Silesian University of Technology

Faculty of Energy and Environmental Engineering

Department of Air Protection

Ph.D. Dissertation

Application of Pure and Mixed Cultures of Bacteria Strains in Synthetic Dyes Removal Processes – Mechanisms and Optimisation of Process Conditions

Author:

Kamran Ayaz

Supervisor:

dr hab. Ewa Zabłocka-Godlewska prof. PŚ

Gliwice, 2026

Dedicated to my parents and my wife, whose love, support, and belief in me made this journey possible

Acknowledgements

First and foremost, I would like to express my deepest gratitude to my supervisor, **Prof. Ewa Zabłocka-Godlewska**, for her continuous guidance, encouragement, and invaluable scientific support throughout my doctoral studies. Her patience, insightful feedback, and trust in my abilities have played a crucial role in shaping this research and my development as a scientist.

I am sincerely thankful to Dr. **Katarzyna Krukiewicz**, for her constant support, constructive discussions, and tireless efforts during both the experimental and publication in part of my PhD work. Her mentorship greatly strengthened the quality and direction of this research.

I would also like to thank all members of the **Department of Air Protection at the Silesian University of Technology** for providing a supportive and collaborative research environment. Special thanks go to my colleagues and laboratory partners who assisted me during experiments, discussions, and challenging moments in the lab.

My appreciation extends to all international collaborators and institutions that contributed to this research through academic discussions, technical assistance, or shared facilities. Their cooperation enriched both the scientific quality and global perspective of this work.

I am deeply grateful to my dear friends **Shakir, Hamza, Faizan, and Abdullah** for their encouragement, support, and companionship throughout this journey. Their presence, advice, and motivation helped me stay strong during both academic and personal challenges.

Finally, and most importantly, I would like to express my heartfelt gratitude to my **parents** and my **wife**. My parents have been my lifelong source of inspiration, teaching me the value of education, perseverance, and integrity. Their prayers, sacrifices, and unwavering belief in me have been the foundation of every success in my life. To my wife, thank you for your patience, understanding, and constant support during the demanding years of my PhD. Your encouragement, love, and strength have helped me overcome every obstacle along the way. This achievement belongs to you as much as it does to me.

Abstract

Synthetic dyes are widely used, especially in textiles, because they give strong color, many shades, and good fastness. A large portion of the applied dye does not bind to fibers and washes out, creating colored wastewater. This is even worse for highly water-soluble, anionic dyes that are built to stay stable in dye baths. Their stability, charge, and structure make them hard to remove with standard physical, chemical, or biological treatment. Azo dyes are the largest group and are often difficult to treat. Upon breaking up of Azo bond removes color quickly but can form aromatic by-products that may persist or need aerobic oxidation to lower toxicity. So, treatment must go beyond decolorization to prove real chemical change, manage by-products, and work across different microbes and reactor designs.

This dissertation examines biological decolorization of several synthetic dyes, but most of the work uses Evans Blue (EB; Direct Blue 53) as the main model compound. EB is a highly sulfonated diazo dye that dissolves easily in water, produces an intense color, and represents the type of anionic azo dye that is difficult to treat in practice. The research follows a staged approach. It starts with tightly controlled biological experiments and then moves toward engineered bioelectrochemical systems that can operate faster and handle higher loads.

Across all stages, treatment is evaluated using mechanistic and chemical evidence, not only UV–Vis estimated color loss. The aim is to build and validate biological and bioelectrochemical routes that accelerate dyes, mainly EB removal with both pure and mixed cultures, while also demonstrating that the dye is chemically transformed rather than temporarily masked by adsorption or partial reduction. The dissertation also makes clear where each approach reaches its limits and identifies the design and operating changes that most effectively improve performance and control

The first experimental chapter focuses on the isolation of selected bacterial species (*Actinomycetes*) involved in decolorization processes. *Actinomycetes* were screened on solid media for dye decolorization, with EB as the target azo dye and Brilliant Green (BG) and Crystal Violet (CrV) as triphenylmethane comparators. In this part of studies, biomass immobilization at low-cost solid carriers were evaluated to stabilize biomass, increase retention, and support later translation to reactor systems. Low-cost solid carriers were tested to optimize the isolated microbe's growth and degradation efficiency. The carriers used were conifer shavings, straw, and leafy chips. Only straw supported visible microbial growth in

initial testing, so we selected the straw for the main experiment as well. After 14 days, straw alone and biomass showed less decolorization or degradation, while combining straw with biomass showed better results. Strain 1K1 removed 66.6% of BG and 80% of EB. Strain EGK2 removed 97.8% of BG and 73% of EB. A key goal was to separate the main mechanism of color loss. In carrier systems, color can be lost because of biosorption, microbial degradation or because dye adsorbs when carriers are introduced. The screening results helped us pick strains for aerobic post-treatment in later experimental chapters. Despite better dye removal there were few limitations that need to be addressed. Long incubation times and mixed physical and biological effects were the main issues. These findings support moving to another model organisms and tighter, controlled optimization in the next experimental chapters.

The second experimental chapter examines EB biodegradation by the electroactive model bacterium *Shewanella oneidensis* MR-1. The design uses Response Surface Methodology (RSM) to optimize key variables: time, temperature, initial dye concentration, and electron-donor concentration. UV–Vis kinetics are used to tracked color loss. While chemical transformation was checked by chromatographic technique HPLC to tracked parent dye loss and GC–MS for the identification of transformed products. This combined approach defines a defensible operating window rather than a single operating point. It clarifies how dye load, temperature, and electron-donor supply control both the rate and the completeness of Evans Blue (EB) bioconversion. Under optimized conditions, nearly complete decolorization (>99%) was achieved. Loss of the chromophore, together with the appearance of aromatic and short-chain acid products, confirmed true dye degradation rather than biosorption. These findings show that *Shewanella oneidensis* MR-1 is an effective single-strain biocatalyst for EB removal and that response surface methodology (RSM) can identify a practical operating window for future applications. This work also reduced the time to complete decolorization from 14 days (experimental section 1) to 3 days. In addition, the pure culture of *S. oneidensis* MR-1 completely mineralized EB when process and growth conditions were fully optimized.

The third experimental chapter investigates efficient decolorization, degradation and complete mineralization of the diazo dye EB using an integrated system that couples a double-chamber microbial fuel cell (DCMFC) with an aerobic bioreactor. This work targets solutions to problem of high concentrations of toxic dyes, with two goals: achieving high decolorization efficiency and characterizing the microbial communities that drive decolorization and degradation. Mixed anaerobic activated sludge from a wastewater treatment plant was used to

evaluate EB removal in the DCMFC anode at initial dye concentrations of 100 and 200 mg/L. In the MFC, the anode creates a low-redox environment that promotes reductive cleavage of azo bonds while enabling energy recovery as electrical current. The aerobic post-treatment step employed two mixed actinomycete strains isolated from garden compost. These *Actinomycetes* consortia oxidized the reduced intermediates and residual organics produced at the anode, supporting full mineralization of the dye.

Decolorization efficiency and microbial community composition were evaluated using 16S rRNA sequencing, and electrochemical impedance spectroscopy (EIS) was used to assess anode and DCMFC resistance. The results demonstrated decolorization efficiencies ranging from 90 ± 2% to 98 ± 1.9% for 100 mg/L and from 79 ± 2% to 87% ± 1% for 200 mg/L after 20-24 h of process. The microbial community analysis revealed a significant presence of *Pseudomonadota* (45.5% in dye-acclimated cultures and 32% in inoculum cultures), with key genera including Actinomarinicola (13.75%), Thermochromatium (4.82%), and *Geobacter* (4.52%). This study highlights the potential of the integrated DCMFC–aerobic system, utilizing mixed *Actinomycetes* strains for the very first time in aerobic step, what may be beneficially applicated in the future for the effective treatment of industrial dye effluents, offering both environmental and bioenergy benefits.

This chapter presents the solutions that cut decolorization time from 3 days to 20–24 hours and achieved complete mineralization by adding a secondary aerobic step. It also treated a higher starting Evans Blue load of 200 mg/L, double that used in experimental chapters 1 and 2. Three limits remain: a long start-up period (adaptation) of about 30 days before we get start the actual experiment of degradation of EB with initial concentration of 100 and 200mg/L, extra energy demand for the aerobic step, and difficult mechanism tracing with a mixed community. These issues point to the need to optimize the reactor and MFC biointerface and attempt to utilize environmentally friendly single chamber microbial fuel cell (SCMFC) so that pure culture can match or exceed this performance while giving clearer mechanisms and easier process control.

Based on the limitation of previous chapter, the final experimental chapter investigates the effect of carbon cloth modifications (anode electrode) using polyaniline (PANI), glucose, and gelatin on biofilm formation, charge transfer, and microbial viability using pure bacterial culture of *Shewanella oneidensis* MR-1. The Pure culture is more prone to toxic effect of dyes and underperformed in high initial dyes concentration. Cyclic voltammetry results and

Biofilm viability studies reveal that carbon cloth in bulk glucose solution (CC.G.B) supports predominantly planktonic growth, limiting bacterial adhesion, while modified carbon cloth (MCC.B) achieves the highest biofilm formation (90.2 ± 0.2 %) and charge storage capacity (CSC, 174.9 ± 10.2 mC/cm^2), corresponding to an approximately 50-fold increase in CSC compared with a bare carbon cloth (CC.B) system (3.3 ± 0.3 mC/cm^2), highlighting the synergistic impact of surface modifications and microbial activity. These findings demonstrate that MCC.B facilitates extracellular electron transfer by optimizing bacterial adhesion and nutrient availability, making it a promising candidate for shortening start-up to 3 days (30 days in experimental section 3) and improving early-stage bioelectrode performance.

In the SCMFC, the modified carbon cloth anode interface achieved about 96–97% decolorization at 150 mg/L in 13 hours (t50 ≈ 5 h; t80 ≈ 9–10 h), 90–91% at 300 mg/L, and 73% at 450 mg/L in 13 hours. Thus, lowering the decolorization time to 13 hours from 24 hours (experimental section 3). The system also operated stably at an initial concentration of 450 mg/L, whereas earlier experiments showed performance limits because of the dye toxicity above 200 mg/L. While GC-MS analysis showed that EB are degraded to less toxic compounds mostly low molecular weight acids 3-methylbutanoic and octanoic acid even without post-treatment aerobic step. These outcomes show a clear, controllable sequence, modified surface chemistry of anode electrode improved bacterial attachment of pure bacterial culture by bearing the toxic effect of high initial dye concentration through well-developed biofilm on modified electrode. This also strengthened electron transfer and increased process rate and capacity. The approach remains simple, uses standard carbon cloth, and is scalable for faster treatment.

STRESZCZENIE

Barwniki syntetyczne są szeroko stosowane, zwłaszcza w przemyśle tekstylnym. Zapewniają one intensywny kolor, wiele odcieni oraz trwałość barwy wybarwionego materiału. Duża część barwników w trakcie aplikacji nie wiąże się z włóknami i pozostając w roztworze oraz ulegając wypłukaniu tworzy barwne ścieki. Największy problem dotyczy barwników dobrze rozpuszczalnych w wodzie i anionowych, które są projektowane tak, aby pozostawały stabilne w kąpielach barwierskich. Ich stabilność, ładunek i budowa sprawiają, że trudno usuwać je ze ścieków standardowymi metodami fizycznymi, chemicznymi lub biologicznymi. Barwniki azowe stanowią największą grupę, jeżeli chodzi o różnorodność jak i stosowane ilości, i często są trudne do usuwania w procesie oczyszczania ścieków. Rozpad wiązania azowego powoduje zanik barwy (dekoloryzację), który nie stanowi gwarancji pełnego rozkładu cząsteczki i może prowadzić do powstania aromatycznych, toksycznych produktów ubocznych, które mogą się utrzymywać w cieczy lub wymagać tlenowego utleniania w celu obniżenia toksyczności. Dlatego oczyszczanie musi wykraczać poza sam efekt dekoloryzacji, aby zapewnić rzeczywistą zmianę chemiczną, kontrolę powstających produktów ubocznych oraz działać w różnych układach mikroorganizmów i reaktorów celem całkowitego usunięcia związku i pochodnych.

W niniejszej rozprawie doktorskiej zaprezentowano wyniki badań usuwania wybranych barwników syntetycznych przez bakterie. Większość wyników dotyczy zastosowania błękitu Evansa (EB, Direct Blue 53) jako głównego barwnika testowego. EB jest silnie sulfonowanym barwnikiem diazowym, bardzo dobrze rozpuszczalnym w wodzie, intensywnie zabarwionym i reprezentatywnym dla trudnych do usunięcia anionowych barwników azowych. Praca realizuje plan etapowo: zaczyna się od kontrolowanych układów biologicznych, a następnie przechodzi do projektowanych układów bioelektrochemicznych. Każdy etap opiera się na dowodach mechanistycznych, a nie wyłącznie na śledzeniu zaniku barwy monitorowanego spektrofotometryczną metodą UV–Vis. Celem jest opracowanie i walidacja strategii biologicznych i bioelektrochemicznych, które przyspieszą usuwanie EB z użyciem czystych i mieszanych kultur bakteryjnych, przy jednoczesnym potwierdzeniu rzeczywistej transformacji chemicznej. Badania określają także praktyczne ograniczenia oraz punkty, które mogą poprawić zarówno wydajność procesu, jak i kontrolę mechanistyczną.

Pierwszy rozdział eksperymentalny skupia się na screeningu ukierunkowanym na pozyskanie wybranych gatunków bakterii (*Actinomycetes*) biorących udział w procesach usuwania

barwników syntetycznych. Screening promieniowców (*Actinomycetes*) prowadzono na podłożach stałych pod kątem dekoloryzacji barwników, disazowego EB, trifenylometanowej zieleni brylantowej (BG) i fioletu krystalicznego (CV). W tej części badań zastosowano również immobilizację biomasy na tanich, naturalnych nośnikach stałych w celu stabilizacji biomasy, zwiększenia retencji i skuteczności degradacji barwników oraz wsparcia zasadności późniejszego przeniesienia do układów reaktorowych.

Zastosowane nośniki to: wióry iglaste, słoma oraz zrębki liściaste. Jedynie na słomie uzyskano widoczny wzrost mikroorganizmów w testach wstępnych, dlatego wybrano ją także do eksperymentu głównego. Po 14 dniach sama słoma oraz sama biomasa wykazywały słabszą dekoloryzację lub degradację barwników, aniżeli połączenie słomy z biomasą, co dawało lepsze wyniki. Szczep 1K1 usunął 66,6% BG oraz 80% EB. Szczep EGK2 usunął 97,8% BG oraz 73% EB. Celem było też określenie głównych mechanizmów zaniku barwy. W układach z nośnikami barwa może zanikać z powodu: biosorpcji, rozkładu barwnika przez mikroorganizmy, lub sorbcji barwnika przez nośnik. Wyniki badań screeningowych pomogły wybrać szczepy do tlenowego doczyszczania w kolejnych rozdziałach eksperymentalnych. Pomimo lepszego usuwania barwnika w układach z immobilizowaną biomasą występowało kilka ograniczeń wymagających rozwiązania. Długi czas inkubacji oraz złożony, niejednoznaczny udział fizycznej sorpcji i procesów biologicznych były głównymi problemami. Wyniki te uzasadniają przejście do badań nad innymi organizmami modelowymi i bardziej ścisłej, kontrolowanej optymalizacji w kolejnych rozdziałach eksperymentalnych.

Drugi rozdział eksperymentalny skupia się na biodegradacji barwnika EB przez elektroaktywną bakterię modelową *Shewanella oneidensis* MR-1. Projekt wykorzystuje statystyczną metodę Response Surface Methodology (RSM) do optymalizacji kluczowych zmiennych: czasu, temperatury, początkowego stężenia barwnika oraz stężenia donora elektronów. Kinetykę UV–Vis zastosowano do śledzenia zaniku barwy. Transformację chemiczną weryfikowano metodą chromatograficzną HPLC w celu śledzenia zaniku macierzystej formy barwnika oraz GC–MS w celu identyfikacji produktów jego transformacji.

Taka komplementarna analiza czynników umożliwia zdefiniowanie procesowego okna pracy zamiast analizy pojedynczego punktu/parametru operacyjnego. Wyjaśnia, w jaki sposób ładunek barwnika, temperatura oraz dopływ donora elektronów kontrolują zarówno szybkość, jak i kompletność biokonwersji Evans Blue (EB). W warunkach zoptymalizowanych uzyskano niemal całkowitą dekoloryzację (>99%). Zanik chromoforu, wraz z pojawieniem się

produktów aromatycznych i krótkołańcuchowych kwasów, potwierdził rzeczywistą degradację barwnika, a nie biosorpcję. Wyniki te pokazują, że czysta kultura *Shewanella oneidensis* MR-1 jest skutecznym biokatalizatorem w usuwaniu EB oraz że metodologia Response Surface Methodology (RSM) pozwala zdefiniować praktyczne okno pracy dla przyszłych zastosowań. Zastosowany układ skrócił również czas pełnej dekoloryzacji z 14 dni (Rozdział 1) do 3 dni. Ponadto czysta hodowla *S. oneidensis* MR-1 całkowicie zmineralizowała EB, gdy warunki procesu i wzrostu były w pełni zoptymalizowane.

Trzeci rozdział eksperymentalny prezentuje wyniki skutecznej dekoloryzacji, degradacji i całkowitej mineralizacji barwnika diazowego Evans Blue, z użyciem mieszanej kultury bakteryjnej oraz zintegrowanego systemu łączącego dwukomorowe mikrobiologiczne ogniwo paliwowe (DCMFC) z tlenowym bioreaktorem. Ta część badań dotyczy roztworów zawierających wysokie stężenia toksycznych barwników, z dwoma wytyczonymi celami: osiągnięciem wysokiej skuteczności dekoloryzacji oraz charakterystyki społeczności mikroorganizmów. Inokulum na bazie beztlenowego osadu czynnego, pobranego z oczyszczalni ścieków, wykorzystano w procesie usuwania Evans Blue na anodzie DCMFC przy początkowych stężeniach barwnika 100 i 200 mg/L. W MFC anoda tworzy środowisko o niskim potencjale redoks, które sprzyja redukcyjnemu rozszczepieniu wiązań azowych, jednocześnie umożliwiając odzysk energii w postaci prądu elektrycznego. W etapie tlenowego doczyszczania wykorzystano dwa mieszane szczepy promieniowców wyizolowane z kompostu ogrodowego. Ta mieszana kultura bakterii utleniała zredukowane intermedianty oraz resztkową materię organiczną wytworzoną na anodzie, wspierając pełną mineralizację barwnika.

Dokonano oceny skuteczności dekoloryzacji, składu społeczności mikroorganizmów za pomocą sekwencjonowania 16S rRNA, a spektroskopię impedancyjną (EIS) zastosowano do oceny oporu anody i DCMFC. Wyniki wykazały skuteczność dekoloryzacji w zakresie 90 ± 2% do 98 ± 1,9% dla stężenia EB 100 mg/L oraz 79 ± 2% do 87% ± 1% dla 200 mg/L, po 20-24 h procesu. Analiza społeczności mikrobiologicznej ujawniła istotną obecność *Pseudomonadota* (45,5% w hodowlach zaadaptowanych do barwnika i 32% w hodowlach inokulum), z kluczowymi rodzajami obejmującymi *Actinomarinicola* (13,75%), *Thermochromatium* (4,82%) oraz *Geobacter* (4,52%). Badania te podkreślają potencjał zintegrowanego systemu DCMFC–tlenowego, wykorzystującego po raz pierwszy w etapie tlenowym mieszane szczepy promieniowców, co w przyszłości może być zastosowane z

korzyścią dla skutecznego oczyszczania przemysłowych ścieków barwnikowych, oferując korzyści środowiskowe i bioenergetyczne. Rozdział ten prezentuje rozwiązania, które skróciły czas dekoloryzacji z 3 dni do 20–24 godzin, osiągając pełną mineralizację poprzez dodanie wtórnego etapu tlenowego. Oczyszczono także wyższy ładunek początkowy Evans Blue wynoszący 200 mg/L, dwukrotnie większy niż w rozdziałach 1 i 2. Pozostały trzy ograniczenia: długi okres rozruchu (adaptacji) około 30 dni zanim można rozpocząć właściwy eksperyment degradacji EB przy początkowym stężeniu 100 i 200 mg/L, dodatkowe zapotrzebowanie energetyczne wynikające z etapu tlenowego oraz trudne śledzenie mechanizmu w układzie z mieszaną mikrospołecznością. Problemy te wskazują na potrzebę optymalizacji reaktora i biointerfejsu MFC i podjęcia próby zastosowania przyjaznego dla środowiska, jednokomorowego mikrobiologicznego ogniwa paliwowego (SCMFC), aby czysta hodowla mogła dorównać lub przewyższyć tę wydajność, zapewniając jednocześnie bardziej interpretowalne mechanizmy i łatwiejszą kontrolę procesu.

Na podstawie ograniczeń poprzedniego rozdziału, zdecydowano się na kierunek badań, którego wyniki zaprezentowano w ostatnim rozdziale eksperymentalnym. Zawarto tu wyniki: wpływu modyfikacji tkaniny węglowej (elektrody anodowej) z użyciem polianiliny (PANI), glukozy i żelatyny na możliwość tworzenia biofilmu; transferu ładunku oraz żywotności mikroorganizmów z wykorzystaniem czystej hodowli *Shewanella oneidensis* MR-1. Czyste hodowle są bardziej podatne na toksyczny wpływ barwników i wykazują gorszą wydajność przy wysokich początkowych stężeniach barwnika. Wyniki cyklicznej woltamperometrii oraz badania żywotności biofilmu dla zastosowanych modyfikacji elektrod wykazały, że tkanina węglowa pracująca w roztworze glukozy (CC.G.B) sprzyja głównie wzrostowi planktonicznemu, ograniczając adhezję bakterii, natomiast zmodyfikowana tkanina węglowa (MCC.B) sprzyja najlepszemu rozwojowi biofilmu (90,2 ± 0,2 %) oraz pojemności magazynowania ładunku (174,9 ± 10,2 mC/cm2), co odpowiada około 50-krotnemu wzrostowi CSC w porównaniu z układem z niezmodyfikowaną tkaniną węglową (CC.B) (3,3 ± 0,3 mC/cm2), podkreślając synergiczny wpływ modyfikacji powierzchni i aktywności mikroorganizmów. Wyniki te pokazują, że MCC.B ułatwia pozakomórkowy transfer elektronów poprzez optymalizację adhezji bakterii i dostępności składników odżywczych, co czyni go obiecującym kandydatem do skrócenia rozruchu układu do 3 dni (30 dni w rozdziale 3) oraz poprawy wczesnej wydajności bioelektrody.

W SCMFC ze zmodyfikowanym interfejsem anody osiągnięto w 13 godzinie procesu około 96–97% dekoloryzacji przy stężeniu EB 150 mg/L (t50 ≈ 5 h; t80 ≈ 9–10 h), 90–91% przy 300 mg/L oraz 73% przy 450 mg/L. Tym samym obniżono czas dekoloryzacji do 13 godzin z 24 godzin (rozdział 3). Układ działał także stabilnie przy początkowym ładunku 450 mg/L, podczas gdy wcześniejsze eksperymenty wykazywały ograniczenia wydajności z powodu toksyczności barwnika powyżej 200 mg/L. Analiza GC–MS wykazała, że EB jest degradowany do mniej toksycznych związków, głównie niskocząsteczkowych kwasów 3-methylbutanowego i oktanowego, nawet bez tlenowego etapu doczyszczania. Wyniki te wskazują na kontrolowalną sekwencję: zmodyfikowana chemia powierzchni elektrody anodowej poprawiła przyczepność czystej kultury bakterii i pozwoliła na zniesienie toksycznego wpływu wysokiego początkowego stężenia barwnika dzięki dobrze rozwiniętemu biofilmowi na zmodyfikowanej elektrodzie. Wzmocniło to również transfer elektronów oraz zwiększyło szybkość i zdolność procesu. Rozwiązanie pozostaje proste, wykorzystuje standardową tkaninę węglową i jest skalowalne do szybszego oczyszczania.

List of Publications Connected with Dissertation

- Ayaz, K., Zabłocka-Godlewska, E., Shakibania, S., Patel, T., Karoń, K., & Krukiewicz, K. (2026b). Enhancing Microbial Adhesion and Electron Transfer of Shewanella oneidensis MR-1 with Polyaniline-Glucose-Gelatin Coating for Bioelectrochemical Applications. (Journal of Environmental Chemical Engineering IF= 7.2) https://doi.org/10.1016/j.jece.2026.121546
- Ayaz, K., Zabłocka-Godlewska, E., Smołka, S., Kudlek, E., Hussain, I., & Ilyas, M. (2026a). Sustainable biodegradation of Evans blue (Direct Blue 53) by Shewanella oneidensis MR-1: Response surface optimization and product analysis. (Journal of Water Process Engineering IF=6.2) https://doi.org/10.1016/j.jwpe.2025.109399
- Ayaz, K., Zabłocka-Godlewska, E., & Li, C. (2024). Enhancing Azo Dye Mineralization and Bioelectricity Generation through Biocathode-Microbial Fuel Cell Integration with Aerobic Bioreactor.(Energies IF=3.4) https://doi.org/10.3390/en17194896
- Ayaz, K., & Zabłocka-Godlewska, E. (2022). Screening of Actinomycetes decolorizing the synthetic dyes from rotten poplar wood and garden compost. Contemporary Problems of (Power Engineering and Environmental Protection; Pikon, K., Bogacka, M., Eds, 119-131)

List of Abbreviations and Variables

List of Abbreviations

Abbreviation	Definition
Ag/AgCl	Silver/silver chloride (reference electrode)
ANOVA	Analysis of variance
AOPs	Advanced oxidation processes
BOD	Biochemical oxygen demand
BG	Brilliant Green (triphenylmethane dye)
CC	Carbon cloth (anode substrate)
CC.B	Carbon cloth anode with bacterial biofilm
CC.G	Carbon cloth with glucose in bulk media
CC.G.B	Carbon cloth with glucose in bulk media and bacterial biofilm
CC.PANI.B	Carbon cloth with polyaniline layer and bacterial biofilm
CE	Coulombic efficiency
CI	Color Index
COD	Chemical oxygen demand
CLSM	Confocal laser scanning microscopy
CSC	Charge storage capacity
CV	Cyclic voltammetry
CrV	Crystal Violet (triphenylmethane dye)
DCMFC	Double-chamber microbial fuel cell
DAQ	Data acquisition system/data logger
DNA	Deoxyribonucleic acid
EB	Evans Blue (Direct Blue 53; CI 23860)
EDS	Energy-dispersive X-ray spectroscopy
EET	Extracellular electron transfer
EIS	Electrochemical impedance spectroscopy
FTIR	Fourier transform infrared spectroscopy
GC-MS	Gas chromatography-mass spectrometry
HPLC	High-performance liquid chromatography
LB	Luria-Bertani (medium)

MCC	Modified carbon cloth (engineered anode samples)
MCC.B	Modified carbon cloth with bacterial biofilm
MSM	Mineral salts medium
MFC	Microbial fuel cell
PANI	Polyaniline
PCR	Polymerase chain reaction
PD	Power density
PBS	Phosphate-buffered saline
Pt/Ti	Platinum/titanium (counter electrode)
RNA	Ribonucleic acid
RSM	Response surface methodology
RMSE	Root mean squared error
SCMFC	Single-chamber microbial fuel cell
SEM	Scanning electron microscopy
TOC	Total organic carbon
UV-Vis	Ultraviolet-visible spectroscopy
16S rRNA	16S ribosomal ribonucleic acid

List of Variables

Symbols are listed with their meaning and units as used in the dissertation.

Symbol	Definition	Units / Notes
A (Absorbance)	Absorbance in UV-Vis calibration and measurements	–
A_s	Measured absorbance of the sample	–
m	Slope of calibration line ($A = m \cdot C + b$)	absorbance per (mg/L)
b	Intercept of calibration line ($A = m \cdot C + b$)	absorbance
C_{sample}	Calculated dye concentration in the sample	mg/L
C_0	Initial dye concentration	mg/L

C_t	Dye concentration at time t	mg/L
D	Dilution factor	–
DD (%)	Decolorization efficiency	%
t	Time/incubation time	h
Y	Predicted response (e.g., dye removal efficiency)	%
A (RSM coded)	Coded factor A: time	coded (–1/0/+1); actual in h
B (RSM coded)	Coded factor B: Evans Blue concentration	coded; actual in mg/L
C (RSM coded)	Coded factor C: glucose concentration	coded; actual in mg/L
D (RSM coded)	Coded factor D: temperature	coded; actual in °C
β_0, β_i	Regression coefficients (intercept, linear, quadratic, interaction terms)	varies
ε	Model error term (residual)	varies
V	Voltage across external load	V (or mV)
I	Current, calculated by Ohm's law ($I = V/R_{ext}$)	A
R, R_{ext}	External resistance/load	Ω
R_{int}	Internal resistance	Ω
P	Power ($P = V \cdot I = V^2/R_{ext}$)	W
j_0	Apparent exchange current density (EIS-derived)	A/m^2 (or mA/cm^2)
E	Electrode potential	V
ν	Scan rate (cyclic voltammetry)	V/s
I(E)	Current as a function of potential	A
E_1, E_2	Cutoff potentials defining integration window	V
IpA	Anodic peak current	mA
IpC	Cathodic peak current	mA
CSC	Charge storage capacity	mC/cm^2
S	Projected geometric electrode area	cm^2
Z	Complex impedance	Ω

R_s (or R1)	Solution/ohmic resistance from equivalent circuit fitting	Ω
R_ct (or R2)	Charge-transfer resistance from equivalent circuit fitting	Ω
W	Warburg impedance (diffusion element)	Ω·s (-1/2) (model-dependent)
P, n (CPE)	Constant phase element parameters	model-dependent
T	Temperature (used in kinetic relations where applicable)	K
n	Number of electrons (used in kinetic relations where applicable)	–
R (gas constant)	Universal gas constant	J/mol·K
F	Faraday constant	C/mol

Chapter 1

1 Introduction

Dyes are widely used in industrial chemicals in sectors such as textiles, printing, cosmetics, and food, where they provide color to materials and products. They are chromophoric compounds that contain light-absorbing groups and can bind to or interact with a substrate through chemical bonds or physical forces. By absorbing selected wavelengths and transmitting or reflecting others, these molecules produce the visible coloration observed on the treated substrate (Alegbe and Uthman 2024). Natural dyes are colorants obtained from renewable biological sources (plants, insects/animals) and minerals, traditionally used in textiles and other crafts, whereas synthetic dyes are predominantly petroleum-derived organic compounds engineered for high color strength, broad shade range, and reproducible performance (Cofrancesco 2009). Since their industrial adoption, synthetic dyes have largely replaced natural dyes in large-scale production. They provide consistent batch-to-batch quality, stronger fastness (to washing, light, and rubbing), and simpler process control, making them more suitable for modern manufacturing (Alegbe and Uthman 2024). Even though synthetic dyes dominate industry, stricter environmental rules and concerns about dye industry wastewater are pushing interest back toward natural and bio-based dyes. These options may be safer and more sustainable. However, they also have drawbacks: the colors can be less consistent, the shade range is smaller, and some fabrics still need extra chemicals (mordants or other helpers) to fix the color and keep it from fading (S. Yadav et al. 2023).

Synthetic dyes and the history of the color industry

Dyes are colorants that attach to materials like textiles, paper, and leather. They keep their color even after washing, sunlight, and heat, so they are hard to remove. Early dyes were natural and came from plants, insects, and minerals used by ancient cultures. Indigo blue (from Indigofera plants or woad) and weld yellow (from Reseda luteola, which contains luteolin) were common and are well documented in archaeology and history (Splitstoser et al. 2016; Pizzicato et al. 2023).

During the Industrial Revolution, dye production moved from natural sources to man-made chemicals. In 1856, William H. Perkin made mauveine, the first synthetic organic dye that succeeded in the market. This discovery started the aniline-dye era. In 1858, Johann Peter Griess found the diazotization reaction, which made azo dye chemistry possible. Early azo dyes soon followed (Figure 1.1), including Yellow aniline in 1862 and Bismarck Brown in

1863, the first azo dye sold commercially (Yates and Yates 2015; Cova, Pais, and Seixas De Melo 2017).

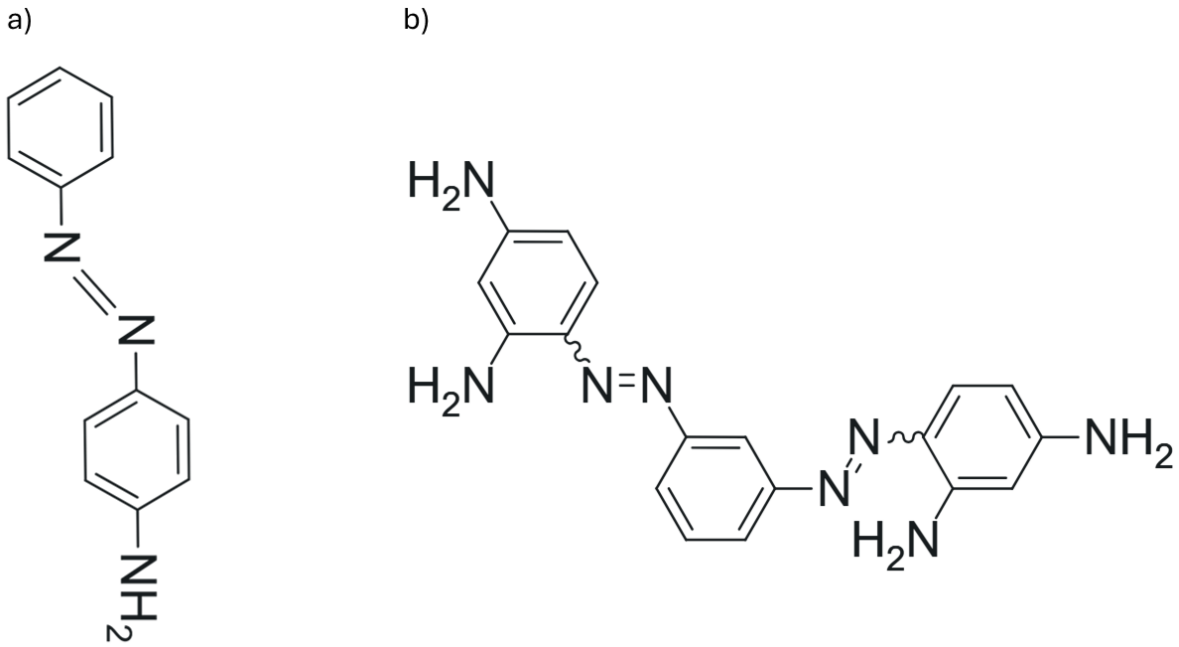

Figure 1.1 The first synthetic azo dyes: (a) Yellow anilinę (b) Bismarck Brown (Bafana, Devi, and Chakrabarti 2011)

Synthetic dyes especially azo dyes changed the colorants industry after the mid-19th-century breakthroughs of mauveine and the diazotization reaction. Compared with natural dyes, they cost less, offered a wider and adjustable range of colors, gave more consistent batch-to-batch results, scaled easily to factory production, and resisted washing, light, heat, and chemicals. These advantages pushed natural dyes out of most industrial uses (Slama et al. 2021; Hagan and Poulin 2021).

Azo dyes became dominant because they are simple to synthesize at larger scale, structurally versatile through the –N=N– chromophore with diverse substituents, and provide strong shades with generally good fastness across many substrates and material. These advantages make the synthetic dyes a favorable matched to needs of a rapidly expanding dye market (Slama et al. 2021). Since the Industrial Revolution, thousands of synthetic dyes have been commercialized. Recent assessments estimate more than 10,000 commercial dyes in use and an annual global production of about 700,000 tons. These figures reflect the widespread application of dyes in dyeing industries (Islam et al. 2025). The textile industry is the largest consumer of azo dyes, with additional use in paper and leather, food and pharmaceuticals industries (Ozturk 2022).

1.1 Types of synthetic dyes and their uses in the color industry

Synthetic dyes are most usefully classified using three complementary criteria: (i) application class, (ii) ionic character and solubility/physical form in water, and (iii) chemical structure (chromophore family)

Synthetic dyes are most commonly classified in the color industry by application class, meaning the class is defined by how the dye is applied and fixed to a specific substrate (especially textile fibres) under a characteristic set of process conditions (Benkhaya, M' rabet, and El Harfi 2020; Hunger 2004). This approach is widely used in industry because it links directly to fixation chemistry, use of auxiliaries, and typical operating windows such as pH, salt demand, temperature, and redox steps. The main application classes used across wet-processing industries are reactive, direct, acid, basic (cationic), disperse, vat, and sulfur dyes.

Reactive dyes are dominant for cellulosics fiber material. They form covalent bonds with cellulose under alkaline conditions, giving bright shades and strong wash fastness. Their drawback is hydrolysis and incomplete fixation, which leaves unfixed dye in the spent bath; effluents often show high color and high salt/alkali loads (J. Sharma, Sharma, and Soni 2021; Benkhaya, M' rabet, and El Harfi 2020).

Direct dyes are widely used for cotton, viscose fiber and also in paper coloration because they apply from water and bind largely by non-covalent bond; they are operationally simple and cost-effective, but generally provide lower wet fastness than reactive or vat systems and can contribute appreciably to color in wastewater because they remain highly water soluble (Berradi et al. 2019).

Acid dyes are anionic (often with sulfonic or carboxylic groups) and are applied from acidic baths. They bind to protonated amino groups on fibers via ionic interactions, often aided by hydrogen bonding and van der Waals forces (Millbern et al. 2024). Acid dyes target wool, silk, and nylon through ionic interactions under acidic conditions and are common in textiles and carpets; their advantage is shade brilliance and controllable dyeing behavior, while the main challenge for wastewater is again linked to their stability and solubility when losses occur (Hassan 2021).

Basic (cationic) dyes are used mainly for acrylic fibers and in inks and paper. They give very strong color strength due to high affinity. Their intense color and strong interactions with solids

mean that apparent “removal” can be dominated by sorption unless chemical transformation is confirmed (P. Yang et al. 2024; M. D. Khan et al. 2023).

Disperse dyes are essential for polyester and other hydrophobic fibers. They are applied as fine dispersions and driven into the fiber at high temperature or with carriers. The advantage is robust polyester coloration. The drawback is wastewater rich in dispersants and colloidal dye particles rather than purely dissolved color (J. Sharma, Sharma, and Soni 2021).

Vat and sulfur dyes remain important for cellulosics when deep shades and high durability are required. In vat dyeing, the dye is chemically reduced to a soluble, colorless form, applied to the fiber, and then re-oxidized in the fiber. This gives very high fastness but increases the chemical and redox footprint of processing (Hunger 2004; J. Sharma, Sharma, and Soni 2021). Common examples often cited for these classes are Reactive Black 5 and Reactive Blue 19 (reactive), Direct Blue 53 (direct), Acid Orange 7 (acid), Methylene Blue (basic), and Indigo (vat). The main value, however, lies in understanding the class-specific processing logic rather than any single dye.

Classifying dyes by ionic character (anionic, cationic, non-ionic, amphoteric) and by solubility form (true solution vs. dispersion; water-soluble vs. sparingly soluble or insoluble) is essential for predicting environmental fate and treatment. These traits control how dyes move in water, how they interact electrostatically, how strongly they adsorb to carriers or biomass, and how available they are to microbes for biodegradation (M. D. Khan et al. 2023; Alegbe and Uthman 2024).

Finally Structure-based classification (e.g., azo, anthraquinone, triphenylmethane, indigoid, phthalocyanine, xanthene, and metal-complex dyes) is critical for mechanism-based interpretation, because each chromophore has distinct redox behavior and biodegradation routes that determine persistence and treatability. Table 1-1 summarizes the major synthetic dye families and representative model dyes, listing their Color Index numbers, scientific names, chemical formulas, and key UV–Vis parameters used for comparison and for monitoring during treatment studies.

1.1.1 Anthraquinone dyes

Anthraquinone dyes contain a fused aromatic, quinone-like backbone that gives high photochemical and chemical stability. Their rigid polycyclic structure and resonance stabilization limit enzymatic attacks and slow down mineralization, leading to persistence.

Effective treatment often requires specialized biocatalysts or combined sequences such as biologically assisted oxidation or reduction. In dye wastewaters, they are challenging pollutants and are commonly used as benchmarks for treatability across chromophore families (Mohanty and Kumar 2025; M. D. Khan et al. 2023; Al-Tohamy et al. 2022a).

1.1.2 Triphenylmethane dyes

Triphenylmethane dyes includes crystal violet, brilliant green and malachite green. They show intense color and are often cationic, which promotes strong interactions with negatively charged biomass and material surfaces. Their removal typically involves both adsorption and biochemical transformation, so experimental controls are required to separate physical uptake from true conversion. They remain important model pollutants in biodegradation studies and wastewater reviews because they can be toxic and persist under suboptimal treatment conditions (Y. Tian et al. 2024; Alegbe and Uthman 2024; Al-Tohamy et al. 2022a).

1.1.3 Indigoid dyes

Indigoid dyes, especially industrial indigo used for denim, are important because denim effluents often have low biodegradability and variable composition. The textile-wastewater literature treats indigo as a priority pollutant in some sectors and recommends green or hybrid treatment trains that combine biological and physicochemical steps to improve removal and enable reuse (Castillo-Suárez et al. 2023; Al-Tohamy et al. 2022a).

1.1.4 Xanthene dyes

Xanthene dyes, including rhodamine-class compounds used as fluorescent models, raise concerns due to strong color/fluorescence and potential toxicity. Apparent removal is often dominated by adsorption, which depends on the matrix and surface chemistry. Therefore, studies should confirm chemical transformation with methods such as chromatographic analysis rather than relying on color or absorbance alone. Including these dyes supports the dissertation goal of distinguishing simple decolorization from verified degradation products (Aragaw 2024a; M. D. Khan et al. 2023; Al-Tohamy et al. 2022a; Alegbe and Uthman 2024).

1.1.5 Azo dyes

Azo dyes contain one or more azo bonds (–N=N–) that link aromatic or heteroaromatic rings. They are the most widely used synthetic colorants, especially in textile wet processing (Aragaw 2024a), and include the reactive, direct, and disperse classes . They are also common

in leather, paper, printing inks, and plastics because they offer broad shade control and flexible preparation chemistry (Benkhaya, M' rabet, and El Harfi 2020; Islam et al. 2025). Their industrial success is due to four factors:

1. Easy synthesis through diazotization and coupling reactions
2. Structural flexibility that creates a very large color range
3. High coloring strength with good fastness on many substrates
4. Cost-effective large-scale production compared with other chromophore families

Table 1-1 Representative synthetic dye families and model dyes (RB19, Crystal Violet, Indigo Carmine, Rhodamine B, and Evans Blue), showing their Color Index/scientific names, chemical formulas, and key UV–Vis parameters (molecular weight and λ_max) used for comparison and monitoring in treatment studies.

Dye family	common name	Scientific name	Chemical formula	Key parameters	Chemical structure	Reference
Anthraquinone dyes	Reactive Blue 19 (RB19;	RB19; C.I. 61200	C22H16N2Na2O11S3	Molecular weight 626.5; λmax 595 nm	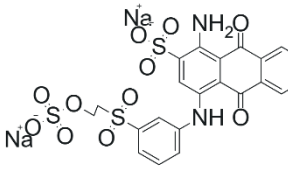	(Ciobanu, Barna, and Harja 2016)
Triphenylmethane dyes	Crystal violet	Crystal violet; C.I. 42555	C25H30N3Cl	Molecular weight 407.98 g/mol; λmax 590 nm	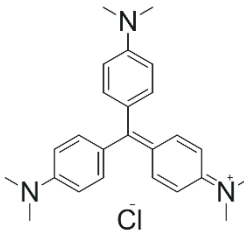	(ZABŁOCKA-GODLEWSKA, PRZYSTAŚ, and GODLEWSKA 2020)
Indigoid dyes	Indigo carmine (IC)	3,3'-dioxo-2,2'-bis-indolyden-5,5-disulfonic acid disodium salt;	C16H8N2Na2O8S2	Molecular weight 466.36 g/mol; λmax 610 nm	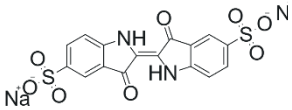	(Białowąs et al. 2024)

Xanthene dyes	Rhodamine B (RhB)	Rhodamine B (also "basic rose red" / "brilliant pink B")	C28H31ClN2O3	λmax 554 nm (UV–Vis measurement)	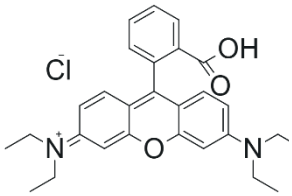	(Lu et al. 2020)
Azo dyes	Evans Blue (EB)	Evans blue; disazo dye; C.I. 23860	C34H24N6Na4O14S4	Molecular weight 960.79 g/mol; λmax 606 nm	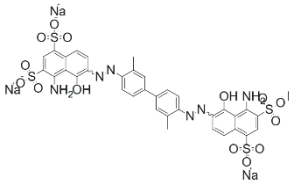	(ZABŁOCKA-GODLEWSKA, PRZYSTAŚ, and GODLEWSKA 2020)

Azo dyes and color

Azo dyes contain the –N=N– group, but strong color appears only when this group is part of a continuous conjugated π system with aromatic rings. Conjugation spreads out electrons and moves the main π→π* and n→π* electronic transitions into the visible range, which explains the vivid color of many aryl azo compounds (Rashid et al. 2020; Benkhaya, M' rabet, and El Harfi 2020). If the azo group is attached to alkyl fragments (Figure 1.2a), there is no extended conjugation, the absorptions stay in the UV range, and the compounds are mostly colorless. In contrast, aryl azo systems such as azobenzenes (Figure 1.2b) show absorption bands partly in the visible range, which gives yellow to orange color (Rashid et al. 2020). This photophysical basis also explains why UV–Vis spectroscopy is routinely used to track decolorization kinetics in treatment studies.

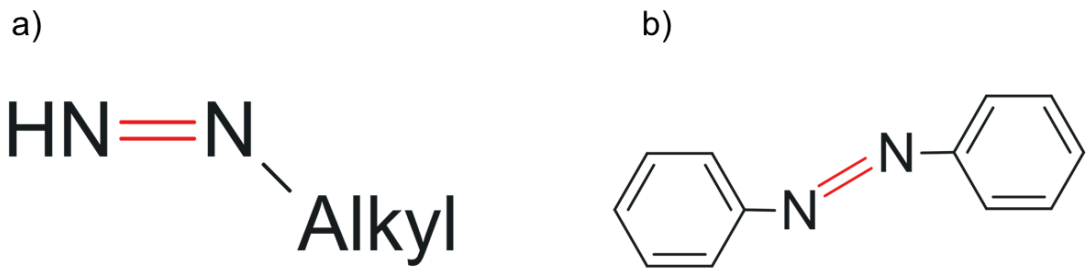

Figure 1.2 Two compounds exemplifying an A) an alkyl azo compound and B) an aryl azo compound (Merino and Ribagorda 2012)

Azobenzenes and the effect of substituent groups on color and solubility

Beyond the azo bond, many commercial dyes carry auxochromes that interact with the π system and change the electronic transitions, which shifts the maximum absorption and tunes color. Electron-donating groups such as NH_2 and OH, and electron-withdrawing groups such as NO_2, CN, and carbonyls, can cause bathochromic or hypsochromic shifts depending on their strength and where they sit on the ring (Yamada et al. 2018). Sulfonic (SO3H) and carboxylic (COOH) groups are widely used to increase water solubility and adjust ionic character without lowering color strength; this in turn affects transport in wastewater and interactions with sorbents and biomass (Thomas and Adegoke 2022). Controlled studies on substituted azobenzenes show systematic λmax shifts with substituent strength and position, supported by spectroscopic and computational analyses (Figure 1.3) (Yamada et al. 2018; Porobić et al. 2020).

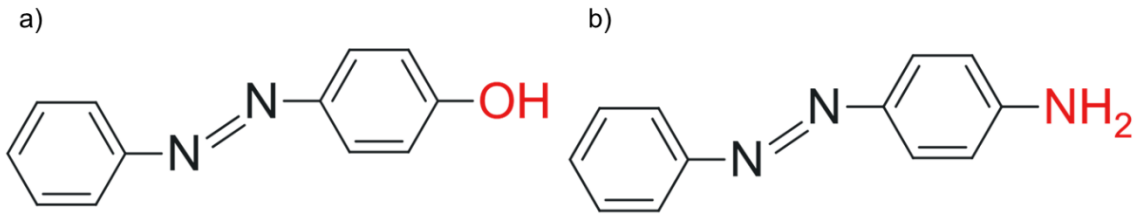

Figure 1.3 The bathochromic shift of –OH substituted azobenzene from 347nm to 386nm when azobenzene is substituted with –NH2 group at the same position of the aryl ring.

Extent of production, usage, and why azo dyes dominate

Recent studies estimate global synthetic dye production at about 0.7–0.8 million tons per year, with more than 10,000 commercial dye types. Within this total, azo dyes remain dominant, typically representing 60–70% of use (Islam et al. 2025). Azo dyes are preferred because they are simple and cost-effective to make, can be tuned to many colors, and provide good fastness when the dye class and process match the fiber, for example reactive azo dyes on cotton and disperse azo dyes on polyester (Alegbe and Uthman 2024). Most azo dyes are produced by diazotization followed by azo coupling from aromatic amine precursors. Recent work also reports intensified methods, including flow synthesis and mechanochemical routes, that improve safety and efficiency while keeping the same core chemistry (Ouyang et al. 2024). The high production volume and broad use create a substantial risk of dye release to wastewater during industrial dyeing.

Azo dye wastewater generation, environmental impacts, and treatment challenge

In conventional dyeing, a large share of dye does not fix to the fiber and is washed out, creating highly colored effluents. In reactive dyeing of cotton, fixation is often only 50–80%, so 20–50% of the applied dye can enter wastewater if conditions are not optimized (Khatri et al. 2015). When this wastewater reaches surface waters, then dissolved and particulate dyes in wastewater can reduce light penetration, suppress photosynthesis, and disrupt aquatic communities; strong color also lowers visual quality and can harm biodiversity (Al-Tohamy et al. 2022b). Many dyes, especially azo dyes, are engineered to resist sunlight, temperature change, and microbial attack, which leads to persistence and buildup unless it is treated effectively (G. B. Singh et al. 2024). Under reducing conditions, azo dyes can partially convert to aromatic amines, and some amines or related intermediates are genotoxic, mutagenic, or carcinogenic depending on their structure (Bienstock, Perera, and Pasquinelli 2022). These points underscore the need to distinguish simple decolorization from verified chemical transformation in dye-removal studies.

Textile dye industries effluents are very complex and typically show high color, elevated COD and TOC, high salinity, and variable pH, and they often contain surfactants and other processing chemicals (Table 1-2). As a result, treatment or reuse is required before discharge to meet permit limits (Berradi et al. 2019). Case studies from major textile regions report pollutant loads that demand effective on-site treatment or centralized treatment to protect receiving waters (Tüfekci, Sivri, and Toroz 2007).

Legislation and regulatory drivers relevant to azo dyes

In Europe, dye-containing wastewater discharge is regulated by the Water Framework Directive (2000/60/EC). In addition, REACH (Annex XVII, Entry 43) restricts azo dyes in textiles and leather that can contact skin or the oral cavity if they can breakdown to listed primary aromatic amines. These rules cover both the parent dyes and the hazardous amines released during chemical or biological reduction (Figure 1.4) (Keshava et al. 2023). Together, these frameworks motivate treatment strategies that go beyond visible color removal and address transformation pathways and by-product control.

Figure 1.4 Textile wastewater contains toxic chemicals from dyes that pollute the environment - like wastewater released from factories into River, in India (pictured). Credit (Noemi Cassanelli/AFP/Getty Images)

Table 1-2 Typical properties of untreated textile wastewater (Al-Kdasi et al. 2004)

Measured parameter	**Typical range**
Chemical Oxygen Demand (COD; mg/L)	150–12,000
Biochemical Oxygen Demand (BOD; mg/L)	80–6,000
Total Dissolved Solids (TDS; mg/L)	2,900–3,100
Chloride (mg/L)	1,000–1,600
Color (Pt–Co scale)	50–2,500
Total Suspended Solids (TSS; mg/L)	15–8,000
Total Kjeldahl Nitrogen (TKN; mg/L)	70–80
pH	7.0–12.0

1.2 Selection of Evans Blue as the model dye

Evans Blue (EB), also called C.I. Direct Blue 53 or T-1824, is a diazo dye with a molecular weight of about 960.8 to 961 Da and with very high water solubility (Yao et al. 2018). These properties make EB a strict model for biological dye removal. EB is also a good “stress-test” dye because it represents a threatening class used in wet processing. These are sulfonated, anionic, aromatic azo dyes that are made to keep strong color while staying stable and highly soluble in water. The sulfonate groups are a key structural feature that increases water solubility in many azo dyes and EB is one of them (Benkhaya, M’ rabet, and El Harfi 2020). These same design features often make treatment difficult. Highly water-soluble anionic dyes show adsorption and removal that depend strongly on conditions such as pH, ionic strength,

and the surface chemistry of the adsorbent. EB has been used in comparative adsorption studies that directly test how its uptake changes with the type of sorbent and with operating conditions (Aguirre-Contreras et al. 2025). In addition, EB are described in recent reviews as environmentally persistent pollutants in dye-containing wastewaters, supporting the need for robust treatment strategies beyond simple color removal (G. B. Singh et al. 2024). Finally, under reducing/low-redox biotransformation conditions typical of many azo-dye removal environments (including anaerobic zones and bioelectrochemical anodes), azo bonds can undergo reductive cleavage to yield aromatic amines, which often require subsequent aerobic treatment steps for further degradation; therefore, decolorization alone is not adequate evidence of detoxification or mineralization (Van Der Zee and Villaverde 2005).

Beyond textile relevance, EB is widely documented in biomedical science as a strongly colored tracer that binds tightly to proteins (notably serum albumin) and therefore remains detectable and stable in aqueous biological environments (Saunders et al. 2015; Yao et al. 2018). Although this biomedical application is different from wastewater treatment, it highlights two points that are important for environmental biotechnology. First, EB is chemically stable under diverse conditions. Second, EB can bind strongly to biological materials. These two features make simple color decolorization testing unreliable on their own and support the need for additional transformation test in biodegradation studies to confirm real transformation. (H. L. Wang and Lai 2014; Yao et al. 2018).

Compared with benchmark azo dyes such as Reactive Black 5, EB is less frequently used as a mechanistic model. Existing EB studies vary in aeration, media, co-substrates, and dye concentration, hindering direct comparison. Accordingly, (Table 1-3) provides an overview for the use of EB as a model dye across application different microorganisms and reactor configurations.

Table 1-3 Comparative analysis of Evans Blue dye biodegradation by different microbial strains, highlighting degradation efficiency, time, and initial dye concentration

No	Microorganism used	Initial dye concentration (mg/L)	Time to max removal (h)	Max. Degradation (%)	Reference
1	*Pseudomonas fluorescens Sz6* (bacteria)	50	48	95	(Zablocka-Godlewska, Przystas, and Grabinska-Sota 2012)
2	*Pseudomonas fluorescens SDz3* (bacteria)	50	48	86	(Zablocka-Godlewska, Przystas, and Grabinska-Sota 2012)
3	*Pleurotus ostreatus, Gloeophyllum odoratum, Fusarium* oxysporum (fungi)	150	96	43	(Przystś, Zabłocka-Godlewska, and Grabińska-Sota 2013)
4	*Pleurotus ostreatus BWPH* (fungi)	20	96	60	(Przystaś, Zabłocka-Godlewska, and Grabińska-Sota 2019)
5	*Pleurotus ostreatus K4* (fungi)	20	72	20	(Przystaś, Zabłocka-Godlewska, and Grabińska-Sota 2019)
6	*Enterobacter cloacae SD4-1* (bacterium)	50	24	75	(Ravi et al. 2025)
7	*Streptomyces spp.* (actinomycetes)	50	120	97	(Kameche et al. 2022)
8	*Staphylococcus lentus*	100	24	19.7	(Chaieb, Hagar, and Radwan 2016)
9	*Shewanella oneidensis MR-1* (bacterium)	100	24	100	(Ayaz, Zabłocka-Godlewska, Smołka, et al. 2026)

Published work demonstrates that EB can be decolorized by diverse taxa, but removal performance is often slow or incomplete unless conditions strongly favor reduction or co-metabolism. For example, Pseudomonas fluorescens strains (Sz6 and SDz3) were reported to remove >85% of EB within 48 h and reach complete decolorization by 120 h under static conditions, with additional discussion of toxicity changes in post-process samples. Mixed fungal cultures have also been evaluated for EB and dye mixtures, illustrating that fungal cultures can contribute to dye removal but may show variable performance depending on strain combinations and dye class. Actinomycetes are likewise relevant: Streptomyces strains have been reported to achieve high EB decolorization (up to ~97% at 50 mg/L) but typically on multi-day timescales, consistent with the broader observation that actinobacterial dye

degradation can be effective yet condition dependent. In contrast, some organisms show limited EB removal under the tested conditions (e.g., low removal reported for Staphylococcus lentus in comparative azo dye decolorization work), reinforcing that removal of EB is not easy across microbial groups and that strain selection and operating-window definition are critical (Zablocka-Godlewska, Przystas, and Grabinska-Sota 2012; Przystś, Zabłocka-Godlewska, and Grabińska-Sota 2013; Przystaś, Zabłocka-Godlewska, and Grabińska-Sota 2019; Ravi et al. 2025; Kameche et al. 2022; Chaieb, Hagar, and Radwan 2016).

Critically, across much of the EB literature, decolorization percentage is frequently the main endpoint, whereas chemical confirmation of degradation (e.g., parent-dye disappearance by HPLC and identification of intermediates by GC–MS/LC–MS and optimization of controllable process variables are less consistently integrated. This creates a clear knowledge gap for treatment-relevant conclusions: for sulfonated diazo dyes such as EB, it is not sufficient to show color loss alone; strong interpretation requires demonstrating transformation and evaluation how operational factors control (electron donor, temperature, dye load, and in bioelectrochemical systems also resistance and electrochemical state) shape both kinetics and completeness.

1.3 Current methods for treatment of color industry wastewater

Due to environmental risks and legal obligations, color industry wastewater needs to be treated for color, organic compounds including toxic ones, inorganic ions such as nitrates, sulphates and phosphates and heavy metal ions. Several technologies are currently in use for color and organics removal. These range from physico-chemical degradation methods to biological degradation methods are shown in Figure 1.5.

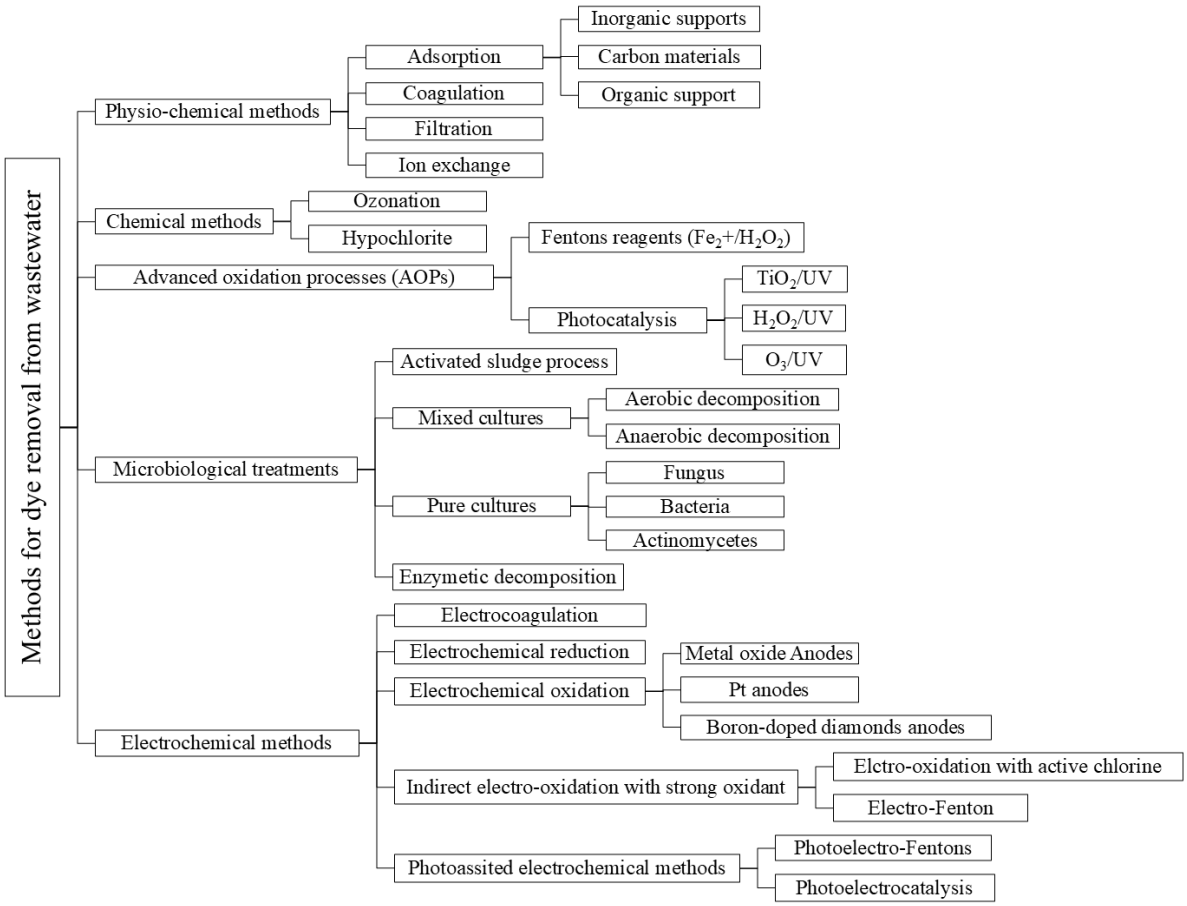

Figure 1.5 Current and proposed methods for removal of synthetic dyes from industrial wastewater

1.3.1 Physio-chemical dye removal methods

The main objective of a physical or physicochemical method to treat textile wastewater is the removal of dissolved and undissolved chemicals and particulate matter present in the wastewater. Below, we discuss several physical and physicochemical methods that are commonly used to treat textile wastewater, including adsorption, ion exchange, membrane technology, irradiation, coagulation-flocculation, and electrocoagulation.

Adsorption

Adsorption removes dyes by moving them from water onto a solid surface, driven by electrostatic attraction, π–π interactions, hydrophobic forces, and, for some materials, ion exchange. Performance depends strongly on dye class and solution chemistry. On many carbons based and organic adsorbents, cationic or basic dyes usually adsorb more readily than anionic reactive or acid dyes. Under comparable conditions, more hydrophobic dyes and those with higher molar mass show higher uptake. Recent reviews summarize these mechanisms and compare behaviors across textile dyes (Al-Zawahreh et al. 2021; Dutta et al. 2021).

Commercial activated carbon (AC) remains a benchmark adsorbent, with high capacities for many disperse, direct, and basic dyes. Uptake of highly hydrophilic reactive or acid dyes is often limited unless the surface is modified or a co-adsorbent is added. AC production is energy intensive, and costs vary with the precursor and the activation method. Techno economic studies report prices of about US$2 per kg for waste-shell carbons made by physical activation, rising to much higher prices for specialty grades. These costs can limit large-scale use for high-volume dye effluents (Al-Tohamy et al. 2022b; Husien et al. 2022). To lower cost and improve circular use, many studies employ biosorbents from agricultural or food wastes (husks, peels, shells), activated sludge, biofilms, and biochar produced from terrestrial or algal biomass. These materials can achieve competitive color removal, especially for cationic dyes, and can be tailored by acid or base activation by metal or heteroatom doping to increase affinity for anionic dyes. However, regeneration and disposal of spent sorbents remain important design concerns (Kainth, Sharma, and Pandey 2024; Suresh et al. 2024). For textile dye effluents, adsorption works best when matched to the dye's chemistry and supported by surface modification to capture anionic or reactive dyes, or by combining with biological or advanced oxidation steps. Selection should consider unit cost, regeneration method, and end-of-life management of sludge or spent sorbent, alongside adsorption capacity and kinetics (Al-Tohamy et al. 2022b; Dutta et al. 2021).

Adsorption is effective for rapid color removal, but it is a phase-transfer method and does not ensure detoxification or mineralization. Spent adsorbents need thermal or chemical regeneration or disposal, which raises operating costs and can shift pollutants into secondary solid wastes. In real dye industries effluents, salts, surfactants, and dissolved organics compete for sites and reduce capacity and selectivity, especially at high salinity. Performance is strongly dependent on dye class, and breakthrough occurs quickly for highly soluble dyes unless very high adsorbent doses are used (Al-Tohamy et al. 2022b; Soltani, Faramarzi, and Parsa 2021).

Ion exchange

Many agricultural by-products, including maize cobs, sugar beet pulp, soybean hulls or pulp, and tree bark, can be chemically modified by introducing acidic or basic groups to function as ion-exchange or biosorbent media for textile wastewater decolorization. These materials remove dyes primarily through electrostatic attraction, aided by additional surface interactions. They are attractive because they are low cost and widely available (Kadhom et al. 2020). For charged dyes, ion-exchange resins can form dye resin complexes that can cluster

into flocs and can be removed by filtration. The main mechanism is ionic exchange between the resin's functional groups and the dye ions. Removal performance depends on the dye class: anionic dyes (acid, reactive, direct or metal-complex) versus cationic dyes (basic) (Dutta et al. 2021). In exchange, non-electrostatic interactions also play important roles. Dye uptake typically involves hydrogen bonding, π–π interactions and van der Waals forces in addition to charge attraction. The number and strength of these interactions strongly influence capacity and selectivity. Such mixed-mode binding is well documented for cellulose-based and magnetic ion-exchange sorbents used on dye industries effluents (Hubbe, Park, and Park 2014). Disperse dyes are mostly nonionic and hydrophobic, so they lack the charge needed for efficient ion exchange. As a result, ion-exchange resins generally perform poorly for removing disperse dyes compared with adsorption processes that rely on hydrophobic and π–π interactions or with advanced oxidation methods. (Dutta et al. 2021).

Ion exchange can remove ionic dyes efficiently, but performance declines when effluents contain mixed anions, high ionic strength, and competing organics that foul resin sites. Regeneration produces a high-salinity, dye-rich brine that needs further treatment or disposal, creating a secondary waste issue. Resins are sensitive to fouling by colloids and macromolecules and often require upstream clarification and periodic chemical cleaning. Costs rise with frequent regeneration and resin replacement, which can be limiting for high-strength or variable textile streams (Yuzer and Selcuk 2021; Moh Rabti et al. 2025).

Membrane technology

Membrane processes are commonly used for color removal and water reuse in textiles industries include ultrafiltration (UF), nanofiltration (NF), and reverse osmosis (RO). Recent assessments reports their operating principles, typical dye and salt rejection ranges, and their suitability for partial improvement of reuse or for full scale recycling (Kamalesh et al. 2024; Yanyan Liu et al. 2025).

Commercial membranes are commonly made from polyamides (thin-film composites), polysulfone/polyethersulfone (PSf/PES), polyacrylonitrile (PAN), and polyvinylidene fluoride (PVDF). These materials are selected for their chemical and thermal stability and resistance to the broad pH range, temperature, and solvent ranges found in dye contaminated effluents (Kamalesh et al. 2024). As selective physical barriers, NF and RO retain dyes and multivalent salts while producing a permeate suitable for on-site reuse. Multiple studies report high color

removal and significant salt recovery, enabling internal recycling of water and auxiliaries (Yanyan Liu et al. 2025). Ultrafiltration (UF) alone has limited decolorization because many dye molecules are smaller than typical UF molecular-weight cutoffs. Even so, using hydrophobic UF membranes such as PES or PVDF can improve retention of dyes and COD through adsorption and sieving. In practice, UF is most effective as a pretreatment step that protects downstream nanofiltration (NF) or reverse osmosis (RO) units (Kamati, Yan, and Fan 2024). UF, and to a lesser extent NF, does not remove all dissolved solids, and even RO produces a concentrated retentate that requires management. High capital and energy demands, fouling, and limited membrane life under variable loads remain major constraints for full-scale deployment (Zhou et al. 2024). Recent reviews present side-by-side comparisons of UF, NF, and RO for textile wastewater recovery and reuse, covering performance, fouling control, and emerging variants such as loose-NF and FO/MD hybrids. These summaries provide design guidance for integrating membranes into treatment trains (Yanyan Liu et al. 2025; Reddy, Kalla, and Murthy 2021).

Irradiation

Gamma irradiation removes color from textile effluents by creating very reactive species that attack dye molecules. These include hydroxyl radicals (OH), hydrated electrons (eaq^-), and hydrogen atoms (H). The rate of degradation increases as the absorbed dose increases. Dissolved oxygen further improves performance because it promotes peroxyl chemistry and additional oxidation. Recent studies and case reports confirm this clear dose–response pattern and the positive effect of oxygen in dye removal from solutions (Al-Abduly et al. 2021). Successful treatment has been shown for reactive, acid, and disperse dyes. Ionizing radiation can also break down other toxic organics present in dye-house wastewater, such as chlorophenols and related aromatics, which improves both color removal and overall organic load. Recent work shows that gamma and electron-beam irradiation can remove dyes and halogenated phenols, supporting their use as a polishing or reuse step (Ahsan et al. 2022). Gamma processes can treat dyes that are difficult for conventional oxidation or reduction. Radiolysis generates nonselective radicals that cleave azo bonds and can mineralize intermediate products, which explains their robustness in complex effluents (Wojnárovits and Takács 2008). However, there are important limitations, e.g. capital and energy costs are high. Light penetration and matrix effects reduce efficiency in real wastewater; turbidity, deep color, and dissolved constituents can shield the beam and scavenge radicals, which lowers effective

photon use. Aeration or oxygen supply is often needed to maintain oxidative pathways in the treated stream. Throughput can also be limited on a large scale. These factors raise operating costs compared with standard physicochemical methods (Emami-Meibodi et al. 2016) (Hübner et al. 2024; Priyadarshini et al. 2022).

Coagulation-Flocculation

Coagulation–flocculation is a physicochemical pretreatment applied before sedimentation or filtration to improve color removal from textile effluents. In this process, coagulants such as Al3+ and Fe3+ salts or polymeric agents neutralize particle charges and lower the zeta potential, which destabilizes dye-bearing colloids. Gentle mixing then promotes the growth of flocs that can settle or be filtered. The underlying principles, the main coagulant types, and the operating ranges for pH, dose, and mixing are well established for industrial wastewaters, including real textile streams (El-taweel et al. 2023; Karam, Bakhoum, and Zaher 2021). The method is effective for many water-insoluble dyes, for example sulfur and disperse dyes, and for dye-containing suspensions. It can also reduce COD to varying degrees and improve downstream biodegradability when followed by biological treatment. Studies on real effluents and model disperse-dye systems report substantial decolorization and solids removal at optimized doses and pH (Karam, Bakhoum, and Zaher 2021). Highly water-soluble dyes, for example many reactive or acid dyes, are harder to remove and often require higher chemical doses or additional treatment steps. Coagulation transfers color from the water phase into a solid phase rather than degrading it, so the resulting-colored sludge or retentate must be managed. Reviews of dye-containing wastewater consistently highlight these limits and the need for integrated treatment trains that combine physicochemical and biological steps (Al-Tohamy et al. 2022b). Drawbacks include chemical and energy costs, sensitivity to wastewater charge and ionic strength, and the generation of sludge that may contain residual aluminum or iron. If this sludge is mismanaged, metal-rich residues and leftover coagulants can harm aquatic organisms, which underscores the need for appropriate sludge handling or valorization pathways (Aragaw and Bogale 2023).

Electrocoagulation

Electrocoagulation (EC) uses a direct current applied to sacrificial metal electrodes, typically aluminum or iron, to generate coagulant particles inside the reactor. At suitable pH, the electro-dissolved Al^{3+} and Fe^{3+}/Fe^{3+} ions form aluminum or iron (hydr)oxides that neutralize surface

charges, sweep-flocculate colloids, and adsorb dissolved dyes. Compared with chemical coagulation, EC requires fewer added chemicals and often produces less sludge, while still achieving high decolorization on real textile effluents (Gasmi et al. 2022; Boinpally et al. 2023), Because the coagulants are created directly from the anode by electro-dissolution, external coagulant addition is minimized. Process performance depends on several controllable variables: solution conductivity, pH, current density, electrode arrangement, spacing and material, hydrodynamics, residence time, and electrode stabilization. Together, these factors determine floc formation, energy use, and overall treatment efficiency (Boinpally et al. 2023; Phu, Nguyen, and Phung 2025). Comparative studies show that disperse dyes, which are less soluble and more hydrophobic, are generally easier to remove by EC than reactive dyes. In contrast, COD removal can be higher for reactive-dye streams, which often contain larger fractions of soluble organics relative to particulates. Similar patterns are reported for chemical coagulation and for EC on both model and real textile effluents (Kim et al. 2004). Practical limitations include anode consumption and the need for periodic replacement, the requirement for sufficient conductivity or added electrolyte, energy demand, and sludge handling even if reduced relative to chemical coagulation. These factors influence operating cost and scale-up, which motivates hybrid treatment trains such as EC followed by filtration or biological steps to meet water reuse or discharge targets (Gasmi et al. 2022).

1.3.2 Chemical methods

Commonly used chemical methods for decolorization of textile wastewater include those based on chemical oxidation and reduction (Holkar et al. 2016). In case of chemical oxidation, the dye molecules are degraded into small colorless molecules such as carbon dioxide, water, nitrogen, aldehydes, acids, and sulfates, depending on the dye structure and on the strength of the oxidant used. Due to the limitations associated with classic oxidation-based approaches and because environmental regulations have become more stringent, new and novel approaches for dye removal and degradation have been developed and implemented. Among these methods, Advanced Oxidation Processes (AOPs) have been proposed as a promising technique for wastewater treatment, as they can efficiently oxidize a wide range of recalcitrant compounds.

Chemical oxidation

Chemical oxidation in textile effluents commonly employs chlorine, chloramine, chlorine dioxide, ozone (O_3), and hydrogen peroxide (H_2O_2), alone or within AOPs (e.g., UV/H_2O_2, O_3/H_2O_2). These reagents target chromophores and auxiliary organics, with selection guided by dye class, matrix salinity, energy, and chemical costs. Recent reviews summarize operating conditions and performance across real dye-house streams (Al-Tohamy et al. 2022b). Hypochlorite is effective for many water-soluble dyes (acid, direct, metal-complex, reactive) but is far less efficient on water insoluble dyes and diazo dyes and demand longer contact times than monoazo dyes for complete decolorization. A key concern is formation of adsorbable organic halogens (AOX) and other chlorinated by-products, especially in chloride rich matrices, which elevates toxicity and necessitates downstream control (Al-Tohamy et al. 2022b). Ozone rapidly attacks unsaturated chromophores, yielding high color removal and appreciable COD decrease; indirect •OH generation can further enhance degradation. However, short O_3 half-life and matrix effects (pH, temperature, salts/bromide) limit mineralization, and ozonation often produces low-molecular-weight aldehydes, ketones, and carboxylic acids, occasionally with increased toxicity, hence the frequent pairing with bio-treatment or carbon (Epelle et al. 2022). Standalone H_2O_2 can decolorize some dye classes and oxidize auxiliary organics with benign end-products versus chlorination or sole O_3; yet, without activation (UV, Fe^{2+}/Cu, persulfate) it often shows slower kinetics, partial dye breakdown, higher doses, and retention times to reach targets, these are the factors that raise operating costs relative to activated AOPs (S. Khan et al. 2024). Overall, the choice of oxidant reflects trade-offs among decolorization rate, mineralization, by-product control, and cost. Contemporary practice favors hybrid treatments (e.g., O_3 or UV/H_2O_2 followed by biological or carbon steps) to capture rapid color removal while managing oxidation by-products and meeting reuse or discharge limits (Al-Tohamy et al. 2022b).

Advanced Oxidation Processes

Advanced oxidation processes (AOPs) generate very reactive oxidants, especially hydroxyl radicals (•OH), in amounts high enough to oxidize organic pollutants in water (Glaze, Kang, and Chapin 1987; O'Shea and Dionysiou 2012). Because •OH and related radicals react quickly and with low selectivity, they attack dye chromophores and other organics, leading to rapid decolorization and, depending on the wastewater matrix and the operating conditions, partial or extensive mineralization (Miklos et al. 2018; Y. Zhang et al. 2021). In textile

wastewater treatment, the main AOP families are UV/H_2O_2, ozone-based AOPs, Fenton and photo-Fenton systems, heterogeneous photocatalysis with semiconductors such as TiO_2 or ZnO under UV or sunlight, and electrochemical AOPs (EAOPs) such as anodic oxidation and electro-Fenton (Y. Zhang et al. 2021; Bilińska, Gmurek, and Ledakowicz 2017; Rodríguez-Narváez et al. 2021).

Photocatalytic oxidation usually follows four steps: (1) the semiconductor is excited by UV or solar photons, (2) electron–hole pairs formation, (3) hydroxyl radicals are generated from water or hydroxide at the catalyst surface, and (4) organic pollutants are oxidized, potentially to CO_2 and H_2O if the reaction goes to completion. This sequence is the standard mechanistic view for TiO_2 and ZnO in dye removal (Miklos et al. 2018; Y. Zhang et al. 2021). A simplified scheme for ZnO is:

1. $ZnO + h\nu\ (UV) \rightarrow ZnO\ (e_{CB}^- + h_{VB}^+)$
2. $ZNO(h_{VB}^+) + H_2O \rightarrow H^+ + \bullet OH$
3. $ZNO(h_{VB}^+) + OH^- \rightarrow ZnO + \bullet OH$
4. $\bullet OH$ + dye → oxidation products → ($CO_2 + H_2O$, if mineralization is complete)

Key advantages include fast degradation for many dye structures, the option for solar-driven operation in photocatalysis and photo-Fenton, and easy pairing with biological or membrane steps to reach cleaned reuse-grade effluent (Oller, Malato, and Sánchez-Pérez 2011; Bilińska, Gmurek, and Ledakowicz 2017). Performance depends strongly on wastewater composition and process variables such as initial dye level, oxidant and catalyst dose, pH, light intensity, irradiation time, and background salts and auxiliaries typical of dye-house effluents (Y. Zhang et al. 2021; Bilińska, Gmurek, and Ledakowicz 2017). Energy and cost can be limiting factors because of chemical inputs and electricity demand. Comparative reviews highlight electrical energy per order and overall operating cost as key metrics, and show that integrated treatment placing AOPs before or after biological treatment often lower costs while improving biodegradability and polishing residual intermediates(Mousset et al. 2021; Oller, Malato, and Sánchez-Pérez 2011).

1.4 Biological degradation methods of dyes removal

Biological treatment is widely applied to dye-containing wastewater because it lowers color and organic load with relatively low chemical use and fits into standard wastewater plants.

Performance depends strongly on reactor design and presence of stages with different redox conditions, since many synthetic dyes, especially azo dyes, do not fully break down under a single set of conditions. Practical systems include aerobic activated sludge and sequencing batch reactors; anaerobic units such as UASB (Upflow Anaerobic Sludge Blanket) and anaerobic biofilm reactors; and sequential anaerobic followed by aerobic stages that pair rapid decolorization with subsequent oxidation of reduced intermediates (S. Zafar, Bukhari, and Rehman 2022; Aragaw 2024a). Biofilm-based technologies (moving bed biofilm reactors, packed-bed or other attached-growth media, and granular sludge) are increasingly used because biofilms improve tolerance to shock loads, salinity, and inhibitory compounds common in dye-industries effluents, while retaining slow growing degraders and enabling higher effective biomass concentrations (Murshid et al. 2023; Aragaw 2024a).

From last one decade, the literature shows a clear shift from single-step batch tests toward integrated treatment that explicitly aim to (i) accelerate decolorization, (ii) manage toxic intermediates, and (iii) improve robustness under real wastewater variability (salinity, pH swings, auxiliary chemicals) (Tripathi, Singh, Pathak, et al. 2023; Balachandran and Sabumon 2025). In parallel, advanced biological reactors or configurations such as immobilized-cell reactors and hybrid systems including (biological and electrochemical cells) have become more prominent as routes to improve treatment process stability and cleaned effluent quality (Rane and Joshi 2021; Tripathi, Singh, Pathak, et al. 2023; Moyo, Makhanya, and Zwane 2022). Parallel to this reactor evolution, biological research of dye-loaded effluents treatment has expanded from single isolates toward microbial consortia and engineered communities, supported by “omics” tools (metagenomics/transcriptomics) to link community function and enzyme potential to measurable treatment outcomes (Murshid et al. 2023).

1.4.1 Biological technologies and reactor systems used for dye treatment

Suspended-growth systems and modified activated sludge.

Technology based on the conventional activated sludge is still the main biological process used at wastewater treatment, yet dye-industry wastewater often stresses it because pH can vary, salinity can be high, many dyes are toxic, and competing electron acceptors can disrupt metabolism. As a result, many studies aim to improve robustness of this technology through bioaugmentation with dye-degrading microbes, selective enrichment of resilient communities, or staged operation that separates key redox steps. Long-term monitoring at full-scale plants

has linked better process quality and more stable sludge properties to measurable shifts in functional genes and in the structure of the microbial community. This evidence base shows a clear movement toward mechanistic understanding in real facilities, rather than reliance on short lab batch tests alone (Santhanarajan et al. 2021; Aragaw 2024a).

Biofilm and attached growth reactors

Biofilm-based treatment has expanded because biofilm's structure provides the microorganisms growth stability in this also helps stabilize slow-growing degraders, increases biomass retention, buffers shock loads, and creates oxygen and redox gradients inside the biofilm that support complex dye transformation. Recent studies report advances in biofilm carrier materials, including low-cost and waste-derived supports, along with progress in kinetics studies, reactor configurations, and economic assessment that points to scalable designs (Murshid et al. 2023; Morgan-Sagastume 2018). Membrane-aerated biofilm systems and hybrid membrane-aerated biofilm reactors deliver oxygen through a membrane directly to the biofilm. This approach can lower aeration losses and provide a controlled oxygen flux. It stabilizes biofilms, improves resilience, and enables tighter control of redox conditions. Although many applications target nutrient removal, the same principles of controlled oxidant delivery and stable attached growth are increasingly relevant for complex industrial wastewaters where oxygen sensitivity and redox staging control contaminant fate (H. He et al. 2021; 2025; Nerenberg 2016).

Moving bed biofilm reactors provide a high protected surface area on mobile carriers under continuous mixing, which supports strong mass transfer and stable operation under variable loading. The material and surface chemistry of the carriers strongly influence biofilm development, activity, and detachment. Purposeful carrier engineering has therefore become a major lever for improving reactor function and robustness (Morgan-Sagastume 2018; Bassin et al. 2016).

Fixed-bed and packed-bed biofilm reactors retain biomass on porous media and can couple phase transfer with biodegradation when high-surface-area carbonaceous supports are used. Initial adsorption can concentrate dyes and intermediates near active biomass and extend contact time, while ongoing biodegradation regenerates sorption capacity during operation (Mohanty and Kumar 2021; Cherif et al. 2024) For azo dyes, attached-growth reactors are commonly placed in sequential anaerobic followed by aerobic treatment. Anaerobic stages

favor rapid reductive cleavage of the azo bond and achieve decolorization. The subsequent aerobic units promote oxidative transformation and mineralization of aromatic intermediates and remove remaining oxygen demand. This staged logic is emphasized in recent reviews of integrated processing for textile wastewaters and is supported by demonstrations that combine anaerobic conversion with aerobic biofilm post-treatment to improve removal of aromatic amine by-products (Bogale, Teffera, and Aragaw 2024; Cui et al. 2019; Kong et al. 2022; Hosseini Koupaie, Alavi Moghaddam, and Hashemi 2011).

Immobilized-cell and immobilized-enzyme systems.

Immobilization has become a major development pathway because it can (i) reduce biomass washout, (ii) protect cells or enzymes from dye toxicity, (iii) increase operational stability and reusability, and (iv) couple adsorption with biodegradation when the carrier has sorptive capacity. Continuous packed-bed operation with immobilized consortia on carbonaceous supports (e.g. biochar) has been repeatedly proposed as a route to improve performance compared with batch operation, and newer reviews evaluate immobilization as a tool for strengthening reproducibility and industrial relevance (Mohanty and Kumar 2021; Saha and Rao 2020)

Staged anaerobic-aerobic biological process

For azo dyes in particular, staged systems remain foundational because anaerobic reduction can cleave azo bonds efficiently but may yield aromatic amines that require an aerobic post treatment step for further oxidation and detoxification. Modern analyses emphasize that single-stage treatment often fails to achieve complete detoxification, and that the number of stages and reactor type can significantly affect outcomes in complex reactive azo dye mixtures. This staged logic has become increasingly considered in textile-focused evaluations of biological treatment design (Aragaw et al. 2024; Azimi, Abdollahzadeh-Sharghi, and Bonakdarpour 2021)

1.4.2 Microbial groups used in biological dye decolorization technologies

Biological dye removal relies on diverse organisms, and the past decade has shown increasing emphasis on selecting organisms not only for color removal but for verified biodegradation capacity under wastewater-relevant stress conditions.

Fungi (including white-rot fungi) and fungal enzymes.

Decolorization by yeasts and fungi generally proceeds through lignin modifying enzymes such as laccases, manganese peroxidases, lignin peroxidases and polyphenol oxidases to transform and mineralize the synthetic dyes using molecular oxygen as electron acceptors. White-rot fungi (e.g., *Trametes*, *Phanerochaete*) secrete laccases, manganese peroxidase, and lignin peroxidase, enabling broad oxidation and decolorization across many dye classes; enzyme immobilization further improves process stability (Costa et al. 2025; Nagraj et al. 2025; Rajhans et al. 2021). However, fungal systems may require longer growth phases and specific nutrients and conditions, which can complicate continuous treatment. But Yeasts (e.g., *Candida*, *Trichosporon*) are gaining attention for faster growth and tolerance, though their dye-degrading breadth is typically narrower than filamentous fungi (Herath et al. 2024; Muniyasamy et al. 2020). At the same time, practical work has increasingly examined fungal enzyme immobilization and hybrid adsorption–biocatalysis concepts to address scale-up barriers (Costa et al. 2025; Nagraj et al. 2025; Rajhans et al. 2021)

Microalgae and bacterial–microalgal consortia

Algae have been studied to remove color through biosorption and enzymatic dye degradation. Micro- and macroalgae remove dyes via biosorption onto cell walls rich in functional groups and, for some taxa, enzymatic transformation. They are attractive in saline and variable effluent because of tolerance level. In general, they require no added organic carbon, lowering operating cost. Performance depends strongly on dye chemistry, pH, biomass concentration, and temperature; recent reviews document effective removal by *Chlorella*, *Oscillatoria*, and seaweeds, and highlight algae derived materials (e.g., biochar) as sorbents (Gayathiri et al. 2022; Suresh et al. 2024). Microalgae-based dye removal is often positioned around coupled pollutant removal and oxygen generation; however, recent literature increasingly frames algae in consortia, where bacteria provide complementary catabolic potential, and algae contribute oxygen release and nutrient uptake, improving stability under variable wastewater conditions (R. K. Rathour et al. 2024)

Actinomycetes

Actinobacteria (*Actinomycetes*) are Gram-positive bacteria that are ubiquitous in soil and other habitats. They are valued in environmental biotechnology for metabolic diversity, production of extracellular enzymes and bioactive metabolites, and tolerance to harsh conditions relevant

to textile effluents, including variable pH, salinity, and inhibitory organics (El Awady et al. 2024). These traits make them attractive and stable biocatalysts for dye treatment. In dye-removal systems, actinobacteria act through multiple mechanisms: (i) enzymatic biotransformation and biodegradation by oxidoreductases such as peroxidases that attack aromatic structures and disrupt chromophores (Adenan, Lim, and Ting 2022); (ii) reductive pathways that initiate azo-bond cleavage when suitable redox conditions and electron donors are present (Takkar et al. 2022); (iii) and biosorption or bioaccumulation driven by filamentous biomass and extracellular polymers (Adenan, Lim, and Ting 2022; Wei et al. 2015).

Within *Actinobacteria*, *Streptomyces* genera are especially prominent. Many strains secrete extracellular oxidoreductases and have confirmed ability for repeated decolorization and transformation of azo dyes under defined conditions. Recent mechanistic work with *Streptomyces albidoflavus* demonstrated effective decolorization and biodegradation of several applied textile azo dyes, emphasizing mechanism rather than color removal as the only endpoint. Broader literature reports show wide dye spectra for *Streptomyces* spp. and enzyme-linked transformation, including EB-focused studies that cite *Streptomyces* strains capable of decolorizing azo orange within 48 h and *Streptomyces pactum* decolorizing methyl red, Navy-Blue HER, Reactive Magenta HB, and Orange 3R, with oxidative biodegradation attributed to lignin-peroxidase-type activities. Enzyme based studies further support the role of actinobacterial peroxidases in hazardous azo-dye decolorization, highlighting extracellular oxidoreductases as key catalytic levers (El Awady et al. 2024).

From an engineering perspective, immobilization on solid carriers such as porous media, packed bed supports, sponges or foams, gels, and carbonaceous materials is widely used to translate actinomycete potential into robust reactor performance. Carriers increase biomass retention, improve resistance to inhibitory dye loads, stabilize activity during hydraulic and operational fluctuations, enhance dye–biocatalyst contact through high surface area and local concentration effects. Because carriers and filamentous biomass can also sorb dyes, rigorous designs include adsorption blanks and controls to separate adsorption-driven color loss from verified biodegradation (Harish et al. 2023; Kurade et al. 2019).

Bacteria

Bacteria are the most frequently applied biological agents for textile dye removal because they combine rapid growth, broad metabolic diversity, and the ability to operate under both aerobic and oxygen-limited conditions that are commonly met in engineered reactors and real

effluents. However, the recent studies emphasizes that dye removal by bacteria must be interpreted carefully: apparent decolorization can reflect true biotransformation, but it can also reflect partial chromophore disruption, adsorption to biomass/support matrices, or transformation to colorless yet potentially toxic intermediates, especially for azo dyes (Aragaw, 2024) (Veluchamy et al. 2024; Aragaw 2024a).

Pure bacterial cultures: strengths and limitations

Pure cultures are widely used to build mechanistic understanding of synthetic dyes removal under controlled conditions. They can help to establish a link between dye removal to specific enzymes, propose pathways, test electron-donor needs, and assess responses to pH, salinity, dye concentration and temperature. The main advantage is interpretability, since binding performance to defined physiology is easier than in the case of mixed community effects. The main limitation is poor robustness in real textile wastewater: single isolates often underperform or destabilize under alkalinity, salinity, auxiliary chemicals, variable COD, and competing electron acceptors (H. hong Li et al. 2019). A pure isolate may work for one dye but often fails with mixtures of dye classes and other wastewater chemicals, which limits practicality for real effluents (Balapure, Bhatt, and Madamwar 2015). Using a single isolation also facilitates detailed pathway resolution. Molecular biology tools provide genetic information to guide regulation of enzyme systems and to modify strains to enhance enzyme activity. In parallel, rigorous quantitative and qualitative analysis of biodegradation kinetics is essential to characterize the biochemical steps of dye removal (Saratale et al. 2011). Consequently, identifying single isolates through physiological, biochemical, and molecular approaches is important for studying intrinsic biological reactions, although in the term of dyes removal this strategy is less effective for most persistent pollutants. Metabolic pathways of single dyes in single cultures can be clarified using FT-IR, GC–MS, HPLC, liquid chromatography–mass spectrometry (LCMS) and nuclear magnetic resonance (NMR) (Aragaw 2024a).

Table 1–4 summarizes bacterial strains that have been reported to decolorize and remove textile dyes under aerobic, anaerobic, and low-oxygen conditions. Many single-strain studies achieve high color removal, but the time needed to reach maximum decolorization differs greatly depending on oxygen conditions, dye type, and the initial dye concentration. The table shows two practical trends: first, many effective bacteria were isolated from wastewater, sludge, or contaminated soils, which suggests these environments promote dye-tolerant

microbes; and second, color removal can result from both real dye transformation and dye binding to biomass, so the most reliable studies support UV–Vis decolorization with COD changes or additional chemical evidence of degradation. Overall, Table 1–4 emphasizes that bacterial dye treatment should be interpreted using verified mechanisms and optimized operating conditions, rather than using color loss alone as proof of effective treatment.

Table 1-4 : Summarizes representative single-strain and selected mixed-isolate studies for textile dye biodecolorization and biodegradation, adapted from Aragaw (2024) with recent single-strain updates included to reflect current literature (Aragaw 2024a)

No.	Microorganism (type)	Dye(s)	Time to max (h)	Condition	Dye conc. (mg/L)	pH, T (°C)	Color removal (%)	Reference
1	*Acinetobacter baumannii*	RB5, RR120, RB171	12	Aerobic	100	8, 30	98=RB5 96=RR120 96.2=RB19	(Ameenudeen, Unnikrishnan, and Ramalingam 2021)
2	*Bacillus cohnni*	Congo red	48	Anaerobic and aerobic	100	7.2, 32	93	
3	*Bacillus albus*	Methylene Blue	6	Aerobic	100	7, 30	99.27	(Kishor et al. 2021)
4	*Klebsiella pneumoniae*	disperse blue-284	24	Anaerobic and aerobic	200	7, 37	95	(Mustafa et al. 2021)
5	*Pseudomonas stutzeri*	Procion Red	20	Microaerophilic	50	8, 32	98	(Bera and Tank 2021)
6	*Klebsiella variicola*	Acid Blue 113	72	Anaerobic	100	8, 35	93.43	(P. K. Singh et al. 2021)
7	*Acinetobacter baumannii*	Reactive Blue 221; Reactive Black 5	48	Aerobic	500	9, 45	90 (RB221); 87 (RB5)	(Sreedharan, Saha, and Rao 2021)
8	Isolates	Seven dyes	216	Anaerobic	50 µL dye/100 mL	7, 30	73.73–92	(Mohamad Hanapi et al. 2022)
9	Isolates	Mixture of azo dyes	96	—	200	—	55.9±3.1 to 87.6±3.1	(Thiruppathi et al. 2021)
10	*Halomonas* sp.	Reactive Red 184	96	Anaerobic/anoxic	150	10.4, 25	98	(Guadie, Gessesse, and Xia 2018)
11	*Acinetobacter baumannii*	Reactive Blue 224	24	Aerobic	100	6, 37	91	(Ullah et al. 2024)

12	*Pseudomonas aeruginosa* MT-2	Congo Red	48	Static (low oxygen)	150	8, 35	94.0	(Tripathi et al. 2024)

Abbreviations used in the tabel: RB5 = Reactive Black 5; RR120 = Reactive Red 120; RB171 = Reactive Blue 171

Mixed cultures and consortia

The toxicity of dyes and their transformation products, including aromatic amines and phenolic compounds, can differ depending on whether degradation is carried out by a single microorganism or by a mixed microbial community. Mixed communities provide greater metabolic diversity, synergistic degradation, multiple detoxification mechanisms, and better environmental adaptability. They comprise distinct microbial groups with complementary pathways and enzyme sets, enabling cleavage of a wider range of chemical bonds in toxic compounds. In contrast, a single microorganism may lack key enzymes required to break specific bonds, limiting degradation and detoxification (R. K. Rathour et al. 2024). A single microorganism might partially degrade dyes and their transformed chemicals into less toxic compounds, subsequently other microorganisms can further metabolize it, thereby their cooperation can reduce the overall toxicity of the chemicals (Das, Cherwoo, and Singh 2023).

Using microbial consortia from environmental samples for dye biodegradation in colored wastewater improves efficiency. Community members can protect each other, better tolerate harsh conditions, and reduce costs associated with isolating and maintaining pure cultures. Sequential biodegradation steps may also require complementary enzymes that are stabilized or protected by different microorganisms within the consortium (Ajaz, Shakeel, and Rehman 2019). Consortia have achieved strong color removal and COD reduction in real textile effluents characterized by high color (1679–1990 Hazen), high COD (1720–2170 mg/L), broad temperature ranges (30–55 °C), and variable pH (7–11).

Consortia-based biodegradation has limitations as well, for mechanistic analysis because multiple extracellular enzymes act simultaneously, making pathways difficult to reconstruct. Aerobic metabolism of some dyes is constrained, whereas under anaerobic conditions several bacterial species act as electron acceptors and, via azoreductases, cleave azo bonds to yield colorless aromatic amines. Integrating anaerobic and aerobic stages enables cooperative removal of these toxic intermediates, aligning oxygen requirements of aerobes and anaerobes to improve overall detoxification (Jamee and Siddique 2019; Bogale, Teffera, and Aragaw 2024).

In biological treatment systems, consortia can also use additional carbon and nutrient sources, which supports resilience and sustained activity. Integrated reactors operated at an optimal hydraulic retention time achieve high color removal and significant reductions in COD and TKN (*Toal Kjeldahl Nitrogen*), demonstrating the performance benefits of staged redox treatment with mixed communities (Aragaw 2024a; Bogale, Teffera, and Aragaw 2024). This is directly relevant for mechanism-focused studies, also in the case of consortia created in biofilms, since biofilms can couple adsorption, enzymatic reduction, and subsequent aerobic metabolism within a single structured matrix. They are also compatible with engineered carrier materials and reactor strengthening strategies that are highlighted in recent reviews, enabling practical integration of mechanism and performance in advanced dye-treatment configurations.

1.5 Mechanisms of azo dye decolorization and removal in biological systems

In biological treatment of azo dyes, the visually dominant endpoint is the loss of color that can arise from fundamentally different processes (reversible reduction, partial chromophore disruption, or true chemical transformation). For this reason, recent dye-removal studies emphasize that UV–Vis decolorization alone is an incomplete endpoint and should be supported by mechanistic controls and chemical transformation evidence (e.g., parent-dye disappearance confirmation by chromatography and metabolite/toxicity assessment) when claims extend to “degradation” or “detoxification.”

1.5.1 Biotransformation enzyme-driven conversion

Biotransformation is an enzyme-driven change to dye molecules that can remove color quickly, but it does not by itself ensure detoxification or full mineralization. For many azo dyes, the first step is reductive cleavage of the azo bond (–N=N–) catalyzed by azoreductases and related reductases. These enzymes use intracellular electron carriers such as NADH or NADPH and often operate with flavin cofactors. Recent studies show that this enzyme class depends strongly on cofactor supply and on the presence of a suitable electron donor, which together control reaction rates. This explains why reductive decolorization is highly sensitive to operating conditions (Aragaw 2024b; Veluchamy et al. 2024). A common outcome is the formation of aromatic amines and other reduced products, so the loss of color can occur at the same time as the appearance of compounds that may persist and may be toxic. Current research

therefore treats the formation of aromatic amines and their post-treatment leads to their disappearance as central issues in azo-dye biotransformation (Balachandran and Sabumon 2025).

1.5.2 Biodegradation, detoxification and mineralization

Biodegradation means further metabolic breakdown beyond the initial color loss step. The dye and its reduced intermediates are converted into smaller molecules that can enter main metabolism and can be mineralized. For azo dyes, recent reports describe a practical sequence: first, reductive decolorization under low-oxygen or low-redox conditions; second, oxidative conversion of aromatic amines and other intermediates, which usually requires an aerobic or otherwise oxidative phase. This reductive → oxidative order is emphasized because the conditions that maximize azo-bond reduction do not necessarily support efficient removal of aromatic amines (Jayapal et al. 2018; Balachandran and Sabumon 2025; Aragaw et al. 2024). Accordingly, recent reports argue that strong confirmation of biodegradation should include apart of results of UV–Vis measurement at least one more line of evidence, most often chromatographic tracking of the parent dye or identification of transformation products, since biodegradation is a chemical-fate claim rather than a color claim (Carrascal-Hernández et al. 2025; Jasińska, Walaszczyk, and Paraszkiewicz 2024). A further trend is growing use of omics and systems-level tools, including genomics, transcriptomics, proteomics, and metabolomics, to support pathway assignments and to identify enzymes and stress responses that govern dye conversion in bacteria and consortia. Omics-focused reviews show that these approaches reduce reliance on UV–Vis alone and enable more rational selection of organisms and operating conditions for reproducible biodegradation processes (Jasińska, Walaszczyk, and Paraszkiewicz 2024).

1.5.3 Biosorption and bioaccumulation

Biosorption is the physicochemical binding of dye molecules to biomass, including cell walls, functional groups, and extracellular polymeric substances (EPS). Also, they participate in biofilm creation, as well as supporting materials within biofilms. It can contribute substantially to apparent removal, particularly for ionic dyes, and it is often rapid. However, the biosorption does not prove that dye is chemical transformed or detoxified, and this biosorption can be reversible, which may shift the environmental burden to sludge or biomass unless its final treatment is managed. Recent studies of microbial and biofilm-based remediation distinguish

biosorption from enzymatic conversion and highlight EPS as a key mediator of dye binding and apparent decolorization in biofilm systems (Tripathi, Singh, Singh, et al. 2023; Oliveira et al. 2024).

Biosorption is not undesirable, recent mechanistic work describes it as helpful, and sometimes the first step that concentrates dyes in the biofilm matrix and increases contact between dye molecules and enzymes, which supports later reduction or oxidation. This coupling is especially relevant in immobilized or biofilm reactors. It also reinforces the need for adsorption blanks and desorption checks when interpreting color loss (Oliveira et al. 2024).

1.6 Factors affecting biological biodegradation performance

The dye biodegradation process is highly sensitive to environmental and operational factors, including reaction temperature, pH, oxygenation, mixing, hydraulic retention time, dye concentration, dye type, the quantity and quality of nitrogen and carbon sources (Aragaw 2024a). These variables influence metabolic processes across operating ranges. Accordingly, the geographical location of treatment plants, optimized process configuration, reaction conditions, selected bioreactor type, and the specific wastewater matrix are critical design considerations for efficient dye degradation. Reports show that biological treatment of textile wastewater is strongly affected by reaction conditions because of the nature of the pollutants to be degraded, including the need for aerobic or anaerobic phases and the effects of dye concentration and molecular structure (Kapoor et al. 2021).

1.6.1 Oxygen regime and redox staging

Azo reduction is typically favored under low redox/anaerobic conditions, while aerobic phases support further oxidation of aromatic intermediates. Hence, oxygen control determines whether systems stop decolorization or proceed toward detoxification. The current consensus across textile-focused evaluations is that integrated anaerobic–aerobic configurations are often necessary for complete degradation treatments, especially for recalcitrant reactive azo dyes and complex real wastewaters (Azimi, Abdollahzadeh-Sharghi, and Bonakdarpour 2021; Aragaw et al. 2024).

1.6.2 Electron-donor availability and co-substrates

Because reductive azo cleavage requires reducing equivalents, carbon source type and concentration strongly control rates and completeness, particularly in bacterial systems.

Azoreductase based analyses emphasizes on the practical limitation, that sustained electron-donor supply is often necessary, and that donor limitation or competition from alternative electron sinks (acceptors) reduces dye conversion efficiency (Veluchamy et al. 2024; Aragaw 2024a).

1.6.3 pH and salinity

Many textile effluents are alkaline and saline, which can inhibit conventional microbial communities and alter dye solubility/ionic interactions. Recent reviews argue that incomplete dyes removal efficiency are due to this conditions mismatch and highlight alkaliphilic/halotolerant strategies and adaptive consortia as routes to improve the biocenosis robustness under realistic conditions (F. Tian et al. 2023; Aragaw 2024a).

1.6.4 Temperature and hydraulic retention conditions

Temperature governs enzymes activity, the enzymatic processes rates and microbial growth. Retention time and biomass retention determine whether slow transformation steps can proceed. They also determine whether the community remains stable during shock loads. In biofilm and immobilized systems, these controls are critical. Reviews of biofilm reactors show that carrier selection, temperature, hydrodynamics, and biomass retention are the main scale-up levers for industrial use (Saha and Rao 2020; Murshid et al. 2023; Mohanty and Kumar 2021).

1.6.5 Dye concentration, dye structure, and matrix composition

Initial dye concentration impacts both toxicity and electron demand. Higher loads place greater stress on cells and require more electrons for reduction. Dye class and chromophore also matter, since these features determine how easily the molecule can be reduced and how susceptible it is to enzyme attack. In real dye-industry effluents, surfactants, salts, and other auxiliaries are common. These additives can inhibit microbes, change membrane permeability, and divert electron flow away from the target dye. Recent studies repeatedly note that such matrix effects explain why “single-factor, single-dye” lab results often do not transfer to practice. This evidence supports the need for integrated treatment designs and for statistically defined operating windows that remain valid across varying dye types, concentrations, and wastewater compositions (Kusumlata et al. 2024; Periyasamy 2025).

1.7 Biological treatment pathways for azo dye wastewater

Operationally, biological dye treatment is implemented as aerobic, anaerobic, or sequential anaerobic-aerobic systems which are most effective and recommended for azo dyes

1.7.1 Aerobic treatment

Aerobic treatment generally shows weaker direct performance on intact azo dyes because oxygen competes for reducing equivalents and suppresses reductive cleavage of azo bond. However, it is essential for the second stage of the pathway: oxidative conversion of aromatic amines and downstream fragments produced after azo reduction. Recent reviews agree that aerobic phases supply the enzymes and oxidizing conditions needed to drive biodegradation toward smaller organics and better detoxification, even when aerobic systems alone do not initiate rapid decolorization of many azo structures (Bogale, Teffera, and Aragaw 2024; Carrascal-Hernández et al. 2025).

Operationally, aerobic treatment offers process stability, supports nitrification, organic post treatment, and fits well within conventional biological infrastructure. For azo dyes, it is most effective as post-treatment step rather than a single decolorization step for recalcitrant reactive or direct dyes (Bogale, Teffera, and Aragaw 2024). However, in recent study *Shewanella oneidensis* MR-1 has been investigated as an aerobic biocatalyst for azo dye decolorization (Methyl Orange and Amaranth), with studies reporting rapid color removal even at relatively high initial dye concentrations, on the order of 270 mg/L. Under fully aerated conditions, this behavior is notable because oxygen often suppresses reductive azo-bond cleavage by competing for cellular reducing equivalents (Y. Wang et al. 2025). The reported performance of *S. oneidensis* MR-1 is therefore commonly interpreted in the context of its versatile respiratory metabolism and strong extracellular electron transfer capability, which can support fast redox process and sustained dye transformation in even oxygenated systems. Collectively, these findings indicate that, for certain azo dyes and operating conditions, *S. oneidensis* MR-1 can maintain high decolorization rates in the presence of oxygen, making it a useful model organism for probing aerobic mechanisms of azo dye removal and for designing aerated biological treatment stages where color loss must be supported by chemical evidence of transformation.

1.7.2 Anaerobic treatment

Anaerobic or low-oxygen treatment is the most kinetically favorable biological route for rapid decolorization of azo dyes, since the azo chromophore (–N=N–) is efficiently reduced under

low redox conditions. Mechanistic reviews agree that many azo dyes act as electron-accepting substrates and that reductive enzymes, notably azoreductases and NADH–DCIP reductases, cleave the azo bond using intracellular reducing equivalents such as NADH or NADPH, often with flavin cofactors (Veluchamy et al. 2024; Carrascal-Hernández et al. 2025). This advantage is especially relevant for dye industries effluents matrices where oxygen transfer is limited and redox control is practical, so anaerobic reduction is widely treated as the first step for azo dye decolorization (Aragaw 2024b).

A critical limitation is that anaerobic decolorization often yields aromatic amines and other reduced intermediates, so color loss is not evidence of detoxification or complete treatment (Balachandran and Sabumon 2025). Current best practice includes chemical confirmation, for example chromatographic disappearance of the parent dye and identification of metabolites, and explicit evaluation of the fate of reduced intermediates rather than reliance on UV–Vis alone (Carrascal-Hernández et al. 2025; Jayapal et al. 2018).

1.7.3 Combined anaerobic/aerobic treatment

Combined anaerobic–aerobic treatment (sequential or integrated anoxic and oxic A/O) is widely regarded as the most defensible biological strategy for azo dye wastewaters (Figure 1.6). Anaerobic or micro-oxygen conditions drive azo-bond reduction and rapid decolorization, while aerobic conditions promote oxidation and biodegradation of aromatic intermediates, improving detoxification and the potential for COD and TOC reduction. Recent textile-wastewater reviews conclude that integrated A/O processes are more practical and effective for complex effluents than single-stage activated sludge, reporting high removal of color and organics when A/O designs are well configured (Bogale, Teffera, and Aragaw 2024). A representative example is a sequential anaerobic–aerobic reactor system for methyl red, where the authors tracked decolorization and aromatic amine by-products using HPLC, FTIR, and GC–MS, showed substantial removal of intermediates after the aerobic phase, and observed reduced biological toxicity (Jayapal et al. 2018). This evidence based approach aligns with systematic reviews that recommend pathway or product level confirmation when the goal is detoxification rather than just color decolorization (Carrascal-Hernández et al. 2025; Balachandran and Sabumon 2025).

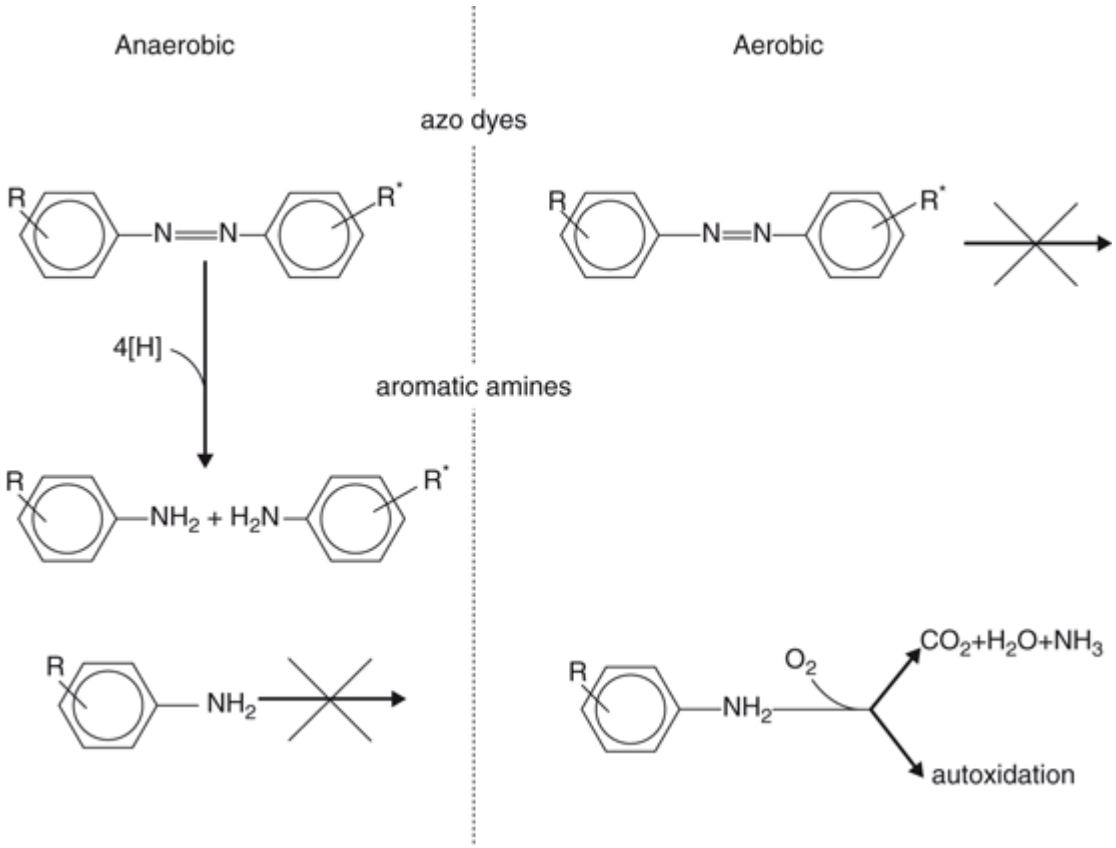

Figure 1.6 Schematic representation of (bacterial) decolorization and demineralization of azo dyes under anaerobic and aerobic conditions (Van Der Zee and Villaverde 2005).

1.8 Anaerobic/aerobic bioelectrochemical systems (BES) and microbial fuel cells (MFCs) for azo dye treatment

As mentioned previously azo dyes complete biodegradation in majority cases requires two stages different in condition (e.g. section 1.8). In anaerobic or micro-oxygen conditions, azo-bond reduction and rapid decolorization, while aerobic conditions promote oxidation and biodegradation of aromatic intermediates (A. Yadav et al. 2022). Bioelectrochemical systems, especially microbial fuel cells (MFCs), put this idea into practice by creating controlled redox environments. The anode operates without oxygen, while the cathode is oxygenated, which establishes separate zones for reduction and oxidation. Systems can also be arranged in sequence, with an anaerobic unit followed by an aerobic unit. MFCs offer two added benefits: they can recover a portion of energy as electrical current, and they provide mechanistic insight through electrochemical measurements and diagnostics (Murali et al. 2013; A. Yadav et al. 2022). In the dye–MFC approach, an electroactive biofilm on the anode oxidizes a co-substrate such as acetate or glucose and transfers the released electrons to the anode. Dye removal then occurs near the low-redox anode by direct reduction on the electrode or by indirect reduction

via redox mediators produced by the microbes. In coupled configurations, the MFC delivers a controlled reductive step, and an aerobic post-treatment oxidizes the reduced intermediates that form in the anode, improving detoxification and mineralization (Figure 1.7) (Danish Khan et al. 2015; Murali et al. 2013; Solanki, Subramanian, and Basu 2013a; Jalili et al. 2024). More detailed information and examples can be found in (Solanki, Subramanian, and Basu 2013b).

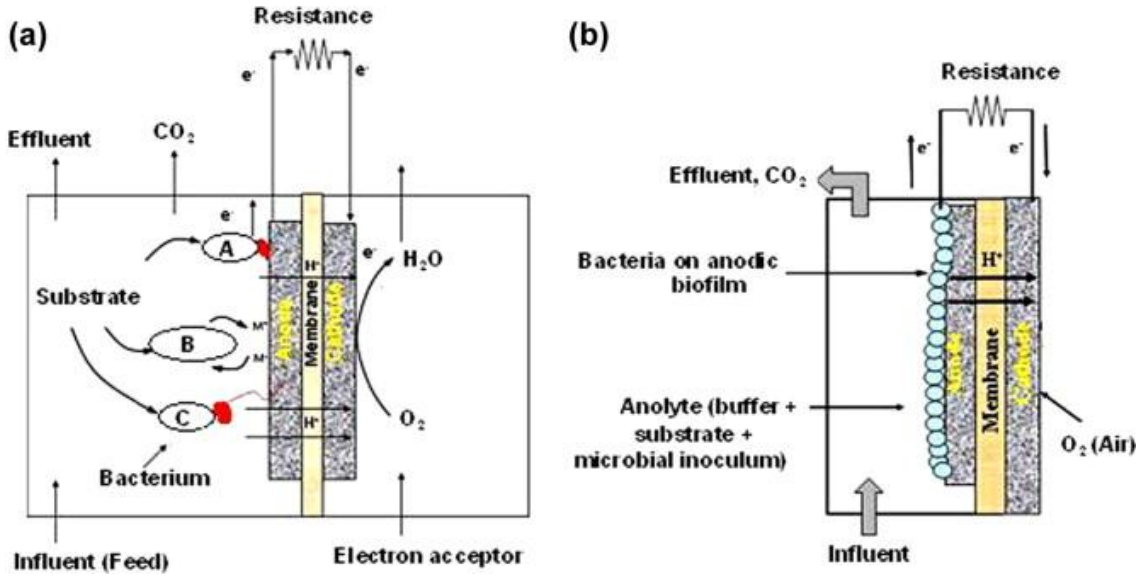

Figure 1.7 (a) Simplified view of a two-chamber microbial fuel cell (MFC) with possible modes of electron transfer , and (b) a single-chamber MFC with open air cathode (Solanki et al. 2013). Modes of electron transfer include (A) direct electron transfer (via outer bacteria membrane cytochromes), (B) electron transfer through mediators, and (C) electron transfer through nanowires (Solanki, Subramanian, and Basu 2013b).

1.8.1 Anaerobic reduction within the MFC (decolorization stage)

Many MFC studies report very high azo-dyes decolorization, reflecting the suitability of the low-redox bioanode for initiating azo-bond reduction. However, high decolorization does not guarantee mineralization, since reductive cleavage can generate aromatic intermediates that retain toxicity (A. Yadav et al. 2022; Danish Khan et al. 2015). A comprehensive review highlights this verification gap, despite frequent reports of approximately 96–100% decolorization, only a minority of studies assess mineralization (for example TOC removal) or characterize intermediates (A. Yadav et al. 2022), which is directly relevant to mechanism-focused claims in this dissertation.

1.8.2 Aerobic post-treatment coupled to MFCs (detoxification Stage)

Because anaerobic azo reduction can generate aromatic amines, many designs add an aerobic post-treatment step. A foundational example showed that an MFC with an aerobic biocathode further treated anaerobically decolorized azo-dye effluent, enabling additional oxidation while

producing electricity (J. Sun et al. 2011). Similarly, in another study was used a single-chamber MFC as the anaerobic and electrogenic stage, which followed by activated-sludge aerobic treatment, creating the transfer from anaerobic to aerobic treatment in which the second stage was targeted to transformation products and improved overall treatment beyond decolorization (Danish Khan et al. 2015). More recent integrated demonstrations extend this approach to mixed or real dye wastewaters, pairing an MFC stage with aerobic treatment to stabilize performance in complex matrices and to improve treated effluent quality (J. Sun et al. 2011).

Microbial fuel cells (MFCs) are well suited to anaerobic followed by aerobic dye treatment. They implement the established sequence of rapid anaerobic reduction and subsequent aerobic oxidation of aromatic intermediates, while adding three distinctive advantages. First, MFCs provide controllable and measurable electron-transfer function. Voltage and current, polarization curves, cyclic voltammetry, and electrochemical impedance can link biofilm development and charge-transfer limitations to dye removal, avoiding black-box interpretation (A. Yadav et al. 2022). Second, MFC architecture enables engineered redox control in the primary stage without intensive aeration, a major energy cost in conventional aerobic treatment. MFCs can therefore serve as lower-aeration front-end units, with aerobic post-treatment applied only as needed to remove intermediates (F. Zhang et al. 2013; A. Yadav et al. 2022). Third, bioelectrochemical systems (BES) offer a unique operational advantage over conventional bioreactors by directly using the microbe–electrode interface and extracellular electron transfer (EET). Unlike traditional systems that rely on chemical electron acceptors (e.g., oxygen, nitrate) in solution, BES utilize solid electrodes to either accept electrons from electroactive bacteria (anode) or donate electrons to them (cathode (Ndive et al. 2025).

Recent reviews note that performance can be constrained by slow biofilm start-up, weak adhesion, high internal resistance, and EET losses, which can decouple dye removal from electrochemical function and reduce electron recovery. These limitations motivate targeted strategies, including anode surface modification targeted for increasing biocompatibility, biofilm engineering, and optimization of external resistance and operating regimes, to increase treatment rate and stabilize power output (Ndive et al. 2025; A. Yadav et al. 2022).

1.9 Problem statement

Synthetic dyes are essential to textile wet processing and to leather, paper, printing inks, and plastics because they provide high color strength, reproducible shades, and strong dying

performance across different types of fibers. Even under controlled conditions, significant fractions of reactive dyes remain unfixed and enter wastewater, yielding colored effluent (Islam et al. 2025; Dutta et al. 2021; Aragaw 2024a) (Kalaivani et al. 2012; Ramamurthy et al. 2024). Azo dyes remain the dominant structural family in industry, leading to frequent environmental detection and a high likelihood of discharge via textile effluents (Islam et al. 2025; Ramamurthy et al. 2024).

1.9.1 Why colored effluents are environmentally and operationally problematic

The presence of dyes in water and causing its coloring is not just a matter of appearance. Even low dye concentrations can cause persistent and harmful contamination. Dyes can block sunlight, reduce water clarity, and limit photosynthesis and primary productivity.

Laboratory and field studies show that dyes can impair growth, development, and reproduction of aquatic organisms. They can also cause multi-organ injury through oxidative stress, depending on dye structure, concentration, and exposure time (Dutta et al. 2021). Textile dye industry is complex. It often contains very high COD or TOC, variable pH, elevated salinity, and mixtures of surfactants, dispersants, and auxiliary chemicals. Hydraulic loading also fluctuates. These factors lower the efficiency of conventional biological treatment and make it harder to select and control cost-effective processes for removal and degradation (Aragaw 2024a). At the same time, physicochemical treatment methods are expensive and do not always solve the problem definitively, generating, for example, further post-process waste. A critical concern for azo dyes removal is reductive cleavage under low-redox or biologically reducing conditions, the azo bond can cleave and form toxic aromatic amines and other intermediates that require further aerobic oxidation to reduce risk (Ravi et al. 2025). Such intermediates may persist and can be toxic. As a result, loss of visible color of water doesn't solve the problem, because it is not the same as detoxification or mineralization. Effective treatment must therefore achieve both color removal and verified chemical transformation, with explicit control of by-products.

1.9.2 Human-health and regulatory drivers

Toxicology-focused reviews link azo dyes and their transformation products to genotoxicity and broader environmental health risks, supporting precautionary management and robust treatment before effluents discharge (T. Li et al. 2025; Ramamurthy et al. 2024). In Europe, environmental protection and product-safety frameworks drive stricter control of hazardous

aromatic amines. REACH Annex XVII (Entry 43) restricts azo colorants that can release listed aromatic amines in certain textile and leather articles and is backed by standardized analytical testing and compliance requirements ("EU REACH Annex XVII Amended | Bureau Veritas CPS," n.d.; "SGS: New European Standard for Aromatic Amines Derived from Azo Colorants Released," n.d.). Industrial water emissions are further governed by the Water Framework Directive and by textile sector best available techniques guidance, which push for stronger wastewater control, monitoring, and higher performance of treatment and reuse (Castro et al. 2019). Compliance requires treatment that is demonstrably effective, reproducible, and aligned with discharge limits and risk reduction, not merely visually acceptable.

1.9.3 Limitations of current treatment approaches and why the problem persists

A broad range of physicochemical methods is used to remove dyes, including coagulation–flocculation, adsorption, advanced oxidation, and membrane filtration. As mentioned above, and also according to the recent reviews, the emphasize drawbacks of these methods are high use of chemicals, large volumes of sludge, high energy demand, incomplete mineralization, and elevated operating costs when complex and variable textile effluents are treated at full scale (Periyasamy 2024; Aragaw 2024a). Biological treatment is, in principle, more sustainable. Yet, high salinity, extreme pH, auxiliary chemicals, and the inherent resistance of many dyes often decrease the effectiveness of conventional activated sludge, which can lead to incomplete removal or unstable performance (Periyasamy 2024).

For azo dyes, the main mechanistic limitation is well established. Low-oxygen or low-redox conditions favor reduction of the azo bond and rapid loss of color, while oxygenated conditions are usually needed to oxidize and mineralize the aromatic amines that form. The literature therefore recommends integrated treatment that links an anaerobic step to a subsequent aerobic step as a practical route to detoxification (S. Zafar, Bukhari, and Rehman 2022). Successful implementation remains challenging because reaction rates and product fate depend on electron-donor supply, hydraulic regime, pH, temperature, and dye loading. This creates a clear need for process optimization and for verification of chemical transformation, not only observation of color loss.

1.9.4 Dissertation relevance and justification of the experimental strategy

There is a clear need for treatment research that links microbial selection, mechanistic verification, and process optimization, while also addressing bioelectrochemical limits on

biofilm formation and extracellular electron transfer (EET). A structured pathway is recommended: first, identify organisms or consortia that reliably transform dyes under controlled conditions; second, use statistically based optimization to define robust operating windows; third, test integrated systems that provide the right redox sequence, with anaerobic reduction followed by aerobic treatment, and track performance with analytical and electrochemical measurements.

1.10 Aim and Scope of the Study

The aim of the study was to use pure and mixed bacterial cultures in the development and integration of synthetic dye removal methods, with particular emphasis on the azo dye Evans Blue removal. This goal was achieved by employing methods combining mechanistic transparency, process condition optimization, bacterial community studies, and electrode engineering, which allowed for the confirmation of real dye degradation rather than just color loss. The detailed objectives of this thesis are:

1. The primary objectives of first stage of study: (i) Evaluation of the decolorization efficiency of selected dyes (EB, BG and CV) by isolated bacteria belonging to actinomycetes group and quantification of the effect of solid carriers on bacterial growth and process efficiency.
2. Define an RSM-based operating window for EB dye decolorization process by single pure strain *S. oneidensis* MR-1 (time, temperature, dye load, electrons donor) for optimisation of process. Determination of the products of biotransformation using UV–Vis/HPLC/GC–MS and explicitly assessing oxygen dependence to determine whether EB degradation can be achieved under aerobic conditions without prior anaerobic azo reduction.
3. In aim to further optimization the dye removal process, implementation of the anaerobic activated sludge as a mixed biocenosis, along with the implementation of a DCMFC anode system coupled with an aerobic stage. Performance of analyses of the dye decolorization and mineralization with GC-MS, EIS (Electrochemical Impedance Spectroscopy), and CV (Cyclic Voltammetry) as well as a metagenomic assessment of the microbial community structure in the system.
4. Evaluate Evans Blue (EB) removal by *Shewanella oneidensis* MR-1 under anaerobic bioelectrochemical conditions in a microbial fuel cell (MFC), with the aim of achieving the highest removal and mineralization without requiring an aerobic post-treatment stage.

In parallel, engineer the anode biointerface with their modifications (e.g., PANI-based with nutrient-cue/controlled-release concepts) to asses possibility of improving the surface biocompatibility and accelerate bacteria adhesion, lower Rct, and increase early-phase current/CSC as next step of optimization of process and improved EB removal rate and tolerance to higher dye load, supported by analytical confirmation beyond UV–Vis where applicable.

5. Integrate findings across pure-culture, mixed-community, and bioelectrochemical stages to establish an experimentaly proved, optimization-driven framework for EB removal that may be transferable to processes of removal of structurally similar sulfonated azo dyes in textile wastewater.

1.10.1 Based on the above-mentioned objectives, the following hypothesis was formulated in Dissertation roadmap and evidence strategy:

This dissertation is structured as a stepwise workflow that moves from basic biological feasibility to statistically optimized pure-culture treatment, to mixed-culture bioelectrochemical operation, and finally to interface engineering that removes the key bottlenecks observed in earlier stages. Throughout the dissertation, decolorization is treated as chromophore loss measured by UV to Vis spectroscopy, while further biochemical transformation (biotransformation or/and biodegradation) is confirmed by changes in chromatographic profiles using HPLC and by identification of transformation products using GC to MS. When a downstream aerobic unit is used, it is presented as aerobic post treatment leading to further oxidation of reduced intermediates formed during reductive azo bond cleavage, which is first indicated by the disappearance of the main UV to Vis peaks.

1. *Actinomycetes* are a group of bacteria with an enzymatic system dedicated to the biodegradation of structurally complex compounds. Screening studies conducted to obtain these microorganisms from samples rich in plant residues allow isolation of the pure strains with a high capacity to remove synthetic dyes. The biomass of selected strains immobilization on low-cost carriers will allow them to stabilize their growth, activity and will impact on increase of dye removal efficiency. The observed dyes removal results will show a main mechanism and will point out the possible participation of sorption by solid carriers and/or the true biodegradation (Section 3.1).

2. The use of a pure culture of electroactive bacteria *Shewanella oneidensis* MR-1 in the removal of a selected azo dye (EB) and the optimization of process conditions opens up prospects not only for increased bioprocess efficiency but also, in subsequent stages, allows for the evaluation of the feasibility of using this bacterium in integrated systems with current generation during the dye biodegradation process. Conducting the process under conditions of unlimited oxygen access will allow us to assess whether, in the case of *Shewanella oneidensis* MR-1, omitting the recommended oxygen deficit for initiating azo dye decomposition is justified. The use of response surface methodology (RSM) will allow us to define a statistically justified operating window for selected process parameters. UV-Vis spectrophotometric analyses will allow us to track the decolorization kinetics, while monitoring the process products using HPLC, GC, and MS will confirm complete dye decomposition and assess the environmental safety of the process. The main effects and interactions will form the basis for subsequent experiments (Section 3.2).

3. Using a pure culture of the electroactive bacterium *Shewanella oneidensis* MR-1 to remove a selected azo dye (Evans Blue, EB), together with optimization of operating conditions, creates an opportunity to improve bioprocess efficiency. It also prepares the next stages of the work, where the feasibility of using this bacterium in integrated systems will be evaluated, including electricity generation during dye biodegradation. Operating the process under aerobic conditions will evaluate, if *S. oneidensis* MR-1, can reasonably omit oxygen-limited conditions that are usually applied to initiate azo dye breakdown. UV-Vis spectrophotometry, GC-MS, and electrochemical diagnostics will allow us to assess the treatment effectiveness, linking the level of biofilm development and charge transfer behavior within the biofilm to dye removal rate. Microbial community profiling, such as 16S rRNA sequencing, illumina sequencing, and microscopy, will allow interpretation of the composition and functioning of the biofilm in the reactor (Section 3.3).

4. The use of the exoelectrogenic bacterium *Shewanella oneidensis* MR-1 in a bioelectrochemical system, such as a microbial fuel cell (MFC), without the oxygen post-treatment stage will allow us to assess whether full biodegradation of the dye is possible under purely anaerobic conditions. Modifications of the anode surface will improve its biocompatibility, accelerate bacterial adhesion and the formation of an active biofilm, reduce the Rct, and increase the early phase current/CSC, which will be the next step in process optimization and improve the removal rate of various EB dye concentrations. UV-visible

analyses, as well as other methods beyond this method, will provide process monitoring. Anode surface characterization and chemical composition methods, including cyclic voltammetry during electropolymerization, FTIR, and SEM with XPS, will be used. It is assumed that reducing interfacial resistance and faster early biofilm formation will increase the rate of EB removal and mineralization without the need for an oxygen-based post-treatment step. This research plan will allow for improved interface performance and increased operational stability, especially at higher initial dye loads. (Section 3.4).

5. Integration of the results of different experiments covering the stages of pure culture, mixed community and bioelectrochemistry can provide input data for improving the efficiency of the technology for removing structurally similar sulfonated azo dyes from textile wastewater.

Chapter 2

2 Materials and Methods

2.1 Chemicals and Reagents

All chemicals used in this study were of analytical grade and were used in accordance with occupational health and safety regulations.

2.1.1 Dyes

The primary model dye investigated throughout this dissertation was Evans Blue (EB; Direct Blue 53; CI 23860,) purchased from (Sigma-Aldrich). Additional dyes used in selected experiments included Brilliant Green (BG) (Sigma-Aldrich) and Crystal Violet (CrV) (Sigma-Aldrich). Stock dye solutions were prepared in sterile deionized water. Dye solutions were filter-sterilized with syringe filters (0.22 μm PES) and stored in the dark at 4 ^{o}C.

2.1.2 Microbiological growth media, buffers, and nutrients

Microbiological and bioelectrochemical experiments employed different culture media and buffer systems according to the study objective and reactor configuration.

- **Pochon medium (solid and liquid)** was used for the isolation and screening of dye-degrading actinomycetes. The medium contained (per 1L): arginine (50 mg), soluble starch (2000 mg), and 50 ml of a standard salt solution (composition per 1L: K_2HPO_4 (5000 mg), $MgSO_4 \cdot 7H_2O$ (2500 mg), NaCl (2500 mg), $FeSO_4 \cdot 7H_2O$ (50 mg), and $MnSO_4 \cdot 5H_2O$ (50 mg); agar (15000 mg/L) was added for solid media. The pH was adjusted to 6.8–7.2.
- **Luria–Bertani (LB) broth/agar** was used for bacterial cultivation. LB medium contained (per 1 L): tryptone (1000 mg), yeast extract (5000 mg), and NaCl (10000 mg) and agar (15000 mg) for solid media.
- **Nutrient Medium** Used in Anodic, Cathodic and Aerobic Chamber (DCMFC) - the anode chamber was supplied with a medium containing acetate (1000 mg/L), and 50 mM phosphate buffer, supplemented with 10 mL/L vitamins and minerals (composition below). The cathode chamber received the same medium composition, except that $NaHCO_3$ (300 mg/L) replaced the acetate. $NaHCO_3$, in the cathodic chamber acts as support for bacterial growth and maintain pH. Aerobic- post treatment

chamber was supplemented with liquid Pochon medium for actinomycetes growth before receiving effluent from anodic chamber.

- **Mineral Salt Medium (MSM)** consisted of (per 1 L): $(NH_4)_2SO_4$ (1000 mg), K_2HPO_4 (6000 mg), KH_2PO_4 (1000 mg), $MgSO_4 \cdot 7H_2O$ (100 mg), and NaCl (5000 mg), with pH adjusted to 7.0.
- **Buffers and electrolytes.** A 50 mM phosphate buffer was used as the anodic electrolyte in microbial fuel cell (MFC) experiments. Phosphate-buffered saline (PBS, pH 7.2) was used for washing steps and for electrochemical measurements (cyclic voltammetry (CV) and electrochemical impedance spectrometry (EIS)) where specified.
- **Trace mineral solution (SL-10; stock, per 1 L):** $FeCl_2 \cdot 4H_2O$ (1500 mg), $ZnCl_2$ (70 mg), $MnCl_2 \cdot 4H_2O$ (100 mg), H_3BO_3 (6 mg), $CoCl_2 \cdot 6H_2O$ (190 mg), $CuCl_2 \cdot 2H_2O$ (2 mg), $NiCl_2 \cdot 6H_2O$ (24 mg), $Na_2MoO_4 \cdot 2H_2O$ (36 mg), and 25% (v/v) HCl (10 mL) to stabilize the solution and minimize precipitation. The mineral stock was stored at 4 °C and added as anolyte at the dosages specified in the respective experimental protocols.
- **Vitamin solution (Wolin-type stock, per 1 L):** biotin (2.0 mg), folic acid (2.0 mg), pyridoxine-HCl (10.0 mg), thiamine-HCl (5.0 mg), riboflavin (5.0 mg), nicotinic acid (5.0 mg), calcium D-pantothenate (5.0 mg), vitamin B_{12} (0.1 mg), p-aminobenzoic acid (5.0 mg), and α-lipoic acid (5.0 mg). The vitamin stock was filter-sterilized (0.22 µm), stored at 4 ºC in amber containers, and added aseptically at the dosages specified in the respective experimental protocols.
- **Carbon and electron donors.** Glucose, sodium lactate, and sodium acetate were used as carbon/electron donors depending on the experimental design. Glucose was applied at concentrations reported in the relevant subsections. Sodium acetate was used at 1 g/L and mentioned in respective sections. In selected runs, sodium bicarbonate (300 mg/L) was added to the cathodic compartment to provide buffering capacity and an inorganic carbon source. Sodium lactate with different concentrations were used and reported in its relevant experimental subsection.

2.1.3 Reagents and polymers used for electrochemical anode modification

For carbon cloth anode modification, aniline 99.5% (Sigma-Aldrich) was used as the monomer for polyaniline (PANI) electropolymerization in acidic sulfuric acid (H_2SO_4) media described in section (2.7.2). For carbon cloth electrodes pretreatment, the acetone and ethanol were used. For further post-polymerization surface modification the coatings from sterile solutions of glucose (10% w/v) and gelatin (10% w/v) prepared in deionized water were performed.

2.1.4 Analytical, microscopy and other reagents

Biofilm quantification employed crystal violet 1% w/v, methanol, and 33% acetic acid. For scanning electron microscopy (SEM), samples were fixed with 2% glutaraldehyde and dehydrated through a graded ethanol series (25–99%). Live/dead biofilm staining was performed using the SYTO9/propidium iodide fluorescent dye system (Sigma-Aldrich). For chromatographic analyses, methanol, acetonitrile, and NaH_2PO_4 (analytical grade) solutions were used as mobile phases and extraction solvents. Nitrogen gas was used to maintain anaerobic conditions in the MFC anode chambers as required.

2.2 Biological Materials

2.2.1 Pure and Mixed bacteria cultures

Actinomycetes strains were isolated from environmental sources, including rotten poplar wood, matured garden compost (SK) and compost from composting plant at different phases (K1 - phase 1compost; K2 - compost with activated sludge, and K3 - matured compost/phase 3). Details of isolation procedure in section 2.4.

A pure bacterial strain, *Shewanella oneidensis* MR-1 (LMG 19005; ATCC 700550; JCM 31522), was obtained from the Belgium Coordinated Collections of Microorganisms (BCCM), University of Gent, Belgium, and used for the pure-culture dye removal experiments and bioelectrochemical/biofilm studies (details in section 2.5 and 2.7).

For mixed-culture MFC studies (details in section 2.6), mixed anaerobic activated sludge (anode inoculum) and aerobic activated sludge (cathode inoculum) were collected from a municipal wastewater treatment plant in Gliwice, Poland. In addition, two actinomycetes strains (SK-2 and SK-3) isolated from matured garden compost were used for the aerobic post-treatment step.

2.2.2 Plant-derived solid carriersFor bacteria strain (actinomyces) immobilization a plant-derived solid carriers were used

1 Two kinds of deciduous wood shavings: oak [*Quercus robur* L.] and European beech [*Fagus sylvatica* L.], average shaving size app. with length 0.5-1.2 cm and width 0.3-0.6 cm were used

2 Two kinds of conifer wood shavings: pine [*Pinus sylvestris* L.] and Norway spruce [*Picea abies* L.], average shaving size app. with length 0.5-1.2 cm and width 0.3-0.6 cm were used.

3 Straw from common oat [*Avena sativa* L.]. – straw was cut into pieces with the size app. length 1.0-1.2 cm and width 0.4-0.5 cm.

2.3 Electrode Materials and Equipment

2.3.1 Reactor systems

Microbial fuel cell (MFC) reactors were constructed from plexiglass in two configurations:

1 A double-chamber microbial fuel cell (DCMFC): two-chambered plexiglass reactor equipped with a cation exchange membrane separator (CMI-7000, RisingSun Membrane, Beijing, China). The total volume was 120 and working volume was 100 ml for each chamber.

2 Single-chamber microbial fuel cell (SCMFC): plexiglass reactor with total volume 70 mL and working volume 50mL.

2.3.2 Electrodes and electrical components

As electrode different materials were used specified in the respective experimental protocols:

1 Carbon brush (CB) - carbon brush electrodes consisting of carbon fiber bristles wound on a titanium wire core, which were used in the double-chamber microbial fuel cell (DCMFC configuration (Mill-Rose, OH, USA) with size of 1 cm × 2 cm (diameter × length).

2 Carbon cloth (CC) - commercial carbon cloth (AC-1071HCB, AvCarb, USA; thickness 356 μm, Electrical Resistivity 1.1 x 10 ohm/cm), which was used predominantly in the single-chamber microbial fuel cell (SCMFC) configuration.

In SCMFC experiments, the air cathode comprised Pt-coated carbon cloth (sputter coated: 100nm layer of Pt) with a geometric area of 16 cm^2. For electrochemical measurements, an Ag/AgCl reference electrode (EDAQ, ET072) was used, and a Pt/Ti rod counter electrode (EDAQ, ET078) served as the counter electrode in selected experiments. Electrical connections to the external circuit were made using copper wire, with alligator clips used for secure wire-to-electrode and circuit connections. Discrete external resistors were applied as fixed loads, with specific resistance values provided in the relevant chapter protocols.

2.3.3 Analytical instruments

- UV–Vis spectrophotometer (Hitachi U-1900) was used for dye concentration and color removal analysis.
- Electrochemical impedance spectroscopy (EIS) and cyclic voltammetry (CV) were performed by using CH Instruments, Inc., type 660C, Austin, TX, USA, and PalmSens4 Potentiostat (Netherlands).
- Multichannel data acquisition (DAQ) voltage logger (PicoLog 1012, Pico Technology Ltd., St Neots, Cambridgeshire, United Kingdom).
- Quorum Q150R Plus Rotary Pumped Coater for Pt coated on carbon cloth
- Nexera lite HPLC system (Shimadzu)with PDA detector for dye and intermediate analysis.
- GC–MS (Agilent 7890B) for degradation product identification.
- FTIR spectrometer (PerkinElmer Spectrum Two) for surface chemistry analysis.
- SEM/EDS (Phenom ProX) for morphological characterization of electrode materials and biofilms.
- X-ray photoelectron spectroscopy was investigated with an AXIS SUPRA+ XPS spectrometer, with an Al K_α X-ray source, used for elemental analysis.
- Confocal laser scanning microscope (FV3000) for biofilm imaging.
- COBAS Microplate reader for biofilm quantification assays.

2.3.4 General laboratory equipment

Standard microbiological and analytical laboratory equipment was used throughout, including incubators (26–30 °C), autoclaves, centrifuges, syringe filters (0.22 µm PES), pipettes, glassware, and sterile consumables.

2.4 Screening, Isolation and Carrier-Assisted Dye Decolorization by Actinomycetes

The experiments for this section were conducted in two sequential stages: (i) screening, isolation and purification of actinomycetes strains from environmental sources and (ii) evaluation of possibility of dyes decolorization, first on solid culture medium (preliminary experiment) and subsequently in liquid culture medium with and without lignocellulosic carriers (main experiment).

2.4.1 Screening, Isolation and Purification of Actinomycetes

Sampling sources

Actinomycetes were isolated from rotten poplar wood (Populus nigra L.), matured garden compost (SK) and compost collected from a composting plant (Pszczyna, South Poland) at different composting stages: K1 (phase 1 compost), K2 (compost mixed with activated sludge), and K3 (matured compost; phase 3).

Material preparation

Compost samples were cleaned by removing extraneous materials (e.g., pebbles, twigs, leaves). All material dilutions were performed in sterile physiological saline (0,85% NaCl aqueous solution). For each source material, 5000 mg of sample was mixed with 45 mL physiological saline to obtain a 10^{-1} dilution, followed by serial dilution up to 10^{-6}.

Primary screening

A primary screening on solid Pochon medium was conducted to assess growth and qualitative dye decolorization by actinomycete isolates. Evans Blue (EB; azo dye) and two triphenylmethane dyes, (BG) and (CrV), were evaluated. Stock dye solutions were prepared in sterile deionized water at 1000 mg/L and added to molten sterile Pochon medium to obtain final dye concentrations of 50 mg/L and 100 mg/L. Dyed media were poured into Petri dishes and allowed to solidify before inoculation. Diluted suspensions were spread onto Petri dishes

dyed media and incubated at 26 °C. After 7 days of incubation, the plates were examined and colonies with discoloration zones around, were selected Discoloration zones indicated the decolorization potential of the strains. selected strains were isolated and subjected to a purification procedure.

Purification and maintenance of isolates

Morphologically distinct colonies were purified by repeated streaking (streak method) on fresh Pochon agar plates under sterile conditions and incubated again for 7 days at 26 °C. Pure cultures were transferred to Pochon agar slants and cultured for 7 days before use in next step of screening procedure. Isolates were coded according to the sampling site (e.g., P1.1, 1K1).

2.4.2 Secondary Screening on Solid Medium

A secondary screening on solid Pochon medium was conducted to assess growth and qualitative dye decolorization by actinomycete isolates. As previously EB, BG and CV dyes were evaluated. Dye concentrations in solid Pochon medium was 50 mg/L and 100 mg/L. Isolated and purified strains obtained at preliminary screening procedure and additional strains from the Department culture collection were used for inoculation of dyed plates by streaking method and incubated at 26 °C. Plates were examined after 24 h, 3 days, 7 days, and 14 days for biomass development and qualitative decolorization, assessed by the presence of decolorized zones surrounding colonies. Based on secondary screening performance, strain 1K1 (isolated in this study) and strain EGK2 (from the departmental strain collection) were selected for liquid-phase experiments.

2.4.3 Main Decolorization Experiment in Liquid Medium with and Without Carriers

The main experiment was performed in 50 ml bottles with the use of liquid Pochon medium using four experimental series prepared in triplicate: (i) 30 mL Pochon medium (substrate) only, (ii) 2500 mg straw + 30 mL substrate, (iii) 2500 mg conifer wood shavings + 30 mL substrate, and (iv) 2500 mg deciduous wood shavings + 30 mL substrate. Plant-derived materials were used as solid carriers for immobilization of actinomyces. All samples were sterilized (autoclaving in temperature 121 °C for 15 min). Samples were divided into abiotic (not inoculated) and biotic (inoculated) ones. Inocula were prepared by rinsing biomass from Pochon agar slants with 9 mL physiological saline. The suspension was adjusted to 1 McFarland standard, and 1 mL was used to inoculate each sample. After inoculation, cultures were incubated for 7 days at 26 °C to allow biomass propagation on the substrate and carrier

materials. Following this propagation step, dyes were added to initiate decolorization experiments. In the main experiment, EB and BG were tested. Dyes stock solutions were prepared at 1000 mg/L and was filter-sterilized with syringe filters (0.22 µm PES). The dyes dosing was performed to obtain in each sample an initial dye concentration of 45 mg/L. The choice of these concentrations was based on the literature data and the experience of the department team in this field (Zabłocka-Godlewska, Przystaå, and Grabińska-Sota 2014; Przystas, Zablocka-Godlewska, and Grabinska-Sota 2012) Decolorization performance was evaluated after 7 days and 14 days according to the applied experimental procedure.

2.4.4 Measurements and Calculations

After 7 days of incubation, samples were centrifuged (10 min at 5500 rpm) to obtain clear supernatant. The absorbance was measured on a "UV-VIS Hi-tachi U-1900" spectrophotometer with the deionized water as a blank sample. The wavelengths were: 624 nm for BG, 606 nm for EB, and 590 nm for CV. After 14 days of culture, the second series were measured. More details about measurements and calculations are included in section 2.8.

2.5 Pure-Culture Biodecolorization of Evans Blue by *Shewanella oneidensis* MR-1

2.5.1 Preparation of Dye and Bacterial Growth Solutions

A stock solution of Evans Blue (Direct Blue 53) was prepared in deionized water at a concentration of 2000 mg/L. Working dye solutions were prepared by appropriate dilution of the stock solution with mineral salt medium (MSM) to obtain initial dye concentrations of 25, 50, and 100 mg/L, depending on the experimental design, along with 10 mL/L each of vitamin solution and trace mineral stock solution as per the methods mentioned previously (Wu et al. 2012; Yanbo Li, Liu, and Shi 2023). The MSM served as the decolorization medium and was adjusted to pH 7.0. Glucose was added as the primary carbon and electron source at concentrations of 250, 500, and 1000 mg/L. For comparative experiments, sodium lactate was used as an alternative electron donor at an equimolar carbon concentration. All media and solutions were sterilized by autoclaving at 121 °C for 30 minutes, except for dye stock solutions, which were filter-sterilized with syringe filters (0.22 µm PES) to avoid thermal degradation.

2.5.2 Bacterial Growth and Inoculum Preparation

Shewanella oneidensis MR-1 (LMG 19005; ATCC 700550; JCM 31522) was obtained from the Belgium Coordinated Collections of Microorganisms (BCCM), Ghent University (Belgium). The bacteria strain *Shewanella oneidensis* MR-1 was used as a pure culture for all Section 2.5 experiments. The strain was revived in Luria–Bertani (LB) broth and incubated overnight at 37 oC with shaking at 200 rpm. A loopful of overnight culture was streaked onto LB agar plates to confirm strain purity. For inoculum preparation, a single colony was transferred into 10 mL LB broth and incubated overnight under the same conditions. The culture was subsequently diluted 1:100 into fresh LB broth and grown for 3–4 h until reaching the exponential growth phase. Cell density was adjusted to 0.5 McFarland standard, corresponding to approximately 1.5×10^8 CFU/mL, and this standardized suspension was used as the inoculum for all biodecolorization experiments to ensure reproducibility.

2.5.3 Experimental Setup for Dye Decolorization

Batch dye decolorization experiments were conducted in 100 mL Erlenmeyer flasks with a working volume of 50 mL. Each flask contained MSM supplemented with Evans Blue (three series with different initial dye EB concentrations of 25, 50, and 100 mg/L) and the selected carbon source at predefined concentrations (250, 500, 1000 mg/L). Flasks were inoculated with 1.0 mL of the standardized *S. oneidensis* MR-1 suspension. To prevent contamination and evaporation, flasks were sealed with sterile cotton plugs wrapped in aluminum foil. Abiotic control flasks (without bacterial inoculation) were prepared in parallel under identical conditions to account for non-biological dye removal. All experiments were conducted under normal aerobic conditions, unless stated otherwise, and incubated at three different temperatures (25, 30, or 37 ^{o}C) using temperature-controlled incubators, according to the experimental design. Samples were withdrawn aseptically after 24, 48, and 72 h of incubation for further processing and analysis. Each experimental condition was performed in triplicate (= 3), Figure 2.1 shows a schematic of the methodology.

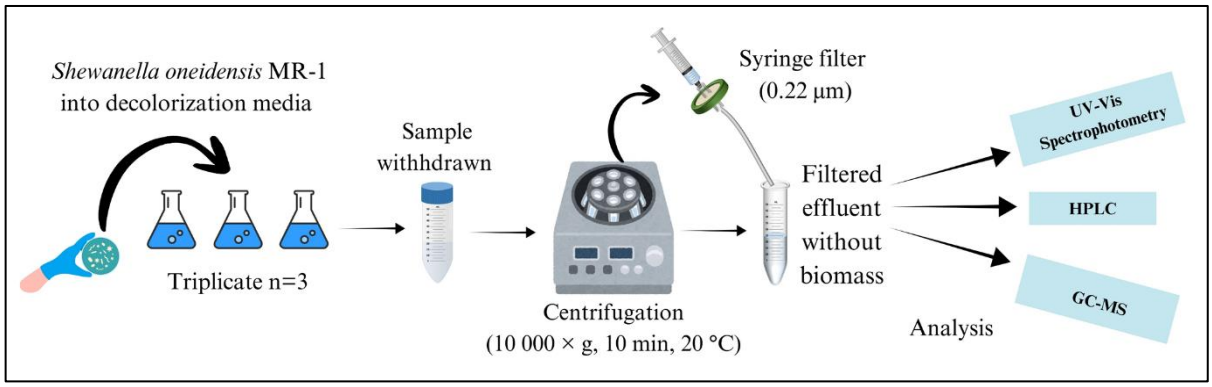

Figure 2.1 Schematic of the experimental workflow for EB decolorization by S. oneidensis MR-1 (K. Ayaz et al 2026a)

2.5.4 Comparative Aerobic vs Anaerobic and Glucose vs Lactate Experiment

To assess the influence of oxygen availability and electron donor type on dye decolorization, a separate comparative experiment was performed under four distinct operating regimes:

1. Aerobic conditions with glucose
2. Aerobic conditions with lactate
3. Anaerobic conditions with glucose
4. Anaerobic conditions with lactate

In this experiment, the initial Evans Blue concentration was fixed at 100 mg/L, and the carbon source concentration was maintained at 250 mg/L. Incubation temperature was set at 37 °C. Aerobic experiments were conducted in Erlenmeyer flasks, incubated. Anaerobic experiments were carried out in butyl-rubber-sealed serum bottles, which were purged with nitrogen gas for 20 minutes to establish anoxic conditions. Samples were collected at 20, 40, and 60 h. Abiotic controls were included for all conditions to verify biological involvement in dye removal. Abiotic controls were included as mentioned earlier in Section 2.5.3.

Measurements (UV-Vis spectrophotometry, HPLC, GC-MS) and calculations details included in section 2.8, 2.11 and 2.12.

2.5.5 Experimental Design Using the Full-Factorial RSM

A full-factorial experiment (3^4) was conducted to evaluate the effects of time (A; 24, 48, 72 h), Evans blue (EB) concentration (B; 25, 50, 100 mg/L), glucose (carbon) concentration (C; 250, 500, 1000 mg/L), and temperature (D; 25, 30, 37 °C) on dye-removal efficiency (%). For response-surface modeling, factors were coded to −1, 0, +1 according to their true midpoint (48 h, 62.5 mg/L, 625 mg/L, 31 °C) (Table 2-1). A second order (full quadratic) model was

fitted in coded space by ordinary least squares, including all main effects, all six two-way interactions, and the four squared terms. To respect the physical bounds of the response, observations were truncated to (0, 100) % before fitting.

Table 2-1 Experimental design and factor levels (coded −1/0/+1) for the 3^4 full factorial RSM for EB removal

Factor	Variable	Low (–1)	Center (0)	High (+1)
A	Time (h)	24	48	72
B	Dye conc. (mg/L)	25	62.5	100
C	Carbon source Conc. (mg/L)	250	625	1000
D	Temp (°C)	25	31	37

2.6 Dual-Chamber Microbial Fuel Cell for Evans Blue Degradation and Energy Recovery

2.6.1 Screening and isolation of Actinomycetes Strains for Aerobic treatment

The actinomycetes obtained in the first screening were not sufficiently effective for the intended aerobic stage, a second isolation and screening were performed using garden compost as a source of additional actinomycetes, applying the same methodology as in Section 2.4 for consistency. Multiple isolates were obtained and their screening outcomes are presented in the Results section (Section 3.3.1) among them, SK-2 and SK-3 showed the strongest and most efficient decolorization and were selected for experiments in the integrated aerobic chamber of DCMFC to evaluate their capacity to oxidativ transformation intermediates, particularly aromatic amines formed during the anaerobic stage.

2.6.2 Media Used in Anodic, Cathodic and Aerobic Chambers

The anode and cathode culture medium composition is described in section 2.1.2. In the case of anode, the medium was additionally enriched by Evans Blue (100 or 200 mg/L), while in cathode the medium replaces EB and acetate with $NaHCO_3$ and acts as support for bacterial growth as inorganic carbon source and acts as buffer to maintain pH.

In the aerobic chamber, actinomycetes were cultivated in liquid Pochon medium to establish active biomass. After 7 days of incubation, the anode effluent from the anaerobic stage was transferred into the aerobic culture to evaluate oxidative transformation of reduced dye intermediates, with particular emphasis on the biodegradation of aromatic amines and further mineralization toward more complete treatment.

Inoculum Preparation

Anodic chamber acclimation: The anode compartment was inoculated with anaerobic activated sludge and sludge-to-dye solution ratio was maintained at 4:1 (Mixed Liquor Suspended Solids (MLSS) 4 g/L; initial OD600 1.5) and acclimated to establish a mature, electroactive mixed-culture biofilm on anode prior to dye experiments. During acclimation Evans Blue concentration increased gradually from 50 mg/L to 100 mg/L in a 50 mM phosphate buffer. The reactor was monitored by cell voltage, and 50% of the medium was refreshed whenever the voltage drops to approximately 10 mV, which served as an operational indicator of substrate depletion and declining electrochemical activity. The system was operated for approximately one month for the acclimation phase until a reproducible voltage response was achieved. The aim of this acclimation was to stabilize biofilm growth and extracellular electron transfer at the anode so that subsequent experiments reflect controlled operating conditions rather than start-up effects.

Cathodic chamber acclimation. The cathode compartment was inoculated with aerobic activated sludge from the same source (MLSS 4 g/L; initial OD600 1.5) and operated as a biocathode to support stable oxygen reduction under aerobic conditions. Like the anode, cathode-side performance was tracked through the overall cell voltage behavior, and the acclimation phase aimed to ensure consistent cathodic biofilm activity and minimize start-up limitations before experimental operation.

Aerobic post-treatment chamber acclimation. Inocula were prepared by rinsing biomass from Pochon agar slants with 9 mL physiological saline and adjusting the suspension to OD_{600} = 0.5. The aerobic post-treatment chamber was then inoculated with 1.0 mL of the actinomycete consortium (SK-2, 0.5 mL; SK-3, 0.5 mL; each OD_{600} = 0.5) and incubated for 7 days to establish active biomass before receiving anode effluent, thereby supporting degradation of aromatic amines formed during anaerobic azo-bond reduction.

2.6.3 Reactor configuration and integrated system layout

The integrated system consisted of a DCMFC coupled to a post-treatment aerobic bioreactor. The DCMFC was constructed using two Plexiglass compartments (120 mL each): one chamber operated under anaerobic conditions (anode) and the other cathodic chamber under aerobic conditions, act as biocathode for oxygen reduction and complete the circuit reaction as shown schematically in the Figure 2.2. A cation-exchange membrane (CMI-7000,

RisingSun Membrane, Beijing, China) was positioned between the two chambers (anodic and cathodic) to separate the anolyte and catholyte. Each DCMFC chamber had an effective working volume of 100 mL. The effluent from the anaerobic anode chamber was subsequently directed to a separate aerobic bioreactor (120 mL working volume, Plexiglass) to further treat the DCMFC effluent and support mineralization of intermediates formed during anaerobic degradation. Both the anode and cathode electrodes were carbon brushes with dimensions reported as 1 cm × 2 cm (diameter × length) and were placed centrally within each chamber. Electrical connections were made using insulated copper wire, and the connection points were sealed using nonconductive epoxy to insulate the interfaces. The carbon brush electrodes were prepared following the approach described by Logan et al., (Logan et al. 2006) using carbon fibers woven around two twisted titanium wire cores. The external circuit was connected to a voltage data logger (PicoLog 1012, Pico Technology Ltd., St Neots, Cambridgeshire, United Kingdom). Voltage output was recorded through a 500 Ω external resistor, and the logging interval was set to 5 min.

Before inoculation, nitrogen gas was sparged through the anodic medium for 15 min, and nitrogen was also supplied to the DCMFC headspace to maintain anaerobic conditions. The reactors were operated in a temperature-controlled chamber (30 ± 1°C). During the acclimatization of biofilm adaptation (start-up) period, Evans Blue concentration increased gradually from 50 mg/L to 100 mg/L in a 50 mM phosphate buffer. The system was operated for approximately one month for the acclimation phase. After acclimation, feasibility experiments were carried out by supplementing DCMFCs with acetate (1000 mg/L) and two dye concentrations (100 and 200 mg/L Evans Blue) together with 10 mL/100 mL of minerals and vitamins, as described in section 2.1. Operational cycling was controlled based on acetate depletion and voltage decline. Specifically, approximately half of the anode chamber medium was replaced with fresh dye-containing medium when the electron donor (acetate) was nearly depleted, and the cell potential dropped below 50 mV, which was used as the practical indicator to complete one cycle.

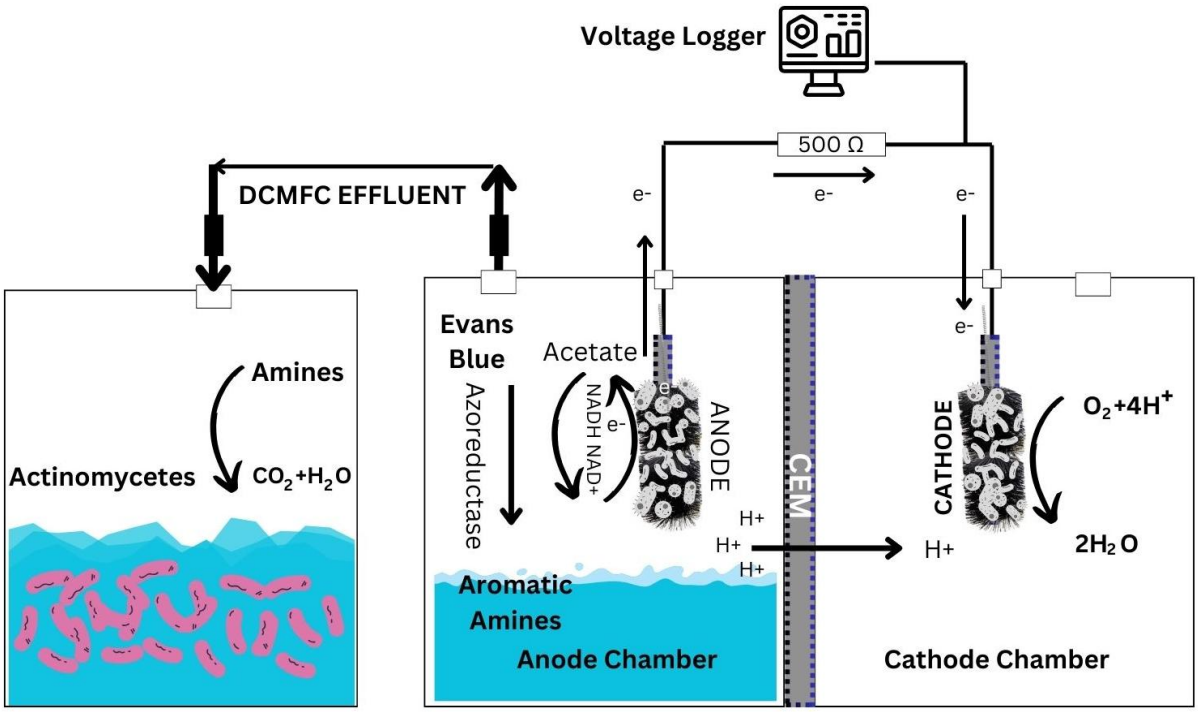

Figure 2.2 Schematic diagram of double − chamber microbial fuel cell (K.Ayaz et al. 2024)

2.7 Single Chamber Microbial Fuel Cell (SCMFC) Anode Modification for Enhanced EB Decolorization and Microbial Adhesion

2.7.1 Bacterial inoculum preparation

Shewanella oneidensis MR-1 was the only bacteria strain used as a pure culture for all Section 2.7 experiments. The details of methodology of bacteria inoculum preparation are included in Section 2.5.2. Cell density was standardized to 0.5 McFarland (≈ 10^8 CFU/mL) using densitometric measurement. This standardized suspension was used as the inoculum for all subsequent experiments unless otherwise stated.

2.7.2 Preparation and chemical characterization of the modified carbon cloth electrode

For microbiological experiments, carbon cloth (CC) electrodes were cut to identical dimensions (1.5 × 0.8 cm; geometric area = 1.2 cm^2) to ensure consistent electrode area across all tests and to enable direct comparison of electrochemical responses. The cut electrodes were rinsed with deionized water (dH_2O) and sterilized under UV irradiation for 10 min (on both sides). For electrochemical experiments, commercial carbon cloth (AC-1071HCB, AvCarb, USA; thickness 356 µm) was used.

Polyaniline (PANI) was deposited onto the pretreated CC by electropolymerization in a three-electrode configuration. The CC (1.5 × 0.8 cm; 1.2 cm^2) served for optimization as the working electrode, a KCl-saturated Ag/AgCl electrode was used as the reference, and a platinum wire acted as the counter electrode. Electrodeposition was carried out in 0.5 M H_2SO_4 containing 0.1 M aniline using cyclic voltammetry (20 cycles; scan rate 50 mV/s; potential window −0.6 to 1.0 V), producing a uniform green PANI coating. After deposition, electrodes were thoroughly rinsed with dH_2O and air-dried overnight to stabilize the coating (CC. PANI). Electropolymerizated electrodes were sterilized under UV irradiation for 10 min (on both sides).

To introduce a readily available carbon source at the anode surface, at aseptic conditions 50 µL of sterile glucose solution (10% w/v in dH_2O) was evenly drop-cast onto the CC.PANI surface and dried on a hot plate at 50 °C for 15–20 min, after which the electrodes were stored at room temperature (CC.PANI.Glucose). To minimize premature glucose dissolution into the surrounding medium, in aseptic conditions a protective gelatin overlayer was applied by drop-casting 20 µL of gelatin solution (sterile 10% w/v in dH_2O). The selected casting volumes were chosen to provide uniform coverage of the 1.2 cm^2 CC surface without overflow or aggregation, thereby producing a consistent, adherent multilayer while maintaining coating integrity during incubation and electrochemical testing. The gelatin layer was dried at 35 °C for 30 min. The resulting multilayer electrode (CC. PANI.Glucose.Gelatin) is hereafter referred to as the modified carbon cloth (MCC). The full preparation workflow is presented in Figure 2.3.

Chemical characterization of bare and modified electrodes was performed by Fourier-transform infrared (FTIR) spectroscopy (PerkinElmer Spectrum Two). Fresh films were scanned over 400–4000 cm^{-1} at 2 cm^{-1} resolution using 16 accumulations. Surface chemical composition was further examined by X-ray photoelectron spectroscopy (XPS) using an AXIS SUPRA+ spectrometer equipped with an Al Kα X-ray source.

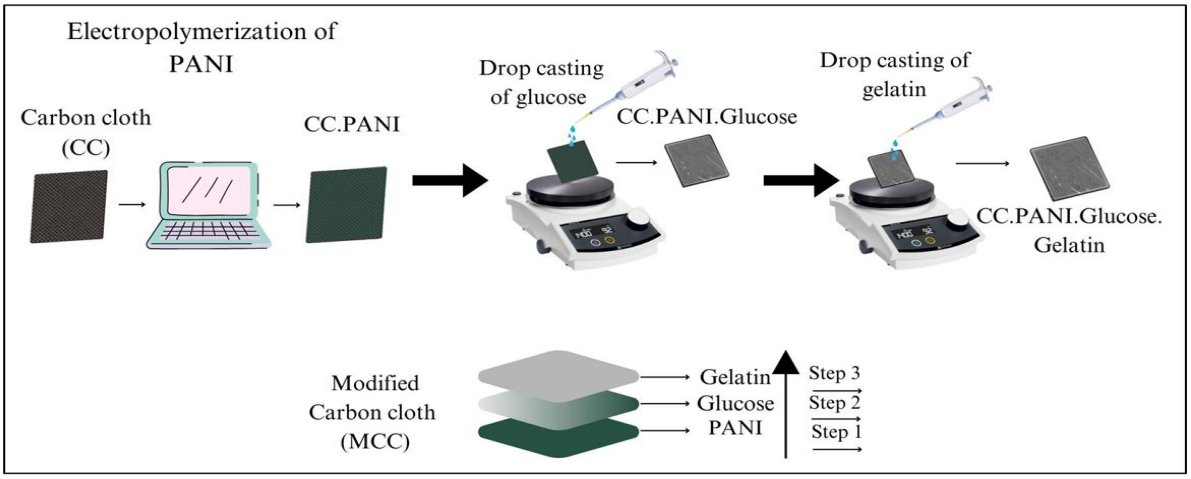

Figure 2.3 Schematic representation of the electrode modification (K. Ayaz et al. 2026b).

2.7.3 SCMFC setup, operation, and electrochemical performance evaluation

Two single-chamber microbial fuel cells (SCMFCs) were assembled using plexiglass reactors (total volume: 70 mL) and operated as (i) a modified carbon cloth MFC (MCC-MFC) and (ii) an unmodified carbon cloth MFC (CC-MFC) with dimensions of (3 × 3 cm; 9 cm^2). In MCC-MFC, the MCC anode was prepared following the procedure described in Section 2.7.2, whereas CC-MFC employed an unmodified carbon cloth anode. In both reactors, a platinum sputter-coated carbon cloth (16 cm^2) was used as the air cathode. The cathode and a cation exchange membrane (CMI-7000) were mounted externally on the reactor wall and positioned over a 4 cm diameter opening. The distance between the anode and cathode was maintained at 5 cm. A stainless-steel mesh (16 cm^2) served as the cathode current collector. Electrical connections were made using titanium wire, and the circuit was completed through a fixed external resistor (1,000 Ω).

Both SCMFCs were inoculated with *Shewanella oneidensis* MR-1. Each reactor was operated at an effective working volume of 50 mL and fed with an anolyte consisting of 10 mM phosphate buffer and supplemented with mineral and vitamin solutions (10mL/100 ml). In the CC-MFC control, glucose was supplied directly to the bulk anolyte (1 mL of 10% w/v) as the carbon source. In contrast, in MCC-MFC, the same glucose dose was introduced as a surface-confined glucose layer beneath the gelatin overcoat on the anode, thereby localizing carbon at the bioanode interface rather than distributing it in the electrolyte. Before the operation, the headspace of each SCMFC was purged with nitrogen gas for 20 min to establish and maintain anaerobic conditions. For feasibility assessment, an initial EB concentration of 150 mg/L was introduced to the SCMFC. The pH was maintained between 7.2 and 7.5, and

the reactors were operated in a temperature-controlled chamber (30 ± 1°C) under dark conditions. Following successful anaerobic degradation of EB, its concentration gradually increased to 300 and 450 mg/L.

2.8 UV–Vis Spectrophotometric Determination of Dye Concentration and Decolorization

UV–Vis spectrophotometry was employed across all experiments described in sections 2.4, 2.5, 2.6, and 2.7 to quantify residual dye concentration and calculate decolorization efficiency. Measurements were performed using a Hitachi U-1900 UV–Vis spectrophotometer with quartz cuvettes, with spectra typically collected over 400–800 nm (or a broader scan where specified). Before UV–Vis measurement, samples were clarified by centrifugation (10,000 × g, 10 min, 20 °C) to remove turbidity and biomass-related light scattering. Then samples were filtered through a 0.22 μm PES syringe filter to remove residual of suspended biomass before UV–Vis determination. Quantification was based on calibration curves prepared in the relevant experimental matrices, and appropriate medium blanks were used in each experimental section to account for matrix effects and ensure reliable absorbance-to-concentration conversion.

In section 2.4 (actinomycete batch cultures), decolorization was evaluated for Evans Blue (EB) and Brilliant Green (BG) after dye addition at initial concentration of 45 mg/L. After 7 days of incubation, 2.5 mL aliquots were withdrawn, clarified by centrifugation (10 min, 5500 rpm), and measured against deionized water. Absorbance was recorded at 606 nm (EB) and 624 nm (BG). The same sampling and measurement procedure was repeated after 14 days, and dye concentrations in test and control samples were calculated from the corresponding calibration relationships (i) and formula (ii) to determine percent removal. In section 2.5, UV–Vis spectroscopy (wavelength range 400–800 nm) was used to monitor Evans Blue, focusing on its characteristic absorbance maximum at 606 nm, with MSM + glucose used as the blank. In section 2.6 (DCMFC system), EB-treated samples were scanned over wavelength 300–900 nm to capture the full spectral profile of sample. EB quantification was performed using the absorbance signal at 606 nm, and concentration values were obtained via a standard calibration curve. In section 2.7 (SCMFC system), EB concentration was determined at 606 nm, with PBS + glucose serving as the matrix blank.

Across all experiments described in sections 2.4 to 2.7, absorbance (A) matrix-matched calibration (linear model A = m·C + b; acceptance: $R^2 \geq 0.995$ and non-significant lack-of-fit) was applied to determine dye concentrations in the samples. Dye concentrations were calculated using the linear calibration model:

$$C_{\text{sample}} = \left(\frac{A_s - b}{m}\right) \times D \qquad (i)$$

where C_{sample} is dye concentration in sample, $A_s$is the measured absorbance, m and b are the slope and intercept of the calibration line, and D is the dilution factor (D = 1 for undiluted samples). Measurements were conducted in triplicate and are reported as mean ± SD. Decolorization percentage efficiency (D%) was expressed as:

$$D(\%) = \frac{C_0 - C_t}{C_0} \times 100 \qquad (ii)$$

where C_0 denotes the initial dye concentration and $C_t$is the concentration at the corresponding sampling time.

2.9 Electrochemical Measurements

Electrochemical characterization was performed only for the MFC-based investigations (sections 2.6 and 2.7) to probe redox activity at the bioanode interface and to quantify interfacial resistances governing electron transfer. CV was used to identify oxidation/reduction features associated with electroactive bacteria species and dye transformation products, whereas EIS was used to resolve solution/ohmic contributions and charge-transfer limitations through frequency-domain analysis.

2.9.1 Monitoring of DCMFC performance

The DCMFC reactor was run in a closed circuit with 500 (Ohms Ω) of external resistance. A Picolog data logging system was used to acquire voltage data from the reactor. Using Ohm's law, the flow of current within the external circuit was determined as follows (R. S. Yadav et al. 2024)

$$I = V/R \qquad (iii)$$

Where I is current, V is the potential difference (voltage) across the exterior load, R is the external resistor (load), and I is the current flow in the exterior circuit.

To calculate the power output of the MFC, the following formula is used (R. S. Yadav et al. 2024):

$$P=IV \quad \text{(iv)}$$

where P (watts) is the power, V is the potential difference (voltage) across the exterior load, I is the current.

Different external resistances, ranging from 10 ohms to 1 million ohms, were attached to exterior circuits at the completion of the MFC experimental setup. By applying the procedure outlined in the equation to normalize the resultant power and current values to the surface area ($21cm^2$) of the anode, polarization curves and power-current graphs were created (A. Yadav et al. 2022).

In the last batch cycle of the acclimation period, DCMFC was given 100 mg/L of EB combined with 1000 mg/L of acetate, and it was able to maintain stability and reach its maximum cell potential. EIS and CV were performed by using CH Instruments, Inc., type 660C, Austin, TX, USA.

There were two different EIS measuring types used. First, the bioanode employed a three-electrode arrangement, including Ag/AgCl (reference), cathode (counter), and bioanode (working) electrodes, at potential amplitudes of 10 mV and frequencies ranging from 100 kHz to 10 mHz. For the entire cell (DCMFC), a two-electrode setup was used with cathode (working), anode (counter) and Ag/AgCl (reference) electrodes at an open-circuit voltage (M. D. Khan et al. 2021). CV was carried out with a scan rate of 10 mV/s over a range of −1 V to 1 V with degrading dye. To assess the electrochemical performance of the DCMFC, Ag/AgCl served as the reference electrode, while the anode served as the working electrode, and the cathode served as the counter electrode.

2.9.2 Electrochemical analysis of modified Anode

Section 2.7 describes the modification of carbon cloth anodes to improve microbial adhesion, shorten the start-up period, increase electron transfer efficiency, decrease resistance, and enhance dye removal within a reduced operating time. To evaluate whether these surface modifications translated into measurable improvements at the bioanode interface, CV and EIS were applied. Together, these techniques provided electrochemical evidence for bacterial attachment and biofilm-mediated electron transfer on the modified anode. Electrochemical analysis was performed using a three-electrode system consisting of CC.B, CC.G.B, and

MCC.B as the working electrodes, an Ag/AgCl reference electrode (EDAQ, ET072), and a Pt/Ti rod counter electrode (EDAQ, ET078). CV and EIS data were acquired using a PalmSens4 Potentiostat (Netherlands). CV measurements were conducted for CC, CC.G, and MCC as control and CC.B, CC.G.B, CC.PANI.B and MCC.B electrodes with bacterial inoculation, over a potential range of -0.8 V to 1 V (vs. Ag/AgCl) at a scan rate of 0.01 V/s. EIS data were collected at a DC voltage of 0 V and an AC voltage of 10 mV across a frequency range of 10 kHz to 0.01 Hz, with six scans per decade. These measurements were carried out in both the presence and absence of biofilms. The charge storage capacity (CSC) was determined using the following equation (Abdullah et al. 2024):

$$\text{CSC} = \frac{1}{Sv} \int_{E_1}^{E_2} I\ (E) dE \qquad \text{(v)}$$

where: ν is a scan rate (V/s), S is a geometrical area of the electrode (1.2 cm^2), E_1 and E_2 are the cutoff potentials (V), and I is a current (A). Here, S refers to the projected geometric area of the carbon cloth electrode immersed in the electrolyte, which is used for normalising CSC values. Because carbon cloth is a porous 3D material and both faces and edges are exposed, the true electrochemically active surface area is larger than S, so the reported CSC values should be interpreted as apparent CSC per projected area. All electrodes were cut from the same sheet using identical dimensions, so the uncertainty in S arising from manual cutting and minor edge fraying is estimated within ± 5%, which is much smaller than the observed multi-fold differences in CSC between samples. In this work, CSC (mC/cm^2) is defined as the total charge obtained by integrating the CV curve over the applied potential window and normalizing by the projected geometric area S; it therefore represents the apparent areal charge density of the entire electrode–electrolyte–biofilm system, and is not the specific capacitance of any individual component (e.g. PANI or biofilm) alone.

To enable quantitative comparison of interfacial kinetics, an apparent exchange current density (j_0) was estimated from the fitted charge-transfer resistance (R_2) using the relationship:

$$j_0 = \frac{RT}{nFAR_2} \qquad \text{(vi)}$$

where: T = 298 K, n = 1, R = 8.314 J/(mol·K), F = 96 485 C/mol, and A = 1.2 cm^2.

2.9.3 SCMFC electrochemical performance evaluation

Voltage monitoring and current calculation

Voltage output (mV) was continuously recorded from the reactor system using a multichannel DAQ logger (PicoLog 1012, Pico Technology Ltd., St Neots, Cambridgeshire, United Kingdom) at fixed 15 min intervals. Current was calculated using Ohm's law:

$$I = \frac{V}{R} \quad \text{(vii)}$$

Where I is current, V is the potential difference (voltage) across the exterior load, R is the external resistor (load), and I is the current flow in the exterior circuit.

Polarization and power density determination

For polarization and power curves, the external resistance was adjusted stepwise from 10 to 10^6 Ω after the voltage stabilized at each load. Current and power were calculated as:

$$P = VI \quad \textit{(viii)}$$

where P (watts) is the power, V is the potential difference (voltage) across the exterior load, I is the current

and normalized by the projected anode area (3 × 3 cm; 9 cm^2) to obtain areal current density and areal power density:

$$j = \frac{I}{A} p = \frac{P}{A} \quad \text{(ix)}$$

Where J is current density, P (watts) is the power, and A is area of anode used in the respective experiment.

All calculations were performed using SI-consistent conversions (mV→V; mA→A) before reporting.

2.9.4 DNA Extraction, PCR Amplification, and Illumina Sequencing

After the DCMFC experiment was completed, the anode carbon brush was removed, and the microbial population of the anode biofilm was investigated using the following methods. Genomic DNA was initially isolated from the biofilm sample using the DNA Isolation DNeasy PowerSoil Pro Kit (Qiagen, Hilden, Germany), as per the manufacturer's instructions. The forward primer 338F (5′-ACTCCTACGGGAGGCAGCA-3′) and the reverse primer 806R (5′-GGACTACHVGGGTWTCTAAT-3′) were utilized to amplify the V3-V4 region of 16S rRNA.

For Actinomycete strains in an integrated aerobic chamber, the actinobacterial primers 243 F (5′-GGATGAGCCCGCGGCCTA-3′) and 513 R (5’-CGGCCGCGGCTGCTGGCACGTA-3′) with 5% DMSO were used during PCR to avoid any metabolites. A GeneAmp® 9700 (Applied Biosystems, California, United States) was used for PCR.The input gDNA sample (5ng) was amplified through PCR using 5×reaction buffer, 1 mM dNTP, 500 nM each of the forward and reverse PCR primers, and DNA polymerase (Herculase II fusion, Agilent Technologies, Santa Clara, CA, USA). Heat activation at 95 °C for 3 min was used for the initial PCR cycle. After that, there were 25 cycles of 30s at 95 °C, 55 °C, and 72 °C and a final 5 min extension at 72 °C. To create the final library with the index, 10 μL of the first PCR product was amplified using Nextera XT Indexed Primer (Illumina Inc., San Diego, CA, USA). The PCR products were purified using the AxyPrepTM DNA GelExtraction Kit (Axygen Biosciences, AXYGEN Union City, CA, USA). After purification and quantification, the samples were delivered to a biotechnology company (Macrogen Europe, Amsterdam, The Netherlands) for 16S rRNA gene sequencing via the Illumina MiSeq platform. The genetic distance model (Tamura–Nei) was used to construct a phylogenetic tree and neighbor-joining tree method in Geneious Prime (version 9.8.1). The tree included 27 ITS sequences representing different strains of Actinomycetes, including 5 sequences, i.e., SK2 and SK3

2.10 HPLC analysis

During the decolorization process in section 2.5 (after 2, 4, 11, 14, and 28 h at 30 ± 2 °C, initial pH 7.0), the culture media were collected and centrifuged at 10000 rpm for 15 min. Then, 1 mL of supernatant from each sample was filtered through a 0.22 μm pore size syringe filter (Qpore® sterile syringe PES Filter); a control sample (untreated EB dye) was also prepared. The filtered samples were analyzed individually by injecting 20 μL into the chromatograph to detect the corresponding peaks and determine the retention time of each sample. Chromatographic analyses were performed using a C18 reversed-phase column maintained at 25°C and a pH of 3. The mobile phase consisted of 60% methanol and a 40% of sodium dihydrogen phosphate (NaH_2PO_4). The flow rate was set to 0.5 mL/min under isocratic conditions. The total run time for each analysis was 10 min. Detection was carried out with a photodiode array (PDA) detector, and chromatograms were recorded at a wavelength of 254 nm.

2.11 Analysis of Dye Degradation by GC–MS

After completion of the incubation period, 5 mL aliquots of the culture supernatant were carefully withdrawn from the Evans blue degradation assays for GC–MS analysis. To eliminate suspended cells and insoluble particulates, the samples were first subjected to centrifugation at 10,000 × g for 10 minutes. The resulting supernatant was subsequently passed through a Qpore® sterile syringe filter (polyethersulfone (PES), 0.22 μm, 25 mm diameter) to ensure the complete removal of any remaining microbial biomass. The cell-free filtrate was then subjected to solid phase extraction via the use of Supelclean™ ENVI-18 cartridges by Supelco. Details of the method are presented in (Pieczykolan et al. 2025). The column bed was activated with 5.0 mL of acetonitrile and 5.0 mL of methanol and then washed with deionized water. The filtrate was added to the prepared bed. After sample filtration, the bed was dried under vacuum for 5 minutes. The compounds remaining on the bed were eluted with 0.8 mL of methanol and 0.8 mL of acetonitrile. The prepared extract was subjected to gas chromatography–mass spectrometry (GC–MS) analysis via a 7890B GC coupled to an MS detector (Agilent Technologies, Santa Clara, USA). Injections were performed automatically with an autosampler syringe speed of 300 μL/min; the inlet temperature was 250 °C. Chromatographic separation was achieved on an SLB™ 5 ms capillary column (30 m × 0.25 mm i.d., 0.25 μm film; Sigma–Aldrich, Poland). The oven program was as follows: 80 °C (6 min hold), ramp at 5 °C min^{-1} to 260 °C, then 20 °C min^{-1} to 300 °C with a 2 min hold. Helium (grade 6.0) served as the carrier gas. The MS was operated in total ion current (TIC) scan mode over m/z 50–500. The ion trap temperature was 150 °C, and the ion source temperature was 230 °C.

2.12 Microscopic analysis

At the end of the experiment in section 2.6, the surface of the bioanode was evaluated by using SEM to determine bacterial attachment and biofilm formation at the anode surface. Also, the control and modified samples of experiment in section 2.7 are CC, CC.G, and MCC, co-cultured overnight with bacteria, and were thoroughly rinsed with PBS before preparation for SEM analysis. All the samples were sectioned and fixed overnight with 2% glutaraldehyde, followed by two washes with phosphate buffer solution (pH 7.2). Dehydration was performed sequentially using ethanol solutions of 25%, 50%, 70%, 80%, 90%, 95%, and 99%. To ensure high-quality imaging, the samples were air-dried for 24 h at room temperature (Ayaz,

Zabłocka-Godlewska, and Li 2024). Once dried, the samples were sputter-coated with gold and imaged using a Phenom ProX SEM at an accelerating voltage of 10 kV. SEM was equipped with an energy-dispersive X-ray spectroscopy (EDS) analyzer for elemental analysis.

2.13 Biomass analysis

Biofilm biomass analysis was performed on the modified anodes to evaluate their ability to promote microbial attachment and biofilm development. As described in Section 2.7, these analyses were conducted to verify whether the anode surface modifications enhanced biofilm formation, which is a critical factor influencing electron transfer efficiency and overall bioelectrochemical performance. Following an overnight co-culture in a 12-well plate, the bacterial growth medium was removed from wells containing CC, CC with glucose in the solution (CC.G), and MCC. The samples were named CC. B, CC.G.B, CC.PANI.B and MCC.B, where 'B' denotes the presence of biofilm. All samples were washed three times with PBS to eliminate non-adherent bacteria. For the PANI-only bioanode (CC.PANI.B), PANI-modified carbon cloth (CC.PANI) was inoculated with *S. oneidensis* MR-1 and operated under the same electrochemical and cultivation conditions as CC.B, CC.G.B, and MCC.B, but without subsequent glucose–gelatin coatings. Subsequently, samples CC.B, CC.G.B, CC.PANI.B and MCC.B were immersed in methanol for 15 min, followed by air-drying at room temperature for 10–20 min. The dried samples were stained with 1% crystal violet/dH_2O solution for 30 min. After staining the dye solution was removed and samples were thoroughly rinsed with PBS. The dye absorbed by samples during staining were desorbed by using 33% acetic acid/dH_2O (samples discoloration). Finally, 300 µL of the solution of desorbed dye (after sample discoloration) was transferred to a 96-well plate, and absorbance was measured at 570 nm using a COBAS microplate reader. The experiments were performed in triplicate, and the average result was calculated using the following equation to determine the degree of biofilm formation:

$$\text{Biofilm formation (\%)} = \left(\frac{A_{CCM}}{A_{CTRL}}\right) * 100\% \quad \text{(x)}$$

where: A_{CCM} is the absorbance of the solution after discoloration of samples CC.B, CC.G.B and MCC.B, and A_{CTRL} is the absorbance of the solution after discoloration of CC control, both recorded at 570 nm.

2.14 Bacteria Viability assay

Bacterial viability was evaluated using the LIVE/DEAD® BacLight Bacterial Viability Kit (Thermo Fisher Scientific, USA). Samples were rinsed briefly with deionized water and stained with 50 µL of staining solution, prepared by mixing 3 µL of SYTO9 and 3 µL of propidium iodide in 1 mL of PBS. The samples were incubated in the dark at room temperature for 60 minutes. Following incubation, CC.B, CC.G.B, and MCC.B films were affixed to microscope slides, covered with a cover slip and a drop of mounting medium, and left to dry for 15 min (Abdullah et al. 2024). Confocal Laser Scanning Microscopy (CLSM) (Model: FV 3000, objective: UPLSAPO 60XS, magnification: 60x) was used to image live cells (excitation at 488 nm) and dead cells (excitation at 561 nm).

2.15 Chemical oxygen demand analysis

Chemical oxygen demand (COD) was measured to quantify the removal of oxidizable organic matter during SCMFC operation. Liquid samples were collected from the anode chamber at defined time points, immediately filtered with (0.22 µm syringe filters, Qpore® sterile syringe PES Filter) to remove suspended biomass and carbon particles and stored at 4 °C until analysis. The COD was monitored by using a HACH COD test kit (Middle range: 20 - 1500 mg/L) to evaluate the organic removal efficiency. For each measurement, 2.0 mL of sample was added to COD test kits. If COD was expected to exceed the vial range, samples were diluted with deionized water, and the dilution factor was included in the final calculation.

COD kits digestion was performed at 160 °C for 2 h in a COD digester (ThermoReactor COD ECO-16, Velp scintifica). After digestion, kits were cooled to room temperature and absorbance was measured using a photometer (MD 100 photometer, Lovibond), following the vial manufacturer's instructions. COD values were calculated using the instrument calibration curve supplied with the COD kits and reported as mg O_2/L. Method blanks (deionized water) were analyzed with each batch to verify accuracy. All samples were analyzed in at least triplicate, and results are presented as mean ± standard deviation. COD removal (%) was calculated as:

$$COD(\%) = \frac{COD_0 - COD_t}{COD_0} \times 100 \quad \text{(xi)}$$

where COD_0 is initial and COD_t is the COD concentrations (mg O_2/L) at time t (hour)

2.16 Software and statistical analysis

Different software for visualization and analysis was used in this dissertation.

1. Data analysis and model fitting for section 2.6 were performed in the Python Software Foundation (2022, version 3.11) via the pandas, statsmodels, and matplotlib libraries. A second-order polynomial regression model was fitted to the experimental data to relate the response variable (dye removal efficiency) to the independent variables. Model adequacy was evaluated via ANOVA, coefficient significance, the coefficient of determination (R^2), adjusted R^2, and root mean squared error (RMSE), together with standard diagnostics (residual normality, independence via Durbin–Watson, and condition number). The general form of the regression model was as follows:
   $$Y = \beta 0 + \beta 1A + \beta 2B + \beta 3C + \beta 4D + \beta 5A2 + \beta 6B2 + \beta 7C2 + \beta 8D2 + \beta 9AB + \beta 10BC + \beta 11AD + \beta 12BC + \beta 13BD + \beta 14CD + \varepsilon \quad \text{(xi)}$$
   where Y is the predicted dye removal percentage, a response, and A, B, C, and D are the coded values of the four process variables.
2. Three-dimensional response surface plots were generated in OriginPro 2025b (OriginLab Corporation, Northampton, MA, USA), varying two factors at a time while holding others at their mean, to visualize interaction effects and determine optimal conditions for dye removal.
3. Visualization of the Live and dead cell results in section 2.7 was achieved using ImageJ 1.54f11. Electrochemical impedance spectra were analyzed and fitted to an equivalent electrical circuit using the EIS Spectrum Analyzer.
4. In this dissertation all the data analysis was performed using Microsoft Excel to calculate each assay's mean and standard deviation from three independent experimental replicates. All the graphs and visualization of the results were achieved by using OriginPro 2025b.

Chapter 3

3 Results And Discussion

3.1 Immobilized Actinomycetes for Azo Dye Removal

Textile dye effluents are difficult to treat because many commercial dyes are engineered to resist photochemical and oxidative degradation, making wastewater highly persistent and intensely colored even at low concentrations. This can reduce light penetration, disturb photosynthesis and cause oxygen deficit, and increase ecotoxicological risks in receiving waters. Although physicochemical methods can rapidly remove color, their broad application is often limited by high chemical demand, sludge generation, and secondary waste handling, which increases cost and can shift pollutants rather than detoxify them, thereby motivating biological options that target transformation and toxicity reduction (Al-Tohamy et al. 2022b; Castillo-Suárez et al. 2023; Islam et al. 2025; Aragaw 2024a).

Within biological approaches, actinomycetes (*Actinobacteria*) are especially relevant to this dissertation because they are metabolically versatile and can express enzyme systems implicated in the transformation of complex aromatic structures, including azo dyes, enabling decolorization that can extend beyond physical sorption. Contemporary literature emphasizes genera *Streptomyces* and related actinobacteria as promising dye-degrading biocatalysts, with evidence of effective azo dye decolorization and mechanistic links to oxidative/reductive enzymatic activity (Bautista-Pinzón et al. 2024; Cuebas-Irizarry and Grunden 2024)

However, actinomycete-based dye effluents treatment remains less developed for reliable application, particularly for azo dyes under aerobic conditions, where both decolorization and downstream mineralization may be limited by kinetics and process instability. Recent studies specifically report strong dyes decolorization potential in Streptomyces-based systems, supporting the rationale for targeted investigation while also underscoring the need to quantify performance under controlled operational conditions (Bautista-Pinzón et al. 2024; El Awady et al. 2024)

Accordingly, to the objectives included at section 2.4, this chapter directly addresses the dissertation objective by (i) screening, isolation and purification of dye decolorizing actinomycetes strains from environmental sources and (ii) evaluation of dye decolorization, first on solid culture medium (preliminary experiment) and subsequently in liquid culture medium with and without lignocellulosic carriers (main experiment

The results of this chapter were published as chapter of monograph entitled "*Screening of Actinomycetes decolorizing the synthetic dyes from rotten poplar wood and garden compost*" by Ayaz, K., & Zabłocka-Godlewska, E. (2022). Contemporary Problems of Power Engineering and Environmental Protection; Pikon, K., Bogacka, M., Eds, 119-131

3.1.1 Preliminary and secondary screening on solid medium: growth and decolorization patterns

The preliminary screening was conducted with the use of poplar rotten wood and 3 kinds of compost as a source material for strains isolation and EB, BG and CV dyes (in concentration 50 and 100 mg/L) as selective agents. After incubation time (7 days) on plates with the CV in both concentrations the growth of bacteria was very weak, and no decolorized zones were observed. From plates with EB and BG, 23 strains which present the biggest decolorization zones were selected. Strains were undergone undergoing the purification procedure. Finally, 15 pure strains (mainly from EB plates) were obtained, and stored on slants. In the next stage – secondary screening – the decolorization potential of the isolated strains was examined. The plate-based screening showed a clear dye-structure (chemical group) dependence in both - actinomycete growth and creation of visible decolorization zones (Table 3.1). For the triphenylmethane dyes, the BG supported only weak growth with decolorized zones in ~50% of strains at 50 mg/L, and no detectable growth at 100 mg/L. In the case of CrV dye a similarly inhibitory pattern was observed also at primary screening: strains exhibited very weak growth without discoloration zones at all plates containing 50 mg/L of CrV dye, whereas growth was not observed at 100 mg/L. In contrast, the azo dye EB allowed growth and decolorization in case of all strains at both 50 mg/L and 100 mg/L; however, intensive growth was only observed at the lower EB concentration, 50 mg/L, in case of ~35% of strains, while the higher EB concentration maintained growth but did not support intensive biomass formation. These outcomes indicate that EB was the most bioavailable dye in this solid-medium screening, whereas triphenylmethane dyes imposed a reduced growth even at the lower concentration tested. In most cases, no stained biomass was observed, indicating that the dye removal mechanism was biodegradation rather than adsorption.

Table 3.1 Results of a preliminary experiment on a solid substrate (Ayaz, K., & Zabłocka-Godlewska 2022)

Strain/selective factor BG or EB	Time	Triphenylmethane dyes				Azo dyes	
		Brilliant green (BG)		Crystal violet (CrV)		Evans blue (EB)	
		50 mg/L	100 mg/L	50 mg/L	100 mg/L	50 mg/L	100 mg/L
	24h	-	-	-	-	G	G
P1.1 /BG	3d	-	-	-	-	G/D	G/D
	7d	Gw/D	-	Gw	-	G! /D/BS	G/D
	24h	-	-	-	-	G	G
P1.2/EB	3d	-	-	-	-	G/D	G/D
	7d	Gw/D	-	Gw	-	G! /D/BS	G/D
	24h	-	-	-	-	G	G
P3.2/EB	3d	-	-	-	-	G/D	G/D
	7d	Gw/D	-	G	-	G/D	G/D
	24h	-	-	-	-	G	G
P3.3/EB	3d	-	-	-	-	G/D	G/D
	7d	Gw/D	-	Gw	-	G/D	G/D
	24h	-	-	-	-	G	G
P3.4/EB	3d	-	-	-	-	G/D	G/D
	7d	Gw/D	-	Gw	-	G/D	G/D
	24h	-	-	-	-	G	G
1K1/EB	3d	-	-	-	-	G/D	G/D
	7d	Gw/D	-	Gw	-	G!/D/BS	G/D
	24h	-	-	-	-	G	G
1K1K2/EB	3d	-	-	-	-	G/D	G/D
	7d	-	-	Gw	-	G/D	G/D
2K1/EB	24h	-	-	-	-	G	G
	3d	-	-	-	-	G/D	G/D
	7d	-	-	Gw	-	G/D	G/D
	24h	-	-	-	-	G	G
3K1/EB	3d	-	-	-	-	G/D	G/D
	7d	-	-	Gw	-	G/D	G/D
4K1/EB	24h	-	-	-	-	G	G
	3d	-	-	-	-	G/D	G/D
	7d	Gw/FC	FC	Gw	-	G/D	G/D
	24h	-	-	-	-	G	G
4K2/EB	3d	-	-	-	-	G/D	G/D
	7d	FC	FC	Gw	-	G/D	G/D
	24h	-	-	-	-	G	G
4K3/BG	3d	-	-	-	-	G/D	G/D
	7d	FC	FC	Gw	-	G/D	G/D
	24h	-	-	-	-	G	-
9K3/EB	3d	-	-	-	-	G/D	G/D
	7d	-	-	Gw	-	G/D/FC	G/D
	24h	-	-	-	-	G	G
9K4/EB	3d	-	-	-	-	G/D	G/D
	7d	-	-	Gw	-	G! /D/FC	G/D/FC
	24h	-	-	-	-	-	-
9K5/EB	3d	-	-	-	-	G/D	G/D
	7d	-	-	Gw	-	G! /D/FC	G/D

Explanation of the designations used in the table: (-) no microbial growth, (G) bacterial growth, (Gw) weak bacterial growth, (G!) intensive growth, (BS) stained biomass, (D) discoloration of medium (decolorized zones), (FC) fungal contamination.

The tolerance pattern showed in this experiment (EB > CV > BG) aligns with dye class–specific toxicity. Triphenylmethane dyes (BG and CV) are widely reported as bioactive inhibitors with antimicrobial and genotoxic effects that suppress microbial growth, thereby inhibiting growth-coupled decolorization. CrV, in particular, is well recognized as persistent and genotoxic, underscoring the need for effective biological detoxification strategies (S. Mani

and Bharagava 2016). BG and other triphenylmethanes have likewise been flagged for adverse health and safety concerns in exposure-focused environmental evaluations, underscoring that these dyes are not merely colorants but can act as biologically active stressors at relatively low levels (Oplatowska et al. 2011). In practical terms, the weak or absent growth on BG and CV plates strongly suggests that, under the conditions tested, toxicity is also a factor and not only recalcitrance is the primary bottleneck for actinomycete-driven removal of triphenylmethane dyes in this screening format.

Mechanistically relevant point is that increasing dye concentration intensified inhibition, which is a well-established pattern for dye–microbe systems: higher dye concentration can elevate membrane stress, redox imbalance, and can also increase the probability of nonspecific binding to biomass and extracellular polymers that impair nutrient uptake bacteria growth and colony expansion. Reviews on dye contamination and treatment consistently stress that concentration is a key determinant of both biodecolorization kinetics and microbial viability, particularly for structurally complex aromatic dyes (Tkaczyk, Mitrowska, and Posyniak 2020). Our EB decolorization results align with this expectation: that although EB allowed growth and decolorization at both 50 and 100 mg/L, the disappearance of intensive growth at 100 mg/L indicates a shift from acceptable to more stressful conditions at higher concentration, even when decolorization remains visually detectable.

Importantly, the comparatively robust decolorization of EB dye is consistent with recent actinomycete-focused evidence showing that *Streptomyces* spp. can biodegrade Evans Blue effectively, while also demonstrating that performance is sensitive to operating factors, including dye concentration and other matrix stressors. For example, Kameche et al. (2022) reported high EB elimination by multiple *Streptomyces* strains and explicitly noted concentration effects on biodegradation performance (Kameche et al. 2022). Taken together, the screening results partially supports the dissertation objective for section 2.4: evaluation of the decolorization efficiency of selected dyes (EB, BG and CV) by isolated bacteria belonging to actinomycetes and indicates that dose-dependent stress is a realistic constraint that should be quantified, particularly when moving from qualitative plate observations to controlled liquid assays and when assessing whether carriers can stabilize performance under higher dye concentration.

Results - main experiment

Following the screening results, carrier-assisted cultivation was applied to enhance actinomycete biomass retention and to improve dye removal performance under submerged conditions. Therefore, several organic lignocellulosic (plant-derived) carriers were evaluated as growth supports. In the first stage of the experiment, the ability of the selected solid carriers to sustain actinomycete growth during liquid incubation was assessed. After 7 days, visible growth was observed in bottles containing the liquid medium without carriers and in systems supplemented with straw, but no growth was detected in the presence of wooden shavings or wood chips. This outcome is consistent with the known antimicrobial activity of wood-derived polyphenols, particularly condensed tannins, which can inhibit bacterial growth by interacting with cell envelopes and proteins. Reports on tannin-rich bark and tannin-containing matrices show measurable growth inhibition against bacteria, supporting the probability that inhibitory phenolics released from wood during sterilization process (autoclaving) suppressed actinomycete growth (Filho et al. 2022; Villanueva et al. 2023).

In the second stage, based on secondary screening performance and the intensity of biomass growth on solid medium, strain 1K1 (isolated in this study) and strain EGK2 (strain from the departmental strain collection with proved abbilty of synthetic dyes decolorization) were selected for liquid-phase experiments. Decolorization efficiency was quantified for BG, (triphenylmethane dye) and EB (diazo azo dye) using UV–Vis–based concentration estimates. In biomass-only systems, BG removal was strongly strain-dependent. After 14 days, EGK2 achieved 89% BG removal, whereas 1K1 reached 61% (Figure 3.1a). Adding straw increased BG removal by both strains, with EGK2 reaching 89% by day 7 and 97% after 14 days and in the case of strain 1K1 it was only 62 and 66% respectively (Figure 3.1b). However, substantial BG removal was also observed in the straw-only control (70% and 74% at 7 and 14 days; Figure 3.1c). This suggests that in samples containing straw and biomass, a significant share of BG removal can be attributed to the sorption process on the lignocellulosic material and not solely to biological transformation, as also reported by other studies (Vyavahare et al. 2021). These results may also suggest that the straw can play a role of easier substrate for both strains, so their attribution in dye removal might be lower in presence of additional substrate. The strong affinity of cationic triphenylmethane dyes for agricultural residues and straw-derived sorbents is well documented, including studies demonstrating efficient BG sorption by straw biochar and other plant-based matrices through surface and functional-group interactions (Vyavahare et al. 2021; Saif Ur Rehman et al. 2016; Ali, Zeidan, and Amar 2023).

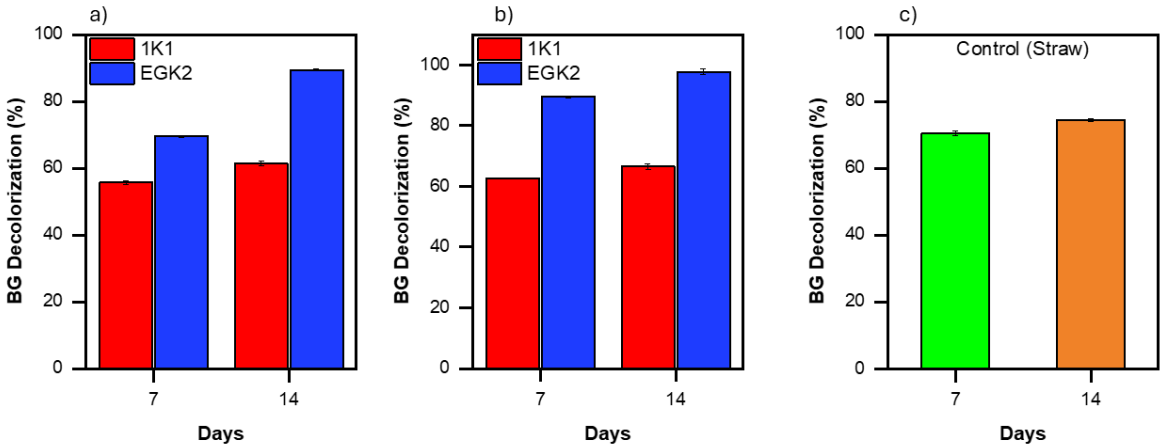

Figure 3.1 Percentage Removal of triphenylmethane brilliant green after 7 and 14 days a)Substrate + biomas, b) Substrate + straw + biomass, c) Straw alone

The EB removal results differed qualitatively from BG removal, suggesting a larger biological contribution. In the presence of substrate and only bacteria biomass without carrier, EB removal by 1K1 was 66% at day 7 and 67% at day 14, while EGK2 achieved 59% and 61% (Figure 3.2a). Such a small or no increase in dye removal efficiency after the next 7 days (14 days of the process) could have been caused by sorption and saturation of the biomass after just 7 days, as well as could have been the result of the accumulation of toxic secondary metabolites inhibiting bacterial growth and therefore decolorization processes. In samples with biomass immobilized on straw, EB removal, compared to biomass alone, increased only after 14 days of the process to 80% for 1K1 and to 64% and 73% for EGK2 at 7 and 14 days, respectively (Figure 3.2b). Straw alone showed limited EB adsorption, 40% on day 7 and 23% on day 14 (Figure. 3.2c). The two-fold lower result after 14 days indicates a dye desorption process, which is probably related to the weak affinity of the dye to the carrier surface. A slight increase of approximately 13% in dye removal in samples with immobilized biomass (in comparison with biomass alone) after 14 days of incubation confirms the weak affinity of the dye for the carrier and the participation of mainly biomass in EB removal. This pattern is consistent with broader evidence that azo dye removal typically depends on enzymatic reduction and downstream transformation steps rather than simple sorption, and that actinobacteria, including *Streptomyces*, can mediate azo dye decolorization via oxidative and reductive enzyme systems (El Awady et al. 2024; Cuebas-Irizarry and Grunden 2024).

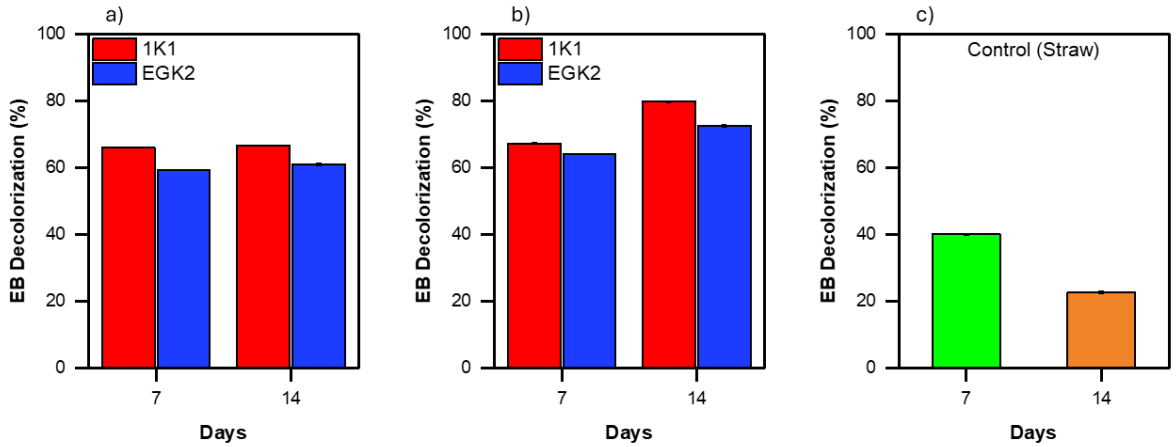

Figure 3.2 Percentage removal of azo dye Evans blue after 7 and 14 days A) Substrate + biomas, B) Substrate + straw + biomass, C) Straw alone

Strain EGK2 removed BG more efficiently (up to 97% with straw) than 1K1. However, strain 1K1 was slightly more effective in removing EB, achieving the highest level of EB removal (80%) when immobilized on straw. Such strain-specific selectivity is typical for actinomycetes, as dye transformation depends on enzyme systems and redox capabilities, that vary among species and even isolates. Recent studies continue to report strong but dye-specific decolorization by Streptomyces and related actinomycetes, reinforcing the value of isolate screening before process scale-up (El Awady et al. 2024; Adenan, Lim, and Ting 2021a).

Overall, straw served as a compatible support that improved observed removal for both dyes, but the mechanistic interpretation is dye specific. For BG, the high removal in straw-only samples demonstrates that straw contributes strongly via physical sorption; therefore, the additional improvement with straw plus biomass likely reflects a combined effect of adsorption (rapid color removal) and biomass retention on the carrier. Nevertheless, it should be noted that results of increased dye removal are not additive.

In the case of EB, the relatively low dye removal by straw alone and the higher removal in the straw-biomass combination suggest a primarily biological process, supported by physical sorption, although to a lesser extent than in the case of BG. Again, no additive effect was observed.

The use of straw as a carrier may have contributed to stabilizing bacterial growth conditions and increasing their decolorization activity against both dyes. At the same time, the low level of increase in decolorization efficiency (5-20%) in the straw-biomass samples in comparison with biomass alone, may indicate a reduced contribution of biological processes to dye removal in the presence of a potentially easier substrate, such as straw.

In summary, the experimental results from section 2.4 highlighted several limitations associated with the use of newly isolated actinomycete strains. First, dye removal in carrier-based systems reflected a combination of physical sorption, biodegradation associated with bacterial growth, and possible desorption during, for example, carrier degradation, making it difficult to separate the biological decolorization activity from physical processes. Second, the relatively long incubation time required to achieve the desired decolorization effect constitutes a significant technological drawback. Similar limitations regarding actinomycete-based decolorization processes, particularly under aerobic conditions, have been reported in other studies, emphasizing the need to better define the systems to elucidate degradation pathways and kinetics (Ramasamy and Sudalaimuhu 2022; Rane and Joshi 2021; Chakravarthi, Mathkala, and Palempalli 2021).

Based on the results presented in this chapter and supporting literature, subsequent experiments in this dissertation were aligned around EB as the principal model dye. Important argument for choosing this dye for further studies is the fact that EB is an azo dye, which means it belongs to the group of dyes used by industry most commonly and in the largest quantities. Dye concentration is a critical operational determinant in biological treatment: increasing dye load can suppress microbial activity and slow decolorization. Accordingly, the remaining experimental work was designed to address this constraint by systematically optimizing operating conditions to achieve efficient EB removal at higher initial concentrations within shorter treatment times.

Conclusions and further research directions

Chapter 3.1 demonstrated that actinomycete isolates can support EB and BG decolorization; however, the efficiency remains strain-dependent and may be enhanced by dye adsorption by the carrier used, the choice of which cannot be random. However, for further studies it was decided to abandon this line of research due to the ambiguity of the results, which hindered mechanistic interpretation and process optimization, lower-than-expected decolorization efficiency, and the required long process time. Therefore, there was made the decision to change the research direction. That is why in the next stage (Chapter 3.2), the research was focused on the EB dye removal optimization using the electroactive model strain *Shewanella oneidensis* MR-1, for which had previously been confirmed abilities to remove other dyes and according to our knowledge *Shewanella oneidensis* MR-1 have never been tested in the term

of EB dye removal. Statistical optimization studies were planned to quantify the interactions of key operational variables in the EB transformation processes.

3.2 Pure-Culture Biodecolorization of Evans Blue by *Shewanella oneidensis* MR-1

EB is a highly sulfonated disazo dye which has aromatic structure and aqueous stability that makes it particularly resistant to biological remediation. Recent literature reviews pointed out that initial dye concentration, temperature, incubation time, and electron-donor availability as dominant factors controlling both biological decolorization kinetics and ultimate removal efficiency for structurally complex azo dyes (G. B. Singh et al. 2024; Balachandran and Sabumon 2025). The results presented in section 3.1 demonstrated that, although actinomycete pure cultures can achieve substantial Evans Blue removal, performance remained strain-dependent and required relatively long incubation periods to approach expected efficiency decolorization. These results led author to focus on another biological system, a pure strain of *Shewanella oneidensis* MR-1, and to attempt to define a mechanistically interpretable framework that would enable methodical identification of the roles and interactions of key operational variables.

To address this requirement, the section 3.2 focuses on the pure culture *Shewanella oneidensis* MR-1 a model exoelectrogenic bacterium. *S. oneidensis* MR-1 is well established for its respiratory versatility and extracellular electron-transfer capability. This bacterial strain has been widely employed to interrogate reductive transformations of complex organic compounds under controlled laboratory conditions. Previous and recent studies confirm that *S. oneidensis* MR-1 can effectively decolorize azo dyes when suitable electron donors and environmental conditions are provided, making it a robust platform for quantitative optimization and mechanistic analysis (G. Liu et al. 2011; Y. Wang et al. 2025). The goal of using *Shewanella oneidensis* MR-1 in studies presented in this chapter was to investigate the process of decolorization and biodegradation of Evans blue by this bacterium, process optimization via response surface methodology (RSM) with parallel determination of degradation products. The central objective of this chapter is therefore to create a statistically rigorous definition of the operating window governing Evans Blue decolorization by a single bacterial strain. Classical one-factor-at-a-time approaches are inadequate for this purpose, as they fail to capture interaction effects that often control real process behavior. Response surface methodology (RSM) is a well-established optimization framework for efficiently evaluating multivariable systems and has been successfully applied to dye biotreatment, where significant interactions among temperature, time, and dye loading have been shown to alter

both predicted optima and process robustness (Zin et al. 2020; P. Sharma, Singh, and Dilbaghi 2009).

Accordingly, the results and discussion in this chapter present an RSM-based evaluation of Evans Blue decolorization by *S. oneidensis* MR-1, in which incubation time, temperature, initial dye and electron donor concentrations are systematically varied. Decolorization efficiency was quantified by UV–Vis's spectroscopy, while molecular-level dye transformation products were verified using complementary HPLC and GC–MS analyses to confirm dye breakdown or mineralization rather than simple color removal because of azo bonds breakdown (methodology in section 2.5). By integrating statistical optimization with product-level verification, this chapter establishes a mechanistically grounded and process-relevant operating window.

Most results presented in this chapter were published in the research paper entitled "*Sustainable biodegradation of Evans blue (Direct Blue 53) by Shewanella oneidensis MR-1: Response surface optimization and product analysis*" by Ayaz, K., Zabłocka-Godlewska, E., Smołka, S., Kudlek, E., Hussain, I., & Ilyas, M. (2026a). *Journal of Water Process Engineering*, *81*, https://doi.org/10.1016/j.jwpe.2025.109399.

3.2.1 Decolorization efficiency

Decolorization efficiency was determined spectrophotometrically. UV–Vis spectra recorded over 400–800 nm exhibited the typical visible absorption band of EB at 606 nm, which decreased steadily during the decolorization process performance (from 2 to 72 h), confirming progressive decolorization. In addition, weak transient features (peaks) appeared in the near-UV region (approximately 250–500 nm) at intermediate time points (about 24–48 h), suggesting the temporary formation of UV-absorbing transformation intermediates that subsequently declined (Figure 3.3). The overall degradation trends for Evans Blue are summarized in Figure 3.5. The corresponding percentage decolorization efficiency are provided in Figure S6.1, while Figure 3.4 presents representative images of EB treatment at carbon-source concentrations of 250, 500, and 1000 mg/L under different temperatures (25, 30, and 37 °C), incubation times (24, 48, and 72 h), and initial dye concentrations (25, 50, and 100 mg/L). However, the images were taken after 72 hours that's only shows complete decolorization in the flasks. Collectively, these results indicate that *Shewanella oneidensis* MR-1 can effectively decolorize EB, with performance dependent on temperature, incubation time, electron-donor availability, and initial dye loading.

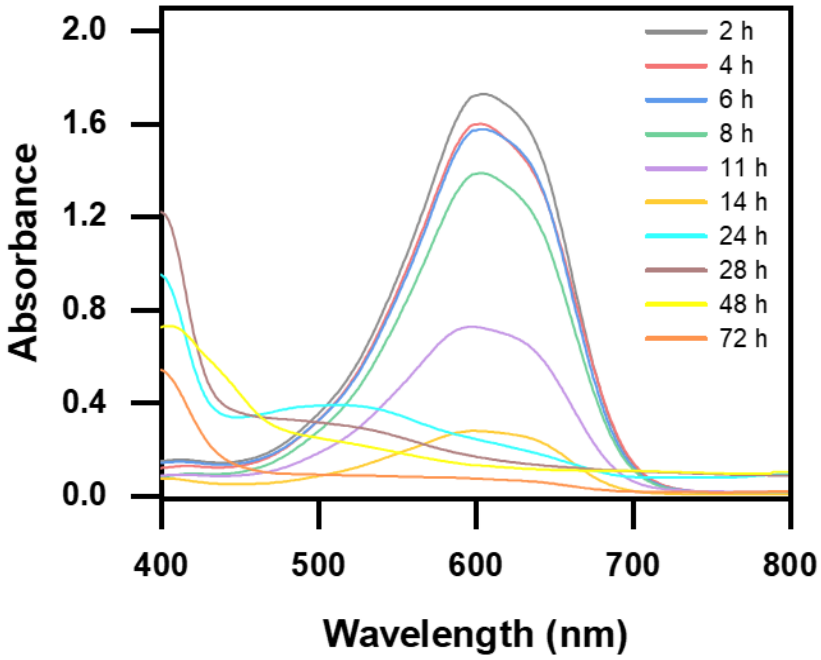

Figure 3.3: UV–Vis spectra (400–800 nm) of Evans blue during treatment with S. oneidensis MR-1 at 50 mg/ L and 30 °C, sampled at 2, 4, 6, 8, 11, 14, 24, 28, 48, and 72 h. The characteristic visible band near 606 nm decreases progressively, indicating decolorization over time (K.Ayaz et al. 2026a).

Figure 3.4 Images of abiotic (left flasks) and biotic (right flasks) samples of Evans Blue dye at different concentrations (25,50, and 100 mg/L) degraded in the presence of 0.25 g/l glucose at different temperatures (25, 30, and 37 °C) after 72 h of incubation (K. Ayaz et al. 2026a Supplementary materials).

At the lowest glucose concentration of 250 mg/L (Figure 3.5a-c, Figure S6.1), the residual dye concentration after 24 h at 25 °C was 16.16 ± 0.03 mg/L (4.7% removal) at 25 mg/L, 33.58 ± 0.34 mg/L (33.1% removal) at 50 mg/L EB, and 77.68 ± 0.22 mg/L (10.3% removal) at 100 mg/L EB, The nominal Evans Blue doses were 25, 50 and 100 mg/L but the measured initial concentrations in the flasks were 16.96 ± 0.01, 50.17 ± 0.64, and 86.59 ± 0.56 mg/L,

respectively, and these values were used as C_0 in all calculations (the lower real initial concentration in samples was a result of the filter sterilization of dye solutions). In abiotic controls, EB remained close to these initial values over 72 h, indicating that physicochemical loss of dye was insignificant for experiment (e.g., adsorption or spontaneous fading). Thus, net biological decolorization in inoculated flasks was interpreted relative to the corresponding abiotic control. This finding demonstrated that the observed dye removal was mostly biotic in nature rather than abiotic.

The low removal of EB dye in different concentrations could be because of low-temperature of incubation at 25°C. Raising temperature to 30°C significantly influenced the efficiency of the decolorization process conducted by *Shewanella oneidensis* MR-1. Higher temperatures probably caused an increase in the activity of the enzymatic systems responsible for this process. At higher temperatures, degradation improved markedly; after 24 h at 30 °C, the dye was almost completely removed, with residual concentration only 1.67 ± 0.16 mg/L (97.8% removal at 100 mg/L). In comparison, at 37 °C, complete removal occurred across all dye concentrations. After 48 h, even at 25 °C, the residual dye concentration decreased to less than 1.2 mg/L across all loads (>98% removal), whereas at 30 °C and 37 °C, nearly complete decolorization occurred (Figure 3.4). These findings are consistent with prior reports that mesophilic bacteria, such as *Shewanella oneidensis* MR-1, achieve maximum azo dye degradation within the 30–37 °C range because of enhanced azoreductase activity and improved membrane permeability (Jiale Liu et al. 2023; Chen, Hopper, and Cerniglia 2005; Abboud et al. 2005; Saratale et al. 2011).

At a glucose concentration of 500 mg/L (Figure 3.5 d-f, Figure S6.1), EB biodegradation followed the same temperature-dependent pattern as that observed at lower glucose concentrations (250 mg/L), but the effect of the initial dye concentration was more apparent. After 24 h of sample incubation at 25 °C, considerable amounts of dye remained. The residual concentrations were 18.77 ± 0.11, 37.11 ± 0.00, and 76.90 ± 0.27 mg/L at initial dye concentrations of 25, 50, and 100 mg/L, corresponding to removal efficiencies of approximately 19%, 24%, and 12%, respectively. Increasing the incubation temperature to 30 °C markedly enhanced EB removal, reducing the residual dye concentration to 6.46 ± 0.32, 24.06 ± 0.13, and 64.33 ± 0.44 mg/L (73%, 47%, and 25% removal), whereas at 37 °C, decolorization was essentially complete across all concentrations (≤ 1 mg/L). Additionally, extending the incubation time to 48 h caused the increase the dye decolorization efficiency; the residual dye concentration decreased to 10.95 ± 0.76 mg/L at 50 mg/L and 23.8 ± 0.008

mg/L at 100 mg/L at 25 °C, and almost complete and complete dye removal occurred at 30 and 37 °C, respectively. After 72 h, residual dye was negligible under nearly all conditions; even at the most challenging condition (100 mg/L at 25 °C), only 5.89 ± 0.38 mg/L remained, whereas all other treatments achieved almost complete removal. These results are consistent with previous reports showing that high azo dye concentrations initially slowdown the dyes degradation (S. Zafar, Bukhari, and Rehman 2022), cause competition for electron-acceptor sites at the cell surface (Balachandran and Sabumon 2025), and the accumulation of inhibitory toxic aromatic amines (Aragaw 2024a). However, this inhibition tends to diminish over time, as cells induce degradative enzymes and accumulate redox mediators, allowing decolorization to proceed more efficiently during prolonged incubation time (El Awady et al. 2024).

At a glucose concentration of 1000 mg/L (Figure 3.5 g-i, Figure S6.1), the initial phase of EB decolorization was notably slower, despite the greater availability of the electron donor. After 24 h of incubation, substantial amounts of dye remained at all series of temperatures. At 25 °C, the dye residual concentrations were 12.78 ± 0.11 mg/L, 33.31 ± 0.11 mg/L, and 77.36 ± 0.53 mg/L for initial loads of 25, 50, and 100 mg/L, respectively. These results are similar to those reached for glucose concentrations of 250 and 500 mg/L at 25 °C. At 30 °C, the heaviest load (100 mg/L) was 71.81 ± 0.08 mg/L, whereas at 37 °C, it was 61.63 ± 0.15 mg/L under the same conditions. This slowdown of process and decrease of efficiency suggests that excess donor availability induced a carbon catabolite repression (CCR)-like effect, in which preferential metabolism of simple in structure and bioavailable carbon sources temporarily suppressed the reductive pathways responsible for complex structure dye degradation. Even the extended incubation time did not overcome this process lag: by 48 h at 37 °C, lower but not complete removal was observed at 25, 50, and 100 mg/L, and by 72 h, the residual dye at 100 mg/L declined to 4.05 ± 0.03 mg/L, corresponding to almost 95% removal. This course of the dye removal process is consistent with previous studies on Shewanella strains , in which an excess of donors or alternative acceptors delayed azo respiration (Y. Hong et al. 2007) until the induction of EET components and azoreductases (Marsili et al. 2008; Zhao et al. 2023).

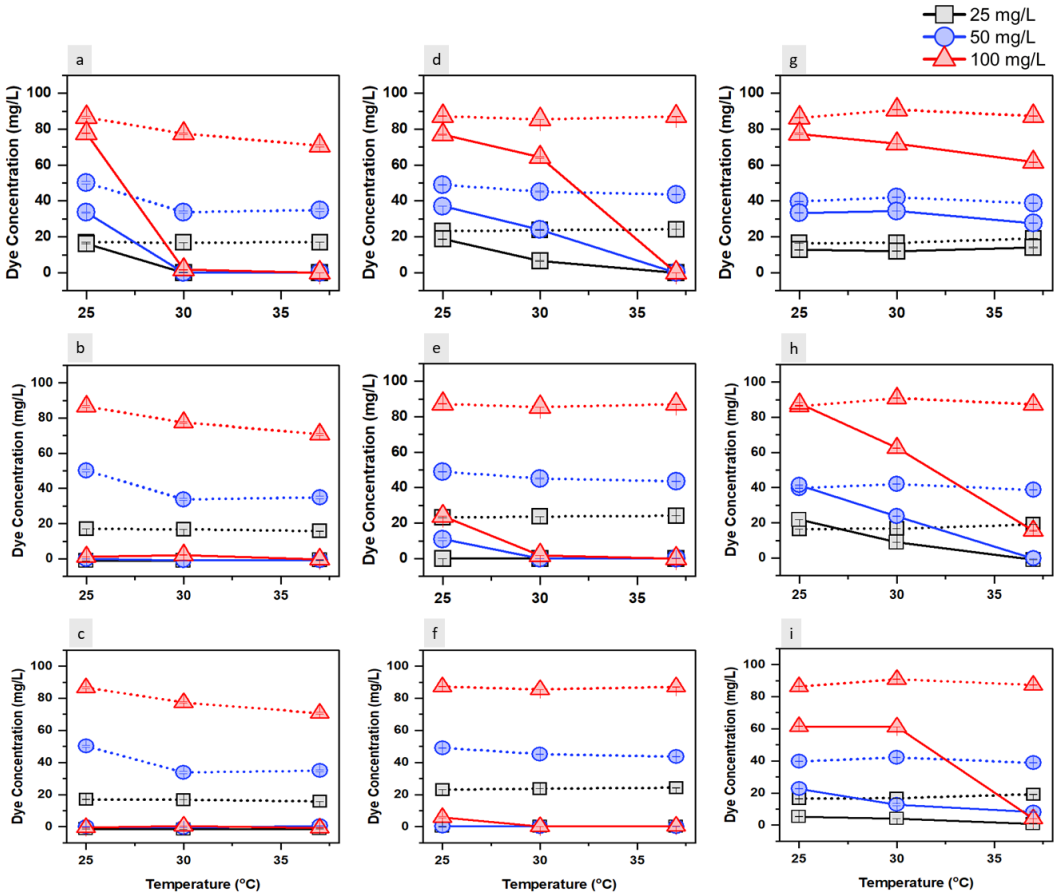

Figure 3.5 Decolorization of Evans blue by Shewanella oneidensis MR-1 at various glucose concentrations, dye concentrations, incubation times, and temperatures. Panels (a–c) represent the results at 250 mg/L glucose, (d–f) 500 mg/L, and (g–i) 1000 mg/L. Each panel shows the residual dye concentrations (mg/L) after 24, 48, and 72 h at three initial dye loads (25, 50, and 100 mg/L) and temperatures (25, 30, and 37 °C). The dotted line represents the abiotic control, whereas the solid line represents Shewanella oneidensis MR-1 degradation (K. Ayaz et al 2026a).

During the literature studies, readers' attention can be drawn to the fact that most of the studies on *Shewanella oneidensis* MR-1 used in decolorization of azo dyes have been conducted in strictly anaerobic, lactate-fed systems. The result obtained in this study shows that EB can be efficiently degraded also under initially aerobic, glucose-amended conditions. This conclusion is additionally supported by the comparative validation experiment (Section 2.5.4) performed at the RSM-derived optimum (100 mg/L EB, 250 mg/L glucose, 37 °C; Figure 3.8), where four operating regimes - (i) aerobic–glucose, (ii) aerobic–lactate, (iii) anaerobic–glucose, and (iv) anaerobic–lactate, were tested. In all four operating regimes EB dye reached 93–96% removal within 60 h of incubation. The comparable endpoint decolorization across redox conditions and with different electron donors, with slightly faster rate under aerobic–lactate, indicates that strain *S. oneidensis* MR-1 can reduce EB dye under both oxic and anoxic conditions when a suitable organic electron donor is present. These findings validate model

predictions and support the mechanistic basis for using aerobic, glucose-amended operation. Consistently, recent studies presented results of rapid oxic decolorization of azo dyes such as methyl orange and amaranth by *S. oneidensis* MR-1 while implicating cytochrome Mtr-associated extracellular electron transfer pathways (Xiao et al. 2012; Wu et al. 2012; Y. Wang et al. 2025).

Considering the mechanistic point of view, the observed patterns are consistent with three interaction features widely reported for *S. oneidensis* MR-1 and likely operate here in our system as well. (i) First, membrane-linked azoreduction and extracellular electron transfer (EET): strain *S. oneidensis* MR-1 couples intracellular catabolism to extracellular acceptors through the inner-membrane quinone pool, periplasmic cytochromes, and outer-membrane Mtr/Omc c-type cytochromes (Coursolle and Gralnick 2010). Secreted flavins (FMN and riboflavin) play a role of soluble and surface-associated electron shuttles, and their time-dependent accumulation may explain the progressive increase in Evans Blue removal from 24 to 72 h, particularly at higher dye loads (Marsili et al. 2008; Y. G. Hong and Gu 2010). (ii) Second, temperature-dependent kinetics: although MR-1 exhibits optimal growth near 30 °C, EET components and dye-reducing enzymes can display higher catalytic activity at moderately elevated temperatures, consistent with faster decolorization at 37 °C than at 30 °C (Abboud et al. 2005; Saratale et al. 2011). (iii) Third, dye structure, its load, and glucose-driven reducing power: EB is a highly sulfonated diazo dye with strong anionic character and high aqueous stability, traits linked to slower early-stage decolorization and greater recalcitrance than simpler monoazo dyes such as Eriochrome Black T, especially at higher initial concentrations (Yao et al. 2018; Chaieb, Hagar, and Radwan 2016). In this system, glucose served as a readily metabolizable electron donor that supports central carbon metabolism and NAD(P)H generation under oxic conditions, supplying reducing equivalents to intracellular azoreductases and the CymA–MtrCAB EET route (Kouzuma et al. 2015; Yanbo Li, Liu, and Shi 2023; Jiale Liu et al. 2023). The combination of these intracellular and extracellular pathways provides a mechanistic basis for the shift from delayed to almost complete removal of Evans Blue dye with increasing incubation time and decreasing load of readily digestible carbon substrate.

The control (abiotic) samples were incubated at the same conditions as the biotic once. A comparison of the results of dye concentration in abiotic and biotic samples after given period of incubation confirmed that EB removal was mostly attributable to microbial activity rather than abiotic degradation. Before discussion of this part of result it should be pointed out that,

despite that initial loads were established as 25, 50, and 100 mg/L, nevertheless after filter sterilization the reached real initial concentrations were lower at 16.96 ± 0.01, 50.17 ± 0.64, and 86.59 ± 0.56 mg/L respectively, and these values were used as C_0 in all calculations. The abiotic controls (MSM + glucose + EB without bacteria biomass), the dye concentrations essentially remained unchanged over 24–72 h at all temperatures; for example, at 250 mg/L glucose and 24 h of incubation, the residual dye concentrations in growing order were 16.96 ± 0.01, 50.17 ± 0.64, and 86.59 ± 0.56 mg/L, which was the same as real initial loads, , and at 500 mg/L glucose, the corresponding values were 23.07 ± 0.04, 49.04 ± 0.20, and 87.27 ± 0.07 mg/L, respectively. respectively. In contrast to abiotic samples, inoculated with bacteria (biotic) samples under optimal conditions (30–37 °C) presented nearly complete decolorization, with residual dye concentrations approaching zero by 24–48 h for 250 and 500 mg/L of glucose and falling below 4.05 ± 0.03 mg/L (~95% removal) at 1000 mg/L electron donor and 100 mg/L dye after 72 h. The clear divergence between the biological and abiotic treatments demonstrated that decolorization was enzymatically driven.

Obtained results showed the enhanced removal at 37 °C, which may be associated with activation of *S. oneidensis* MR-1's EET system, which relies on outer-membrane c-type cytochromes (Mtr/Omc) to reduce extracellular substrates (Coursolle and Gralnick 2010). The flavins (FMN, riboflavin) secretion caused the further accelerate azo bond reduction by acting as soluble shuttles (Marsili et al. 2008). The time-dependent improvement, therefore, likely reflects flavin accumulation and azoreductase induction under anaerobic or microaerophilic conditions (Y. G. Hong and Gu 2010). In contrast, the high residual dye levels in the abiotic controls confirmed the structural recalcitrance of EB, a sulfonated diazo dye resistant to abiotic degradation, e.g., at various temperatures (Zabłocka-Godlewska, Przystaå, and Grabińska-Sota 2014). These findings highlight the strong potential of *Shewanella oneidensis* MR-1 for bioremediating persistent azo dyes and allow us to consider this bacterial strain as a promising candidate for further research on the decolorization of other azo dyes and dyes from other groups. All these data together support a model in which moderate donor availability (250, 500 mg/L), temperatures optimal for mesophiles (30–37 °C), and adequate time of incubation (48–72 h at the highest loads) accelerate EB decolorization by *Shewanella oneidensis* MR-1. These findings agree with broader literature data about azo-dye biodegradation that emphasizes temperature-activated azoreduction, load-dependent lags, and the central role of EET and redox mediators in the cells of bacteria species (Y. Hong et al. 2007; Saratale et al. 2011). Our results presented in this part of dissertation, did not apply an electrode, redox

mediator, or targeted inhibition of the CymA–MtrCAB pathway, and no direct measurement of EET-linked currents or flavin dynamics were performed. Accordingly, the proposed contribution of EET to Evans Blue degradation should be viewed as a hypothesis in this dissertation grounded in established *S. oneidensis* MR-1 physiology, rather than a mechanism demonstrated experimentally here. Dedicated follow-up studies combining dye decolorization with electrochemical measurements and genetic or chemical perturbation of key EET components will be required to quantify the specific role of EET in Evans Blue reduction by *S. oneidensis* MR-1. This will be the direction of further experiments.

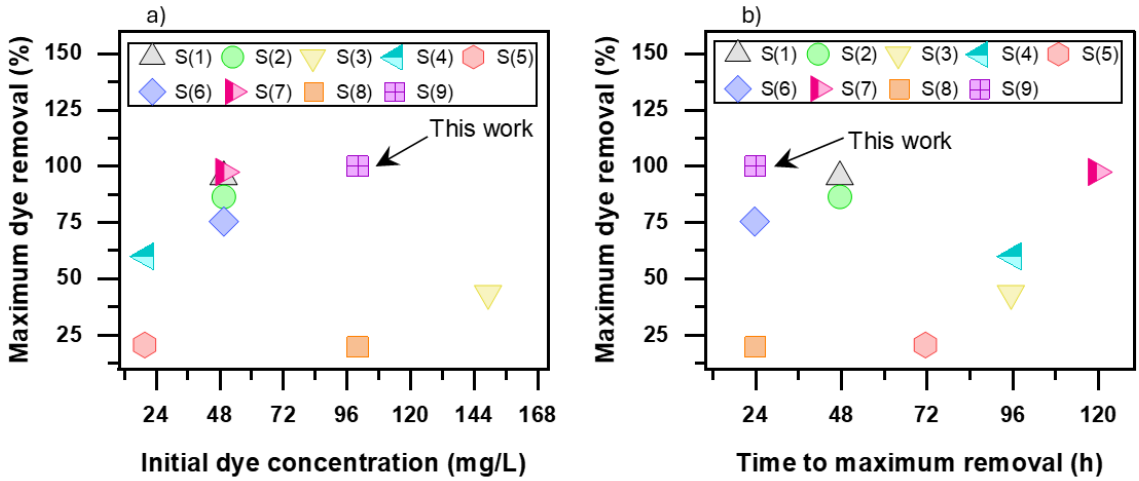

Figure 3.6 (a) Comparison of time required to achieve peak Evans Blue decolorization across microbial strains from multiple studies, highlighting the superior rapidity of Shewanella oneidensis MR-1 in this study, and (b) Comparison of Effect of initial dye concentration on maximum Evans Blue removal efficiency across microbial strains, highlighting variability among bacteria, fungi, actinomycetes (from other studies), and Shewanella oneidensis MR-1 from this study. Each symbol (S1–S9) represents a literature study as taken from the original publications, and experimental conditions (temperature, medium composition, carbon source, etc.) differ between studies. Details are provided in Table 3 (K. Ayaz et al. 2026a)

The comparison of the efficiency of EB dye decolorization (%) by different microorganisms species and the corresponding incubation time reported in the various literature sources are presented in Table 1-3 and Figure 3.6 a,b (Zablocka-Godlewska, Przystas, and Grabinska-Sota 2012; Przystś, Zabłocka-Godlewska, and Grabińska-Sota 2013; Przystaś, Zabłocka-Godlewska, and Grabińska-Sota 2019; Ravi et al. 2025; Kameche et al. 2022; Chaieb, Hagar, and Radwan 2016). In Figure 3.6 a-b, each point represents a single study plotted at its own reported maximum decolorization and time, so the plots are intended as a visual overview of reported results rather than a strict head-to-head comparison under identical experimental conditions (temperature, medium composition, carbon source, etc.). While many bacteria, fungi, and actinomycetes have shown promising results, examined in this study *Shewanella oneidensis* MR-1 stands out for achieving complete decolorization (100%) within just 24 hours

at 100 mg/L, which is much faster than other microorganisms presented in these figures and table (Figure 3.6 a-b, Table 1-3). In comparison, *Streptomyces* spp. achieved up to 97% removal in 120 hours at 50 mg/L, whereas *Pseudomonas fluorescens* strains Sz6 and SDz3 removed 95% and 86% of the dye, respectively, within 48 hours at 50 mg/L. Fungal strains such as *Pleurotus ostreatus* BWPH and K4 exhibited 60% and 20% removal, respectively, at 20 mg/L over 72–96 hours. These findings underscore *S. oneidensis MR-1* high efficiency and possibility of the rapid biodegradation of EB dye. This pointing out the strong potential of this bacteria strain and recommendation for practical application in wastewater treatment systems.

3.2.2 Response Surface Methodology (RSM) Model Fitting and Regression Analysis

Response surface methodology was used to evaluate the influence of several variables (factors): time (A), dye concentration (B), glucose concentration (C), and temperature (D) on EB removal (%). RSM quantified main, interaction, and quadratic effects with an economical number of runs and reliable in-region prediction (Kitanou et al. 2025; Anusi et al. 2025). The data set used for modeling is given in Supplementary Table S6-1. All factors were analyzed in coded units (−1, 0, +1). The full quadratic model was significant ($R^2 = 0.786$; adjusted $R^2 = 0.741$; $F_{14,\ 66} = 17.32$, $p = 6.39\times10^{-17}$). The difference between R^2 and adjusted R^2 was 0.045, which is less than 0.2 and indicates limited overfitting (Ameenudeen, Unnikrishnan, and Ramalingam 2021). Overall, the model explained 78.6% of the variability in dye removal.

The regression equation (in terms of coded variables) was as follows:

$$Y= 85.3939 + 18.0071A - 4.7327B - 23.0559C + 19.5085D - 10.5985A2 + 2.7069B2 - 8.6063C2 - 5.9484D2 - 0.6185AB + 2.2108AC - 10.7710AD - 3.3324BC + 2.3965BD + 5.6948CD + \varepsilon$$

where Y is the predicted dye removal efficiency, and A, B, C, and D represent the coded values of time, dye concentration, carbon concentration, and temperature, respectively.

ANOVA and Model Interpretation

Model adequacy depends on how well the fitted function represents the experimental data. We assessed fit by analysis of variance (ANOVA), which tests how changes in one factor affect the response while accounting for other factors (Bezerra et al. 2008). ANOVA showed a highly significant overall model ($F_{14,\ 66} = 17.32$, $p < 0.001$) and good ability to describe response variation within the studied range (Table 3-1). Among the Linear terms effects: time (A) and temperature (D) were strongly positive (both $p < 0.001$). Glucose as the carbon source (C) was strongly negative ($p < 0.001$). Dye concentration (B) showed negative effect of borderline (p

= 0.072). whereas Quadratic effects: the time-squared term (A^2) was significant (p = 0.015), indicating diminishing returns at longer times. The carbon-squared term (C^2) was borderline (p = 0.083). The dye-squared (B^2) and temperature-squared (D^2) terms were not significant.

Interactions between the terms showed that time × temperature term (AD) was significant and negative (p = 0.001). Thus, the marginal benefit of longer time decreases as temperature increases. The carbon × temperature term (CD) was borderline positive (p = 0.058), suggesting that higher temperature partly offsets the adverse effect of higher carbon. Other two-way interactions were not significant (p > 0.05).

Model diagnostics supported adequacy. Residuals were approximately normal (Omnibus p = 0.897; Jarque–Bera p = 0.902). There was no evidence of autocorrelation (Durbin–Watson = 2.26). The condition number was 7.08, indicating no problematic multicollinearity in the coded design space. Residuals were randomly scattered around zero in the residuals versus fitted plot. Points followed a straight line in the Q–Q plot (Figure S6.2). These patterns indicate normality and constant variance of errors (Roriz et al. 2009; Ameenudeen, Unnikrishnan, and Ramalingam 2021).

Table 3-1 Analysis of variance (ANOVA) results for the decolorization of Evans blue by Shewanella oneidensis MR-1 (K. Ayaz et al. 2026a)

Term	Sum of Squares	DF	F value	P value	Significance
Model	79 371.91	14	17.32	<0.001	Significant
Time (A)	18 339.06	1	56.04	<0.001	Significant
Dye (B)	1 091.33	1	3.33	0.072	Borderline
Carbon source (C)	28 571.05	1	87.30	<0.001	Significant
Temperature (D)	18 700.79	1	57.14	<0.001	Significant
A^2	2 021.90	1	6.18	0.015	Significant
B^2	100.49	1	0.31	0.581	Not significant
C^2	1 015.80	1	3.10	0.083	Borderline
D^2	596.50	1	1.82	0.182	Not significant
A×B	14.28	1	0.04	0.835	Not significant
A×C	182.48	1	0.56	0.458	Not significant
A×D	4 215.23	1	12.88	<0.001	Significant
B×C	429.94	1	1.31	0.256	Not significant
B×D	216.40	1	0.66	0.419	Not significant
C×D	1 221.96	1	3.73	0.058	Borderline
Residual (Error)	21 599.01	66	—	—	—
Total	100 970.91	80	—	—	—

Interactive Effects of Process Parameters

Three-dimensional response surfaces and two-dimensional contour plots were used to systematically explore the effect of key process parameters interactions on dye removal efficiency. (Figure 3.7). This method has been used in several studies (Shahi et al. 2021; Ameenudeen, Unnikrishnan, and Ramalingam 2021; Öge, Nural Yaman, and Buruk Şahin 2023; Jegan Durai et al. 2020).

The interaction between incubation time and temperature (A×D) was significant ($P = 0.001$; Figure 3.7a, b). The response surface showed steep increases toward longer times and higher temperatures. Together with the significant time curvature ($time^2$, $P = 0.015$), this indicates diminishing returns at extended durations.

The temperature × carbon interaction (C×D) was borderline ($P = 0.058$; Figure 3.7c, d). Higher temperature partly offset the inhibitory effect of higher glucose. In contrast, the time × dye interaction (A×B) was not significant ($P = 0.835$). The surface (Figure 3.7e, f) shows that longer time markedly increased removal, while changing dye from 25 to 100 mg/L had only minor effects. The dye × carbon interaction (B×C) was also not significant ($P = 0.256$). Even so, the surface (Figure 3.7g, h) indicates that higher glucose consistently depressed removal, confirming the independent negative effect of carbon. The time × carbon interaction (A×C) and the temperature × dye interaction (B×D) was not significant ($P = 0.458$ and $P = 0.419$; Figures 3.7i, j and 3.7k, l). Patterns were near-additive and dominated by strong main effects.

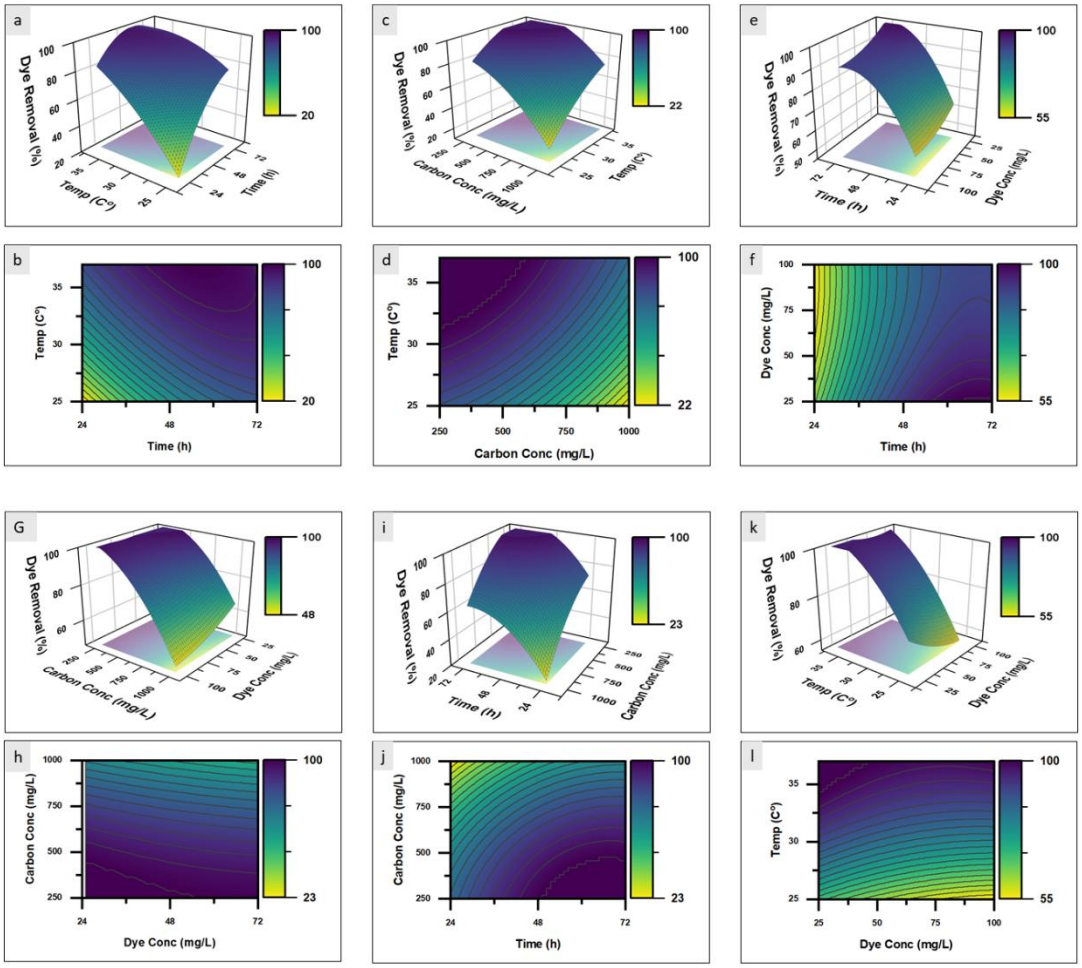

Figure 3.7 Three-dimensional response surfaces and contour plots for EB removal (%) with the remaining two factors fixed at their midpoint: (a, b) time with temperature, (c, d) carbon concentration with temperature, (e, f) dye concentration with time, (g, h) dye concentration with carbon concentration, (I, j) time with carbon concentration, and (k, l) dye concentration with temperature.). (a, c, e, g, I, k) 3D surface plot and (b, d, f, h, j, l) contour plot. (K. Ayaz et al. 2026a)

Observed the strong positive time and temperature effects are aligned with current reports on azo-dye bioremediation, which identify incubation time and temperature adequate for mesophilic bacteria growth and activity as primary levers for accelerating reductive cleavage of azo bonds and subsequent transformations (G. B. Singh et al. 2024). In particular, Evans blue is repeatedly flagged as recalcitrant among azo dyes, which is consistent with its significant curvature over time (Balachandran and Sabumon 2025).

The negative effect of increasing the glucose is mechanistically sound and aligns with recent studies on co-substrate impacts. Co-substrate type and dose control the redox balance. Oversupplying a readily fermentable carbon substrates can cause acid build-up and pH drop, which may inhibits bacterial growth and enzyme activity and reduces decolorization (Nguyen et al. 2025). This result is also consistent with *S. oneidensis* MR-1 physiology. The wild type is not a strong glucose utilizer without adaptation or engineering. It prefers organic acids such

as lactate and pyruvate. This helps explain why adding glucose did not substantially improve dye removal in our system (Nakagawa et al. 2015; J. Zhang et al. 2025).

Obtained results of this experiment the graphical trends align with the ANOVA results, highlighting incubation time and temperature as the dominant positive factors of EB removal, and glucose as a strong negative factor, and dye concentration as a secondary contributor within the tested range. It was proved that the high-performance region lies at long times of incubation and high temperatures with low glucose concentration. Based on the fitted quadratic RSM, the most favorable conditions within the studied ranges were identified at 53.65 h: dye = 100 mg/L, carbon = 250 mg/L, and temperature = 37 °C. Under these conditions, the model's uncapped prediction is 111.86%, which is capped at 100% to respect the physical bounds of the response, indicating complete removal under these conditions. To validate this prediction, an independent batch experiment in oxic and anoxic condition and addition two different electron donors (lactate and glucose) at the same factor levels (100 mg/L Evans Blue, 250 mg/L glucose, 37 °C) was performed with monitoring of decolorization process up to 60 h. Under these conditions, EB removal reached 93–96% across all four tested regimes (aerobic–glucose, aerobic–lactate, anaerobic–glucose, anaerobic–lactate). Reached results confirmed that almost complete decolorization is experimentally achievable at the point predicted by the RSM model. The corresponding time-course profiles for the four regimes are shown in (Figure 3.8 a), after 20 h, all systems exhibited low to moderate decolorization (<20%), whereas by 60 h, all regimes converged to >93% removal, with aerobic–lactate giving the highest final value (95.9 ± 1.0%) while aerobic and anaerobic glucose both giving values around 93.5%. These results are fully consistent with RSM, confirming the predictive power and practical usefulness of the statistical optimization approach used in this study. To assess whether our inoculum level adversely affected EB decolorization, we performed an additional experiment in which the inoculum volume of *S. oneidensis* MR-1 (0.5 McFarland suspension) was systematically varied while keeping all other conditions identical to the RSM optimized values (100 mg/L EB, 250 mg/L carbon source, 37 °C) (Figure 3.8 b) Triplicate cultures *S. oneidensis* MR-1 (0.5 McFarland suspension) were prepared with 1.0, 0.5, and 0.1 mL initial inoculum in both glucose- and lactate-amended media. Under glucose-fed conditions, EB removal remained high across this range, with 94.5 ± 1.5%, 92.5 ± 1.2% and 88.1 ± 0.5% decolorization for 1.0, 0.5, and 0.1 mL inoculum, respectively. In lactate-fed cultures, removal was 93.7 ± 0.2%, 92.0 ± 1.2% and 86.3 ± 2.2% for the same inoculum volumes. Thus, even at the lowest inoculum, EB decolorization exceeded ~86%, and there was no indication of

impaired performance at the highest inoculum, but removal increased modestly with higher biomass. Together with the increase in EB removal over time and the absence of drastic pH change in the main experiments, these results suggest that any oxygen depletion or partial fermentation that may occurred did not inhibit dye degradation within the studied window.

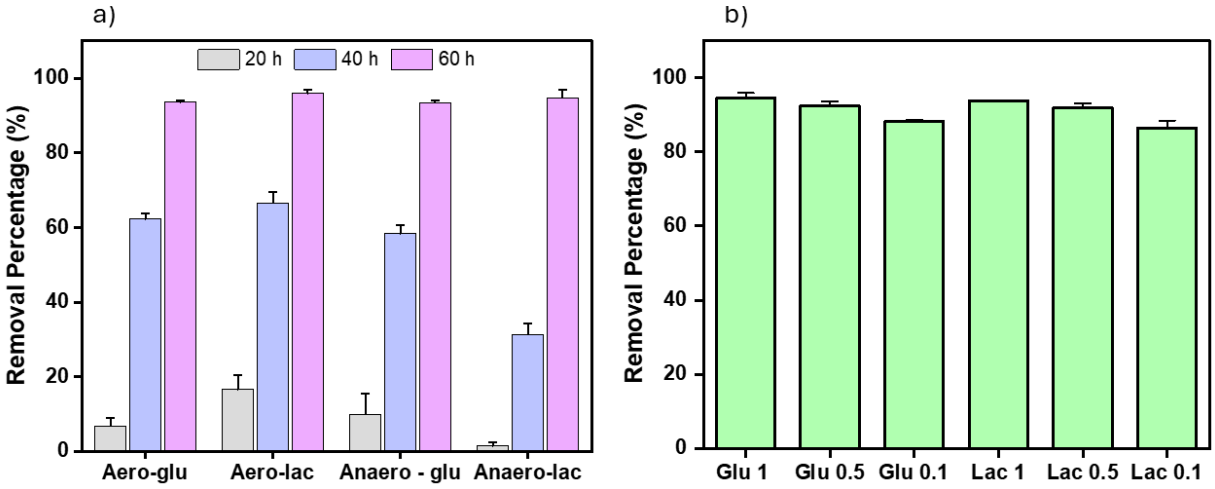

Figure 3.8 (a) Evans Blue decolorization (%) at 100 mg/L, 250 mg/L carbon source and 37 °C under four regimes: aero-glu (aerobic–glucose) ,aero-lac (aerobic–lactate), anaero-glu (anaerobic–glucose), andanaero-lac (anaerobic–lactate), measured at 20, 40, and 60 hours (bars represents mean ± SD, n = 3).(K. Ayaz et al;. 2026a) *(b) Evans blue dye removal percentages by using different incolum concetration in glucose and lactate fed media*

To summarize the discussion of this part of studies beyond statistical significance, the RSM model identifies incubation time and temperature as the dominant positive factors, with increasing glucose concentration acting as a strong negative factor and dye concentration as a secondary contributor within the range of tested values of factors.

The significant interactions show clear trends. Higher initial dye can be offset by longer contact time and moderately higher temperature. Raising glucose above the optimum gives diminishing returns. The RSM model fits the data and defines a practical operating window: about 100 mg/L EB, 250–500 mg/L glucose, 37 °C, and 48–72 h. This window is useful for process design and scale-up. Unlike many RSM studies that focus only on numerical optimization, our model is tied to mechanistic evidence from UV–Vis, HPLC, and GC–MS. This linkage allows us to interpret the dominant factors and interactions, and dye concentration, incubation time, temperature, and carbon supplying terms of *S. oneidensis* MR-1 pathways for Evans Blue breakdown

3.2.3 HPLC analysis

The UV–Vis at 606 nm measurement provided quantitative decolorization of EB but it did not identify end-products (Figure 3.3). To complement this analysis, we used HPLC with a

photodiode array (PDA) to track low-molecular-weight aromatic intermediates during bacterial degradation. Samples taken at 2, 4, 11, 14, and 28 h were injected on a C18 column. PDA spectra were recorded from 210 to 800 nm. Figure 3.9a shows chromatograms at 254 nm.

Three peaks appeared by 2 h and increased through 28 h: A with RT at 4.9 min, B at RT = 5.6 min, and C at RT = 6.3 min. Peak A shifted from deep-UV absorption to a clear λ_max of 258 nm and split after 14 h, which indicates conversion of an initial fragment pool into at least two downstream aromatics. Peak B showed a hypsochromic shift from 260 to 255 nm, consistent with loss of conjugation during side-chain removal or stepwise ring opening. Peak C kept a stable λ_max of 277 nm, consistent with a persistent benzenoid or phenolic intermediate. The absorbance of all three peaks rose with time, which indicates progressive accumulation of these intermediates (Figure 3.9b). This time–spectral pattern matches the mid-pathway phase of bacterial azo-dye transformation (Ngo and Tischler 2022).

The EB parent peak was expected near 606 nm, but EB did not retain on the C18 column and eluted at the void time, nevertheless, degradation was confirmed by UV–Vis spectrophotometry (Figure 3.3). From the HPLC data, the inferred sequence is azo reduction to aromatic intermediates A–C, followed by oxidative ring cleavage or β-oxidation toward mineralization. This agrees with prior reports of bacterial azo-dye pathways. In *Shewanella oneidensis* MR-1, fast early reduction is consistent with its extracellular electron transfer capacity, which can accelerate initial reductive steps (G. Liu et al. 2011). Other bacteria that degrade EB, such as *Enterobacter cloacae* SD4-1, also show transient aromatic intermediates before deeper oxidation, with profiles that depend on the organism and conditions (Ravi et al. 2025). Our HPLC traces capture this aromatic intermediate window. Later acids expected in the pathway have weak absorbance at 254 nm and contribute minimally to these chromatograms.

Concluding this part of results, the HPLC dataset alone confirms rapid decolorization with the timed accumulation and biotransformation of aromatic intermediates, precisely the mid-pathway chemistry anticipated for EB biodegradation under the given conditions.

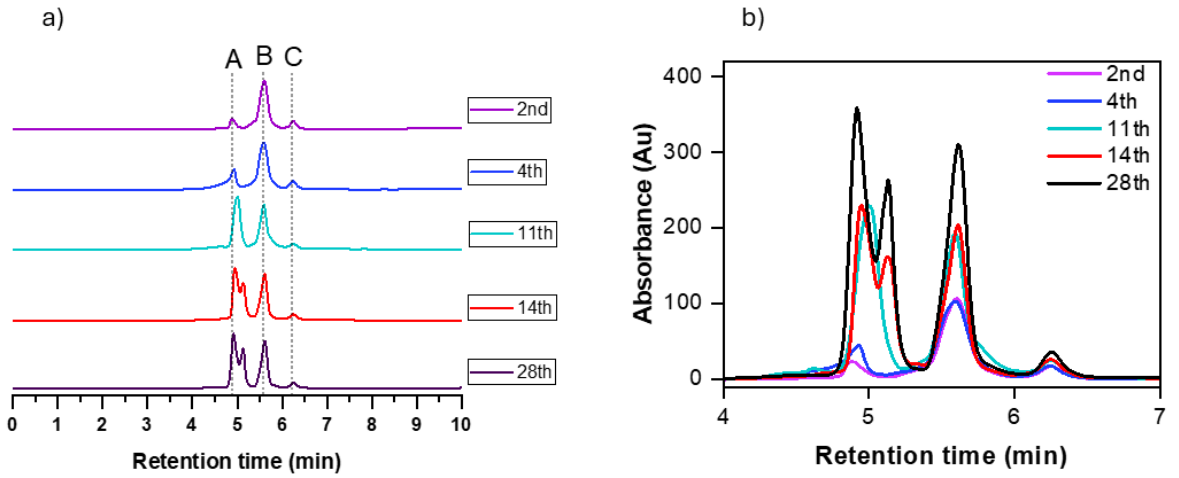

Figure 3.9 HPLC chromatograms (a) collected at 254 nm for samples after various durations of treatment, (b) stacked chromatograms indicating changes in absorbance with time (K. Ayaz et a;. 2026a)

3.2.4 Analysis of degradation pathways via GC–MS

Among many factors influencing the efficiency of dye biodegradation, the compound structure, presence and type of functional groups in dye molecules significantly influence the rate and degree of dye degradation (Sarkar et al. 2017). The chromatogram of the GC–MS profile of the sample treated with *Shewanella oneidensis* MR-1 in aerobic conditions revealed a suite of distinct degradation products, confirming advanced dye transformation (Table 3-2, Figure S6.3).

According to the chromatogram three mechanistic classes of compounds were revealed: (i) Aromatic/phenolic intermediates indicative of initial azo-bond reduction and aromatic remodeling were observed as a phenolic signal assigned to 2,4-di-tert-butylphenol (RT 22.38 min; MW 206.32; CF $C_{14}H_{22}O$) together with two late-eluting amine-bearing aromatics tentatively matched by library search to biphenyl-diamine-type–type structures (RT 38.99 and 39.10 min; low-abundance peaks). (ii) Heteroatom-bearing products were represented by diethyl trisulfide (RT 30.12 min; MW 154.31; CF $C_4H_{10}S_3$), which is consistent with sulfur processing during EB breakdown. (iii) Low-molecular-weight aliphatic acids, characteristic of oxidative ring cleavage and chain shortening, were detected at low abundance: 3-methylbutanoic acid (RT 5.21 min; MW 102.13; CF $C_5H_{10}O_2$) and octanoic acid (RT 13.28 min; MW 144.21; CF $C_8H_{16}O_2$). In addition, a dominant series of 2,5-diketopiperazines (DKPs), namely, pyrrolo[1,2-a]pyrazine-1,4-dione, hexahydro derivatives, was recorded (a major RT of 28.68 min with related signals at 29.56, 31.47, 31.85, 32.04, and 36.28 min); these nitrogenous cyclic dipeptides are interpreted as culture-matrix metabolites rather than dye-derived fragments. A late hexamethylcyclotrisiloxane feature (RT 45.90 min) was treated as a

silicone background artifact. Summarizing obtained results: the product spectrum is consistent with stepwise EB degradation sequence under the present conditions - azo-bond reduction to aromatic amine/phenolic intermediates → heteroatom processing → oxidative ring opening and β-oxidation to short-chain acids—mirroring the functional-class progression reported for EB biodegradation in the reference study while differing in the specific aromatic and sulfur species accumulated in our MR-1 system.

Obtained results align well with the product-based pathway used in the previous study (Ravi et al. 2025), which involves initial azo-bond reduction, followed by heteroatom processing, oxidative ring cleavage, and finally chain shortening. We observe the same classes of products (aromatic/phenolic, S/N-bearing, and aliphatic acids), even though the exact molecules differ due to the different organisms used in the previous study, *Enterobacter cloacae* SD4-1 (Ravi et al. 2025; Stolz et al. 2001).

The aromatic/phenolic signals we observe—tentative aromatic diamines and 2,4-di-tert-butylphenol—indicate an aromatic intermediate phase after azo reduction, which has also been reported in other studies (Al-Tohamy et al. 2023; Mustafa et al. 2025). The formation of aromatic amines after N═N cleavage is a core expectation in chemistry of microbial transformation of azo-dye (Stolz 2001; Ngo and Tischler 2022; Pandey, Singh, and Iyengar 2007). The fact that presented study shows amine-bearing aromatics, rather than the alkyl-benzenes emphasized in *Enterobacter* SD4-1 (Ravi et al. 2025), is plausible because *Shewanella oneidensis* MR-1 uses extracellular electron transfer (EET) and flavin shuttles that favor reductive transformations under low O_2 concentration (Marsili et al. 2008).

The sulfur-bearing product (diethyl trisulfide) supports S-chemistry during breakdown, analogous in function to the thiophene-3-sulfonic acid seen in the literature; the exact sulfur species can vary with redox state, thiol pools, and media (Ravi et al. 2025). The detection of short-chain aliphatic acids (e.g., 3-methylbutanoate, octanoate) has progressed beyond aromatic intermediates toward ring-opened, β-oxidation-like products, matching the expected direction of aromatic ring cleavage into fatty acids or esters in bacterial pathways and consistent with EB product patterns reported in related studies (Ravi et al. 2025; Antonin et al. 2015; Stolz 2001).

The abundant 2,5-diketopiperazines (DKPs) are typical culture-matrix metabolites from peptide turnover common via GC–MS; there are reported but not assigned to the dye degradation pathway (Borthwick 2012). In summary, observed the GC–MS classes support a

stepwise EB pathway under our conditions: azoreductive cleavage → aromatic (amine/phenolic) intermediates with S/N processing → oxidative ring opening and β-oxidation to short-chain acids. This mirrors the functional sequence in the reference while reflecting organism- and condition-specific intermediate identities (Ravi et al. 2025).

However, because GC–MS was performed at a single late time point, the exact chronological order and quantitative contribution of each intermediate cannot be conclusively established, and the proposed sequence should be viewed as a functional-class pathway inferred from these data and published EB studies rather than a fully resolved, stepwise mechanism. Notably, within this MR-1 system, classic mutagenic aromatic amines such as benzidine, aniline, and phenylenediamine were not detected, indicating that EB transformation proceeds predominantly toward phenolic and aliphatic products rather than the accumulation of high-risk aromatic amines (Figure 3.10). Presented findings are consistent with the broader view that dye structure and functional groups (e.g. azo linkages, sulfonated aromatic rings, and sulfur-containing moieties) influence both decolorization and subsequent biodegradation. *S. oneidensis* MR-1 can transform these features into phenolic/aromatic intermediates, S-bearing products and short-chain acids. At the same time, the present data does not allow specific reaction steps to individual functional groups or to reconstruct the full sequence of transformations. In this study, the influence of dye structure is therefore demonstrated qualitatively through the classes of products observed, and explicitly it was recognized that detailed, time-resolved GC–MS, isotope-labelled substrates and targeted manipulation of MR-1 reductive pathways will be required to confirm the proposed stepwise degradation pathway and to more rigorously distinguish MR-1 from other Evans Blue–degrading strains.

These findings present, for the first time, a tentative pathway supported by the identification of specific intermediates and end products produced by *S. oneidensis* MR-1, in contrast to the metabolite profiles previously described for *E. cloacae* SD4-1 (Ravi et al. 2025). Thus, the GC–MS data presented here confirm the efficient and environmentally friendly degradation of EB by *S. oneidensis* MR-1, affirming the disappearance of the parent dye and accumulation of simpler, less hazardous than aromatic amines metabolites.

Table 3-2 Mass spectral data of identified intermediates of EB biodegradation by Shewanella oneidensis MR-1 (K. Ayaz et al. 2026a)

Identified metabolite	**RT (min)**	**MW (g/mol)**	**Formula**	**Pathway role**
Putative aromatic diamines (biphenyl-diamine type)	38.991/39.098	(tentative)	(tentative)	Azo-bond cleavage intermediates (amine-bearing aromatics formed after N═N reduction)
2,4-Di-tert-butylphenol	22.377	206.32	C14H22O	Phenolic aromatic intermediate (aromatic remodeling after azo reduction)
Diethyl trisulfide	30.115	154.31	C4H10S3	Heteroatom (S) processing byproduct during dye breakdown
3-Methylbutanoic acid	5.212	102.13	C5H10O2	Late-stage oxidation product (ring-cleavage → β-oxidation; short-chain acid)
Octanoic acid	13.275	144.21	C8H16O2	Late-stage oxidation product (ring-cleavage → β-oxidation; medium-chain acid)

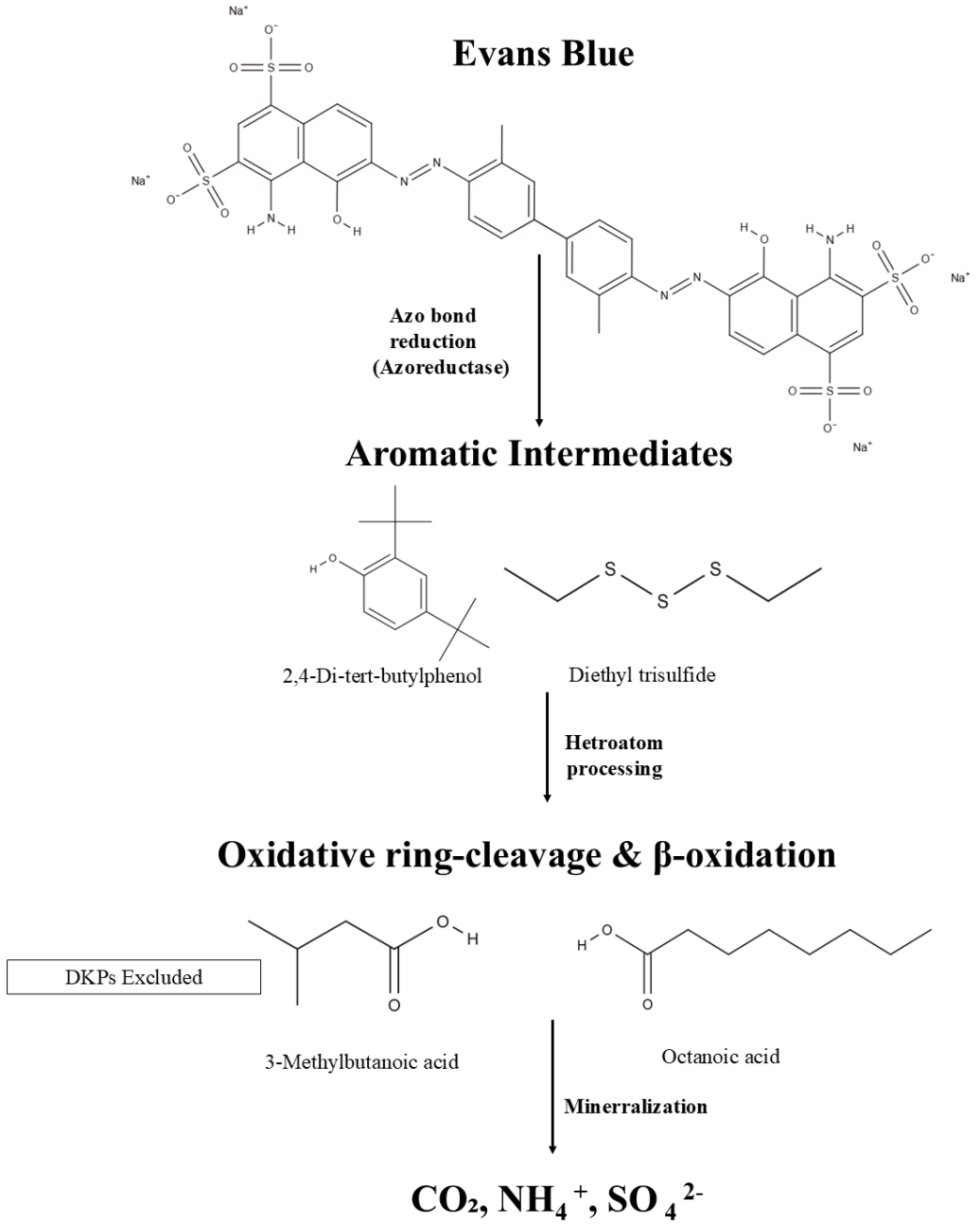

Figure 3.10 End compounds of Evans blue dye degradation by Shewanella oneidensis MR-1and proposal of tentative pathway of EB biodegradation (K. Ayaz et al. 2026a)

Conclusions and further research directions

Section 3.2 defined an optimized operating window for Evans Blue decolorization using a pure culture of *Shewanella oneidensis* MR-1 and confirmed dye transformation and degradation under controlled conditions. Statistical optimization of the process was performed using the response surface methodology (RSM). The analysis results were interpreted in conjunction with the results of degradation product assays. By integrating statistical optimization with product-level verification, this chapter establishes a mechanistically grounded and process-relevant operational window. The obtained results defined further research directions, namely, a transition to bioelectrochemical systems and mixed cultures in subsequent chapters. Pure culture also cleaved the azo bond and fully mineralized EB under aerobic conditions, without an initial anaerobic step, contrary to common reports in the literature. Despite these positive results, several practical limitations were also identified. Complete or near-complete decolorization of higher dye loads (100 mg/L) required relatively long incubation times of approximately 60–72 h, which limits its applicability under realistic wastewater treatment scenarios. This limitation was also highlighted through literature that most single strains take long time for dyes removal. To address these limitations, the research direction is moved deliberately from dye removal by pure-cultures, and optimization of these processes (section 3.1–3.2) to a reactor-based bioelectrochemical platform with application of mixed-microbial cultures, where functional microbiocenosis can act synergistically to accelerate decolorization and support complete mineralization in short time. Specifically, a double-chamber microbial fuel cell (DCMFC) combined with an aerobic post-treatment stage will be implemented to improve EB removal at appropriate loads while simultaneously enabling energy recovery and the intermediate products mineralization. This is a recognized advantage of MFC-based treatment over to conventional aerobic processes, which typically require net energy input.

3.3 Dual-Chamber Microbial Fuel Cell for Evans Blue Degradation and Energy Recovery

The results presented in this section build directly on the findings of section 3.2, where Evans Blue decolorization by a pure culture of *Shewanella oneidensis* MR-1 was successfully optimized using response surface methodology (RSM). Although high removal efficiencies were achieved under defined conditions, the process required extended incubation times (up to 60–72 h at 100 mg/L), highlighting kinetic and functional limitations inherent to single-strain aerobic systems. This limitation gave a base to transition to another issue of experiment, which was mixed-microbial bioelectrochemical treatment, where metabolic variety and complementarity and extracellular electron transfer can be utilized to accelerate dye transformation and enhance overall process performance.

Accordingly, this chapter evaluates a double-chamber microbial fuel cell (DCMFC) operated with a mixed microbial consortium, coupled with an aerobic post-treatment unit, for the treatment of EB from the environmentally dangerous concentrations onto ecofriendly end-products. The integration of bioelectrochemical conversion was designed to simultaneously promote reductive cleavage of azo bonds at the anode, enable downstream oxidation of intermediates in aerobic reactors, and recover electrical energy during treatment. The research focused on linking the decolorization and mineralization efficiency with changes in the bio-composition of the microbial communities forming the biofilm on the anode, biofilm morphology, as well as cyclic voltammetry and electrochemical impedance spectroscopy. By moving from pure cultures to a mixed-community MFC platform, this section addresses the scalability, kinetics, and functional resilience limitations identified in section 3.2 and advances the dissertation objective of developing optimized, energy-positive biological systems for dye-laden wastewater treatment.

Most results presented in this chapter were published in the research paper entitled "*Enhancing Azo Dye Mineralization and Bioelectricity Generation through Biocathode-Microbial Fuel Cell Integration with Aerobic Bioreactor*" by Ayaz, K., Zabłocka-Godlewska, E., & Li, C. (2024). Energies, 17(19), 4896.*Engineering*, *81*, 109399.

3.3.1 Actinomycetes screening and isolation for aerobic chamber

Table 3-4 summarizes the qualitative plate-screening results for *Actinomycetes* strains isolated from garden compost and evaluated as possible candidates for aerobic post-treatment in the

DCMFC system. Each strain was assessed in media containing a representative triphenylmethane dye BG and the target azo dye EB at concentration 100 mg/L. Performance was evaluated by growth and decolorization of dyes (complete, intermediate, partial, or none). The table also records either color loss was associated with sorption, which is important for separating true biodecolorization from dye sorption by biomass and defining the mechanism of decolorization. Overall, the results in the (Table 3-3) show that in the presence of EB the growth of most isolates was possible, but the extent of decolorization varied markedly among strains; SK-2 and SK-3 displayed the most consistent and strong decolorization zones across both dye types, supporting their selection for further evaluation in the aerobic chamber.

Table 3-3 Results of a Acitnomycetes strains isolated from garden compost for aerobic post-treatment in DCMFC

Strain	**Triphenylmethane dyes**			**Azo dyes**		
	Brilliant green (100 mg/L)			**Evans blue (100 mg/L)**		
	Growth	Decolorization	Sorption	Growth	Decolorization	Sorption
SK-1	-	-	-	Gi	Dc	Sc
SK-2	Gp	Dp	Sp	Gi	Di	Sp
SK-3	Gp	Dp	Si	Gi	Di	Sp
SK-4	-	-	-	Gi	Dc	Sc
SK-5		-	-	Gi	Dc	Si
SK-6	Gi	Dp	Sp	Gi	Dc	Si
SK-7	-	-	-	Gi	Dc	So
SK-9	-	-	-	Gi	Di	Sc
SK-10	Gp	Dp	-	Gi	Dc	Sp
SK-11	Gp	-	-	Gi	Di	Sp

Explanation of the designations used in the table (-): no microbial growth, (G): bacterial growth, (Gi): intensive growth (D): Decolorization, (c): Complete (50+ mm zone) (i): Intermediate (20-30 mm zone) (p): Partial (lower than 10 mm zone)

3.3.2 Decolorization efficiency of the dyes

UV–Vis spectra were recorded for the dual-chamber microbial fuel cell (DCMFC) effluent and for a pure solution of EB (100 mg/L) as reference (Figure 3.11a). The reference spectrum showed distinct visible-band absorptions, with a dominant peak at 606 nm that corresponds to the azo chromophore (–N=N–) responsible for the deep blue color. We therefore used the decrease in absorbance at 606 nm to calculate decolorization efficiency (DE%) in DCMFC effluents. In the anaerobically treated effluent, additional bands appeared at 389 nm and 500 nm, consistent with naphthalene-type fragments (389 nm) (M. D. Khan et al. 2021) and secondary amine-containing products (500 nm) (Y. Fu et al. 2014). These features indicate formation of biotransformation products during biodegradation. An absorption near 800 nm was also observed; its origin is unknown and will be investigated in future work.

Thus, color loss arose from reductive cleavage of the azo bond and conversion to aromatic amines under DCMFC anaerobic conditions. After transfer effluents from anaerobic to the aerobic chamber, no distinct absorption peaks remained. This indicates complete biodegradation of aromatic amines and other anaerobic products in the integrated DCMFC–aerobic system.

Before the double-chamber microbial fuel cell (DCMFC) experiment, a new carbon brush was subjected to an adsorption test, and the results were negligible. DCMFC-aerobic system was used to do comparative test at two initial dye concentration (100 and 200 mg/L), and it showed a concentration effect. At 100 mg/L, average color removal exceeded 90%. At 200 mg/L initial dye concentration, removal of EB was about 80% (Figure 3.11b). These values align with literature reports. Quan et al. achieved 98.0% EB removal with a palladium-nanoparticle-modified anode, whereas the unmodified control reached 90% (Quan et al. 2018). Higher dye concentrations inhibited bacteria and prolonged degradation time. Prior studies report greater toxicity at higher dye levels, which suppresses growth and enzyme activity and lowers decolorization efficiency (Long et al. 2019). The reduced tolerance to EB and observed decrease of decolorization efficiency was likely a result of limitation of electron transfer, acetate oxidation. Consistent with this, Fang et al. showed that high concentrations of Active Brilliant Red X-3B inhibited microorganisms, decreasing their number and activity due to toxic, resistant products that could not be directly utilized, which lowered decolorization efficiency (Fang et al. 2015). Finally, complete decolorization in DCMFCs does not guarantee complete mineralization. Anaerobic biotransformation can yield colorless aromatic amines that may persist without an aerobic post-treatment step.

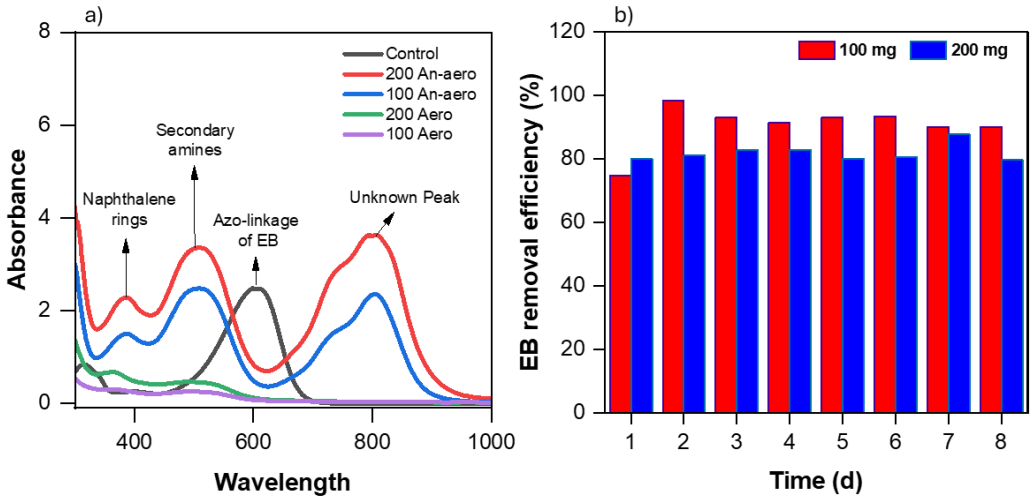

Figure 3.11 a) UV-visible absorption spectra of 100 mg/L and 200 mg/L of DCMFC anaerobic effluent, pure dye solution (control), and aerobically treated effluent. (b) Decolorization of EB in DCMFC with time (K.Ayaz et al. 2024)

3.3.3 Bioelectrochemical Performance of DCMFCs

Voltage behavior and adaptation

The DCMFC voltage outputs were monitored from the startup and are displayed in Figure 3.12. Bacterial adaptation to DCMFC environment is critical for dye removal and can be improved by co-feeding a cosubstrate to the treated azo dye solution and by gradually increasing influent dye concentration (Kong et al. 2018). During enrichment low voltage output was observed (Figure 3.12a). Voltage value was mostly below 20 mV in this phase. The low output reflects adaptation of electrogenic bacteria to the new anode environment (solution) containing Evans Blue (J. Sun et al. 2016).

After enriching Figure 3.12a, the reactor was allowed to stabilize for 3 days until voltage fell to 50 mV. At that point, acetate and medium were replenished to start with experimental stage called enriched stage. In the enriched stage, voltage was much higher than during initial enrichment. The maximum voltage reached 337 mV at 100 mg/L EB while at 200 mg/L causing an initial drop to about 180 mV for three cycles, but the voltage then recovered to 304 mV by the end of experiment. This pattern suggests initial inhibition followed by adaptation. Similar trends were reported for varying dye levels by Sultana et al. (Sultana et al. 2015). Another explanation for our results is that a high concentration of EB may require more electrons to cleave the azo bond, which decreases the output voltage. This was also explained by Khan et al. (M. D. Khan et al. 2021). Furthermore, Thung et al. also observed a decrease in voltage from 167 mV to 148 mV when acid orange 7 concentration increased, indicating that electrons were diverted from the anode to the dye after acetate oxidation (Thung et al. 2015).

Batch operation and peak voltages

Biofilm and freshly acclimated cells gradually attached to the anode after adjustment to the electrogenic environment. The EB dye concentration increased stepwise from 100 to 200 mg/L. In batch mode, voltage peaks declined as acetate was consumed, however, the highest voltage recovered upon the addition of new feed portion (Figure 3.12b). Peak voltages were 280.2 mV at 100 mg/L and 287.34 mV at 200 mg/L under a 500 Ω external resistance. Despite high concentration of electrogens bacteria in the acclimated anaerobic biofilm, overall voltage remained limited. The bioelectricity pathway was active, but further optimization is needed to increase voltage output.

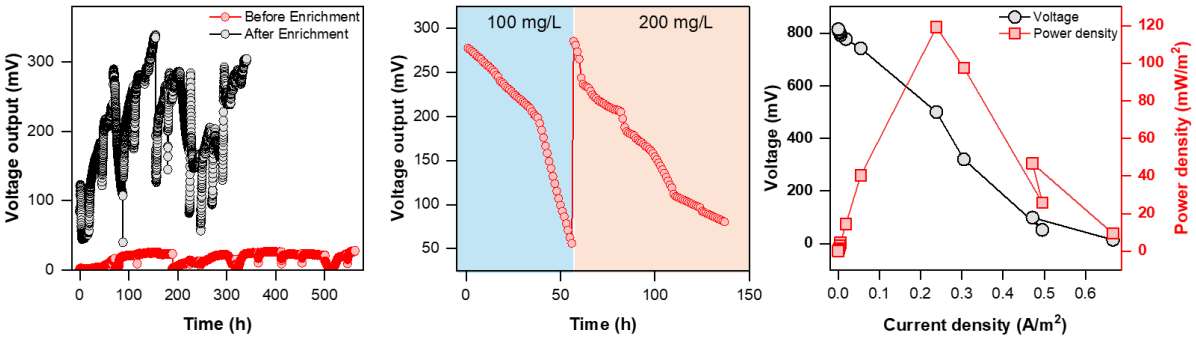

Figure 3.12 (a) Voltage output-time curves of MFCs with enrichment stage and after enrichment (b) Impact of EB concentrations on the production of bioelectric power (500 Ω external load (c) Polarization curves: power density as a function of current density in DCMFC (K. Ayaz et al 2024)

Polarization performance and power

At the end of the operational run, polarization tests characterized electrochemical performance of DCMFC (Figure 3.12c) were conducted. A maximum power density of 119.2 mW/m^2 and a maximum current density of 0.238 mA/m^2 were achieved. These results show that the DCMFC bioreactor can both degrade EB and generate electricity. Interestingly, the current density decreased with increasing resistance, but the voltage increased with increasing resistance. This behavior follows the maximum power transfer theorem. Peak power occurs when external load equals internal resistance. Thus, current is a key driver of MFC power, and P_{max} occurs when R_{ext} equals R_{int}. Our data are consistent with this relationship and support the observation of P_{max} at 550 Ω reported by . (Z. Zafar et al. 2019). However, Raturi et al. (Katuri et al. 2011) reported found higher power densities when shifting from high to low loads. The findings of the present study agree with the maximum power theorem, as stated by (Potrykus et al. 2021) and other previous research.

3.3.4 Electrochemical Characteristics of the Anode Biofilms

Cyclic voltammetry

Cyclic voltammetry (CV) is a standard technique for probing electroactive species in liquid media and anode surface. Electroactive species on the anode were investigated using cyclic voltammetry (CV). We compared the baseline CV at zero with the CV recorded after enrichment of the anode. In the initial scan, the first oxidation and reduction peaks appeared at 0.99 V and −0.54 V, with peak currents of 0.016 A and −0.0001 A, respectively, referenced to Ag/AgCl. After the anode had been enriched with degraded products, the follow-up CV showed a comparable oxidation peak at 0.99 V and a shifted reduction peak at −0.73 V. The corresponding peak currents increased to 0.10 A for oxidation and −0.0003 A for reduction (Figure 3.13a). These features align with literature reports. Mani et al. (2019) observed

characteristic redox couples during EB degradation, with notable peaks near 0.89 V and 0.70 V. Our data show a similar pattern, which supports the presence of redox-active intermediates formed during cleavage of the azo bond (N=N) (P. Mani et al. 2019). Consistent behavior was also reported by Khan et al. (2021), who documented redox couples associated with dye breakdown and noted distinct oxidation signals in the spectra of degraded products. Taken together, our CV results and prior studies point to a common mechanism in which EB reduction generates electroactive intermediates that can be detected as reproducible redox pairs (M. D. Khan et al. 2021).

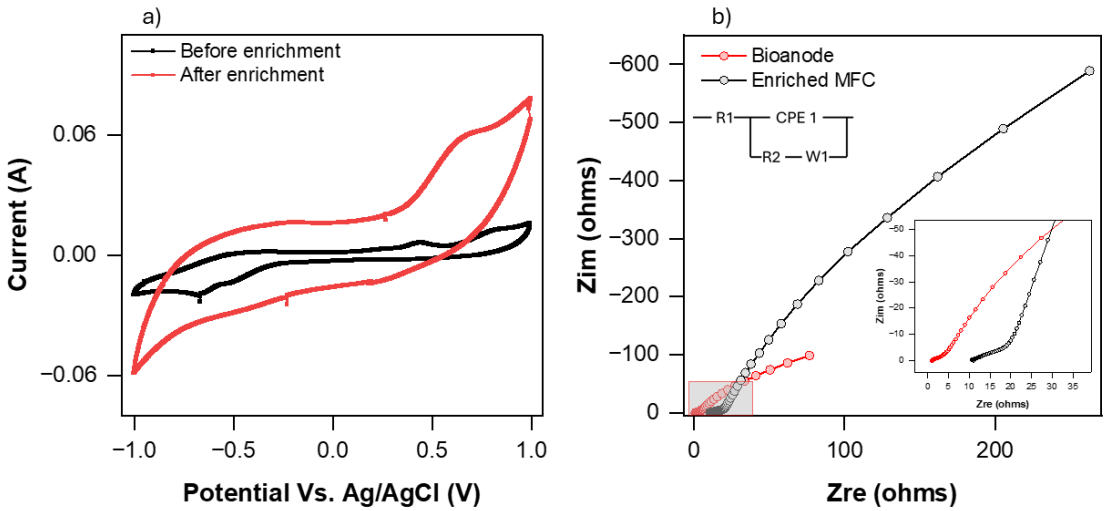

Figure 3.13 (a) Zero time and EB−enriched anode cyclic voltammetry in DCMFC, and (b) EIS Nyquist plots and fitted circuit drawings of the bioanode and DCMFC treated with EB (K. Ayaz et al 2024)

Electrochemical impedance spectroscopy

Electrochemical impedance spectroscopy (EIS) is well suited technique to resolve transport and kinetic phenomena in bioelectrochemical reactors. The method is widely used to estimate solution or ohmic resistance (Rs), charge-transfer resistance (Rct), and diffusion-related Warburg elements (W). These quantities are central to interpreting reaction rates and mass transport (Sanchez-Herrera et al. 2014; H. Wang et al. 2022). Complex impedance data were plotted as Nyquist diagrams and fitted with an equivalent circuit containing Rs, Rct, W, and a constant phase element (CPE) (Figure 3.13b). For the DCMFC, the total internal resistance was 12.48 Ω, based on Rs = 11.19 Ω and Rct = 1.29 Ω. The apparent magnitude of system resistance likely reflects electrode spacing and electrolyte conductivity. In contrast, the bioanode-specific resistance (Rs + Rct) measured in a dedicated configuration was only 1.4 Ω. This low value indicates a mature, well-connected biofilm on the anode surface and supports faster electron transfer at the electrolyte bioanode interface. Enhanced electron

delivery from the anode translates into higher electron flux to the cathode and, in turn, greater bioelectricity generation. These impedance results therefore corroborate the CV evidence and confirm that the developed biofilm lowers interfacial barriers while sustaining efficient charge transfer during EB degradation.

3.3.5 Biofilm Surface Characterization and Community Analysis

Biofilm surface characterization (SEM analysis)

SEM was used to examine bacterial adhesion and biofilm development on the carbon-brush anode. After completion of the DCMFC experiment, bioanodes were removed and prepared for imaging. Baseline SEM micrographs of the unused carbon brush at the start of the experiment are shown in Figure 3.14a, whereas Figure 3.14b presents SEM images of the same anode after operation, demonstrating the presences of distinct biofilm that indicates a compact and continuous microbial population on the electrode surface. Electron micrographs of the pristine (not inoculated) carbon brush display a smooth and orderly fiber network, with clearly visible carbon strands that provide a high specific surface area and abundant attachment points for microbial cells. Consistent with earlier reports, most of the adherent structures observed in our samples are biofilm matrices populated by coccoid bacteria (N. Khan et al. 2018; Offei et al. 2016; S. Yang, Du, and Liu 2012). The biofilm formation generally enhances electron transfer by establishing intimate contact between cells and the conductive substrate, excessively thick or densely packed biofilms can hinder charge transport and reduce DCMFC power output.

A detailed analysis of the microbial community would further clarify how morphology, cell shape, and extracellular polymeric substances contribute to interfacial electron transfer and overall reactor performance. Such population profiling can help resolve the specific roles of dominant taxa in initiating adhesion, forming stable biofilms, and sustaining long-term electrogenic activity on carbon-based anodes.

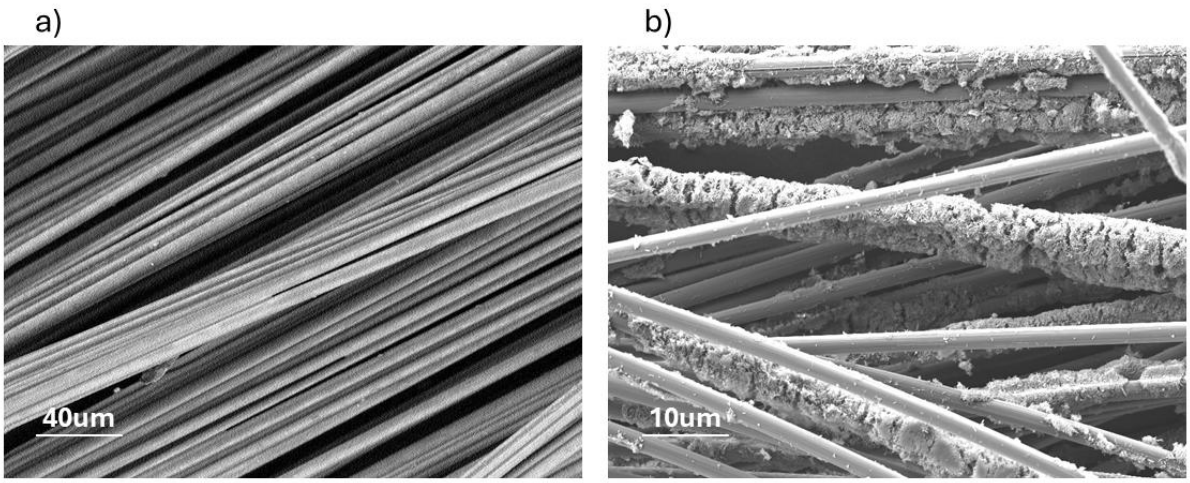

Figure 3.14 (a) SEM Images plain carbon brush at 1000× magnification. (b) SEM Images of anodic biofilm in the DCMFC at 5000× magnification. (K. Ayaz et al. 2024)

A clear understanding of how DCMFCs generate current and degrade dyes requires detailed analysis of the microbial community present in the activated-sludge biofilm. To Evaluate overall MFC performance involves surveying multiple functional bacteria groups, including classic electricigens, dye-degrading organisms, exoelectrogens, fermentative bacteria, and related auxiliaries. These guilds act together to deliver stable power output and sustained contaminant removal, so community structure and balance directly influence reactor function.

To characterize these contributors, we profiled the microbial communities in the anode biofilm by Illumina sequencing and the inoculum using in aerobic reactor by 16S rRNA gene sequencing. Taxa were identified and assigned at the phylum and genus levels. In the discussion below, we focus on the principal functional microorganisms detected at each taxonomic level, restricting attention to those with relative abundances greater than 2%. This threshold highlights the dominant groups most likely to influence electron transfer, co-metabolism, and dye transformation within the DCMFC.

Community shifts at phylum and genus levels

The community changes at the phylum and genus levels between the inoculum and the acclimated DCMFC anode biofilms, respectively are summarized at Figure 3.15a, b. In the inoculum, the dominant phyla were *Pseudomonadota* (45.55%), *Bacteroidota* (13.86%), *Actinomycetota* (10.87%), *Chloroflexota* (8.83%), *Campylobacterota* (6.85%), *Bacillota* (3.41%), *Nitrospirota* (2.90%), with the remaining taxa grouped as others (3.30%) (Figure 3.15a). After acclimation in dye-containing wastewater with a cosubstrate, the DCMFC enriched anode biofilm showed a marked increase in *Actinomycetota* to 28.8% and a

concurrent shift in *Pseudomonadota* to 32.0%. Additional phyla that remained prevalent in the anode biofilm included *Thermodesulfobacteriot*a (4.77%), *Bacteroidota* (4.14%), *Chloroflexota* (9.94%), *Bacillota* (16.42%), with others at 1.42% (Figure 3.15a). These patterns are consistent with known functional roles. *Pseudomonadota* and *Thermodesulfobacteriota* are frequently reported in systems that degrade a wide range of organics, including azo dyes, and they can participate in direct electron transfer to electrodes (Z. Zafar et al. 2019; Pham et al. 2008).

Bacteroidota are often detected under anaerobic conditions that favor azo-dye breakdown and they have been proposed as potential exoelectrogens on bioanodes (Quan et al. 2018). *Actinomycetota* are regularly detected in MFCs and are effective degraders of recalcitrant organic pollutant (Hemdan et al. 2023; Arbour, Gilbert, and Banfield 2020). However, their direct contribution in anode electron transfer is less clear, but they can support electrogenic activity by enhancing community diversity and by providing complementary metabolism (Jimenez et al. 2020; De La Cruz-Noriega et al. 2023). Members of *Bacillota* may contribute to electron transfer and bioelectricity generation (De La Cruz-Noriega et al. 2023). Phyllum *Chloroflexota* have been linked to azo dye degradation and current production in MFCs (Q. Dai et al. 2020). Overall, anode chambers that process dye-laden wastewater are commonly enriched with electrochemically active lineages bacteria from these six phyla, which aligns with reports for similar systems (M. D. Khan et al. 2021; Q. Dai et al. 2020; R. Rathour et al. 2019).

At the genus level, Figure 3.15b shows the relative abundance of major taxa. In the inoculum, dominant genera included *Methylotenera* (20.3%), *Thermochromatium* (6.9%), *Actinomarinicola* (4.5%), *Caldilinea* (3.0%), *Acidothermus* (2.5%), and others (3.3%). After enrichment on the anode, the principal genera were *Actinomarinicola* (13.7%), *Methylotenera* (9.4%), *Thermochromatium* (4.8%), *Geobacter* (4.5%), *Acidothermus* (4.04%), *Soehngenia* (3.6%), *Propionivibrio* (2.4%), *Janibacter* (2.4%), *Proteiniclasticum* (2.3%), *Romboutsia* (2.2%), *Bellilinea* (2.2%), with others at 1.42%. The strong prevalence of *Actinomarinicola* in the dye-treated anode chamber is noteworthy. This genus was first described by He YQ in 2020 and is often associated with sulfur and iron bioleaching contexts under aerobic conditions (Y. Q. He et al. 2020). Our observations are compatible with that ecological link, given the elevated sulfur derivatives present in the dye matrix. Although *Actinomarinicola* has been described as aerobics, we detected it in an anaerobic anode compartment. This outcome may reflect environmental flexibility, where facultative or microaerotolerant behavior permits

perseverance in low-oxygen niches. Such adaptability would be reasonable for taxa originating from deep-sea or resource-limited habitats, and it may help explain their enrichment in a MFC biofilm on the anode.

Geobacter and *Methylotenera* are key contributors to azo-dye conversion and current generation in microbial fuel cells. Species belonging to the genera *Geobacter* are frequently linked to electricity production in the presence of azo dyes (L. Sun, Mo, and Zhang 2022) while *Methylotenera* has been implicated in pathways relevant to Evans Blue degradation, where the secondary metabolite nitrobenzene can form during dye breakdown (Antonin et al. 2015). *Methylotenera* can use nitrobenzene as a substrate and remove nitro groups from the aromatic ring, which supports further detoxification. Consistent with this role, Dai et al. reported *Methylotenera* enrichment on anodes with a connection to denitrification activity (M. Dai et al. 2021).

Thermophilic bacteria thrive in high temperatures, generally with an optimal growth range between 45°C and 80°C. Despite studying MFC did not work at high temperatures (incubation temperature 30°C), the *Thermochromatium* and other thermophilic microorganisms were detected. Thermophilic bacteria also show promise for bioelectricity production. Direct studies on *Thermochromatium* in MFCs are not yet available, but several thermophiles have demonstrated electrogenic potential. Choi et al. showed that *Bacillus licheniformis* and *Bacillus thermoglucosidasius* can generate substantial current, with performance dependent on temperature and carbon source (Choi et al. 2004). Fu et al. identified *Caloramator*-related bacteria as possible current producers in a thermophilic MFC (Q. Fu et al. 2013). Jong et al. enriched diverse thermophilic communities in a mediator-free MFC and achieved high power density and electron recovery (Jong et al. 2006). Taken together, these findings indicate that thermophiles, potentially including *Thermochromatium*, can support electrogenesis under elevated temperatures.

The presence of *Acidothermus* in our system may relate to dye removal at higher temperatures, not available in studied system. Chao Li et al. linked *Acidothermus* to textile wastewater treatment with high COD removal in the 40–45 °C range (C. Li et al. 2015) This temperature window overlaps with our operational conditions and may explain its enrichment.

The role of *Soehngenia* in MFCs has not been directly defined. However, *Soehngenia* was detected by Zhang et al. in sludge from anaerobic or anoxic tanks of municipal treatment plants (G. Zhang et al. 2017). We also detected *Soehngenia* in the anoxic inoculum. Given that

Soehngenia is anaerobic or facultatively anaerobic, and both saccharolytic and proteolytic, it likely acts as a fermenter within the anode biofilm, converting carbohydrates or proteins to intermediates that feed downstream electron-transfer processes (Nazina et al. 2020).

Multiple studies report *Propionivibrio* on anode biofilms, though its specific function is rarely detailed (Naz et al. 2018; G. Wang et al. 2019; Fischer et al. 2022). Work by Brune et al. indicates that fermentative *Propionivibrio* specialize in degrading hydroaromatic compounds, which could supply electron donors or intermediates to electrogens within mixed communities (Brune, Ludwig, and Schink 2002).

In this study, *Proteiniclasticum* was enriched on anode biofilms derived from anaerobic sludge, consistent with prior isolation from anaerobic acetochlor-degrading consortia (Junwei Liu et al. 2021). Evidence also links *Proteiniclasticum* to interspecies electron transfer. Pérez-Díaz et al. showed that in acetate-fed systems amended with Fe_3O_4, direct electron-transfer routes were promoted, and *Proteiniclasticum* became predominant when the mineral was present on the anode, suggesting a role in mineral-mediated electron exchange between community members (Pérez-Díaz et al. 2020).

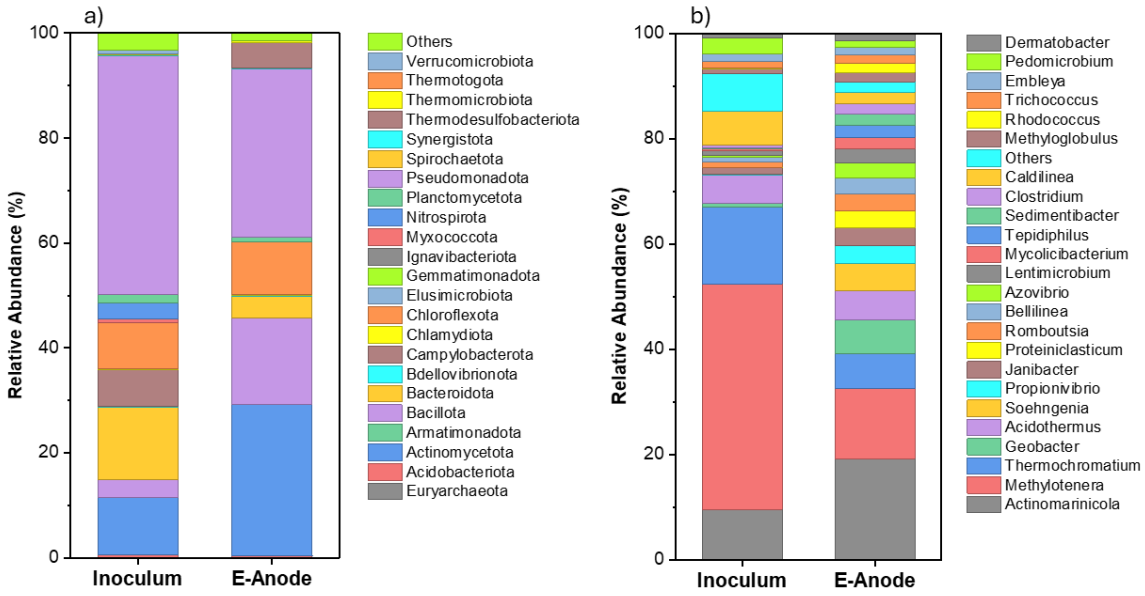

Figure 3.15 Microbial relative abundance at the (a) phylum and (b) genus level. (E anode = enriched bioanode) (K.Ayaz et al. 2024).

In this study, *Janibacter* participated in Evans Blue degradation under anaerobic conditions within the anode biofilm. This observation agrees with Ravadelli et al., who identified *Janibacter* as a dominant azo-dye degrader in an anoxic–oxic membrane bioreactor treating dye-laden wastewater, where it accounted for about 60% of classified sequences (Ravadelli et

al. 2021). Our detection of *Janibacter* on the anode surface is therefore consistent with its documented capacity to attack azo chromophores under low-oxygen conditions and to persist in studying concentrations of EB due to prove persistence in engineered systems exposed to textile effluents.

The genus *Romboutsia* may contribute to bioelectricity generation and to electron transfer toward the anode, and it may also assist in azo-dye breakdown. In our reactor, *Romboutsia* abundance near the anode showed a positive association with voltage output, which mirrors the findings of Li et al., who proposed that *Romboutsia* can behave as an electrogen or a functionally similar organism. The same work linked *Romboutsia* activity to the transformation of chlorinated pesticides, indicating broad redox flexibility that could extend to dye intermediates (Yue Li et al. 2018). Together, these lines of evidence support a dual role for *Romboutsia* in both metabolism of complex organics and facilitation of electron flow to conductive surfaces.

Bellilinea has been linked to anaerobic azo-dye degradation and has shown electrochemical activity consistent with extracellular electron transfer. Recent reports demonstrate that *Bellilinea* can participate in redox exchange with the anode, which aligns with its enrichment in communities that process aromatic contaminants and generate current under strictly anaerobic conditions (S. Liu et al. 2022). The presence of *Bellilinea* in our anode biofilm therefore supports a community structure that couples dye conversion with sustained electrogenesis.

Functional grouping of genera within the anode community

The genera identified here display complementary metabolic functions that can be organized into three practical groups. (i) exoelectrogen-focused genera, including *Geobacter*, *Thermochromatium*, and *Proteiniclasticum*, act primarily as electron exporters. These taxes deliver electrons to the anode during oxidation of available substrates and thereby support current generation in microbial fuel cells. (ii) Second, dual-function genera, such as *Methylotenera*, *Romboutsia*, and *Bellilinea*, serve both as effective dye degraders and as exoelectrogenic contributors. Their flexible metabolism enables simultaneous conversion of dye molecules or intermediates and transfer of electrons to the electrode, which stabilizes power output while advancing contaminant removal. (iii) Third, dye-degrader focused genera, including *Actinomarinicola*, *Acidothermus*, *Soehngenia*, *Propionivibrio*, and *Janibacter*, specialize in breaking down dye structures and related aromatics. These organisms enhance

environmental remediation by attacking chromophores and side chains, thereby reducing color and preparing intermediates for further oxidation or mineralization by aerobic post-treatment. This functional classification clarifies how specific taxa supports electron flow, pollutant breakdown, or both, and it helps explain why mixed communities outperform single isolates in complex wastewater matrices.

Community shifts driven by the DCMFC environment

The anode biofilm diverged markedly from the starting inoculum, indicating strong selection by the DCMFC conditions. We observed substantial differences in community composition between the beginning and the end of the run, consisting of adaptation to continuous redox cycling, exposure to Evans Blue, and contact with the conductive anode surface. Earlier studies reached similar conclusions: the combination of an azo dye in the feed and an anode as an electron sink promotes the growth of both dye-degrading organisms and exoelectrogenic bacteria in the anode compartment of DCMFCs (J. Sun et al. 2013; Zhong et al. 2018). Our results align with this pattern and suggest that stable dye removal and current generation arise from a cooperative network that merges specialized degraders with efficient electron-transferring partners.

Phylogenetic analysis

The phylogenetic analysis produced a well-resolved hierarchical tree with several strongly supported clades that we refer to here as six distinct lineages. Each lineage is shown in a different color for clarity. The query sequences SK-2 and SK-3 group within the third lineage of this tree, indicating close relatedness to members of that clade.

Identification was based on 16S rRNA gene sequencing of two actinobacterial isolates from the aerobic chamber and comparison with reference taxa in GenBank. The strains were designated SK-2 and SK-3. Sequence alignment assigned SK-2 to *Streptomyces* sp. strain actinomycetes (KY235922.1) and SK-3 to *Streptomyces* sp. strain actinomycetes (KY236012). Both isolates therefore fall within the genus *Streptomyces*, as shown in Figure 3.16.

The detection of these *Streptomyces* isolates is consistent with prior reports on dye biodegradation. *Streptomyces* spp. have been shown to degrade Evans Blue at greater than 97% removal and to transform other dyes, including Brilliant Green, triphenylmethane dyes, Nigrosine, Amido Black 10B, Congo Red, and Methyl Red, under shaken conditions

(Kameche et al. 2022; Ayaz, K., & Zabłocka-Godlewska 2022; Adenan, Lim, and Ting 2021b). These findings confirm the strong capacity of *Streptomyces* to attack a wide range of azo and related chromophores.

To our knowledge, no prior study has combined a DCMFC front-end with a defined *Streptomyces* aerobic stage and provided evidence of complete mineralization for Evans Blue. Prior integrated MFC→aerobic reports rely on mixed aerobic consortia and focus on other dyes (e.g., AB29), while actinomycete work documenting azo dye degradation is typically performed in standalone aerobic cultures rather than as the aerobic stage of an MFC train (M. D. Khan et al. 2021; P. Mani et al. 2019).

Our results address two recurring gaps identified in reviews: (i) verification of chemical fate of dye beyond decolorization in dye–MFC systems and (ii) organism-resolved aerobic post-treatment after anaerobic reduction. By specifying *Streptomyces* SK-2/SK-3 in the aerobic chamber and tracking aromatic amines to disappearance, we demonstrate a redox-staged, mechanism-consistent route to detoxification and mineralization of a sulfonated diazo dye.

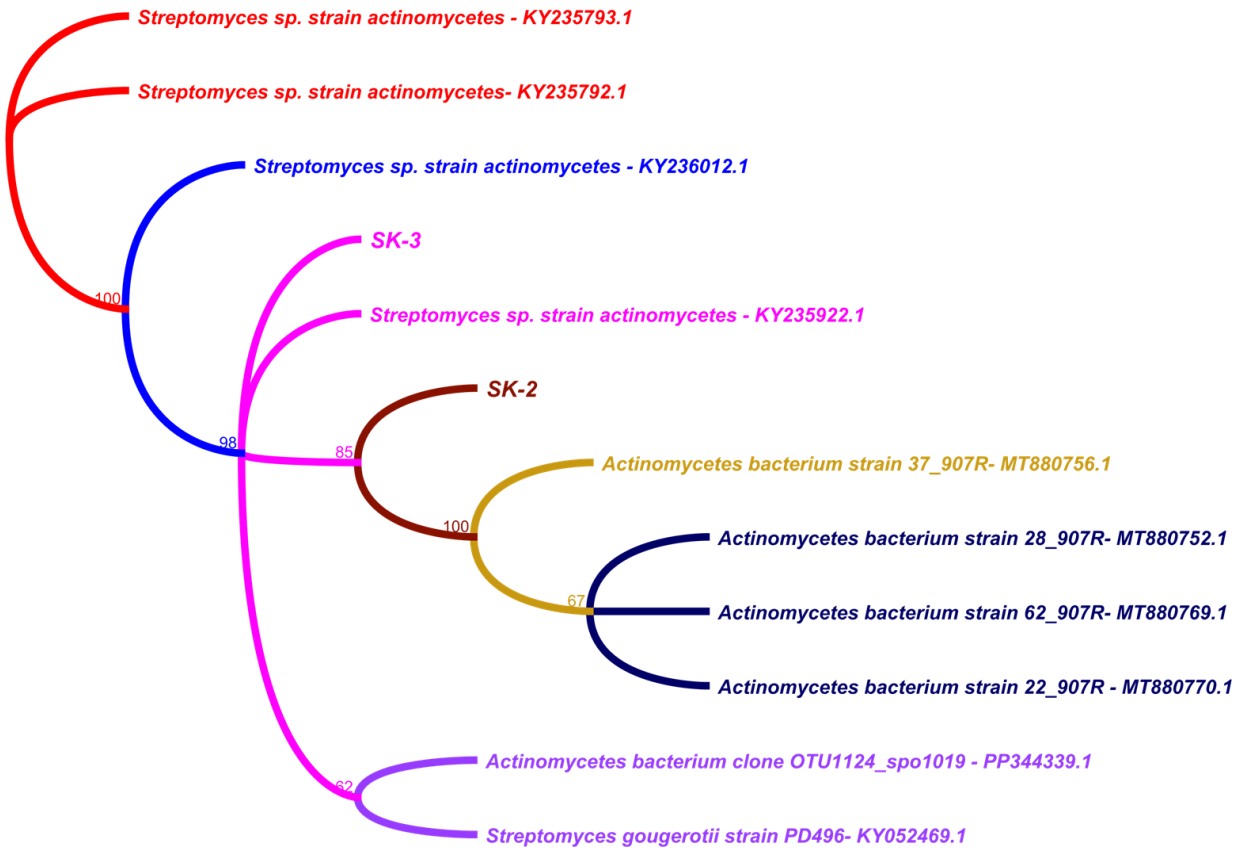

Figure 3.16 Phylogenetic tree of 16s RNA sequences of Streptomyces spp (K.Ayaz et al. 2024)

3.3.6 Analysis of degraded compound by GC-MS

GC–MS was used to identify transformation products of Evans Blue after treatment in an anaerobic anodic chamber operated with mixed anaerobic sludge for biofilm development, followed by aerobic post-treatment using two *Streptomyces* spp. A sequential anaerobic to aerobic concept is widely used for azo dyes because anaerobic conditions favor reductive transformation of azo linkages, while aerobic conditions are typically required to degrade the resulting reduced aromatic products toward mineralization (Van Der Zee and Villaverde 2005; M. D. Khan et al. 2021; 2022)

The tentative pathway followed during degradation of EB (Figure 3.17). (Evans Blue) → *(anaerobic bioanode; azoreductase-mediated reduction and reductive decolorization)* → aromatic/phenolic intermediates *(represented by 2,4-di-tert-butylphenol; RT 22.383–22.396 min)* → *(aerobic Streptomyces oxidation; hydroxylation and de carboxylation)* → phenylacetic acid (RT 15.508–15.684 min) → *(aerobic ring cleavage and chain shortening)* → C4–C5 acids *(butanoic acid; 2-methylbutanoic acid; 3-methylbutanoic acid; RT 5.337–5.556 min)* → *(further oxidation)* → CO_2 + H_2O. A parallel heteroatom-processing branch is supported by the persistence of sulfur-containing aromatic fragments: EB (sulfonated aromatic dye) → *(heteroatom-associated fragmentation during redox transformation)* → 2-pentanone, 3-(3-thienyl)- (RT 27.300–27.325 min) → *(aerobic oxidation)* → aromatic acids and short-chain acids → CO_2 + H_2O. All the identified compounds during an EB degradation are listed in the (Table 3-4).

In the anaerobic samples, an aromatic oxime derivative identified as methyl N hydroxybenzenecarboximidate (reported as “Oxime-, methoxy-phenyl-) was detected at RT 6.219 to 6.307 min, indicating formation of a low molecular weight aromatic derivative during the anaerobic step.

In MFC anodes operated under anaerobic conditions, azo dyes are reduced through azoreductase activity and electron transfer linked to the respiratory chain. This reduction or cleavage of azo bonds causes rapid decolorization and generates a pool of reduced aromatic and phenolic intermediates. Many of these products are highly polar or remain sulfonated, so they are not efficiently detected by GC–MS, as noted in recent work (Veluchamy et al. 2024). In the present anodic effluent, GC–MS identified a phenolic aromatic compound, 2,4-di-tert-butylphenol, at a retention time of 22.383–22.396 minutes. The presence of this peak supports the accumulation of phenolic and other aromatic intermediates during the anaerobic stage.

Phenolic species are frequently reported as mid-pathway products in azo dye transformation and are consistent with partial remodeling of the aromatic framework following the initial reductive steps (Mishra et al. 2022).

A sulfur-containing aromatic ketone, identified as 2-pentanone, 3-(3-thienyl)-, was detected in the anode effluent at RT 27.3–27.3 min and remained detectable during the subsequent aerobic stage. Its perseverance indicates the formation of a relatively stable heteroaromatic-linked fragment that resists rapid oxidation. The detection of sulfur- and other heteroatom-bearing aromatic fragments is consistent with the stepwise transformation of sulfonated aromatic dyes, where ring-substituted sulfur functionalities are carried through intermediate pools before further breakdown. Reports on Evans Blue biodegradation frequently describe sulfur-related intermediates as the sulfonated aromatic framework undergoes sequential reduction and oxidation, supporting the interpretation that this compound represents a mid-pathway product formed during staged redox processing. (Ravi et al. 2025).

Aerobic post-treatment is routinely applied after anaerobic azo reduction because oxygen-dependent oxidoreductases and aromatic-degrading enzyme systems can oxidize the reduced aromatic intermediates first to aromatic acids and then to small organic acids (M. D. Khan et al. 2021). In our aerobic chamber, benzeneacetic acid (phenylacetic acid) was detected at RT 15.508–15.684 min, which supports the conversion of upstream aromatic fragments into carboxylated aromatics under oxidative conditions. Phenylacetic acid is a well-known node in aerobic aromatic metabolism via the phenylacetate pathway, so its appearance is consistent with channeling of dye-derived aromatics into downstream oxidative catabolism (Cuebas-Irizarry and Grunden 2024)

Short-chain acids were abundant in the aerobic effluent, including butanoic acid (RT 5.337 min), 2-methylbutanoic acid (RT 5.556 min), and 3-methylbutanoic acid (RT 5.443 min). Their presence indicates advanced oxidative breakdown and carbon-chain shortening following aromatic ring cleavage. Formation of low-molecular-weight organic acids is widely taken as evidence of late-stage oxidation and progressive mineralization in integrated MFC–aerobic treatment of azo dyes (M. D. Khan et al. 2021). An oxygenated aromatic/cyclic acid, 4-(4-methoxyphenyl) tetrahydro-2H-pyran-4-carboxylic acid (RT 7.383 min), was also detected, which further supports oxygen insertion and oxidative remodeling during aerobic post-treatment. Such oxidoreductase-driven oxidation and ring activation by actinomycetes, including Streptomyces, are well documented for dyes and other aromatic pollutants and align

with the observed shift from aromatic/phenolic signals in the anode to organic acids in the aerobic stage (El Awady et al. 2024).

Table 3-4 Selected GC–MS intermediates supporting the EB pathway in the integrated DCMFC–aerobic system.

No.	Compound (pathway-supporting)	Chamber(s) detected	RT (min)	Molecular formula	MW (g/mol)	Pathway role
1	2,4-Di-tert-butylphenol	Anode, Anaerobic	22.383–22.396	C14H22O	206.32	Representative phenolic/aromatic intermediate pool after reductive initiation
2	2-Pentanone, 3-(3-thienyl)-	Anode, Anaerobic	27.300–27.325	C9H10OS	166.24	Sulfur-containing aromatic fragment supporting heteroatom-processing branch
3	4-(4-Methoxyphenyl) tetrahydro-2H-pyran-4-carboxylic acid	Aerobic	7.383	C13H16O4	236.26	Oxygenated intermediate produced during aerobic oxidation
4	Benzeneacetic acid (phenylacetic acid)	Aerobic	15.508–15.684	C8H8O2	136.15	Aromatic acid intermediate indicating aerobic carboxylation/oxidation
5	Butanoic acid	Aerobic	5.337	C4H8O2	88.11	Low-molecular-weight acid consistent with late-stage breakdown
6	2-Methylbutanoic acid	Aerobic	5.556	C5H10O2	102.13	Low-molecular-weight acid consistent with late-stage breakdown
7	3-Methylbutanoic acid	Aerobic	5.443	C5H10O2	102.13	Low-molecular-weight acid consistent with late-stage breakdown

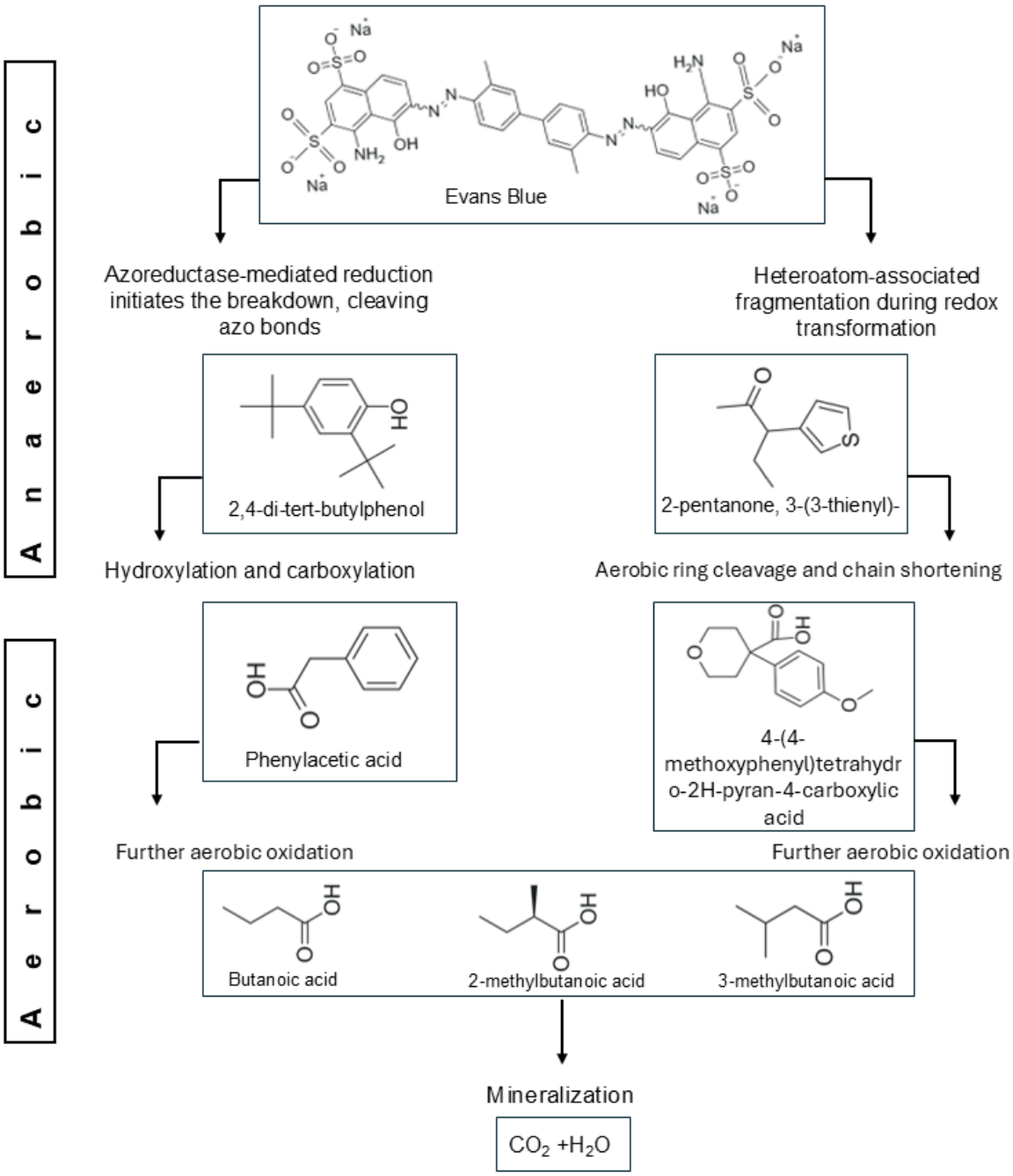

Figure 3.17 Anaerobic-Aerobic degradation pathway of Evans blue in DCMFC – preliminary proposal

Conclusions and further research directions

The results presented in Section 3.3 demonstrate that a double-chamber microbial fuel cell (DCMFC) inoculated with a mixed microbial community can effectively decolorize Evans Blue while simultaneously generating electrical power. Electrochemical analyses (CV and EIS) confirmed active extracellular electron transfer at the bioanode, and community profiling indicated enrichment of electroactive and dye-degrading taxa during reactor operation. In addition, coupling the DCMFC with an aerobic treatment step supported downstream

mineralization of reduced intermediates, addressing a key limitation (toxic intermediates) of strictly anaerobic azo dye reduction. Such process optimization allows us to obtain in terms of synthetic dyes removal environmentally safe solutions. The results were clearly concentration dependent. At 100 mg/L EB, decolorization reached 90 ± 2% to 98 ± 1.9%. When the initial dye concentration was doubled to 200 mg/L, performance decreased to 79 ± 2% to 87 ± 1%, but the combined anaerobic–aerobic sequence still completed treatment within ~20–24 hours.

However, despite these advantages, the DCMFC configuration remained constrained by bioelectrode performance (unmodified anode surface). An additional disadvantage of this system was the system's long adaptation time. The EB removal achieved in the present work is comparable to literature benchmarks reported by Quan et al., where palladium nanoparticle modification of the anode increased Evans Blue removal to 98.0%, while the corresponding unmodified control achieved 90%. This comparison highlights that the bioanode interface is a major performance lever and suggests that targeted anode surface modification can strengthen bacterial attachment, intensify interfacial electron transfer, and ultimately increase decolorization efficiency and robustness under load. Therefore, these outcomes directly motivated the next step of this dissertation: shifting from community-driven optimization within a complex dual-chamber configuration to electrode-driven enhancement in a simplified architecture.

Accordingly, in the next stage of research focused on the implementation of a single-chamber microbial fuel cell (SCMFC) equipped with a rationally engineered bioanode. By integrating a conductive polyaniline layer with localized carbon availability and a protective coating concept, the SCMFC design aims to accelerate early-stage adhesion, reduce charge-transfer limitations, shorten start-up time, and maintain rapid Evans Blue decolorization at higher dye concentrations. This progression preserves continuity with the mixed-culture findings in Section 3.3 while testing whether engineered anode biointerfaces can deliver faster treatment and improved electrochemical performance with reduced reactor complexity and applying the pure strain of electroactive bacteria *Shewanella oneidensis* MR-1.

3.4 Performance of SCMFC with Modified Bioanode (MCC.B

Microbial fuel cells provide a route to couple wastewater treatment with energy recovery by exploiting exoelectrogenic bacteria that transfer electrons from organic substrates to electrodes. Among the best-studied model exoelectrogens, *Shewanella oneidensis* MR-1 supports both direct and mediator-assisted extracellular electron transfer through a cytochrome-based transmembrane pathway and soluble redox shuttles. Nevertheless, practical application remains constrained by slow biofilm establishment and inefficient interfacial charge transfer, which translate into prolonged start-up periods and limited early-stage current production. Consequently, anode biointerface engineering is widely pursued as the most direct way to improve microbial adhesion and electron mobility while maintaining mild operating conditions.

Accordingly, Section 3.4 advances the dissertation objective by shifting from reactor- and community-scale optimization to biointerface engineering at the anode level, while retaining a defined microbial system. Building on the mechanistic insights from section 3.3, this chapter investigates whether rational modification of the anode surface using a conductive polyaniline-based coating combined with localized nutrient-deposition and controlled-release concepts can enhance microbial adhesion, reduce charge-transfer resistance, and increase apparent charge storage capacity during the critical early operational phase. The central hypothesis of this part of dissertation is that accelerating biofilm formation and extracellular electron transfer at the anode–biofilm interface will translate directly into faster Evans Blue decolorization and improved electrochemical performance, thereby addressing the kinetic and resistance-related limitations identified in the DCMFC system and providing a scalable strategy for rapid treatment of dye-laden wastewaters

The detailed reactor configuration, electrode preparation steps, and operating conditions for the SCMFC experiments are described in Section 2.7 (Materials & Methods). The present section (3.4) focuses exclusively on performance outcomes and their interpretation (decolorization kinetics, electrochemical response, and surface/chemical characterization evidence).

The part of results presented in this chapter were published in the research paper entitled "*Enhancing Microbial Adhesion and Electron Transfer of Shewanella oneidensis MR-1 with Polyaniline-Glucose-Gelatin Coating for Bioelectrochemical Applications*" by Ayaz, K., Zabłocka-Godlewska, E., Shakibania, S., Patel, T., Karoń, K., & Krukiewicz, K.

(2026b). *Journal of Environmental Chemical Engineering*, 121546. (Ayaz, Zabłocka-Godlewska, Abdullah, et al. 2026b)

3.4.1 Electrode modification

Polyaniline (PANI) modification of carbon-cloth electrodes has been widely explored across multiple domains, including enhancing of microbial attachment, wastewater treatment, supercapacitor development, and enhancement of electrical output (Huang et al. 2016; J. Li, Zhao, and Liu 2023; Khalil, Ridha, and Al-Mashhadani 2023). Despite this broad interest, the approach carries important constraints. A central limitation reported for PANI-modified electrodes is suboptimal bacterial adhesion (Gizdavic-Nikolaidis et al. 2011; Ramos et al. 2019; Guo et al. 2023), which necessitates deliberate interfacial modification to improve biofilm–electrode contact in bioelectrochemical systems. Reduced attachment directly hinders efficient charge transfer between the biofilm and the conductive substrate, thereby lowering electron recovery and stability of electron flow. To overcome this limitation, in the present work carbon cloth was first electrochemically polymerized with PANI and then overlayered with glucose to attract bacteria to the modified surface, followed by a protective gelatin film to limit glucose leaching into the bulk solution. We selected drop casting because of its operational simplicity and compatibility with lab-scale fabrication. Although drop-cast coatings can be vulnerable to abrasion in some contexts, the glucose and gelatin layers exhibited strong adhesion on the carbon cloth and preserved their integrity throughout the experiments.

Electrochemical evidence for successful PANI growth was obtained from the (CV) response during aniline electropolymerization (Figure 3.18a). The CV displays three well-defined redox couples that map onto the stepwise formation and oxidation states of PANI. The first couple corresponds to conversion from the fully reduced leucoemeraldine state to the partially oxidized emeraldine state (1, 1’). The second couple (2, 2′) is associated with reactions of intermediate species such as p-benzoquinone, p-aminophenol, and dimeric products, which contribute to the evolving electrochemical activity of the film. The third couple (3, 3′) reflects the transition from emeraldine to the fully oxidized pernigraniline state (Belgherbi et al. 2021; Prasad and Munichandraiah 2002; Pournaghi-Azar and Habibi 2007; Shakibania et al. 2025). A progressive rise in peak currents over successive cycles indicates continuous PANI deposition, enlargement of the electroactive surface area, and improved film conductivity.

Taken together, these features confirm the formation of a conductive PANI network and support its suitability as a tailored anode interface for bioelectrochemical applications.

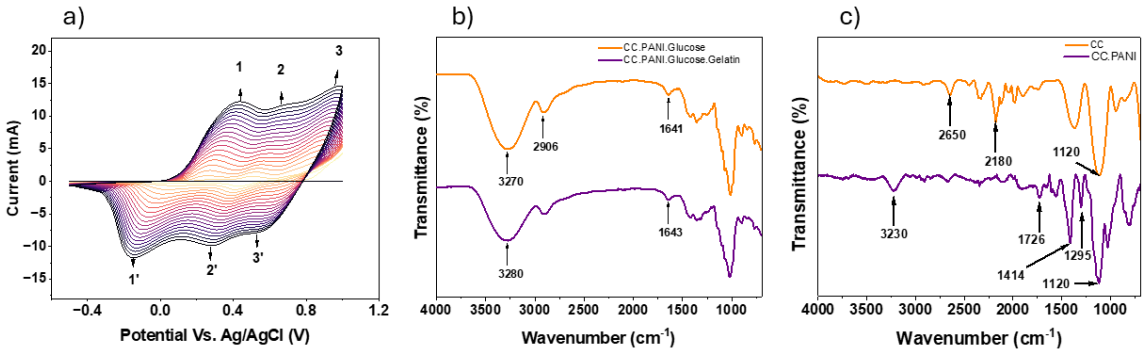

Figure 3.18 (a) Cyclic voltammogram presenting the electrochemical polymerization of aniline on the surface of carbon cloth. (b-c) FTIR spectra of experimental samples, including (c) carbon cloth (CC), CC electropolymerized with PANI (CC.PANI), and (b) CC-PANI coated with glucose (CC.PANI.Glucose), and a protection layer of gelatin (CC.PANI.Glucose.Gelatin referred to as MCC) (K. Ayaz et al. 2026b).

Four samples were analyzed by FTIR: bare carbon cloth (CC), carbon cloth with polyaniline (CC.PANI), CC.PANI coated with glucose (CC.PANI.Glucose), and the final glucose–gelatin composite anode (MCC). The spectra show clear, stage-specific shifts that reflect the expected functional groups and their interactions (Figure 3.18b–c).

For CC, the major bands appear at 1120 cm^{-1}, assigned to C–O stretching, and at 2180 cm^{-1}, attributed to C–O–C vibrations. A peak near 2650 cm^{-1} is consistent with low-intensity C–H stretching from aliphatic residues. After PANI deposition (CC.PANI), the spectrum changes markedly, showing new peaks at 1726 cm^{-1} (C=O stretching), 1414 cm^{-1} (C=C of benzenoid rings), and 1295 cm^{-1} (C–N stretching). These bands are characteristic of protonated PANI films and confirm successful electropolymerization on the carbon fibers, in agreement with prior reports (Jiang and Cui 2006; Shahabuddin et al. 2016; Shirani et al. 2020). Addition of the glucose layer introduces broad O–H stretching centered at 3270 cm^{-1} and a C–H stretching band near 2906 cm^{-1}, together with a shifted carbonyl signal at 1641 cm^{-1}. The downshift of the carbonyl region indicates hydrogen-bond formation between glucose and the underlying PANI or surface oxygen groups (Nybacka, n.d.; Abdullah et al. 2024), and a shifted C=O peak at 1641 cm^{-1}, indicating hydrogen bonding. Applying the gelatin overlayer maintains the strong hydroxyl/amine envelope near 3280 cm^{-1} (O–H/N–H) and gives a carbonyl band at 1643 cm^{-1}, consistent with amide I vibrations from protein backbones (Sultan et al. 2024).

Taken together, these spectral features validate the stepwise functionalization pathway. The baseline CC signals are modified by PANI growth, then further enriched by glucose, and finally stabilized by gelatin. The sequential appearance and position of O–H, C–H, C=O, C–

N, and aromatic C=C bands provide direct chemical evidence that each coating was successfully applied and that interlayer interactions, including hydrogen bonding, were established during the assembly of the MCC bioanode.

Further confirmation of the presence of an organic moiety on the surface of carbon cloth was provided by the XPS analysis (Figure S6.4-S6.7). A wide XPS spectrum of CC (Figure S6.4) revealed the presence of two peaks centered at 285 eV (C1s), and 532 eV (O1s). Here, C1s could be deconvoluted with three peaks, namely 285.02 eV, 285.47eV and 283.07 eV representing C–C, C-H and C=C. Additionally, a weak backbone with the higher binding energy (~290 eV) could be derived from the presence of carbonyl or carboxyl groups or is related to the pi to pi* transition (Biesinger 2022; Grey, Nie, and Biesinger 2024). On the other hand, O1s can be divided to two peak lines at binding energies of 530 eV and 532 eV, representing C—O and C–OH, respectively. The XPS spectrum of CC.PANI (Figure S6.5) presents four peaks centered at 285 eV (C1s), 400 eV (N1s), 532 eV (O1s), and 168 (S2p), the last one derived from the remaining supporting electrolyte. Here, C1s consists of three components located at 284.77 eV, 285.69 eV, and 287.12 eV representing C=C, C–C and C–N, respectively. Also here, two oxygen components are present at 531.94 eV, and 533.24 eV, derived from C—O and C–OH, respectively. The signal in nitrogen region can be decomposed into two lines at 400.08 eV and 400.96 eV that correspond to pyrrolic and pyridinic nitrogen, respectively (Fenniche et al. 2022; Mohtasebi et al. 2016). Having the same composition as CC.PANI, XPS spectrum of CC.PANI.Glucose (Figure S6.6) is represented by a different content of given elements at slightly different peak positions. For instance, C1s signal can be deconvoluted into peaks at 284.91 eV, 286.46 eV, and 288.03 eV, assigned to C=C, C–C, and C–N, respectively. The dominant O1s signal (532.86 eV) is derived from C–OH from glucose, while the nitrogen band can be assigned to pyrrolic and pyridinic nitrogen from PANI at 400.17 eV and 401.79 eV, respectively. The XPS spectrum of CC.PANI.Glucose.Gelatin (Figure S6.7) also consists of three peaks for C1s, O1s and N1s, probably all derived from gelatine. The peaks can be deconvoluted to 284.90 eV, 286.21 eV, 287.76 eV, assigned to C=C, C–C and C–N, respectively, 532.98 eV assigned to C–OH, and 400.15 eV, 401.23 eV, assigned to pyrrolic and pyridinic nitrogen.

To gain insight into the degradation behavior of the outer gelatin layer, time-resolved FTIR was used to track, with spectra collected for MCC after 0.5 to 12 h in water (Figure S6.8). This approach is widely applied to follow structural changes in hydrated proteins and gelatin films (Hermida-Merino et al. 2022; Ji et al. 2022).

The amide I band near 1640 cm^{-1} and the broad O–H/N–H envelope around 3280 cm^{-1}, both characteristic of gelatin, progressively decreased in intensity as immersion time increased. This trend matches published FTIR signatures of gelatin-based films and hybrids, where amide I and the high-wavenumber N–H/O–H region are standard markers for gelatin content and hydration state (Radhika Rajasree et al. 2020; Hermida-Merino et al. 2022; Usoltsev et al. 2019).

In parallel, a band in the 1020–1040 cm^{-1} window, assigned to C–O stretching of glucose and related polysaccharide units, became relatively more prominent with time, which agrees with reports that identify strong carbohydrate C–O and C–O–C vibrations near 1030–1040 cm^{-1} in polysaccharide-rich matrices. Taken together, these spectral changes indicate gradual rather than instantaneous dissolution of the gelatin overlayer and a progressive exposure of the glucose-rich surface on a timescale that is relevant to initial bacterial attachment. Although we did not quantify glucose release kinetics, the observations support a controlled exposure mechanism instead of a measured controlled-release rate, which is consistent with hydration-driven dissolution behavior reported for gelatin films (Qu, Qader, and Abbott 2021; Ji et al. 2022).

3.4.2 Electrode and biofilm-electrode system surface morphology

Scanning electron microscopy (SEM) highlights how surface morphology influences stable biofilm formation and electrochemical performance. The SEM image of the unmodified carbon cloth (CC) (Figure 3.19a) shows the expected smooth, fibrous topography of pristine carbon fibers, with minimal surface features as reported in the literature (Yundan Liu et al. 2016; Ahirrao et al. 2021). The carbon cloth displays a uniform bundle-like architecture, and the plain weave pattern provides mechanical integrity and consistent interfacial contact, attributes that are ideal for electrochemical use. After aniline electropolymerization (Figure 3.19b), the CC surface is markedly altered. The fibers are coated with a polyaniline (PANI) film that appears rough and granular, a morphology consistent with successful polymer growth and the creation of a more developed electroactive area suitable for subsequent bioelectrochemical operation (Yuan Li et al. 2021).

Further modification with glucose produces a continuous, smooth overlayer on the PANI-coated fibers (Figure 3.19c). The CC.PANI.Glucose surface appears uniformly covered, indicating effective incorporation of the carbohydrate while preserving the underlying fibrous scaffold of the cloth (Abdullah et al. 2024). The final composite, formed by adding a gelatin

overcoat (MCC), exhibits an even more homogeneous and smoother appearance than CC.PANI.Glucose (Figure 3.19d). This morphology is consistent with effective encapsulation of the glucose layer by gelatin, which improves stability in aqueous media and helps maintain the overall structural integrity of the modified electrode. Together, these sequential SEM observations confirm the stepwise modification, and this protective coating ensures stability in liquid environments, preserving the glucose layer against rinsing into bulk solution, while maintaining the overall structural integrity of the modified electrode.

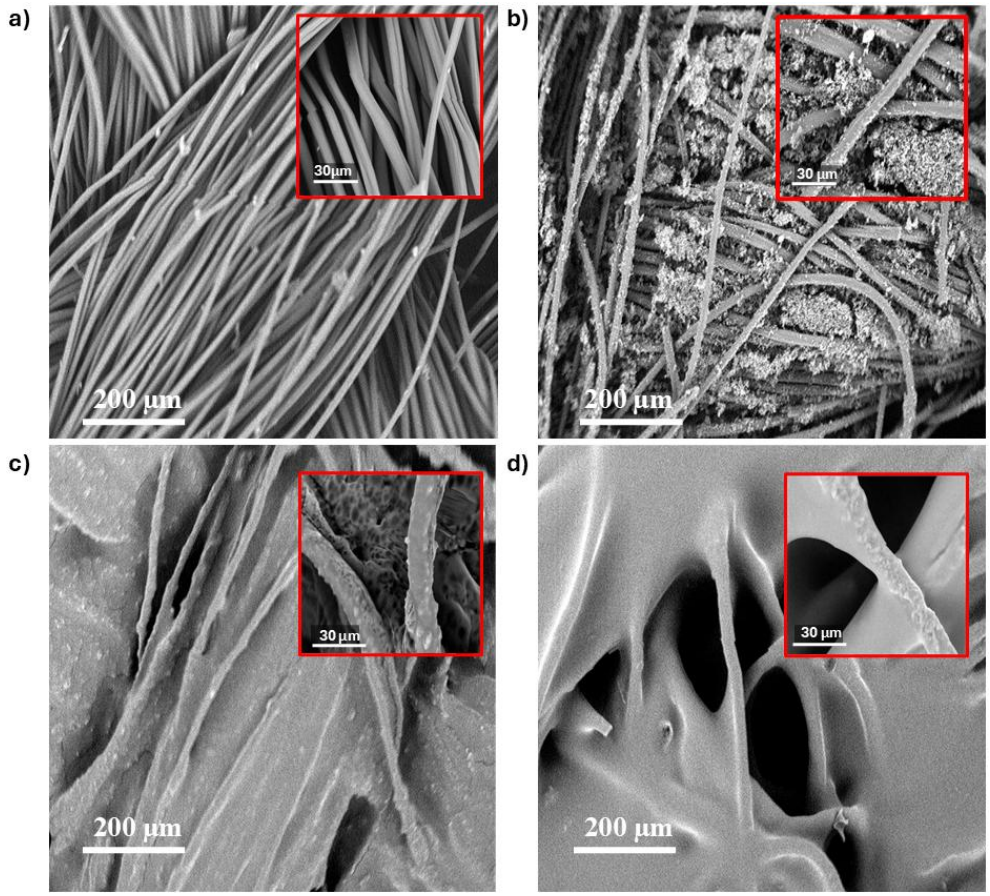

Figure 3.19: SEM images of (A) CC (B) CC.PANI (C) CC.PANI.Glucose and (D) MCC; scale bar is 200 µm, inset – high magnification images (scale bar is 30 µm).(K.Ayaz et al. 2026b)

3.4.3 Biofilm formation and cell viability

Cell viability in biofilm (Figure 3.20a–d) and electrode biofilm coverage (Figure 3.20e) show clear differences among CC.B, CC.G.B, and MCC.B that arise from surface chemistry and layering. The unmodified carbon cloth supports high cell viability at 97 ± 2 %, but it does not promote robust attachment, yielding only 7.1 ± 0.3% biofilm coverage. Adding glucose to the medium (CC.G.B) increases biofilm formation to 52.9 ± 0.9%, but viability drops to 24 ± 5%. This pattern suggests that when glucose is freely available in solution it promotes bacteria growth in suspension as well as encourages initial adhesion but does not sustain a healthy,

stable biofilm. The multilayer anode MCC.B performs best, with the highest coverage at 71.5 ± 0.3% and the highest fraction of live cells at 99 ± 1%, indicating strong compatibility of the modified interface with bacterial growth and persistence.

To isolate the effect of the alone PANI layer, we quantified biofilm coverage on PANI.B under identical conditions (Figure 3.20e). On day 1, PANI.B reached 23.9 ± 0.7% coverage, which already exceeds the bare CC.B and indicates that PANI alone promotes early attachment. By day 7, coverage on PANI.B rose to 53.8 ± 0.2%, yet it remained below MCC.B, which retained the highest coverage of all electrodes. These observations support a two-part mechanism: PANI improves initial adhesion and provides a conductive interface for electron exchange, while the glucose–gelatin overlayer is required to achieve the dense, rapidly established biofilm observed on MCC.B.

Prior work reported approximately 55% biofilm formation with 98% viability for *S. oneidensis* on PEDOT:PSS electrodes functionalized with glucose (Abdullah et al. 2024). The higher surface (71.5 ± 0.3%) coverage and similarly high viability (99 ± 1%) observed in the case of MCC.B electrode surface are consistent with stable retention of glucose at the surface, aided by the gelatin intermediate layer. Gelatin likely serves as the first accessible carbon source and attracts cells to the electrode. As the gelatin layer hydrates, digests and gradually dissolves (Figure S6.8), the underlying glucose becomes more available, which promotes localized attachment and maturation of the biofilm at the anode interface. This stepwise exposure matches the FTIR trends for gelatin hydration and dissolution (Figure S6.8) and aligns with the sustained rise in live-cell coverage and the reduction in charge-transfer resistance measured for MCC.B (Figure 3.20d and Figure 3.22). Although extracellular polymeric substances were not quantified, the combination of high viability, high coverage, and lower R_2 values is typical of dense, electroactive biofilms documented for *S. oneidensis* and related electroactive bacteria on optimized anodes. By day 7, all samples increased in coverage, with MCC.B reaching 90.2 ± 0.2%, clearly higher than CC.B at 42.1 ± 0.2% and CC.G.B at 51.0 ± 0.1%, which highlights stability and sustained growth supported by multilayer design. Future work will combine the present electrochemical and imaging data with direct measurements of glucose release and EPS production to further resolve the underlying biological mechanisms.

The low early coverage on CC.B on day 1 reflects the absence of a local carbon source. After glucose addition in liquid medium on days 3 and 5, coverage increased to 42.1%, which is comparable to CC.G.B at days 1 and 7. These dynamics indicate that when carbon is available

in the bulk liquid, bacteria form a thin outer layer of biofilm on CC, but the outer strata rapidly consume nutrients, leaving inner cells starved. This creates gradients in both electron acceptors and carbon-energy substrates. Because matrix turnover in young biofilms is slow, inner cells enter a survival state while outer cells proliferate. Over time the inner layer transition toward inactivity or death, and the outer layers dominates growth. Such structure decreases the electron transfer. Similar layer-wise dynamics have been reported elsewhere (L. Zhang et al. 2024)(Greenman et al. 2021).

Phosphate-buffered saline washing then removes loosely attached outer cells, leaving the inner layers that contain a high fraction of damaged or dead cells. This behavior corresponds with the confocal viability data in Figure 3.20d and explains the high proportion of dead-stained cells on CC.G.B. Importantly, a low fraction of live-stained cells at the surface does not mean that all cells are electrochemically inactive. A small portion of live bacteria can still generate the modest electrochemical signals seen for CC.G.B, however that current is much weaker than MCC.B, as indicated by lower CSC and higher R_2.

MCC.B exhibited the highest viability and coverage on both day 1 and day 7, which points to enhanced early-stage establishment and sustained maturation. These biological outcomes are consistent with the short-term electrochemical improvements observed over the same period. The results also agree with reports that slow-release carbon immobilized in polymer matrices sustains long-term power output and enriches electrode-associated biomass relative to the bulk anolyte (W. Li et al. 2020). In our design, positioning the carbon source directly on the electrode promotes local growth on MCC.B. The glucose–gelatin layers support early attachment and local nutrient availability, while the PANI underlayer likely reduces interfacial losses by improving electronic connectivity. The combined effect is a more viable and better-attached biofilm, a higher fraction of metabolism coupled to the anode, and increased current and power output, which is consistent with the higher current responses recorded in this study.

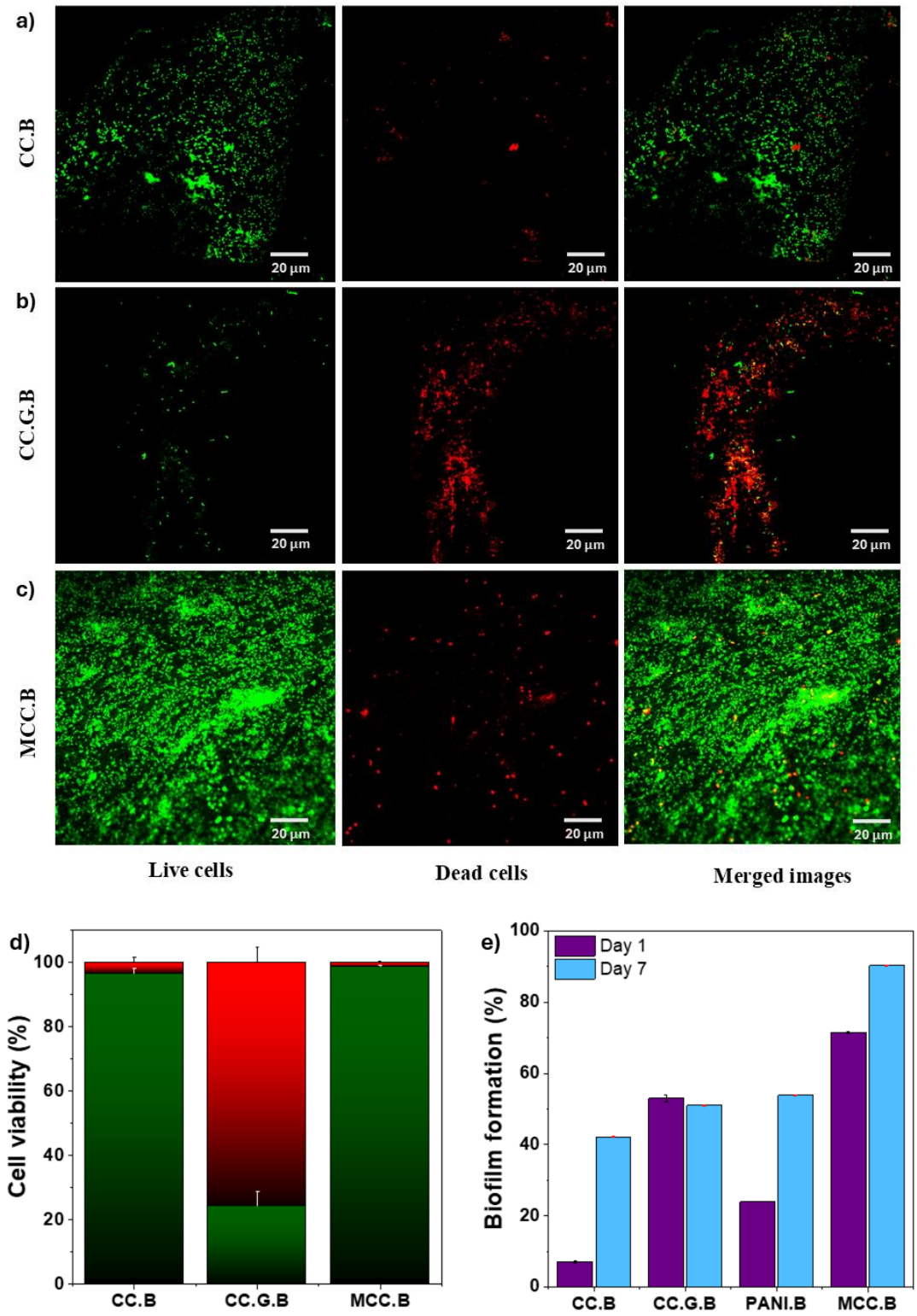

Figure 3.20 Confocal fluorescent microscope images of S. oneidensis cells cultured on the surface of (a) CC, (b) CC.G, (c) MCC, green staining represents live bacteria, while red staining represents dead bacterial cells. (d) Cell viability percentage, (e) Biofilm formation percentage (absorbance of the medium over a CC control was used as the baseline for biofilm quantification). (K.Ayaz et al. 2026b)

3.4.4 Electrochemical analysis

Cyclic voltammetry

CV was applied to compare how each electrode modification stage affected the electroactivity of *S. oneidensis*. We evaluated characteristic anodic and cathodic peak currents IpA, IpC respectively, Figure 3.21a–d) and the total charge transferred via extracellular electron transfer (EET), expressed as charge storage capacity, CSC (Figure 3.21e). All CSC values refer to the apparent areal charge density defined in Section 2.7. The CV results show that bacterial biofilms markedly increase electrochemical activity relative to abiotic controls. On CC.B (Figure 3.21a), a clear anodic peak appears at 0.28 V with IpA = 0.070 mA, whereas unmodified CC displays no distinct peaks, indicating that biofilm formation improves charge transfer through EET. The cathodic response also strengthens, with IpC ≈ −0.17 mA for CC.B and negligible response for CC. Consistent with these trends, CSC rises from 3.3 ± 0.3 mC/cm^{-2} on CC to 14.8 ± 0.1 mC/cm^{-2} on CC.B, confirming greater charge storage and redox engagement once a biofilm is established.

A similar pattern is observed for glucose-containing in bulk system. Abiotic CC.G (Figure 3.21b) shows no distinct IpA or IpC peaks and yields a CSC of 2.0 ± 0.1 mC/cm^{-2}. In contrast, CC.G.B presents IpA = 0.04 mA at 0.3 V and IpC = −0.14 mA at −0.4 V, with CSC increased to 7.2 ± 0.7 mC cm^{-2}. The lower oxidation current on CC.G.B likely reflects the high fraction of non-viable cells indicated by LIVE/DEAD staining and prior reports (Greenman et al. 2021). Given the low surface viability measured for CC.G.B (Figure 3.21b), the CV response is best interpreted as residual activity from a small population of electroactive cells combined with non-faradaic double-layer charging, rather than as evidence of a thick, well-coupled biofilm. The low live-cell fraction of 24% agrees with the reduced CSC and higher R_2 values for CC.G.B when compared with MCC.B.

The multilayer bioanode MCC.B delivers the strongest response. MCC.B (Figure 3.21d) exhibits IpA = 0.40 mA at 0.4 V and IpC = −0.41 mA at −0.4 V, together with CSC = 44.0 ± 7.12 mC/cm^{-2}. The corresponding abiotic electrode, MCC, shows a much smaller CSC of 1.1 ± 0.05 mC/cm^{-2}. To isolate the contribution of PANI from that of the glucose–gelatin overlayer, we compared a PANI-only bioanode (CC.PANI.B) with the abiotic PANI-coated electrode (CC.PANI) (Figure 3.21c). CC.PANI increases CSC to 17.1 ± 3 mC cm^{-2} relative to CC.B, consistent with the larger electroactive area and redox capacity of the PANI film. Establishing a biofilm on the PANI surface further raises CSC to 36.1 ± 7 mC cm^{-2} and broadens the CV

loop, which indicates improved charge storage and faster interfacial electron exchange. Even so, CC.PANI.B does not reach the CSC of MCC.B, confirming that the highest charge storage occurs when PANI is combined with the glucose–gelatin layers that promote rapid, dense, and viable biofilm development.

Overall, the CC.PANI, CC.G.B, CC.PANI.B, and MCC.B datasets point to complementary roles for the layers. PANI serves mainly as a conductive, redox-active scaffold that enhances electronic wiring and adds pseudocapacitance. The glucose–gelatin layers primarily regulate local carbon availability and control biofilm density and viability. The combination yields higher CSC alongside lower R_2 and higher j_0 for MCC.B, which should be interpreted as apparent interfacial kinetics for the complete bioelectrode rather than as a direct measure of intrinsic microbial EET alone.

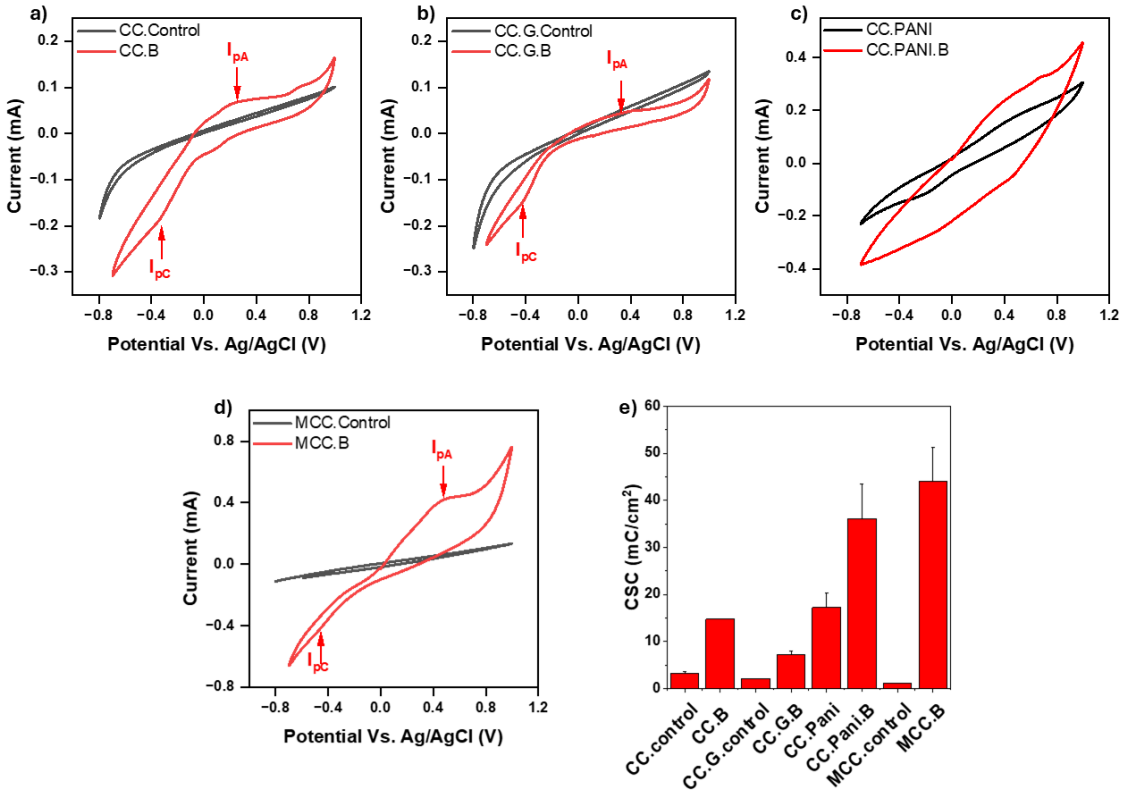

Figure 3.21 Cyclic voltammograms of (a) CC.Control and CC.B, (b) CC.G.Control and CC.G.B (c) CC.PANI and CC.PANI.B (d) MCC.Control and MCC.B. (e) Charge storage capacity values derived from CV curves.(K. Ayaz et al. 2026b)

Electrochemical impedance spectroscopy

EIS results (Figure 3.22a–c) support the CV findings by showing consistently higher resistances for abiotic controls than for biofilm-bearing electrodes, with one exception. CC.G.B displays increased resistance despite the presence of a biofilm, which is consistent

with a biofilm that behaves as a physical barrier when cell viability is low. To obtain reliable parameter estimates, we fitted the spectra with alternative equivalent circuits following (Santoni et al. 2024) and selected models that minimized χ^2 and the relative errors of the fitted elements. The complete parameter sets (R_1, R_2, constant-phase element parameters, (P, n), and the Warburg coefficient W) where applicable, together with fitting errors are reported in Tables S6-2 and S6-3. In all models, R_1 represents the solution resistance governed by electrolyte conductivity, and R_2 captures the interfacial charge-transfer resistance at the electrode surface. For CC.B, two parallel CPEs were required to reflect double-layer storage and biofilm heterogeneity. For CC.G.B, a single CPE was sufficient, indicating a more uniform interfacial response with lower heterogeneity. For MCC.B, the Nyquist plot exhibits a 45° low-frequency tail, so the circuit includes a Warburg element in addition to R_1, R_2, and a CPE, consistent with diffusion-limited transport through the gelatin overlayer or the biofilm matrix. Notably, W decreases from 270 $\Omega \cdot s^{-1/2}$ for the abiotic MCC control to 157 $\Omega \cdot s^{-1/2}$ for MCC.B (Table S6-2), which implies that partial degradation of gelatin and biofilm restructuring reduce diffusional limitations while keeping R_2 low.

Quantitative comparisons of R_2 underscore these trends (Figure 3.22c). CC.B yields $R_2 = 2883 \pm 64$ Ω, which indicates moderate interfacial resistance. CC.G.B rises to $R_2 = 3390 \pm 61$ Ω, consistent with low surface viability and growth biased toward the bulk phase when glucose is available in solution. The abiotic multilayer MCC, comprising PANI, glucose, and gelatin, shows $R_2 = 2900 \pm 92$ Ω; this value is attributed to the insulating effect of intact gelatin that restricts charge transfer. In contrast, MCC.B achieves $R_2 = 952 \pm 21$ Ω. The lower value reflects bacterial degradation of gelatin, greater exposure of glucose at the interface, improved adhesion, and more efficient electron transport across the biofilm–electrode contact. Taken together, these results show a synergistic effect of surface modification and microbial activity. MCC.B provides the most favorable interfacial kinetics among the tested electrodes and is therefore the strongest candidate for bioelectrochemical operation.

To compare kinetics on a common basis, we estimated the apparent exchange current density j_0 from the EIS fits (Table S6-4). The PANI-only bioanode CC.PANI.B exhibits an intermediate R_2 of 2304 ± 322 Ω and $j_o = 0.0093$ mA/cm^{-2}. This value is higher than CC.B (0.0074 mA/cm^{-2}) and CC.G.B (0.0021 mA/cm^{-2}), yet lower than MCC.B (0.022 mA/cm^{-2}). Thus, MCC.B shows roughly a threefold increase in j_o relative to CC.B and an order-of-magnitude increase relative to CC.G.B. These differences are consistent with the lower R_2 and

higher CSC measured for MCC.B and fall within the ranges reported for high-performance bioanodes in microbial fuel cells (Y. B. Fu et al. 2016; Rajesh, Noori, and Ghangrekar 2020).

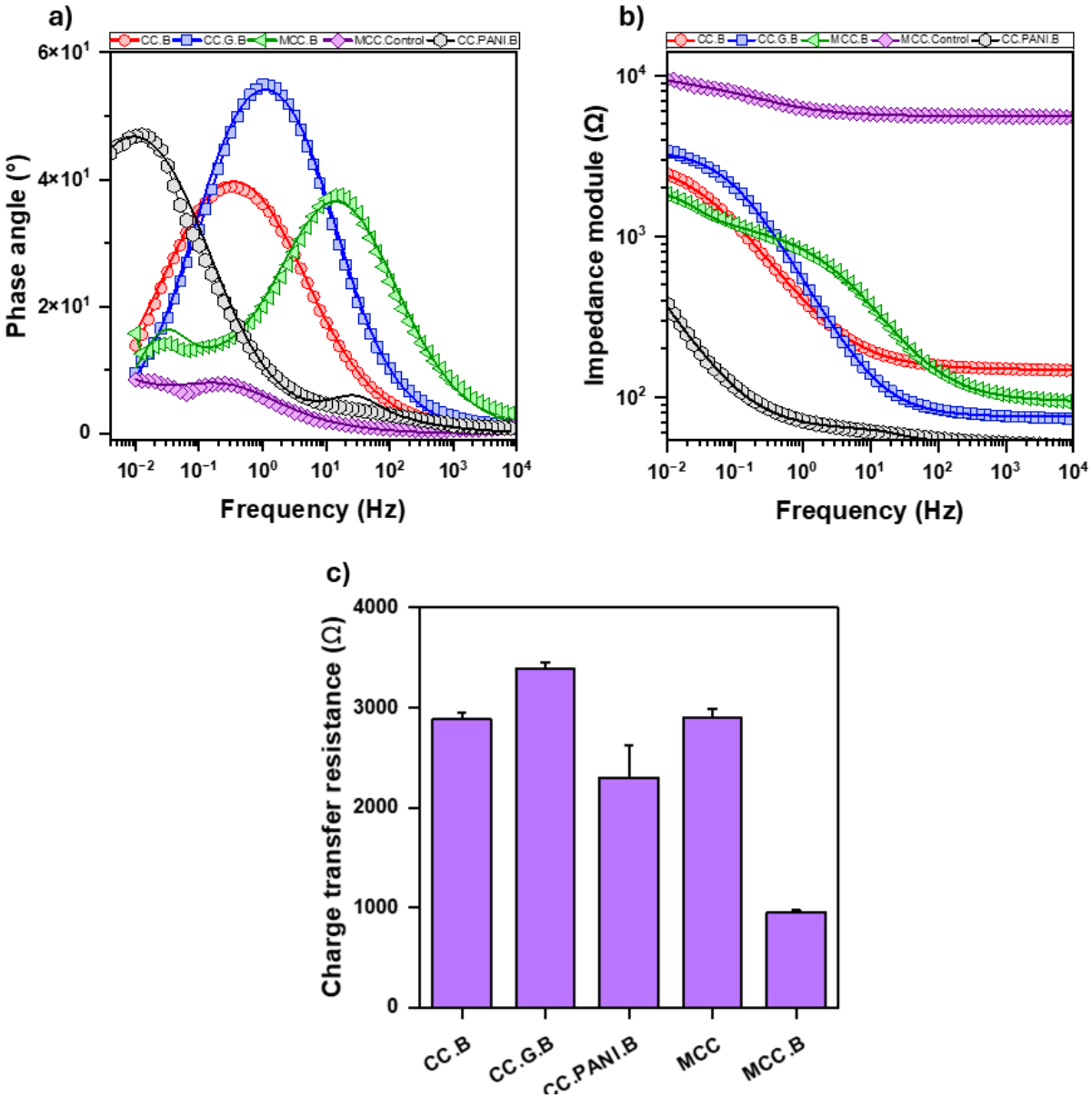

Figure 3.22 Bode plots presenting the behavior of bare and modified carbon cloth electrodes: (a) Impedance vs. frequency, (b) Phase angle vs. frequency. Hollow shapes represent experimental points, while the solid lines represent fitting curves. (c) Comparison of charge transfer resistance for CC.B, CC.G.B,CC.PANI.B, MCC.control, and MCC.B.(K. Ayaz et al. 2026b)

3.4.5 Stability Analysis

The electrochemical behavior of CC.B, CC.G.B, and MCC.B depends on biofilm stability, bacterial activity, and substrate supply. Time-series CV curves (Figure S6.9), CSC values (Figure 3.23a), and EIS data (Figure S6.10; Figure 3.23b) collected on days 1, 3, 5, and 7 capture the effects of glucose depletion and biofilm maturation on charge transfer. These trends

highlight the central role of localized carbon availability in sustaining cell attachment and electron transfer at the electrode.

For CC.B, the anodic and cathodic peak currents decline between day 1 and day 3 in the absence of an added carbon source (IpA1 = 0.06 mA) and (IpC1 = −0.04 mA). Glucose supplementation of 1% on day 3 stabilizes the redox response on day 5 (IpA3 = 0.03 mA) (IpC3 = −0.13 mA). The addition of 1% glucose dose on day 5 increases the response by day 7 (IpA4 = 0.08 mA) (IpC4 = −0.04 mA), which is consistent with continued biofilm growth and improved charge transfer. CSC follows the same pattern, rising from 10 ± 2 mC cm^{-2} on day 1 to 13 ± 1 mC cm^{-2} on day 7, indicating progressive biofilm development on the unmodified carbon cloth.

For CC.G.B, the day-1 peaks are (IpA1 = 0.03 mA) and (IpC1 = −0.07 mA) and they remain similar by day 3 (IpA2 = 0.03 mA) and (IpC2 = −0.10 mA). Adding 1% glucose on day 3 gives (IpA3 = 0.02 mA) and (IpC3 = −0.08 mA) on day 5. A second addition on day 5 yields (IpA4 = 0.07 mA) and (IpC4 = −0.04 mA) on day 7. CSC stays low throughout 10 ± 7 to 9 ± 2 mC/cm^{-2} from day 1 to day 7. The lower IpA on day-7 relative to CC.B indicates limited adhesion to the carbon cloth when glucose is freely available in the bulk liquid. These observations match Figure 3.20b and support the view that a soluble carbon source encourages planktonic growth and diverts electrons away from the anode. Prior work (Pereira et al. 2022) suggesting that optimizing operating conditions to reduce planktonic growth and promote biofilm formation is crucial for enhancing Coulombic efficiency in microbial fuel cells.

For MCC.B, electrochemical activity is highest. Day-1 peaks are (IpA1 = 0.50 mA) and (IpC1 = −0.49 mA). By day 3, glucose depletion at the surface reduces the peaks to (IpA2 = 0.30 mA) and (IpC2 = −0.31 mA). A 1% glucose addition on day 3 restores (IpA3 = 0.50 mA) and (IpC3 = −0.43 mA) by day 5. A second dose on day 5 raises the response on day 7 to (IpA4 = 1.05 mA) and (IpC4 = −0.94 mA). CSC is initially 104 ± 3 mC/cm^{-2}, declines to 46 ± 11 mC/cm^{-2} by day 5 with carbon depletion, then increases sharply to 175 ± 10 mC/cm^{-2} by day 7. This evolution indicates robust biofilm growth on the PANI-based trilayer and improved electron transfer at the interface. The concurrent increase in CSC and biofilm coverage supports a direct link between biofilm maturation and charge storage. The combined visual evidence and electrochemical metrics show that a localized carbon source at the electrode surface promotes attachment and electroactivity more effectively than dissolved glucose in the medium.

Within the 7-day window, MCC.B maintains lower R_2 and higher CSC than CC.B and CC.G.B. This indicates better short-term stability of the biofilm–electrode interface during and immediately after start-up. Because the primary goal was to shorten acclimation and strengthen early biofilm formation and extracellular electron transfer, the stability assessment was confined to the first 7 days. Longer tests beyond 30 days will be needed to quantify carbon-release kinetics and the mechanical durability of the gelatin layer under continuous operation.

After the first 24 h, all reactors received the same bulk glucose feed. The day-7 differences therefore arise mainly from the interfacial architecture and the biofilm structure, rather than from continued advantages of immobilized glucose. Under these matched conditions, the PANI-glucose-gelatin trilayer sustains lower R_2 and higher CSC, which is consistent with stronger biofilm–electrode coupling and lower interfacial losses over the short period examined.

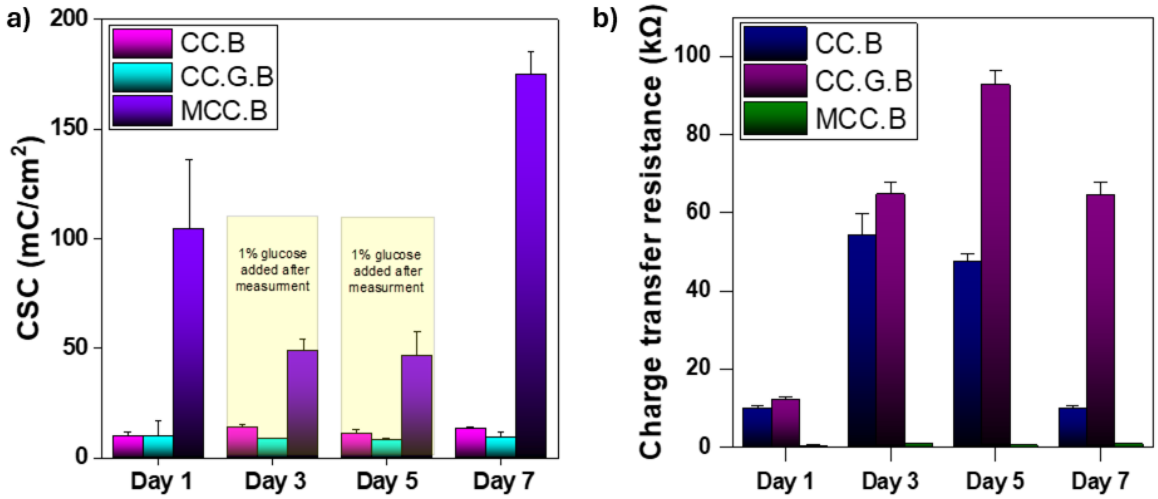

Figure 3.23 (a) Charge storage capacity values (b) comparison of charge transfer resistance values for CC.B, CC.G.B, and MCC.B. (K. Ayaz et al. 2026b)

EIS acquired during the stability experiment confirms the CV trends. The same equivalent-circuit families were used for fitting and for representing charge-transfer and mass-transport behavior (Table S6-3). The R_2 values show clear differences among electrodes and time points (Figure S6.10; Figure 3.23b). For CC.B, R_2 starts at 10 ± 1 kΩ on day 1, rises to 54 ± 6 kΩ on day 3 with carbon depletion, decreases to 48 ± 2 kΩ on day 5 after feeding, and returns to 10 ± 1 kΩ on day 7 as the biofilm stabilizes. For CC.G.B, R_2 remains high: 12 ± 1 kΩ on day 1, 64 ± 3 kΩ on day 3, 93 ± 4 kΩ on day 5, and 64 ± 3 kΩ on day 7. These values are consistent with weak adhesion on the electrode when glucose is available in the liquid phase. For MCC.B,

R_2 is much lower: 199 ± 6 Ω on day 1, 904 ± 40 Ω on day 3, 427 ± 3 Ω on day 5, and 837 ± 17 Ω on day 7. The low-ohmic regime for MCC.B reflects the role of PANI in facilitating electron transfer. The partial dissolution of the gelatin layer supports attachment and biofilm restructuring, which further improves interfacial kinetics within the first week of operation.

3.4.6 SCMFC Electrochemical Performance

During SCMFC operation at a fixed external resistance (R_{ext} =1000 Ω), the MCC anode produced consistently higher voltage output during the biofilm formation phase than the unmodified carbon cloth system (Figure S6.11). MCC reached a peak voltage of 171 mV (I_{peak}=0.171 mA), whereas CC reached 87.5 mV (I_{peak}=0.0875 mA). The higher voltage and recovered charge of MCC compared with CC are consistent with the improved interfacial kinetics (lower R_2, higher j_0) observed during the electrochemical characterization of electrodes. PANI-based coatings can improve the electrical connectivity between biofilm and electrode, provide redox-active pathways, and increase effective electroactive surface area, which collectively lowers interfacial losses and raises current generation relative to bare carbon electrodes. In addition, the feed-dependent "rise–decay" voltage behavior commonly observed in batch or semi-continuous MFC operation is frequently attributed to substrate depletion or product accumulation followed by recovery after replenishment. The comparatively higher output of MCC over the monitored period (up to day 7) supports the interpretation that the modified interface improves biofilm–electrode coupling during start-up, aligning with the primary objective of reducing acclimation time.

As shown in Figure S6.11, the MCC anode exhibited a much shorter start-up period of approximately 3 days compared to about 500 h approximately 20 days for the dual-chamber DCMFC early reported in section 3.3. After stable biofilm formation, MCC-MFC the efficiency of decolorization of Evans blue dye at concentrations of 150, 300, and 450 mg/L. The maximum cell potential recorded during the first cycle of SCMFC was 192 mV, while in subsequent cycles it remained stable around 187 mV, indicating the steady performance of the bioanode. The shortened start-up time of the MCC anode can be attributed to its high biocompatibility, which enhances the attachment and electron transfer from electrogenic bacteria to the anode surface. The PANI polymerization, glucose, and gelatin coating collectively contributed to improved bacterial adhesion and facilitated extracellular electron transfer (EET), further reducing the start-up time. When the initial dye concentration increased from 150 mg/L to 300 mg/L, the voltage slightly rose to 198 mV across three cycles. However,

at 450 mg/L, the maximum voltage decreased to 150 mV in the first cycle and further dropped to 116 mV in the third cycle (Figure 3.24a). The decline at higher dye concentrations suggests toxic effects or competitive inhibition of bacterial metabolism and EET due to excessive dye loading.

Similar findings were reported by Lai et al. (2011), where PANI-modified MFCs achieved a cell voltage of 380 mV (with 510 Ω resistance) compared to 290 mV for unmodified MFCs, and the start-up period was reduced by 33.3% (from 6 to 4 days). The relatively low voltage observed in CC.B (unmodified carbon cloth) MFCs results from its limited biocompatibility, which restricts bacterial growth and electron transfer. In contrast, the MCC anode provided superior performance due to its enhanced conductivity, high surface area, and low activation overpotential, all of which promote efficient electron transfer at the biofilm–electrode interface.

At the end of each cycle, the voltage of SCMFCs dropped sharply, corresponding to the depletion of carbon source. (Figure 3.24b) presents the polarization and power density curves for SCMFCs at different dye concentrations, recorded at maximum cell potential. The results clearly demonstrate the improved electrochemical performance of the modified anode. The maximum power density obtained at 150 mg/L EB dye concentration was 67 ± 0.33 mW/m², while at 450 mg/L it decreased to 21 ± 0.21 mW/m². The power density at lower dye concentration was 3.8 times higher than at higher dye loading.

Direct numerical comparison must be qualified because the systems were evaluated at different loads of EB dye. The DCMFC exhibited a higher areal power density (119 mW m^{-2}) at 100 mg/L EB, whereas the SCMFC delivered 55 ± 0.31 mW m^{-2} at a three-fold higher EB concentration (300 mg/L). This indicates a load-dependent performance at higher dye concentrations, while also showing that the SCMFC configuration maintained stable power generation under a substantially higher inhibitory burden. Similar improvements in MFC performance after PANI modification have been reported by (Mehdinia, Dejaloud, and Jabbari 2013) , (Hou, Liu, and Li 2015), (Sonawane et al. 2018). According to Khan et al (M. D. Khan et al. 2021) An SCMFC treating 200 mg/L Acid Blue 29 achieved a maximum power density of 56 ± 2.7 mW m^{-2}, which aligns with the present study's value of 55 ± 0.31 mW/m² at higher dye concentration. The higher power and faster dye removal arise because the thin PANI layer increases anode conductivity and lowers the biofilm–electrode charge-transfer resistance without blocking the MCC macropores. The preserved porous structure allows dye and

substrates to diffuse into the electrode and supports deeper bacterial colonization, increasing the effective electroactive area. This improves extracellular electron transfer to the anode, sustains a more reducing biofilm microenvironment, and thereby accelerates azo-bond (–N=N–) reduction and overall dye degradation .

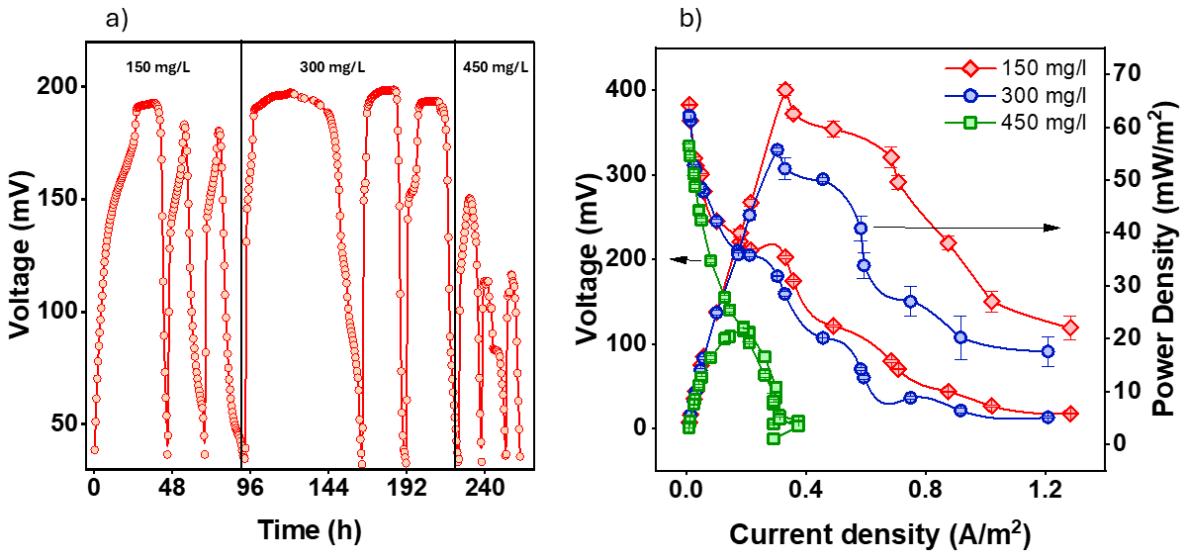

Figure 3.24: (a) Output cell potential of the SCMFCs during the final experiment – decolorization of EB at concentrations:150,300 and 450 mg/L; and (b) polarization and power density curves of the MCC- SCMFC containing EB (150,300 and 450 mg/L)

3.4.7 SCMFC-MCC - Evans Blue Decolorization Efficiency

During the 13-hour experiment of EB removal, the UV–Vis absorbance steadily decreased from an initial value, showing continuous loss of dye color intensity and confirming effective chromophore degradation (Figure 3.25a). The dye removal efficiency increased with time for all initial dye concentrations. For 150 mg/L of EB, the removal reached (96.56%) after 13 hours; for 300 mg/L, (90.22%), and for 450 mg/L (77.28%) (Figure 3.25b). This results again confirm that the decolorization rate and efficiency are concentration dependent. In the early stage (0–3 h), the rate of dye degradation was highest at the lowest dye concentration, with initial rates of 14.08, 11.23, and 10.01 $\%\cdot h^{-1}$ for 150, 300, and 450 mg/L, respectively. This confirms that a lower dye concentration enables faster reduction due to reduced competition for active sites and electrons. The degradation followed pseudo–first-order kinetics for the 0–8 h range ($\ln(C/C_o)$ vs. time), yielding rate constants (k) of 0.121, 0.109, and 0.106 h^{-1} for 150, 300, and 450 mg/L, respectively, with strong correlation (R^2 = 0.95–0.99). The corresponding half-lives ($t_{1/2}$) were 5.71, 6.33, and 6.56 hours, respectively, showing only a slight decrease in rate with increasing dye load.

The time required for 50% removal (t_{50}) was 5.00 h, 5.95 h, and 6.18 h for 150, 300, and 450 mg/L, respectively. For 80% removal (t_{80}), the times were 9.78 h and 10.75 h for 150 and 300 mg/L, while 450 mg/L did not reach 80% within 13 hours. Similarly, 90% removal (t_{90}) was achieved at 11.30 h for 150 mg/L and 12.97 h for 300 mg/L, but not for 450 mg/L (Figure 3.25c).

These results suggest that the microbial fuel cell (MFC) with the modified anode (MCC) can achieve high treatment efficiency (≥80–90%) within the experimental time at concentrations up to 300 mg/L. However, at 450 mg/L, longer hydraulic retention time (HRT) or further process optimization would be needed. The variability of removal increased with dye load, with standard deviations of 1.66, 2.72, and 2.83 for 150, 300, and 450 mg/L, respectively, indicating more stable performance at lower concentrations and higher sensitivity to local conditions at higher loads.

At the end of the experiment, the 150 mg/L test reached a stable plateau around 96.56% of decolorization, while at 300 mg/L process was slightly continued up to 90.22%, and at 450 mg/L decolorization rose slowly and finally reached 77.28%. These results confirm that the modified anode, with its enhanced biofilm adhesion and extracellular electron transfer (EET) capability, significantly reduces treatment time and improves performance, especially at moderate dye loads (≤300 mg/L). However, for higher concentrations (450 mg/L), additional improvements such as increasing electroactive surface area, optimizing nutrient release, or extending HRT are necessary.

Overall, the modified anode showed faster early phase decolorization, shorter treatment times (t_{80}/t_{90}), and higher overall removal efficiency. Even at the highest concentration (450 mg/L), removal remained around 75%, highlighting both strong performance and opportunities for further enhancement.

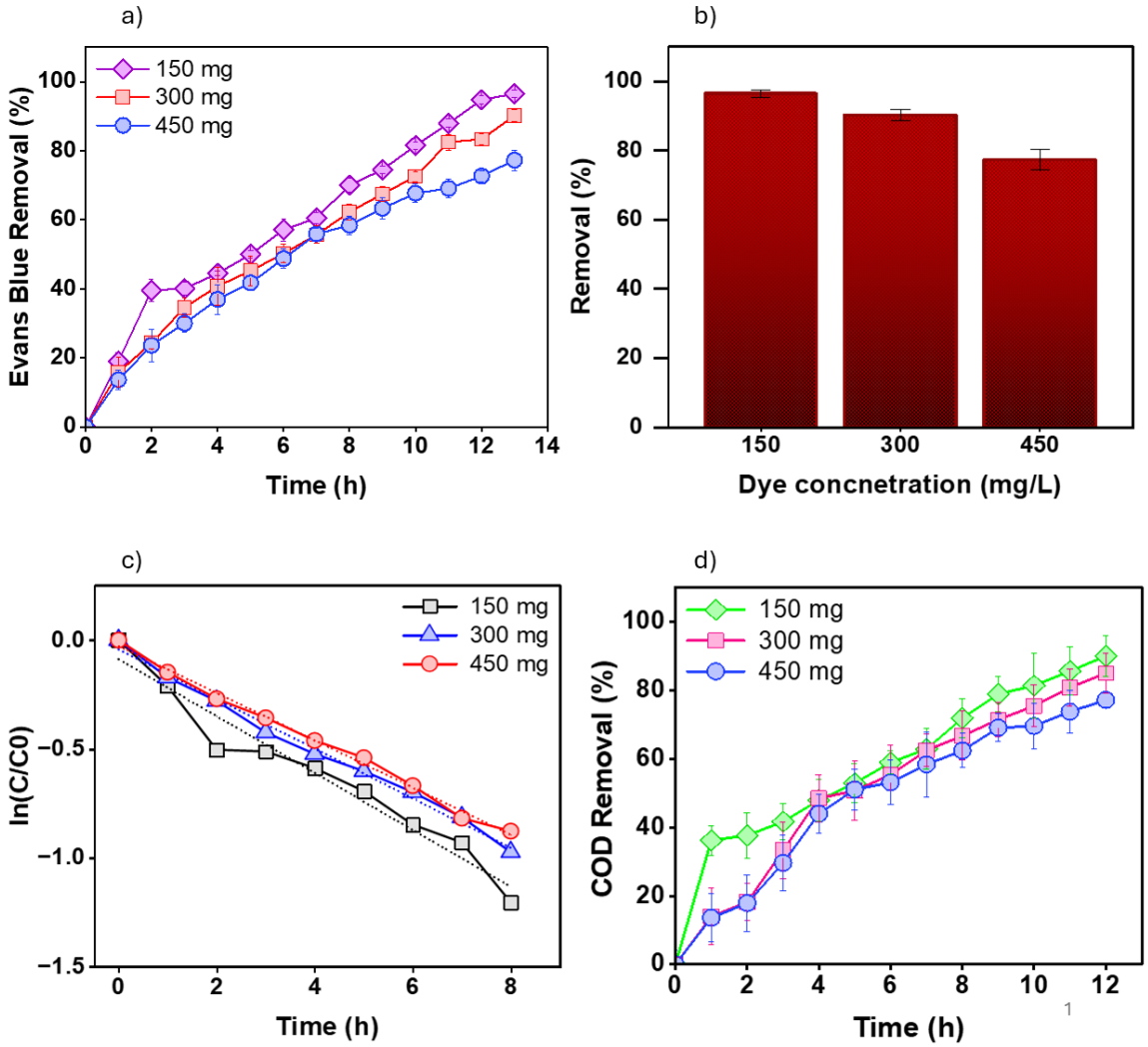

Figure 3.25: (a) Percent dye removal over time in SCMFC for initial Evans blue dye concentrations of 150, 300, and 450 mg/L (b) Maximum dye removal for all concentrations (c) Kinetic analysis of Evans Blue decolorization in SCMFC based on pseudo–first-order model fitting ($ln(C/C_0)$ vs time) for the 0–8 h region, doted line represent fitted line (d) COD removal efficiency of SCMFC at various initial Evans Blue concentrations (150, 300, and 450 mg/L) over 13 hours of operation.

COD removal increased steadily for all initial dye concentrations but as commonly observed in azo dye systems, it occurred more slowly than color removal. After 13 hours, COD removal reached about 90% at 150 mg/L, around 85% at 300 mg/L, and approximately 77% at 450 mg/L (Figure 3.25d). This trend is consistent with the typical two-stage degradation pathway, where the microbial fuel cell (MFC) anode rapidly breaks azo bonds to remove color, followed by slower oxidation processes that reduce organic content (J. Sun et al. 2013; M. D. Khan et al. 2021). At the highest dye concentration (450 mg/L), the lower final COD value reflects the common challenges reported in previous studies: increased oxygen demand for further oxidation, thicker or partially inactive biofilms that limit mass transfer, and reduced availability of electron donors or mediators (Kong et al. 2018; Q. Dai et al. 2020). However, earlier research also suggests that improving anode and biofilm properties can minimize this

gap by enhancing bacterial adhesion and electron transfer efficiency. For Evans Blue, in particular, modified anodes have shown improved COD removal and higher power generation (Quan et al. 2018). Overall, these findings demonstrate strong performance of the system. Even at the highest dye load, decolorization was achieved more effectively than in previous experiments described in section 3.4. At the same time, the results highlight clear opportunities, such as further anode modification or process optimization to enhance COD removal under higher dye loading conditions.

3.4.8 GC–MS-based analysis of EB transformation in the SCMFC-MCC anode

GC–MS was used to identify products formed during EB treatment in the anaerobic anode MCC of a single-chamber microbial fuel cell, inoculated with *Shewanella oneidensis* MR-1. In the case of this bacteria, azo-dye reduction is tightly coupled to extracellular electron transfer through the Mtr pathway, and synthetic azo dyes can function as terminal electron acceptors that are reduced at or near the cell surface (Morales-Florez et al. 2025).

Recent studies further show that EB and related dye-reduction rates in the case of *S. oneidensis* MR-1 depend strongly on electron-transfer control and on the presence or activity of electron shuttles. These findings support the interpretation that dyes decolorization by *Shewanella oneidensis* MR-1 is governed by electron-transfer processes rather than by purely intracellular metabolism, which is consistent with the EET-centered mechanism described above (Y. Wang et al. 2025).

Based on the known azo-bond reduction capability of *S. oneidensis* MR-1 under anode anaerobic conditions and the GC–MS profile obtained, EB transformation in the SCMFC is best interpreted as (i) rapid reductive decolorization initiated by azo-bond cleavage and formation of an intermediate aromatic pool and (ii) partial downstream conversion of a fraction of extractable intermediates to smaller organic acids under co-substrate supported, oxygen-limited conditions. Because many expected azo-cleavage products, especially highly polar sulfonated aromatic amines, are poorly recovered by standard GC–MS without derivatization, the detected compounds represent the GC-amenable fraction rather than a complete mass balance of EB transformation products. (Y. G. Hong and Gu 2010; S. Zafar, Bukhari, and Rehman 2022). The compounds detected during EB degradation in SCMFC-MCC system are presented in Table 3.5, and the proposed pathway for EB is shown in Figure 3.26

In the anodic chamber in anaerobic condition, a prominent aromatic signal is 2,4-di-tert-butylphenol (RT 22.377–22.396 min). Anaerobic azo-dye studies frequently detect phenolic

and other aromatic fragments as intermediates after the initial reductive step, consistent with our observation in section 3.2 and 3.3 and also with earlier reports (Balachandran and Sabumon 2025). Similar aromatic/phenolic features have been reported by other groups as well, reinforcing the interpretation that these compounds form part of the intermediate pool during early-stage azo-bond reduction (Al-Tohamy et al. 2023; Mustafa et al. 2025)

The chromatographic peak annotated as a "methoxy-phenyl oxime" at RT 6.219 min indicates the presence of substituted aromatic derivatives in the anode extract. Under anaerobic conditions, azo dyes typically undergo a first reductive step that generates aromatic-type products. However, many authentic azo-cleavage products, especially highly polar sulfonated amines, are difficult to detect by standard GC–MS unless derivatized or analyzed by alternative LC–MS methods. Therefore, the GC–MS profile should be interpreted as the recoverable fraction of the intermediate pool rather than a complete mass balance of Evans Blue cleavage products (Edebali et al. 2024; Balachandran and Sabumon 2025).

Low-molecular-weight acids indicate late anaerobic breakdown and possibly co-metabolism. The detection of 3-methylbutanoic acid at RT 5.212 min and octanoic acid at RT 13.275 min points to the formation and accumulation of fatty acids during anode operation. The same acids were reported in a section 3.2 where *Shewanella oneidensis* MR-1 achieved complete degradation of EB, reinforcing their relevance as pathway markers (Ayaz, Zabłocka-Godlewska, Smołka, et al. 2026). The detected short- and medium-chain acids are consistent with downstream carbon flow during anode operation and suggest partial conversion of organic intermediates, however for their conversion oxygen is required and oxygen intrusion to anode could be possible during sampling, thus because of this intrusion the aromatic amines could be converted into these low molecular weight compounds. Another possible interpretation is; because similar acids can arise from donor (glucose/yeast extract/peptone) metabolism, they can possibly support a co-metabolic pathway rather than a closed mineralization mass balance. This interpretation aligns with current consensus that anaerobic stages are well suited for initiating azo-bond reduction and rapid decolorization, whereas complete oxidative breakdown and mineralization typically require a subsequent aerobic phase to process reduced aromatic intermediates and residual organics (Balachandran and Sabumon 2025).

Table 3-5 GC–MS-identified compounds in the anaerobic anode of single-chamber MFC inoculated with Shewanella oneidensis MR-1 (Evans Blue)

No	Identified compound (GC–MS library hit)	RT (min)	Molecular formula	MW (g/mol)	Interpreted role in EB transformation	Dominant process (reaction type)
1	Oxime-, methoxy-phenyl- (tentative)	6.219	Not uniquely confirmed (library-type)	166.24	Recoverable aromatic derivative within early "aromatic pool"	Functional-group modification of aromatics (transformation/derivatization marker)
2	2,4-Di-tert-butylphenol	22.377–22.396	C14H22O	206.3239–206.33	Representative phenolic/aromatic intermediate pool detected under anaerobic operation	Aromatic remodeling after reductive initiation
3	3-Methylbutanoic acid (isovaleric acid)	5.212	C5H10O2	102.1317	Low-MW acid indicating anaerobic carbon flow and partial breakdown products	Fermentative acid formation; chain-shortening pool
4	Octanoic acid	13.275	C8H16O2	144.2114	Medium-chain fatty acid; co-metabolic product/end-pool under anaerobic operation	Lipid/fatty-acid pool; partial oxidation products

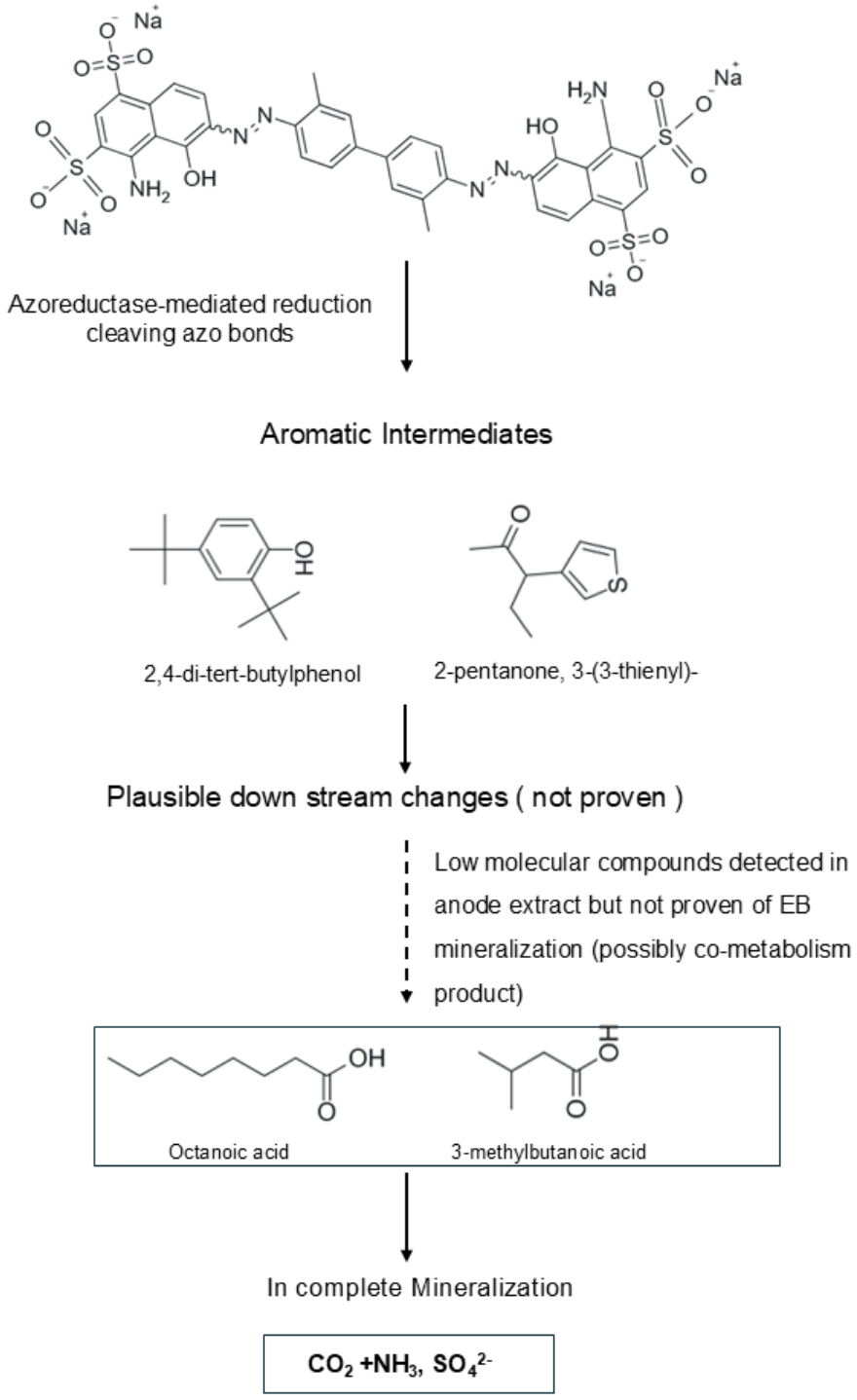

Figure 3.26 Proposed pathway-driven reductive decolorization of Evans blue in SCMFC-MCC. Dashed arrows indicate non-specific matrix changes; 3-methylbutanoic acid and octanoic acid are reported only as detected end-pool compounds, not confirmed dye-derived products. Complete mineralization was not demonstrated

Conclusions and further research directions

Section 3.4 showed that anode surface engineering is a practical and controllable way to improve EB removal in a single-chamber MFC. The modified carbon-cloth anode supported

faster biofilm attachment and stronger extracellular electron transfer, which translated into rapid treatment at high initial dye concentration that were difficult to remove with pure-culture and mixed-consortia tests over similar time periods. In the SCMFC, EB decolorization reached 96.56% at 150 mg/L, 90.22% at 300 mg/L, and 77.28% at 450 mg/L within 13 h. These results show that improving the bio interface directly reduces the kinetic limitations identified in earlier stages and increases the system's tolerance to inhibitory dye levels. GC–MS detected 3-methylbutanoic acid and octanoic acid as extractable low-molecular compounds in the anode matrix. However, the data do not confirm complete mineralization within the tested timeframe, and GC–MS alone cannot prove that these acids originate from EB degradation. Overall, Section 3.4 supports fast reductive transformation with partial downstream conversion, but it does not establish a complete degradation pathway under single-chamber anaerobic anode conditions. Future work should focus on confirming the transformation pathway and demonstrating treatment safety under realistic operation. Key steps include LC–MS/MS to track polar sulfonated intermediates that GC–MS is likely to miss, long-term durability testing of the coating under continuous-flow and shear to assess stability, fouling, and performance drift. For scale-up, the same interface-engineering approach should be transferred from flat carbon cloth to 3D high-surface electrodes (e.g., brush, felt, foam), since start-up time and high-load stability will remain the main barriers to real deployment.

CHAPTER 4

4 Conclusion:

This dissertation aimed to develop and experimentally validate an integrated, optimization-driven and mechanistically tested pathway for removing synthetic dyes, with a primary focus on the recalcitrant sulfonated azo dye Evans Blue (Direct Blue 53), using both pure cultures and mixed microbial communities and translating the work into bioelectrochemical reactor configurations. Also, one of the primary conclusions is that treatment effectiveness cannot be judged by UV–Vis color loss alone, because for highly water-soluble sulfonated azo dyes apparent decolorization can result from reversible adsorption, biosorption, partial chromophore disruption, or matrix effects, even when the parent dye is not fully transformed. For this reason, the thesis adopted a staged experimental strategy in which each step strengthened mechanistic certainty and process relevance by combining decolorization kinetics with chemical verification of transformation products and parent-dye disappearance, statistical optimization of operating conditions, evaluation of mixed-community performance in MFC systems, and anode biointerface engineering to improve adhesion and extracellular electron transfer.

Through the full experimental ladder, this work solved the main practical problem in Evans Blue treatment: i.e. how to move from slow, sometimes misleading “color loss” to fast, controlled, and chemically proved dyes removal because of biodegradation processes. The initial immobilized actinomycete based experiments showed the difficulties connected with real dye removal estimation, due to contribution of physical adsorption on solid carriers, as well as observed desorption process. Additional drawbacks were long time needed to biomass growth and dye removal. Switching to a defined pure bacterial culture *Schewanalla oneidensis* MR-1 and optimizing conditions with RSM made the process both rapid and easier to interpret, pushing EB decolorization to above 99% within 3 days with supporting by chemical transformation results. Application of mixed-community DCMFC plus aerobic step reduced the treatment time further to about 20–24 hours at 100 to 200 mg/L of EB, but it also showed the real engineering limits, especially start-up time and weaker pathway clarity in complex consortia. The final step of studies showed to reduce the degradation time further by fixing the microbe–electrode interface. A modified anode surface improved early biofilm attachment and electron transfer, which shortened treatment to 13 hours at 150 mg/L and kept removal high even as the dye load increased to 300 and 450 mg/L. In short, according to the obtained results, EB removal becomes faster and more controllable when operating conditions are selected as

an optimized, and bioelectrochemical performance is intentionally engineered at the biofilm–electrode interface.

In first experimental chapter the question was, can actinomycetes remove synthetic dyes, and can low-cost natural solid carriers improve process performance? *Actinomycetes* isolates could remove dyes, confirming that this group can contribute to biological dye treatment, especially for aerobic applications. Testing of immobilization of bacteria biomass on solid carriers has shown that decolorization results are the effect of both dye biotransformation and physical adsorption on the solid carriers. Straw alone and biomass alone showed lower removal, while combining straw with biomass improved apparent removal. This combination makes it difficult to truly assess dye removal, especially in the context of proved lack of additive effect of both processes and observed dye desorption from the support during it., Under these conditions (14 days), strain 1K1 achieved 66.6% removal of Brilliant Green and 80% removal of Evans Blue, while strain EGK2 achieved 97.8% removal of Brilliant Green and 73% removal of Evans Blue. These results solved the first objective by confirming that actinomycetes can remove dyes and that carriers can support biomass retention, but they also revealed the main limitation of these processes: long incubation time and difficulties with estimation of real dye removal in the case of immobilization on solid carrier as straw. Results obtained in this part additionally pointed out that not all plant-derived material is suitable for bacteria biomass immobilization. These results justified moving to a mechanistically clearer and faster model system.

The next stage of research was how to optimize the process condition in the case of use of single well-defined bacterium strain *Shewanella oneidensis* MR-1, with proved possibilities of removal of synthetic dyes. The studies were focused on the issue of how to make the removal of azo EB dye faster and more reliably, and how to define an operating window that guarantees repeatability and make it transferable. *S. oneidensis* MR-1 was confirmed as an effective pure-culture biocatalyst for EB removal when conditions were optimized. Response Surface Methodology (RSM) showed that time, temperature, dye concentration, and electron donor jointly control EB conversion, allowing selection of a statistically defensible operating window rather than a single “best parameter condition.” Importantly, in this stage multi-methods estimation of “dye removal” was introduced. Combining UV–Vis, with HPLC tracking of the fate of parent dye and GC–MS identification of transformation products, is core and strength the argument in evaluation whether the removal process is complete and the process is environmentally friendly. According to the results of multi analytical methods the

preliminary pathway of EB biotransformation was performed. Under optimized conditions, greater than 99% decolorization was achieved within 3 days, reducing the treatment time from 14 days obtained in the case of *Actinomycetes* to 3 days and proving that process optimization plus chemical verification is a strong strategy for reliable dye treatment. The RSM quadratic model was statistically significant (R = 0.79; adjusted R = 0.74), indicating a good fit to the experimental data. Time and temperature were the main positive parameters of Evans Blue removal, whereas excess glucose inhibited decolorization, and dye concentration had a smaller effect within the tested range. Based on the fitted quadratic RSM, the most favorable conditions within the studied ranges were identified at 53.65 h: dye =100 mg/L, carbon =250 mg/L, and temperature =37 ◦C. Although the pure-culture approach showed clear decolorization potential, treating higher dye loads (100 mg/L) still required long incubation (≈60–72 h). Therefore, the dissertation shifted from optimized pure-culture treatment to a reactor-based bioelectrochemical system using mixed microbial communities, where synergistic interactions can accelerate decolorization and better support faster, more complete mineralization

In the 3rd stage of study, the main achievement was moving from slow, single-strain treatment to a reactor-based, mixed-culture bioelectrochemical system that delivered fast, concentration-dependent decolorization with improved treatment completeness. In practical terms, the EB treatment time dropped from about 3 days (pure culture) to roughly 24 hours. The double-chamber microbial fuel cell provided a low-redox anode environment that supported azo-bond reduction while allowing energy recovery. To make sure the process went beyond color loss only, and further the intermediates biotransformation took place, the anaerobic step was followed by an aerobic reactor inoculated with the *Actinomycetes* (SK-2 and SK-3) isolated in experimental section 1. This aerobic post-treatment step converted the reduced intermediates formed in the anode chamber of MFC into low-molecular products such as 2-methylbutanoic acid and 3-methylbutanoic acid, which can be further mineralized to CO_2 and H_2O. Both pure single strain (*Shewanella oneidensis* MR-1) in experimental section 2 and reactor based mixed culture (experimental section 3) achieved complete mineralization. However, reactor based mixed culture reduced the treatment time significantly which is the main achievement in this stage.

The results were clearly concentration dependent. At 100 mg/L EB, decolorization reached 90 ± 2% to 98 ± 1.9%. When the initial dye concentration was doubled to 200 mg/L, performance decreased to 79 ± 2% to 87 ± 1%, but the combined anaerobic–aerobic sequence still

completed treatment within ~20–24 hours. This stage demonstrated that mixed microbial communities could provide robust removal and fast decolorization, but this stage also defined practical constraints for real application (long start-up time, added complexity and aeration energy demand, and reduced mechanistic traceability due to complex community interactions). These limitations provide the rationale for the next stage, which targets process intensification and reactor simplification (reducing start-up and removing aeration demand) and improving traceability through better bioanode and reactor design and operational control while maintaining rapid and high concentration dyes treatment.

In the final experimental chapter, we tackled the key weakness of Stage 3 that is the need for a complex dual-step setup to achieve fast treatment at higher dye loads. Here, the strategy was to strengthen the microbe–electrode interface so the MFC could work faster and handle more initial dye concentration in a simpler, single-chamber design. The carbon cloth anode was modified with a conductive PANI layer and a nutrient–protective coating concept, which promoted earlier cell attachment and supported stronger extracellular electron transfer. As a result, the modified anode delivered rapid and high-load decolorization: 96–97% at 150 mg/L, 90–91% at 300 mg/L, and 73% at 450 mg/L within 13 h, showing a clear improvement in tolerance to increasing dye concentration compared with earlier stages.

Crucially, this stage did not provide the total dye biodegradation. End-product analysis (GC–MS) showed formation of low-molecular compounds, including 3-methylbutanoic acid and octanoic acid, indicating that EB was possibly transformed toward smaller, more biodegradable products, what additionally confirmed the possibility of *Shewanella oneidensis* MR-1 to further transformation of the first product of anaerobic azo dye transformation - aromatic amines. However, the profiles also suggested incomplete mineralization, meaning some organic intermediates persisted at the end of the run.

This chapter links tightly to what we learned earlier. The RSM study defined the operating window and the stress-test range for key variables, especially time, carbon source level, and dye loading. Stages 1 and 3 then made it clear that performance drops as the dye concentration increases, and that faster removal depends on more efficient electron transfer by bacteria to cleave azo bond. In this chapter, those insights were translated into a controllable design change: engineering the carbon-cloth anode to strengthen the *Shewanella oneidensis* MR-1 biofilm and its electron-transfer activity in a simpler single-chamber MFC. As a result, the same strain that needed about 3 days to treat 100 mg/L EB could handle much higher loads,

achieving strong decolorization at 300 mg/L and measurable treatment even at 450 mg/L within ~13–20 hours.

In practical terms, the main conclusion of this thesis is that the most scalable route for EB treatment is a bioelectrochemical system where the operating conditions are tuned to biology and electron transfer is actively strengthened by engineering. Across all configurations tested, the single-chamber MFC with the engineered carbon-cloth anode (PANI plus nutrient/protective coating) inoculated with *Shewanella oneidensis* MR-1 was the most promising because it combined strong performance with a simple, controllable design. It reached 96–97% decolorization at 150 mg/L in ~13 h, maintained 90–91% at 300 mg/L, and still achieved ~73% at 450 mg/L, showing a level of high-load tolerance that earlier stages did not achieve. GC–MS confirmed conversion to smaller products, including 3-methylbutanoic acid and octanoic acid, although mineralization remained incomplete within the tested timeframe.

The double-chamber MFC followed by aerobic *Actinomycete* post-treatment addressed a different goal. It provided the clearest evidence that treatment can move beyond color removal effect toward deeper transformation and mineralization, completing treatment in ~20–24 h at 100–200 mg/L, but with added complexity and energy demand.

In summary, this work demonstrated the rapid azo dye removal while ensuring environmental safety was achieved by using appropriate systems of microbial activity, an optimized operating window, and electrode biointerface design as a single integrated engineering solution. This approach makes the Evans Blue removal method faster, more robust at higher loadings, and more closely aligned with what is required in real-world wastewater treatment conditions.

CHAPTER 5

5 Future directions

The next and most important step is to test the developed approach at pilot scale using real textile wastewater in continuous-flow operation. This is necessary because real dyehouse effluents are more complex than synthetic solutions and often contain high salinity, surfactants, auxiliary chemicals, mixed dyes, and variable pH and COD. Pilot testing should apply the response-surface operating window identified in this thesis and use the engineered anode as the main performance tool. The system should include online electrochemical monitoring, such as voltage and current trends and periodic impedance checks, to support simple real-time control of key settings including electron-donor feeding rate, external resistance, and flow conditions.

In parallel, the anode modification strategy should be expanded from flat carbon cloth to high-surface-area 3D electrodes such as carbon brushes, carbon felt, and carbon foam. These materials can hold more biomass, improve mass transfer, and reduce start-up time, which is important for high dye loads. However, scale-up must be supported by durability evidence. Future work should measure coating lifetime, performance drift, and sensitivity to fouling and mechanical shear under continuous operation. Stress tests should include shock increases in dye concentration, salinity changes, pH swings, and flow-rate disturbances.

Another priority is improving how reducing power is supplied to the process. Azo dye reduction depends strongly on electron availability, so future work should test low-cost or waste-derived carbon sources as electron donors to maintain fast treatment while lowering operating cost. If electron shuttles are used, they should be environmentally safe, and their benefit should be quantified clearly. The goal is to shorten the time to reach key performance targets at high dye loads while avoiding excessive planktonic growth that weakens biofilm stability.

To strengthen environmental credibility, future studies should combine chemical transformation evidence with routine toxicity confirmation. LC–MS or GC–MS product tracking should be paired with a small set of standardized toxicity tests so that color loss can be linked to real risk reduction. Finally, a combined techno-economic and life-cycle assessment should quantify cost drivers, energy demand, and emissions to guide scale-up and select the most practical configuration for deployment.

CHAPTER 6

6 Supplementary Information (Appendices)

All supplementary items are numbered with the prefix “S” (e.g., Figure S1, Table S1) and are cited in the main text using the same identifiers.

6.1 Appendices 1. Section 3.2

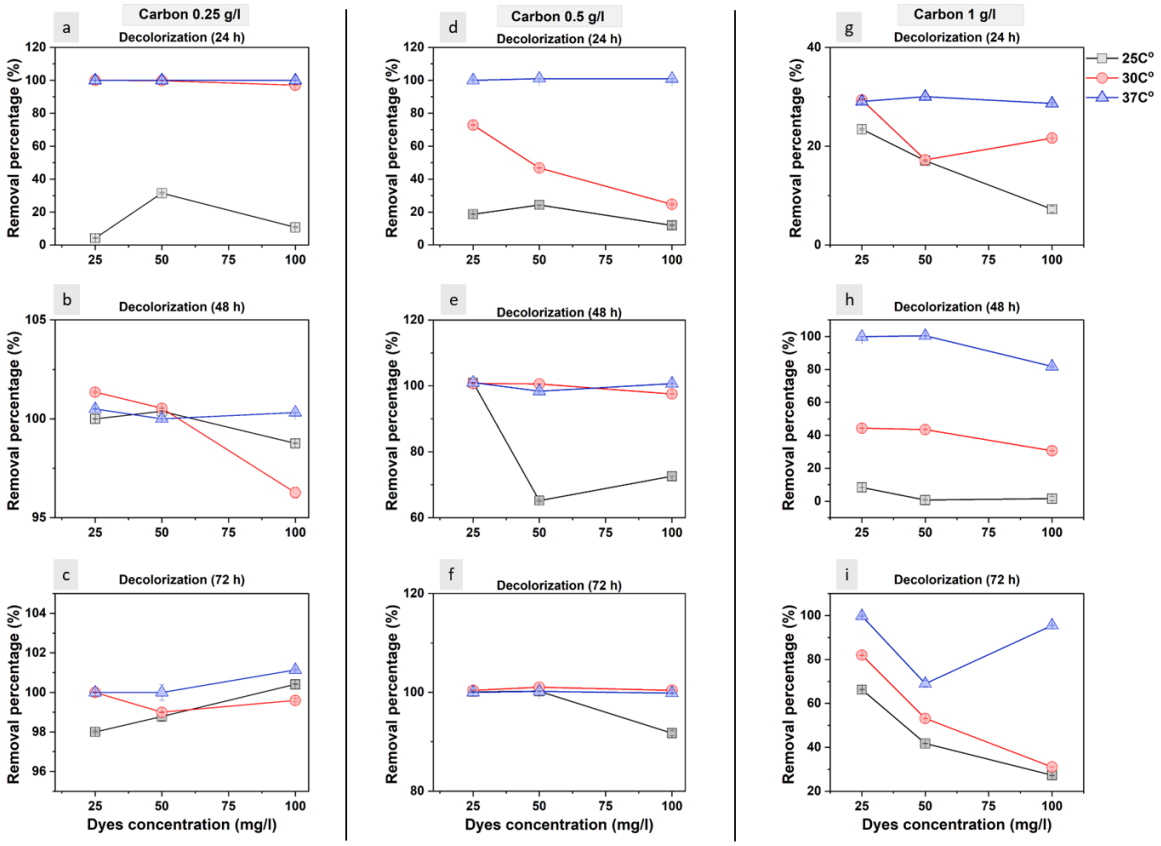

Figure S6.1: a-I Removal efficiency of Evans blue dye at three carbon concentrations (0.25, 0.5, and 1 g/L) and incubation times (24, 48, and 72 hours) under varying temperatures (25°C, 30°C, and 37°C), and dye concentrations (25, 50, and 100 mg/L) (K. Ayaz et al. 2026a)

Table S6-1 Design table for full factorial response surface for Shewanella oneidensis MR-1. (K. Ayaz et al. 2026a)

time (h)	dye_conc (mg/L)	carbon_conc (mg/L)	temp	removal (%)	removal_capped	time_coded	dye_conc_coded	carbon_conc_coded	temp_coded	Predicted_removal (%)
24	25	250	25	4.19	4.19	-1	-1	-1	-1	48.80
24	25	250	30	101.00	100.00	-1	-1	-1	0	73.07
24	25	250	37	100.90	100.00	-1	-1	-1	1	93.18
24	50	250	25	31.48	31.48	-1	0	-1	-1	44.28
24	50	250	30	100.60	100.00	-1	0	-1	0	69.88
24	50	250	37	103.38	100.00	-1	0	-1	1	91.85
24	100	250	25	10.73	10.73	-1	1	-1	-1	42.44
24	100	250	30	97.01	97.01	-1	1	-1	0	70.71
24	100	250	37	101.13	100.00	-1	1	-1	1	96.41
48	25	250	25	100.60	100.00	0	-1	-1	-1	86.59
48	25	250	30	100.50	100.00	0	-1	-1	0	101.88
48	25	250	37	100.50	100.00	0	-1	-1	1	109.42
48	50	250	25	100.38	100.00	0	0	-1	-1	81.65
48	50	250	30	100.20	100.00	0	0	-1	0	98.28
48	50	250	37	101.93	100.00	0	0	-1	1	107.68
48	100	250	25	98.76	98.76	0	1	-1	-1	78.99
48	100	250	30	96.27	96.27	0	1	-1	0	98.28
48	100	250	37	100.32	100.00	0	1	-1	1	111.41
72	25	250	25	100.90	100.00	1	-1	-1	-1	103.17
72	25	250	30	100.90	100.00	1	-1	-1	0	109.49
72	25	250	37	100.80	100.00	1	-1	-1	1	104.46
72	50	250	25	98.78	98.78	1	0	-1	-1	97.82
72	50	250	30	101.51	100.00	1	0	-1	0	105.48
72	50	250	37	94.95	94.95	1	0	-1	1	102.31
72	100	250	25	100.41	100.00	1	1	-1	-1	94.34
72	100	250	30	99.59	99.59	1	1	-1	0	104.66
72	100	250	37	101.14	100.00	1	1	-1	1	105.22
24	25	500	25	18.66	18.66	-1	-1	0	-1	38.03
24	25	500	30	72.78	72.78	-1	-1	0	0	65.47
24	25	500	37	100.50	100.00	-1	-1	0	1	90.00
24	50	500	25	24.32	24.32	-1	0	0	-1	32.03
24	50	500	30	46.74	46.74	-1	0	0	0	60.79
24	50	500	37	100.40	100.00	-1	0	0	1	87.19
24	100	500	25	11.88	11.88	-1	1	0	-1	27.23
24	100	500	30	24.69	24.69	-1	1	0	0	58.66
24	100	500	37	100.95	100.00	-1	1	0	1	88.79
48	25	500	25	100.50	100.00	0	-1	0	-1	77.29
48	25	500	30	100.71	100.00	0	-1	0	0	95.75
48	25	500	37	100.30	100.00	0	-1	0	1	107.72
48	50	500	25	65.18	65.18	0	0	0	-1	70.87
48	50	500	30	100.56	100.00	0	0	0	0	90.66
48	50	500	37	98.37	98.37	0	0	0	1	104.49
48	100	500	25	72.56	72.56	0	1	0	-1	65.25

48	100	500	30	97.51	97.51	0	1	0	0	87.71
48	100	500	37	100.70	100.00	0	1	0	1	105.27
72	25	500	25	100.40	100.00	1	-1	0	-1	95.35
72	25	500	30	100.40	100.00	1	-1	0	0	104.84
72	25	500	37	100.50	100.00	1	-1	0	1	104.24
72	50	500	25	100.21	100.00	1	0	0	-1	88.52
72	50	500	30	101.03	100.00	1	0	0	0	99.34
72	50	500	37	100.20	100.00	1	0	0	1	100.60
72	100	500	25	91.73	91.73	1	1	0	-1	82.08
72	100	500	30	100.41	100.00	1	1	0	0	95.56
72	100	500	37	99.85	99.85	1	1	0	1	100.55
24	25	1000	25	23.45	23.45	-1	-1	1	-1	-6.46
24	25	1000	30	29.37	29.37	-1	-1	1	0	27.31
24	25	1000	37	29.07	29.07	-1	-1	1	1	60.70
24	50	1000	25	17.07	17.07	-1	0	1	-1	-15.43
24	50	1000	30	17.23	17.23	-1	0	1	0	19.67
24	50	1000	37	30.02	30.02	-1	0	1	1	54.93
24	100	1000	25	7.24	7.24	-1	1	1	-1	-26.14
24	100	1000	30	31.02	31.02	-1	1	1	0	11.62
24	100	1000	37	28.66	28.66	-1	1	1	1	50.60
48	25	1000	25	8.37	8.37	0	-1	1	-1	35.75
48	25	1000	30	44.31	44.31	0	-1	1	0	60.54
48	25	1000	37	99.84	99.84	0	-1	1	1	81.36
48	50	1000	25	0.71	0.71	0	0	1	-1	26.37
48	50	1000	30	43.48	43.48	0	0	1	0	52.49
48	50	1000	37	100.42	100.00	0	0	1	1	75.18
48	100	1000	25	1.54	1.54	0	1	1	-1	14.83
48	100	1000	30	30.63	30.63	0	1	1	0	43.61
48	100	1000	37	81.80	81.80	0	1	1	1	70.02
72	25	1000	25	66.29	66.29	1	-1	1	-1	56.76
72	25	1000	30	81.96	81.96	1	-1	1	0	72.57
72	25	1000	37	99.82	99.82	1	-1	1	1	80.83
72	50	1000	25	41.76	41.76	1	0	1	-1	46.96
72	50	1000	30	53.16	53.16	1	0	1	0	64.11
72	50	1000	37	68.98	68.98	1	0	1	1	74.23
72	100	1000	25	27.28	27.28	1	1	1	-1	34.60
72	100	1000	30	31.07	31.07	1	1	1	0	54.40
72	100	1000	37	95.52	95.52	1	1	1	1	68.25

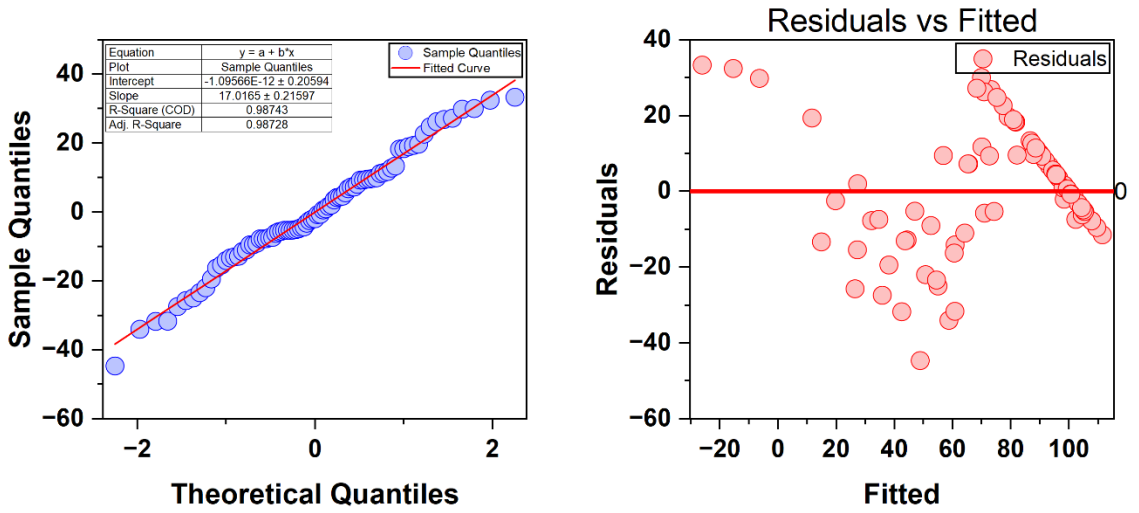

Figure S6.2 (a) Normal Q-Q plot and (b) residuals versus fitted values plot for the quadratic model of dye removal efficiency. Both plots indicate that the model residuals are normally distributed and randomly scattered, supporting the adequacy of the model fit. (K. Ayaz et al. 2026a)

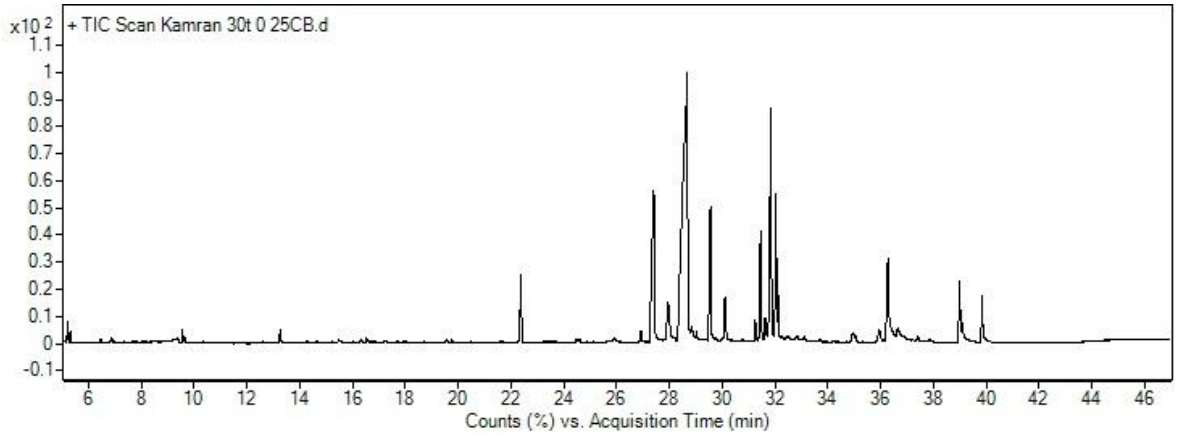

Figure S6.3 Chromatogram of GC–MS analysis of effluent after bacterial treatment. (K. Ayaz et al. 2026a)

6.2 Appendices 2. Section 3.4

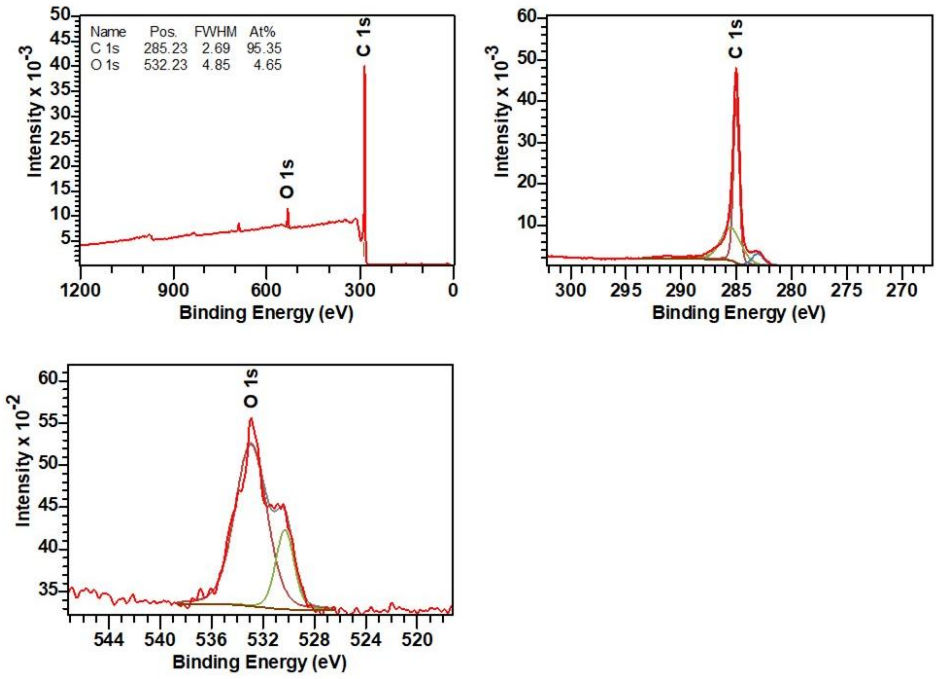

Figure S6.4 XPS spectra collected on the surface of a carbon cloth (CC): a) wide spectrum, b) C spectrum, and c) O spectrum. (K. Ayaz et al. 2026b)

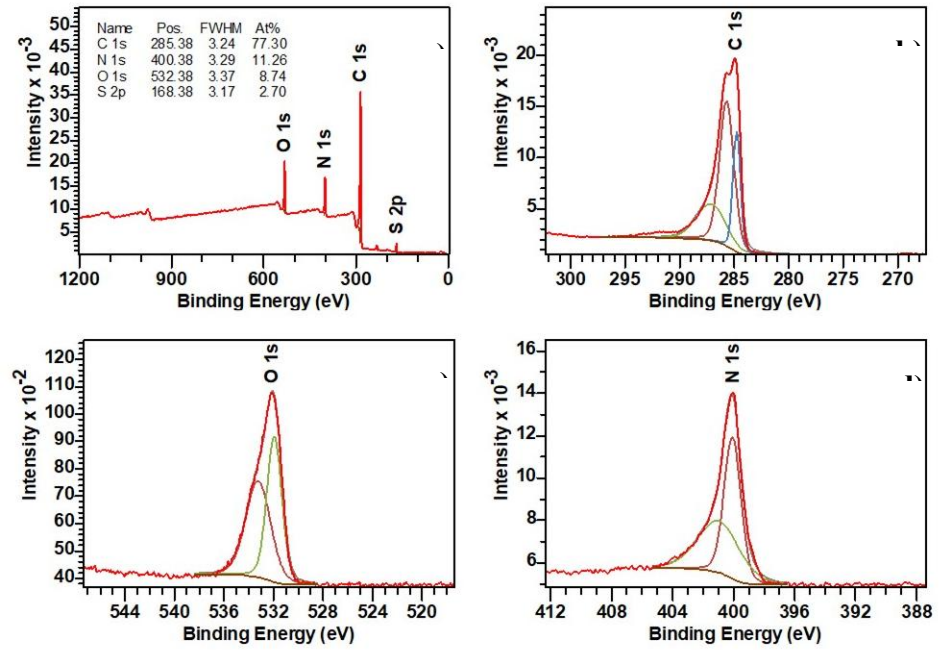

Figure S6.5 XPS spectra collected on the surface of a carbon cloth coated with polyaniline (CC.PANI): a) wide spectrum, b) C spectrum, and c) O spectrum, d) N spectrum. (K. Ayaz et al. 2026b)

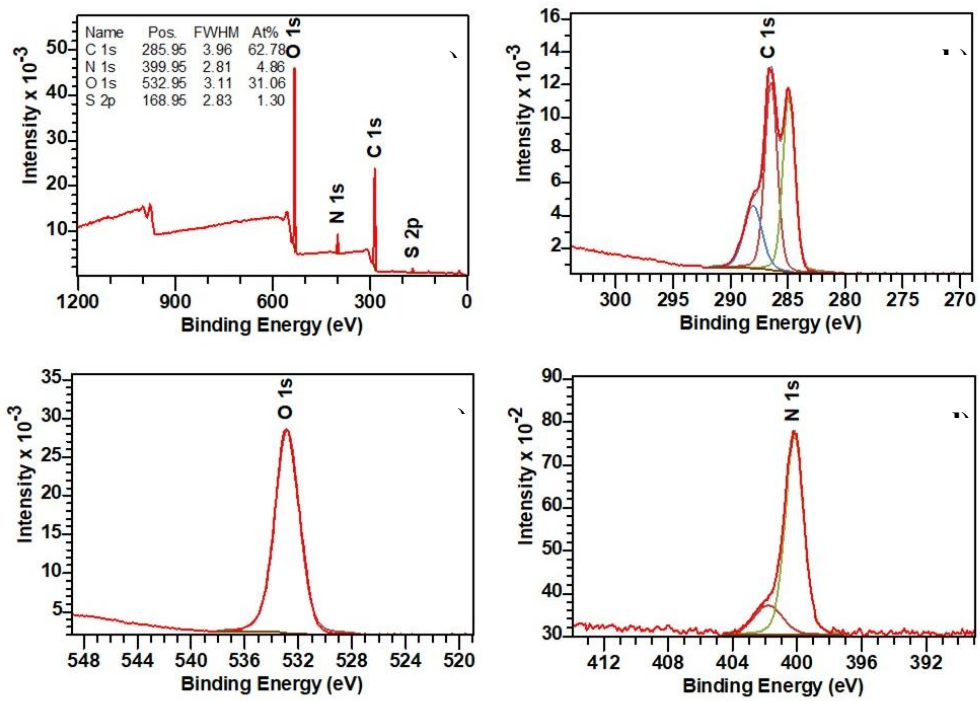

Figure S6.6 XPS spectra collected on the surface of a carbon cloth coated with polyaniline and glucose (CC.PANI.Glucose): a) wide spectrum, b) C spectrum, and c) O spectrum, d) N spectrum. (K. Ayaz et al. 2026b)

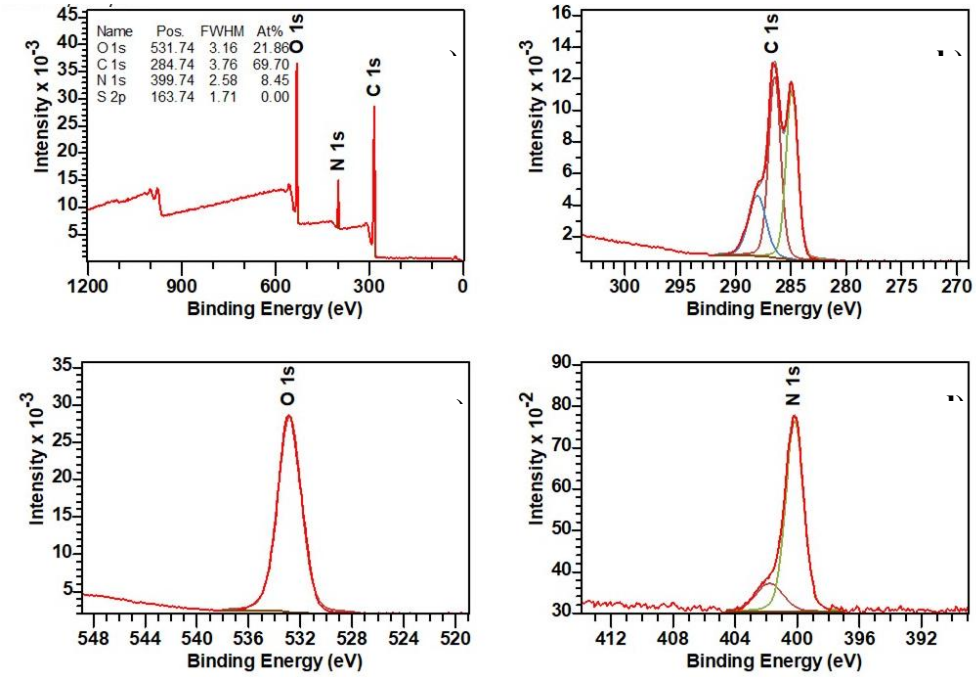

Figure S6.7 XPS spectra collected on the surface of a carbon cloth coated with polyaniline, glucose and gelatin (CC.PANI.Glucose.Gelatin referred to as MCC): a) wide spectrum, b) C spectrum, and c) O spectrum, d) N spectrum. (K. Ayaz et al. 2026b)

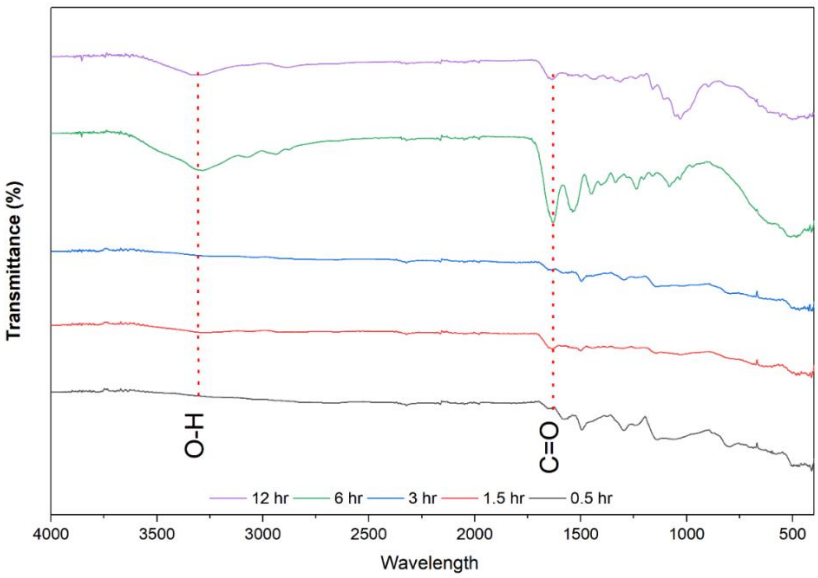

Figure S6.8 FTIR spectra of CC-PANI coated with glucose (CC.PANI.Glucose), and a protection layer of Gelatin (CC.PANI.Glucose.Gelatin referred to as MCC) after different immersion times (0.5 h, 1.5 h, 3 h, 6 h, and 12 h) in water. (K. Ayaz et al. 2026b)

Table S6-2 Equivalent circuit design and fitted values of circuit parameters for pristine and modified Carbon cloth; R1 – solution resistance, R2 – charge transfer resistance, W – Warburg impedance, P and n – CPE parameters.

Sample	Equivalent circuit	Parameter	Value	Unit	Error (%)	x^2
CC.B	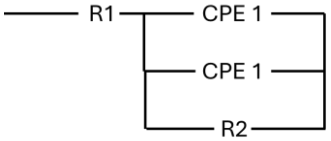	R1	148.33	Ω	0.75	0.0003
		R2	2883.9	Ω	2.21	
		P1	0.0004		2.72	
		n1	0.65508		1.59	
		P2	0.00049		2.23	
		n2	0.65508		1.37	
CC.B.G	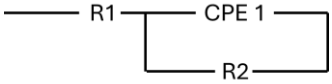	R1	75.5	Ω	0.9845	0.0006
		R2	10	kΩ	1.8742	
		P1	0.000453		1.285	
		n1	0.76661		0.5379	
			3.1			
MCC.control	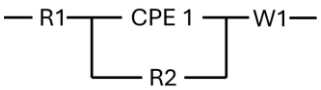	R 1	5.57	kΩ	0.36	0.0001
		R2	2.90	kΩ	3.19	
		Aw1	270.29		6.61	
		P1	0.0003		4.99	
		n1	0.6250		3.53	
MCC.B	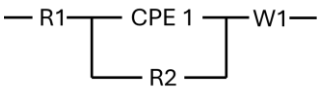	R1	93.851		1.63	0.0008
		R2	952.07		2.17	
		P1	0.00015		2.50	
		n1	0.6951		0.70	
		Aw1	156.99		5.98	

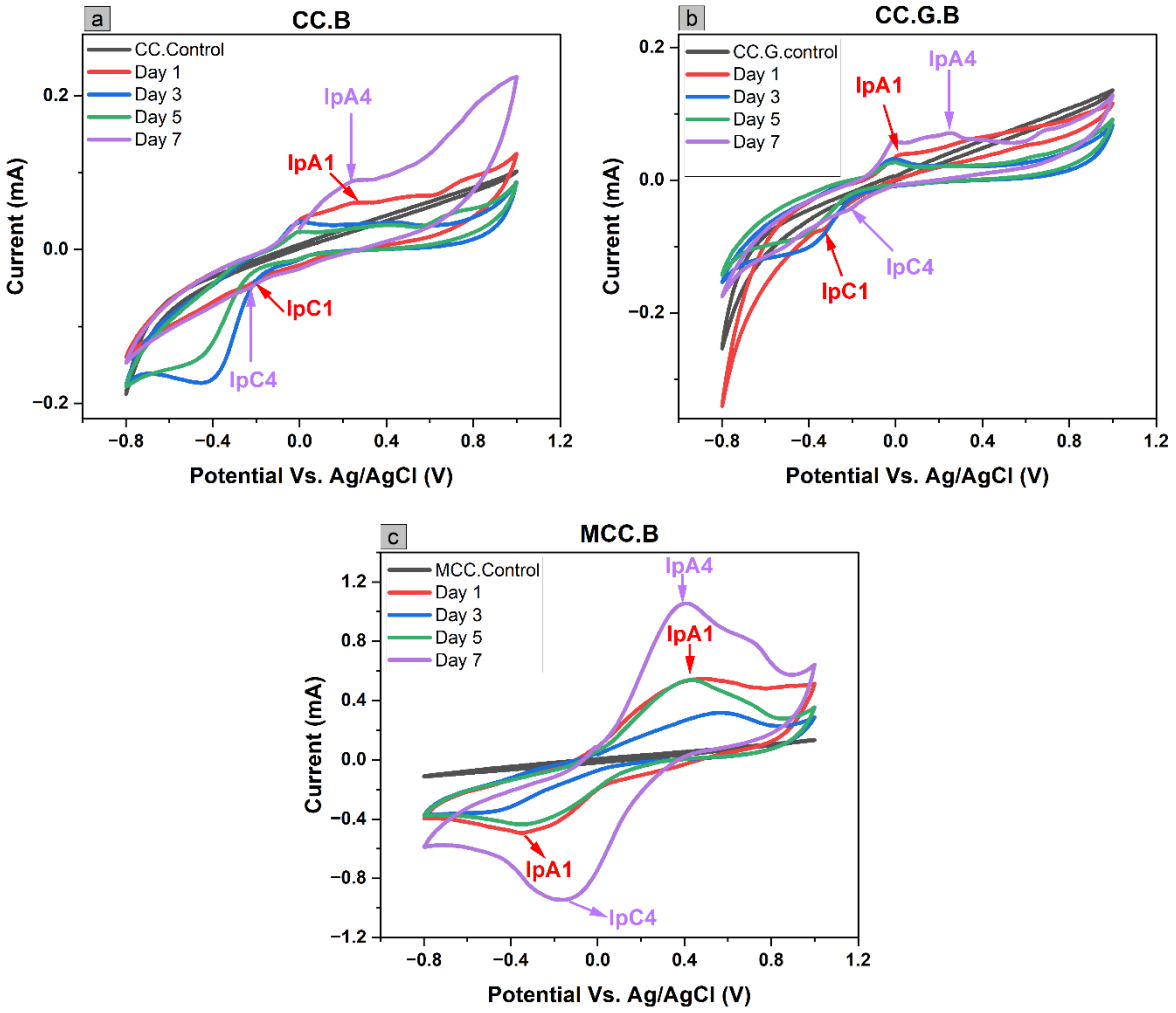

Figure S6.9 Cyclic voltammetry curves recorded over 1, 3, 5, and 7 days, showing progressive biofilm growth and enhanced electrochemical activity for (a) CC.B , (b) CC.G.B (c) MCC.B. (K. Ayaz et al. 2026b)

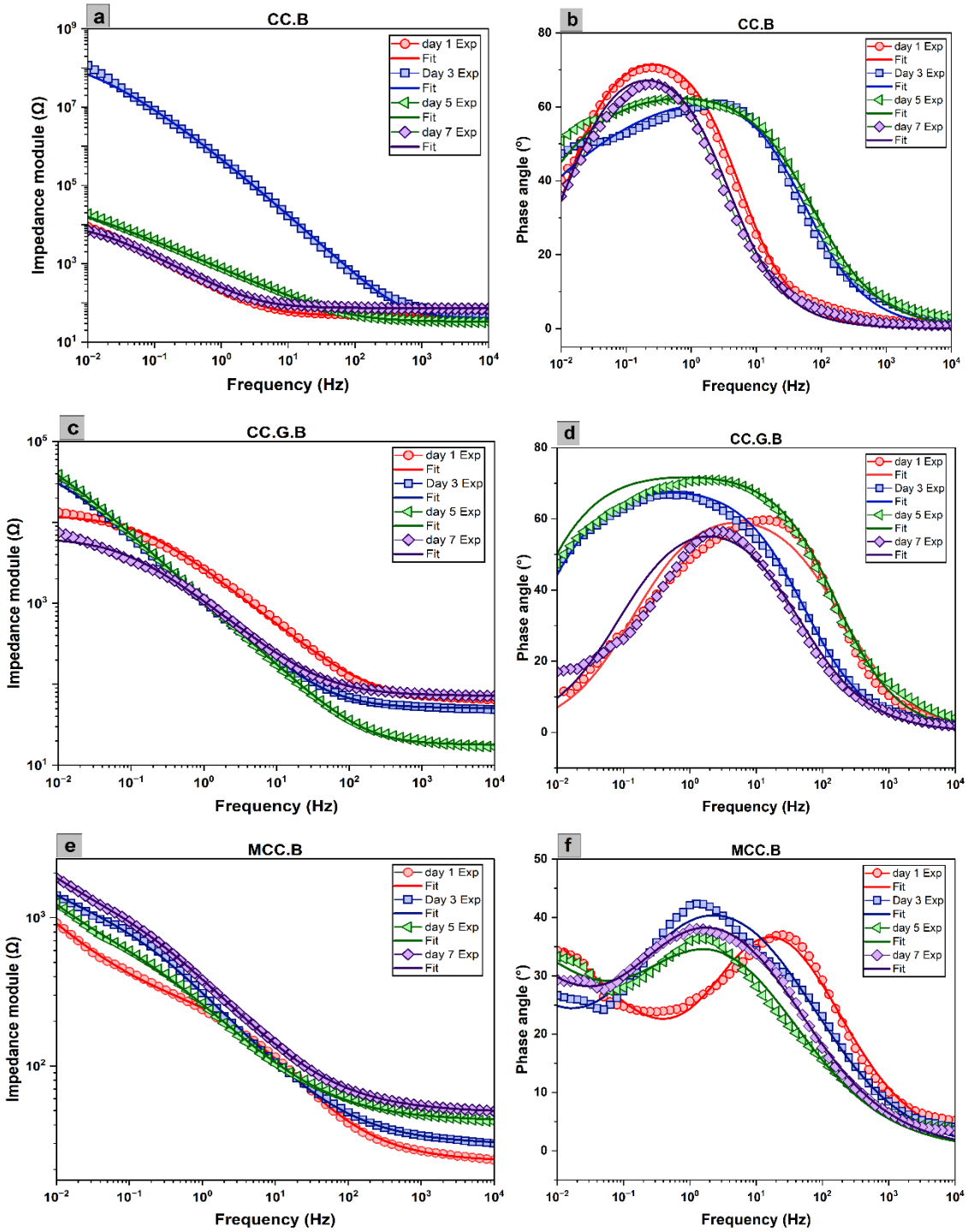

Figure S6.10 Bode plots of CC.B, CC.G.B and MCC.B (a-f) presenting the behavior of impedance modulus and phase angle vs. frequency; symbol represent experimental points on different days, while lines represent fitting curves. (K. Ayaz et al. 2026b)

Table S6-3 Equivalent circuit design and fitted values of circuit parameters for pristine and modified Carbon cloth covered with S. onediensis for stability Performance; R1 – solution resistance, R2 – charge transfer resistance, W – Warburg impedance, P and n – CPE parameters. (K. Ayaz et al. 2026b)

Sample	Equivalent circuit	Parameter	Value	Unit	Error (%)	x^2
CC.B day 1	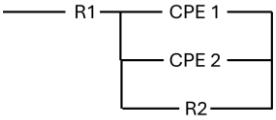	R1	47.229	Ω	2.6881	0.0003
		R2	10	kΩ	5.4798	
		P1	0.0004907		6.4245	
		n1	0.87868		2.8628	
		P2	0.00046661		6.7562	
		n2	0.87868		2.997	
CC.B Day 3	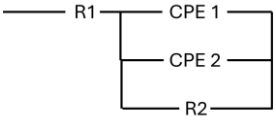	R1	40.871	Ω	2.9127	0.003
		R2	54.3	kΩ	10.245	
		P1	0.0001657		2.6992	
		n1	0.46209		3.093	
		P2	0.00021565		2.9328	
		n2	0.806		1.4739	
CC.B Day 5	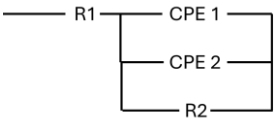	R1	32.771	Ω	2.8704	0.002
		R2	47.562	kΩ	4.5396	
		P1	0.00028315		0.9951	
		n1	0.75643		1.2444	
		P2	7.7114E-05		3.0221	
		n2	0.55183		4.6523	
CC.B Day 7	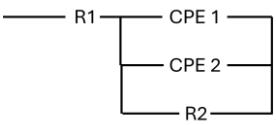	R1	73.596	Ω	2.1209	0.002
		R2	9.8	kΩ	9.5234	
		P1	0.00049683		5.2651	
		n1	0.85071		2.5285	
		P1	0.00044149		5.9251	
		n1	0.85071		2.8295	
CC.G.B Day 1	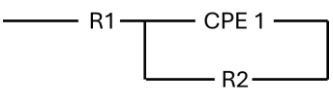	R1	62.005	Ω	4.4393	0.007
		R2	12.2	kΩ	6.012	
		P1	8.8713E-05		13.585	
		n1	0.73496		1.0288	
CC.G.B Day 3	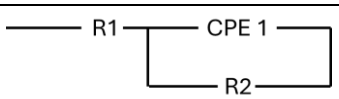	R1	50.507	Ω	2.2607	0.002
		R2	64.7	kΩ	4.9113	
		P1	0.00021367		1.5359	
		n1	0.78129		1.0937	
CC.G.B Day 5	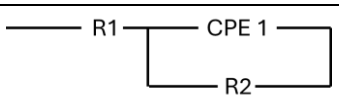	R1	17.71	Ω	2.7216	0.003
		R2	92.7	kΩ	3.8859	
		P1	0.0002017		2.3746	
		n1	0.81321		0.37346	
CC.G.B Day 7	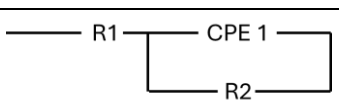	R1	71.835	Ω	3.8445	0.007
		R2	64.55	kΩ	4.9741	
		P1	0.00023827		4.4978	
		n1	0.72806		1.3404	
MCC.B Day 1	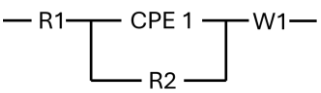	R1	22.52	Ω	1.6555	0.001
		R2	199.16	Ω	2.8977	
		Aw1	132.26		2.2689	
		P1	0.00063438		3.0811	
		n1	0.6895		0.80986	
MCC.B Day 3	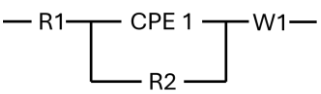	R1	29.544	Ω	1.9843	0.001
		R2	903.94	Ω	4.4061	
		Aw1	119.47		4.858	
		P1	0.0012486		2.7216	
		n1	0.59998		1.1436	
MCC.B Day 5		R1	42.468	Ω	1.5595	0.001
		R2	427.28	Ω	4.9908	
		Aw1	153.59		2.7605	
		P1	0.0018516		3.5516	
		n1	0.58588		1.5693	
MCC.B Day 7		R1	48.468	Ω	0.71693	
		R2	836.72	Ω	2.006	
		Aw1	206.9		1.3587	
		P1	0.0011606		1.3146	
		n1	0.60595		0.56023	

Table S6-4 Fitted charge-transfer resistance (R_2) and apparent exchange current density (j_0) for selected electrodes.

Sample	R_2 (Ω)	j_0 (A/m^2)	j_0 (mA/cm^2)
CC.B	2884	0.074	0.0074
CC.G.B	10 000	0.021	0.0021
CC.PANI.B	2303	0.093	0.0093
MCC.control	2900	0.074	0.0074
MCC.B	952	0.225	0.0220

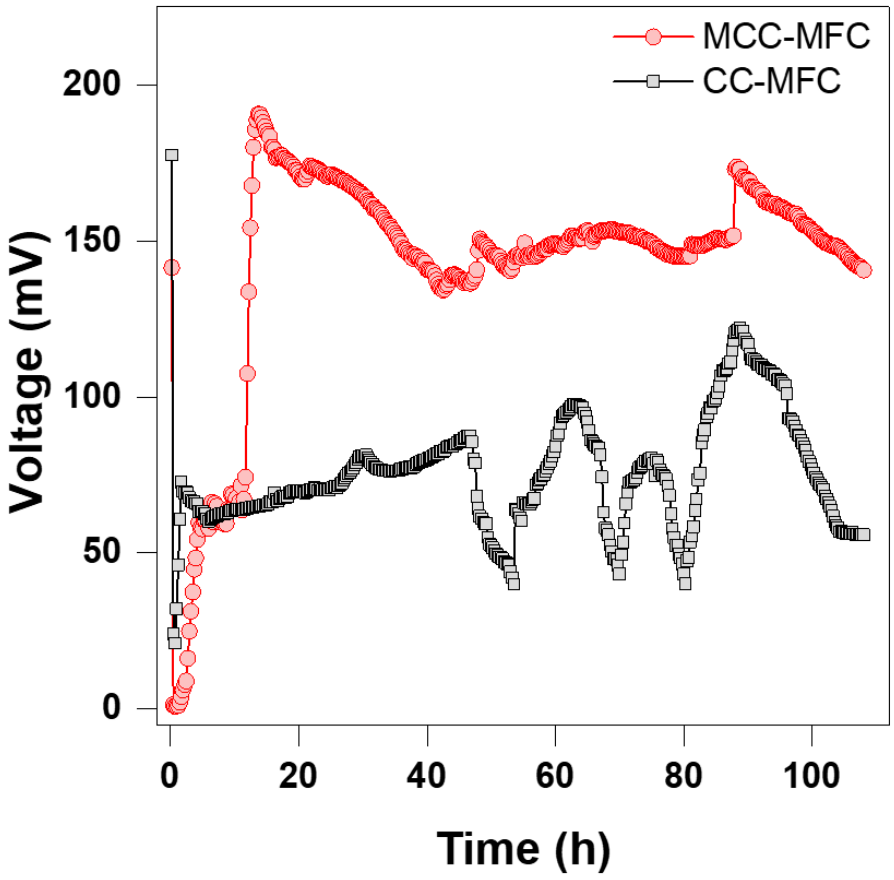

Figure S6.11 Voltage output of MCC-anode and Bare CC-MFC during biofilm formation phase. (K. Ayaz et al. 2026b)

CHAPTER 7

7 References

Abboud, Randa, Radu Popa, Virginia Souza-Egipsy, Carol S. Giometti, Sandra Tollaksen, Jennifer J. Mosher, Robert H. Findlay, and Kenneth H. Nealson. **2005**. "Low-Temperature Growth of Shewanella Oneidensis MR-1." Applied and Environmental Microbiology 71 (2): 811. https://doi.org/10.1128/AEM.71.2.811-816.2005

Abdullah, None, Sara Shakibania, Taral Patel, Divine Yufetar Shyntum, and Katarzyna Krukiewicz. **2024**. "Surface-Functionalized PEDOT:PSS Interfaces for Improved Adhesion, Viability, and Extracellular Charge Transfer of Shewanella Oneidensis MR-1." ACS Sustainable Chemistry and Engineering, December. https://doi.org/10.1021/ACSSUSCHEMENG.4C05458.

Adenan, Nurul Hidayah, Yau Yan Lim, and Adeline Su Yien Ting. **2021a**. "Identification and Optimization of Triphenylmethane Dyes Removal by Streptomyces Sp. from Forest Soil." Sustainable Environment Research 31 (1). https://doi.org/10.1186/S42834-021-00081-Z.

———. **2021b**. "Identification and Optimization of Triphenylmethane Dyes Removal by Streptomyces Sp. from Forest Soil." Sustainable Environment Research 31 (1): 1–15. https://doi.org/10.1186/S42834-021-00081-Z.

———. **2022**. "Removal of Triphenylmethane Dyes by Streptomyces Bacillaris: A Study on Decolorization, Enzymatic Reactions and Toxicity of Treated Dye Solutions." Journal of Environmental Management 318 (September). https://doi.org/10.1016/j.jenvman.2022.115520.

Aguirre-Contreras, Samuel, María Victoria López-Ramón, Inmaculada Velo-Gala, Miguel Ángel Álvarez-Merino, Angélica Aguilar-Aguilar, and Raúl Ocampo-Pérez. **2025**. "A Comparative Study of the Adsorption of Industrial Anionic Dyes with Bone Char and Activated Carbon Cloth." Water 2025, Vol. 17, 17 (23). https://doi.org/10.3390/W17233422.

Ahirrao, Dinesh J., Ajay Kumar Pal, Vikalp Singh, and Neetu Jha. **2021**. "Nanostructured Porous Polyaniline (PANI) Coated Carbon Cloth (CC) as Electrodes for Flexible Supercapacitor Device." Journal of Materials Science & Technology 88 (October):168–82. https://doi.org/10.1016/J.JMST.2021.01.075.

Ahsan, Md Ariful, M. Safiur Rahman, Md Abdul Quaiyum Bhuiyan, Md Saifur Rahaman, Mir Tamzid Rahman, and Mubarak Ahmad Khan. **2022**. "Reuse of Gamma-Ray Irradiated Textile Wastewater: Implications on the Growth of Capsicum Frutescens Plant." Heliyon 8 (8): e10009. https://doi.org/10.1016/J.HELIYON.2022.E10009.

Ajaz, Mehvish, Sana Shakeel, and Abdul Rehman. **2019**. "Microbial Use for Azo Dye Degradation—a Strategy for Dye Bioremediation." International Microbiology 2019 23:2 23 (2): 149–59. https://doi.org/10.1007/S10123-019-00103-2.

Al-Abduly, Abdullah J., Ahmed A. Basfar, Mohammed S. Algamdi, Ibrahim H. Alsohaimi, Ahmed A. Alharbi, and Abdullah M. Alkhedhair. **2021**. "Remediation and Detoxification of Water Samples Contaminated with 2, 4, 6-Trichlorophenol by Gamma Radiation and Ozonation." Radiation Physics and Chemistry 184 (July):109423. https://doi.org/10.1016/J.RADPHYSCHEM.2021.109423.

Al-Kdasi, Adel, Azni Idris, Katayon Saed, and Chuah Teong Guan. **2004**. "Treatment of Textile Wastewater by Advanced Oxidation Processes– A Review." Global Nest Journal 6 (1): 222–30. https://doi.org/10.30955/gnj.000288.

Al-Tohamy, Rania, Sameh S. Ali, Fanghua Li, Kamal M. Okasha, Yehia A.G. Mahmoud, Tamer Elsamahy, Haixin Jiao, Yinyi Fu, and Jianzhong Sun. **2022a**. "A Critical Review on the Treatment of Dye-Containing Wastewater: Ecotoxicological and Health Concerns of Textile Dyes and Possible Remediation Approaches for Environmental Safety." Ecotoxicology and Environmental Safety 231 (February):113160. https://doi.org/10.1016/J.ECOENV.2021.113160.

———. **2022b**. "A Critical Review on the Treatment of Dye-Containing Wastewater: Ecotoxicological and Health Concerns of Textile Dyes and Possible Remediation Approaches for Environmental Safety." Ecotoxicology and Environmental Safety 231 (February):113160. https://doi.org/10.1016/J.ECOENV.2021.113160.

Al-Tohamy, Rania, Sameh S. Ali, Rongrong Xie, Michael Schagerl, Maha A. Khalil, and Jianzhong Sun. **2023**. "Decolorization of Reactive Azo Dye Using Novel Halotolerant Yeast Consortium HYC and Proposed Degradation Pathway." Ecotoxicology and Environmental Safety 263 (September):115258. https://doi.org/10.1016/J.ECOENV.2023.115258.

Al-Zawahreh, Khaled, María Teresa Barral, Yahya Al-Degs, and Remigio Paradelo. **2021**. "Comparison of the Sorption Capacity of Basic, Acid, Direct and Reactive Dyes by Compost in Batch Conditions." Journal of Environmental Management 294 (September):113005. https://doi.org/10.1016/J.JENVMAN.2021.113005.

Alegbe, Emmanuel Ohifueme, and Taofik Olatunde Uthman. **2024**. "A Review of History, Properties, Classification, Applications and Challenges of Natural and Synthetic Dyes." Heliyon 10 (13): e33646. https://doi.org/10.1016/J.HELIYON.2024.E33646.

Ali, Khalid, Hani Zeidan, and Raja Ben Amar. **2023**. "Evaluation of the Use of Agricultural Waste Materials as Low-Cost and Eco-Friendly Sorbents to Remove Dyes from Water: A Review." Desalination and Water Treatment 302 (August):231–52. https://doi.org/10.5004/DWT.2023.29725.

Ameenudeen, Shabnam, Sneha Unnikrishnan, and Karthikeyan Ramalingam. **2021**. "Statistical Optimization for the Efficacious Degradation of Reactive Azo Dyes Using Acinetobacter Baumannii JC359." Journal of Environmental Management 279 (February):111512. https://doi.org/10.1016/J.JENVMAN.2020.111512.

Antonin, Vanessa S., Sergi Garcia-Segura, Mauro C. Santos, and Enric Brillas. **2015**. "Degradation of Evans Blue Diazo Dye by Electrochemical Processes Based on Fenton's Reaction Chemistry." Journal of Electroanalytical Chemistry 747 (June):1–11. https://doi.org/10.1016/J.JELECHEM.2015.03.032.

Anusi, Modestus O., Mathew C. Menkiti, Alexander I. Ikeuba, Chigoziri N. Njoku, Chukwuma E. Iloegbunam, Chinaza J. Nnamani, and Anselem C. Orga. **2025**. "Comparative Analysis of the Response Surface Methodology (RSM) and Artificial Neural Network (ANN) Modelling for the Removal of Diclofenac Potassium from Synthesized Pharmaceutical Wastewater Using a Palm Sheath Fiber Nano-Filtration Membrane and Optimization." Current Research in Green and Sustainable Chemistry 11 (January):100466.

https://doi.org/10.1016/J.CRGSC.2025.100466.

Aragaw, Tadele Assefa. 2024a. “A Review of Dye Biodegradation in Textile Wastewater, Challenges Due to Wastewater Characteristics, and the Potential of Alkaliphiles.” Journal of Hazardous Materials Advances 16 (November):100493. https://doi.org/10.1016/J.HAZADV.2024.100493.

———. **2024b**. “Potential and Prospects of Reductases in Azo Dye Degradation: A Review.” The Microbe 4 (September):100162. https://doi.org/10.1016/J.MICROB.2024.100162.

Aragaw, Tadele Assefa, and Fekadu Mazengiaw Bogale. **2023**. “Role of Coagulation/Flocculation as a Pretreatment Option to Reduce Colloidal/Bio-Colloidal Fouling in Tertiary Filtration of Textile Wastewater: A Review and Future Outlooks.” Frontiers in Environmental Science 11 (April):1142227. https://doi.org/10.3389/FENVS.2023.1142227.

Aragaw, Tadele Assefa, Carolina Suarez, Catherine J. Paul, and Addis Simachew. **2024**. “Evaluation of Integrated Anaerobic/Aerobic Conditions for Treating Dye-Rich Synthetic and Real Textile Wastewater Using a Soda Lake Derived Alkaliphilic Microbial Consortia.” Water 2024, Vol. 16, 16 (20). https://doi.org/10.3390/W16202937.

Arbour, Tyler J., Benjamin Gilbert, and Jillian F. Banfield. **2020**. “Diverse Microorganisms in Sediment and Groundwater Are Implicated in Extracellular Redox Processes Based on Genomic Analysis of Bioanode Communities.” Frontiers in Microbiology 11 (July):508335. https://doi.org/10.3389/FMICB.2020.01694.

Awady, Mohamed E. El, Fatma N. El-Shall, Ghada E. Mohamed, Ahmed M. Abd-Elaziz, Mohamed O. Abdel-Monem, and Mervat G. Hassan. **2024**. “Exploring the Decolorization Efficiency and Biodegradation Mechanisms of Different Functional Textile Azo Dyes by Streptomyces Albidoflavus 3MGH.” BMC Microbiology 24 (1): 1–22. https://doi.org/10.1186/S12866-024-03347-9.

Ayaz, K., & Zabłocka-Godlewska, E. **2022.** “Screening of Actinomycetes Decolorizing the Synthetic Dyes from Rotten Poplar Wood and Garden Compost.” In Contemporary Problems of Power Engineering and Environmental Protection 2022, edited by K. Pikoń & M. Bogacka, 119–31.

Ayaz, Kamran, Ewa Zabłocka-Godlewska, Abdullah, Sara Shakibania, Taral Patel, Krzysztof Karoń, and Katarzyna Krukiewicz. **2026.** “Enhancing Microbial Adhesion and Electron Transfer of Shewanella Oneidensis MR-1 with Polyaniline-Glucose-Gelatin Coating for Bioelectrochemical Applications.” Journal of Environmental Chemical Engineering 14 (2): 121546. https://doi.org/10.1016/j.jece.2026.121546.

Ayaz, Kamran, Ewa Zabłocka-Godlewska, and Chao Li. **2024**. “Enhancing Azo Dye Mineralization and Bioelectricity Generation through Biocathode-Microbial Fuel Cell Integration with Aerobic Bioreactor.” Energies 2024, Vol. 17, Page 4896 17 (19): 4896. https://doi.org/10.3390/EN17194896.

Ayaz, Kamran, Ewa Zabłocka-Godlewska, Szymon Smołka, Edyta Kudlek, Ijaz Hussain, and Muhammad Ilyas. **2026.** “Sustainable Biodegradation of Evans Blue (Direct Blue 53) by Shewanella Oneidensis MR-1: Response Surface Optimization and Product Analysis.” Journal of Water Process Engineering 81 (January):109399. https://doi.org/10.1016/J.JWPE.2025.109399.

Azimi, Banafsheh, Elham Abdollahzadeh-Sharghi, and Babak Bonakdarpour. **2021**. "Anaerobic-Aerobic Processes for the Treatment of Textile Dyeing Wastewater Containing Three Commercial Reactive Azo Dyes: Effect of Number of Stages and Bioreactor Type." Chinese Journal of Chemical Engineering 39 (November):228–39. https://doi.org/10.1016/J.CJCHE.2020.10.006.

Bafana, Amit, Sivanesan Saravana Devi, and Tapan Chakrabarti. **2011**. "Azo Dyes: Past, Present and the Future." Https://Doi.Org/10.1139/A11-018 19 (1): 350–70. https://doi.org/10.1139/a11-018.

Balachandran, Bhavana, and P. C. Sabumon. **2025**. "A Comprehensive Review on Biodegradation of Azo Dye Mixtures, Metabolite Profiling with Health Implications and Removal Strategies." Journal of Hazardous Materials Advances 19 (August):100834. https://doi.org/10.1016/J.HAZADV.2025.100834.

Balapure, Kshama, Nikhil Bhatt, and Datta Madamwar. **2015**. "Mineralization of Reactive Azo Dyes Present in Simulated Textile Waste Water Using down Flow Microaerophilic Fixed Film Bioreactor." Bioresource Technology 175 (January):1–7. https://doi.org/10.1016/J.BIORTECH.2014.10.040.

Bassin, J. P., I. N. Dias, S. M.S. Cao, E. Senra, Y. Laranjeira, and M. Dezotti. **2016.** "Effect of Increasing Organic Loading Rates on the Performance of Moving-Bed Biofilm Reactors Filled with Different Support Media: Assessing the Activity of Suspended and Attached Biomass Fractions." Process Safety and Environmental Protection 100 (March):131–41. https://doi.org/10.1016/J.PSEP.2016.01.007.

Bautista-Pinzón, Fernando, Juan Fonseca-Ordoñez, Mayerlen Falla-Obando, Jairo Gonzales-Tuta, Luis Diaz-Barrera, Fernando Bautista-Pinzón, Juan Fonseca-Ordoñez, Mayerlen Falla-Obando, Jairo Gonzales-Tuta, and Luis Diaz-Barrera. **2024**. "Streptomyces as a Novel Biotool for Azo Pigments Remediation in Contaminated Scenarios." Frontiers in Bioscience-Elite 2024 16 (3) 16 (3). https://doi.org/10.31083/J.FBE1603029.

Belgherbi, O., L. Seid, D. Lakhdari, D. Chouder, M. S. Akhtar, and M. A. Saeed. **2021**. "Optical and Morphological Properties of Electropolymerized Semiconductor Polyaniline Thin Films: Effect of Thickness." Journal of Electronic Materials 50 (7): 3876–84. https://doi.org/10.1007/S11664-021-08896-7.

Benkhaya, Said, Souad M' rabet, and Ahmed El Harfi. **2020**. "A Review on Classifications, Recent Synthesis and Applications of Textile Dyes." Inorganic Chemistry Communications 115 (May):107891. https://doi.org/10.1016/J.INOCHE.2020.107891.

Bera, Sweta Parimita, and S. K. Tank. **2021**. "Microbial Degradation of Procion Red by Pseudomonas Stutzeri." Scientific Reports 11 (1): 1–12. https://doi.org/10.1038/S41598-021-82494-9.

Berradi, Mohamed, Rachid Hsissou, Mohammed Khudhair, Mohammed Assouag, Omar Cherkaoui, Abderrahim El Bachiri, and Ahmed El Harfi. **2019**. "Textile Finishing Dyes and Their Impact on Aquatic Environs." Heliyon 5 (11): e02711. https://doi.org/10.1016/J.HELIYON.2019.E02711.

Bezerra, Marcos Almeida, Ricardo Erthal Santelli, Eliane Padua Oliveira, Leonardo Silveira Villar, and Luciane Amélia Escaleira. **2008.** "Response Surface Methodology (RSM) as a Tool for Optimization in Analytical Chemistry." Talanta 76 (5): 965–77. https://doi.org/10.1016/J.TALANTA.2008.05.019.

Białowąs, Małgorzata, Beata Kończak, Stanisław Chałupnik, and Joanna Kalka. 2024. "Analysis of the Feasibility of Using Biopolymers of Different Viscosities as Immobilization Carriers for Laccase in Synthetic Dye Removal." Archives of Environmental Protection Vol. 50 (1): 19–34. https://doi.org/10.24425/aep.2024.149429.

Bienstock, Rachelle J., Lalith Perera, and Melissa A. Pasquinelli. **2022**. "Molecular Modeling Study of the Genotoxicity of the Sudan I and Sudan II Azo Dyes and Their Metabolites." Frontiers in Chemistry 10 (June):880782. https://doi.org/10.3389/FCHEM.2022.880782.

Biesinger, Mark C. **2022**. "Accessing the Robustness of Adventitious Carbon for Charge Referencing (Correction) Purposes in XPS Analysis: Insights from a Multi-User Facility Data Review." Applied Surface Science 597 (September):153681. https://doi.org/10.1016/J.APSUSC.2022.153681.

Bilińska, L., M. Gmurek, and S. Ledakowicz. **2017**. "Textile Wastewater Treatment by AOPs for Brine Reuse." Process Safety and Environmental Protection 109 (July):420–28. https://doi.org/10.1016/J.PSEP.2017.04.019.

Bogale, Fekadu Mazengiaw, Belay Teffera, and Tadele Assefa Aragaw. **2024**. "Recent Developments in Integrated Anaerobic/Aerobic (A/O) Process for Textile Industry Wastewater Treatment: A Review." Journal of Hazardous Materials Advances 15 (August):100438. https://doi.org/10.1016/J.HAZADV.2024.100438.

Boinpally, Sriram, Abhinav Kolla, Jyoti Kainthola, Ruthviz Kodali, and Jayaprakash Vemuri. **2023.** "A State-of-the-Art Review of the Electrocoagulation Technology for Wastewater Treatment." Water Cycle 4 (January):26–36. https://doi.org/10.1016/J.WATCYC.2023.01.001.

Borthwick, Alan D. **2012.** "2,5-Diketopiperazines: Synthesis, Reactions, Medicinal Chemistry, and Bioactive Natural Products." Chemical Reviews 112 (7): 3641–3716. https://doi.org/10.1021/CR200398.

Brune, Andreas, Wolfgang Ludwig, and Bernhard Schink. **2002**. "Propionivibrio Limicola Sp. Nov., a Fermentative Bacterium Specialized in the Degradation of Hydroaromatic Compounds, Reclassification of Propionibacter Pelophilus as Propionivibrio Pelophilus Comb. Nov. and Amended Description of the Genus Propionivibrio." International Journal of Systematic and Evolutionary Microbiology 52 (Pt 2): 441–44. https://doi.org/10.1099/00207713-52-2-441.

Carrascal-Hernández, Domingo Cesar, Erney José Orozco-Beltrán, Daniel Insuasty, Edgar Márquez, and Carlos David Grande-Tovar. **2025**. "Systematic Evaluation of Biodegradation of Azo Dyes by Microorganisms: Efficient Species, Physicochemical Factors, and Enzymatic Systems." International Journal of Molecular Sciences 2025, Vol. 26, 26 (16). https://doi.org/10.3390/IJMS26167973.

Castillo-Suárez, L. A., A. G. Sierra-Sánchez, I. Linares-Hernández, V. Martínez-Miranda, and E. A. Teutli-Sequeira. **2023**. "A Critical Review of Textile Industry Wastewater: Green Technologies for the Removal of Indigo Dyes." International Journal of Environmental Science and Technology 20 (9): 1. https://doi.org/10.1007/S13762-023-04810-2.

Castro, Ana Margarida, Verónica Nogueira, Isabel Lopes, Teresa Rocha-Santos, and Ruth Pereira. **2019.**

"Evaluation of the Potential Toxicity of Effluents from the Textile Industry before and after Treatment." Applied Sciences 2019, Vol. 9, 9 (18). https://doi.org/10.3390/APP9183804.

Chaieb, Kamel, Mohamed Hagar, and Nagi R.E. Radwan. **2016**. "Biodegradation and Decolorization of Azo Dyes by Adherent Staphylococcus Lentus Strain." Applied Biological Chemistry 59 (3): 405–13. https://doi.org/10.1007/S13765-016-0169-4.

Chakravarthi, Bhoodevi, Vani Mathkala, and Uma Maheswari Devi Palempalli. **2021**. "Degradation and Detoxification of Congo Red Azo Dye by Immobilized Laccase of Streptomyces Sviceus." Journal of Pure and Applied Microbiology 15 (2): 864–76. https://doi.org/10.22207/JPAM.15.2.41.

Chen, Huizhong, Sherryll L. Hopper, and Carl E. Cerniglia. **2005**. "Biochemical and Molecular Characterization of an Azoreductase from Staphylococcus Aureus, a Tetrameric NADPH-Dependent Flavoprotein." Microbiology (Reading, England) 151 (Pt 5): 1433. https://doi.org/10.1099/MIC.0.27805-0.

Cherif, Sonia, Hynda Rezzaz-Yazid, Salima Ayachine, Imene Toukal, Noreddine Boudechiche, Mohamed Belmedani, Hayet Djelal, and Zahra Sadaoui. **2024**. "Continuous Fixed Bed Bioreactor for the Degradation of Textile Dyes: Phytotoxicity Assessment." Processes 2024, Vol. 12, 12 (10). https://doi.org/10.3390/PR12102222.

Choi, Youngjin, Eunkyoung Jung, Hyunjoo Park, Seung R. Paik, Seunho Jung, and Sunghyun Kim. 2004. "Construction of Microbial Fuel Cells Using Thermophilic Microorganisms, Bacillus Licheniformis and Bacillus Thermoglucosidasius." Bulletin of The Korean Chemical Society 25 (6): 813–18. https://doi.org/10.5012/BKCS.2004.25.6.813.

Ciobanu, Gabriela, Simona Barna, and Maria Harja. **2016**. "Kinetic and Equilibrium Studies on Adsorption of Reactive Blue 19 Dye from Aqueous Solutions by Nanohydroxyapatite Adsorbent." Archives of Environmental Protection 42 (2): 3–11. https://doi.org/10.1515/AEP-2016-0014.

Cofrancesco, A. J. **2009.** "Dyes, Natural." Kirk-Othmer Encyclopedia of Chemical Technology, April, 1–30. https://doi.org/10.1002/0471238961.0425051903150618.A01.PUB2.

Costa, Flávia C.R., Fábio S.L. Brito, Maria Júlia R. de Grandi, and Juliana F.S. Daniel. **2025**. "White Rot Fungi for Biodegradation of Dyes: Potential for Industrial Uses - A Review." Journal of the Brazilian Chemical Society 36 (6): e-20250024. https://doi.org/10.21577/0103-5053.20250024.

Coursolle, Dan, and Jeffrey A. Gralnick. **2010**. "Modularity of the Mtr Respiratory Pathway of Shewanella Oneidensis Strain MR-1." Molecular Microbiology 77 (4): 995–1008. https://doi.org/10.1111/J.1365-2958.2010.07266.X.

Cova, Tânia F.G.G., Alberto A.C.C. Pais, and J. Sérgio Seixas De Melo. **2017**. "Reconstructing the Historical Synthesis of Mauveine from Perkin and Caro: Procedure and Details." Scientific Reports 7 (1): 1–9. https://doi.org/10.1038/S41598-017-07239-Z.

Cuebas-Irizarry, Mara F., and Amy M. Grunden. **2024**. "Streptomyces Spp. as Biocatalyst Sources in Pulp and Paper and Textile Industries: Biodegradation, Bioconversion and Valorization of Waste." Microbial Biotechnology 17 (1): e14258. https://doi.org/10.1111/1751-7915.14258.

Cui, Min Hua, Jian Gao, Ai Jie Wang, and Thangavel Sangeetha. **2019**. "Azo Dye Wastewater Treatment in a Bioelectrochemical-Aerobic Integrated System: Effect of Initial Azo Dye Concentration and Aerobic Sludge Concentration." Desalination and Water Treatment 165:314–20. https://doi.org/10.5004/DWT.2019.24395.

Dai, Meixue, Yujia Zhang, Yiming Wu, Ruipeng Sun, Wansong Zong, and Qiang Kong. **2021**. "Mechanism Involved in the Treatment of Sulfamethoxazole in Wastewater Using a Constructed Wetland Microbial Fuel Cell System." Journal of Environmental Chemical Engineering 9 (5): 106193. https://doi.org/10.1016/J.JECE.2021.106193.

Dai, Qin, Sai Zhang, Hao Liu, Jun Huang, and Li Li. **2020**. "Sulfide-Mediated Azo Dye Degradation and Microbial Community Analysis in a Single-Chamber Air Cathode Microbial Fuel Cell." Bioelectrochemistry 131 (February):107349. https://doi.org/10.1016/J.BIOELECHEM.2019.107349.

Danish Khan, Mohammad, Huda Abdulateif, Iqbal M. Ismail, Suhail Sabir, and Mohammad Zain Khan. 2**015**. "Bioelectricity Generation and Bioremediation of an Azo-Dye in a Microbial Fuel Cell Coupled Activated Sludge Process." PLOS ONE 10 (10): e0138448. https://doi.org/10.1371/JOURNAL.PONE.0138448.

Das, Soumyajit, Lubhan Cherwoo, and Ravinder Singh. **2023**. "Decoding Dye Degradation: Microbial Remediation of Textile Industry Effluents." Biotechnology Notes 4:64–76. https://doi.org/10.1016/J.BIOTNO.2023.10.001.

Dutta, Soumi, Bramha Gupta, Suneel Kumar Srivastava, and Ashok Kumar Gupta. 2021. "Recent Advances on the Removal of Dyes from Wastewater Using Various Adsorbents: A Critical Review." Materials Advances 2 (14): 4497–4531. https://doi.org/10.1039/D1MA00354B.

Edebali, Özge, Simona Krupčíková, Anna Goellner, Branislav Vrana, Melis Muz, and Lisa Melymuk. **2024**. "Tracking Aromatic Amines from Sources to Surface Waters." Environmental Science & Technology Letters 11 (5): 397–409. https://doi.org/10.1021/acs.estlett.4c00032.

El-taweel, Reem M., Nora Mohamed, Khlood A. Alrefaey, Sh Husien, A. B. Abdel-Aziz, Alyaa I. Salim, Nagwan G. Mostafa, Lobna A. Said, Irene Samy Fahim, and Ahmed G. Radwan. **2023**. "A Review of Coagulation Explaining Its Definition, Mechanism, Coagulant Types, and Optimization Models; RSM, and ANN." Current Research in Green and Sustainable Chemistry 6 (January):100358. https://doi.org/10.1016/J.CRGSC.2023.100358.

Emami-Meibodi, M., M. R. Parsaeian, R. Amraei, M. Banaei, F. Anvari, S. M.R. Tahami, B. Vakhshoor, et al. **2016**. "An Experimental Investigation of Wastewater Treatment Using Electron Beam Irradiation." Radiation Physics and Chemistry 125 (August):82–87. https://doi.org/10.1016/J.RADPHYSCHEM.2016.03.011.

Epelle, Emmanuel I., Andrew Macfarlane, Michael Cusack, Anthony Burns, Jude A. Okolie, William Mackay, Mostafa Rateb, and Mohammed Yaseen. **2022.** "Ozone Application in Different Industries: A Review of Recent Developments." Chemical Engineering Journal 454 (February):140188. https://doi.org/10.1016/J.CEJ.2022.140188.

"EU REACH Annex XVII Amended | Bureau Veritas CPS." n.d. Accessed January 25, **2026**. https://www.cps.bureauveritas.com/newsroom/eu-reach-annex-xvii-amended.

Fang, Zhou, Hai Liang Song, Ning Cang, and Xian Ning Li. **2015**. "Electricity Production from Azo Dye Wastewater Using a Microbial Fuel Cell Coupled Constructed Wetland Operating under Different Operating Conditions." Biosensors and Bioelectronics 68 (June):135–41. https://doi.org/10.1016/J.BIOS.2014.12.047.

Fenniche, Fares, Yasmina Khane, Abdellah Henni, Djaber Aouf, and Dhiya Elhak Djafri. **2022**. "Synthesis and Characterization of PANI Nanofibers High-Performance Thin Films via Electrochemical Methods." Results in Chemistry 4 (January):100596. https://doi.org/10.1016/J.RECHEM.2022.100596.

Filho, João Gilberto Meza Ucella, Mário Sérgio Lorenço, Elias Costa Souza, Geraldo Márcio da Costa, Roberta Hilsdorf Piccolo, Ananias Francisco Dias Junior, and Fábio Akira Mori. **2022.** "Tannin-Rich Tree Bark Extracts Inhibit the Development of Bacteria Associated with Bovine Mastitis." BioResources 17 (4): 6578–87. https://ojs.bioresources.com/index.php/BRJ/article/view/22106.

Fischer, Fabian, Nancy Merino, Marc Sugnaux, Gérald Huguenin, and Kenneth H. Nealson. **2022**. "Microbial Community Diversity Changes during Voltage Reversal Repair in a 12-Unit Microbial Fuel Cell." Chemical Engineering Journal 446 (October):137334. https://doi.org/10.1016/J.CEJ.2022.137334.

Fu, Qian, Hajime Kobayashi, Hideo Kawaguchi, Javier Vilcaez, Tatsuki Wakayama, Haruo Maeda, and Kozo Sato. **2013**. "Electrochemical and Phylogenetic Analyses of Current-Generating Microorganisms in a Thermophilic Microbial Fuel Cell." Journal of Bioscience and Bioengineering 115 (3): 268–71. https://doi.org/10.1016/J.JBIOSC.2012.10.007.

Fu, Y. B., Z. H. Liu, G. Su, X. R. Zai, M. Ying, and J. Yu. **2016**. "Modified Carbon Anode by MWCNTs/PANI Used in Marine Sediment Microbial Fuel Cell and Its Electrochemical Performance." Fuel Cells 16 (3): 377–83. https://doi.org/10.1002/FUCE.201500103.

Fu, Yanyan, Yixun Gao, Lei Chen, Qingguo He, Defeng Zhu, Huimin Cao, and Jiangong Cheng. **2014**. "Highly Efficient Single Fluorescent Probe for Multiple Amine Vapours via Reaction between Amine and Aldehyde/Dioxaborolane." RSC Advances 4 (87): 46631–34. https://doi.org/10.1039/C4RA08995B.

Gasmi, Aicha, Soumaya Ibrahimi, Noureddine Elboughdiri, Mohamed Aymen Tekaya, Djamel Ghernaout, Ahmed Hannachi, Abdelhakim Mesloub, Badreddine Ayadi, and Lioua Kolsi. **2022**. "Comparative Study of Chemical Coagulation and Electrocoagulation for the Treatment of Real Textile Wastewater: Optimization and Operating Cost Estimation." ACS Omega 7 (26): 22456–76. https://doi.org/10.1021/ACSOMEGA.2C01652.

Gayathiri, Ekambaram, Palanisamy Prakash, Kuppusamy Selvam, Mukesh Kumar Awasthi, Ravindran Gobinath, Rama Rao Karri, Manikkavalli Gurunathan Ragunathan, et al. **2022**. "Plant Microbe Based Remediation Approaches in Dye Removal: A Review." Bioengineered 13 (3): 7798. https://doi.org/10.1080/21655979.2022.2049100.

Gizdavic-Nikolaidis, Marija R., Jared R. Bennett, Simon Swift, Allan J. Easteal, and Mark Ambrose. **2011**.

"Broad Spectrum Antimicrobial Activity of Functionalized Polyanilines." Acta Biomaterialia 7 (12): 4204–9. https://doi.org/10.1016/J.ACTBIO.2011.07.018.

Glaze, William H., Joon Wun Kang, and Douglas H. Chapin. **1987**. "The Chemistry of Water Treatment Processes Involving Ozone, Hydrogen Peroxide and Ultraviolet Radiation." Ozone: Science & Engineering 9 (4): 335–52. https://doi.org/10.1080/01919518708552148.

Greenman, John, Iwona Gajda, Jiseon You, Buddhi Arjuna Mendis, Oluwatosin Obata, Grzegorz Pasternak, and Ioannis Ieropoulos. **2021**. "Microbial Fuel Cells and Their Electrified Biofilms." Biofilm 3 (December):100057. https://doi.org/10.1016/J.BIOFLM.2021.100057.

Grey, Lauren H., Heng Yong Nie, and Mark C. Biesinger. 2024. "Defining the Nature of Adventitious Carbon and Improving Its Merit as a Charge Correction Reference for XPS." Applied Surface Science 653 (April):159319. https://doi.org/10.1016/J.APSUSC.2024.159319.

Guadie, Awoke, Amare Gessesse, and Siqing Xia. **2018**. "Halomonas Sp. Strain A55, a Novel Dye Decolorizing Bacterium from Dye-Uncontaminated Rift Valley Soda Lake." Chemosphere 206 (September):59–69. https://doi.org/10.1016/J.CHEMOSPHERE.2018.04.134.

Guo, Yarui, Yuhong Qi, Chen Zhang, Shukun Zhang, and Zhanping Zhang. **2023**. "The Effect of Conductive Polyaniline on the Anti-Fouling and Electromagnetic Properties of Polydimethylsiloxane Coatings." Polymers 2023, Vol. 15, Page 2944 15 (13): 2944. https://doi.org/10.3390/POLYM15132944.

Hagan, Eric, and Jennifer Poulin. **2021**. "Statistics of the Early Synthetic Dye Industry." Heritage Science 9 (1): 1–14. https://doi.org/10.1186/S40494-021-00493-5.

Harish, B S, Tha Thayumanavan, Veerasekar Nambukrishnan, and K Sakthishobana. **2023.** "Heterogeneous Biocatalytic System for Effective Decolorization of Textile Dye Effluent." 3 Biotech 13 (6): 165. https://doi.org/10.1007/S13205-023-03586-Z.

Hassan, Mohammad M. **2021**. "Energy-Efficient Dyeing of Wool Fabrics with Sulfonic Acid Derivatives of Aniline by Oxidation Polymerization." Sustainable Materials and Technologies 29 (September):e00290. https://doi.org/10.1016/J.SUSMAT.2021.E00290.

He, Huanqi, Avery Lachlann Carlson, Brett Wagner, Cheng Yang, Yi Cao, Mohammed Dilshaad Uzair, and Glen T. Daigger. **2025**. "An Update on Hybrid Membrane Aerated Biofilm Reactor Technology." Water Environment Research 97 (4): e70065. https://doi.org/10.1002/WER.70065;ISSUE:ISSUE:DOI.

He, Huanqi, Brett M. Wagner, Avery L. Carlson, Cheng Yang, and Glen T. Daigger. **2021**. "Recent Progress Using Membrane Aerated Biofilm Reactors for Wastewater Treatment." Water Science and Technology 84 (9): 2131–57. https://doi.org/10.2166/WST.2021.443.

He, Yuan Qiu, Rou Wen Chen, Cun Li, Song Biao Shi, Lin Qing Cui, Li Juan Long, and Xin Peng Tian. **2020**. "Actinomarinicola Tropica Gen. Nov. Sp. Nov., a New Marine Actinobacterium of the Family Iamiaceae, Isolated from South China Sea Sediment Environments." International Journal of Systematic and Evolutionary Microbiology 70 (6): 3852–58. https://doi.org/10.1099/IJSEM.0.004251.

Hemdan, Bahaa A., Gamila E. El-Taweel, Sunandan Naha, and Pranab Goswami. **2023**. "Bacterial Community

Structure of Electrogenic Biofilm Developed on Modified Graphite Anode in Microbial Fuel Cell." Scientific Reports 13 (1): 1255. https://doi.org/10.1038/S41598-023-27795-X.

Herath, Indunil S., Dhanushka Udayanga, D. J. Jayasanka, and Choolaka Hewawasam. **2024.** "Textile Dye Decolorization by White Rot Fungi – A Review." Bioresource Technology Reports 25 (February):101687. https://doi.org/10.1016/J.BITEB.2023.101687.

Hermida-Merino, Carolina, David Cabaleiro, Luis Lugo, Jesus Valcarcel, Jose Antonio Vázquez, Ivan Bravo, Alessandro Longo, et al. **2022**. "Characterization of Tuna Gelatin-Based Hydrogels as a Matrix for Drug Delivery." Gels 8 (4): 237. https://doi.org/10.3390/GELS8040237.

Hong, Yi Guo, and Ji Dong Gu. **2010.** "Physiology and Biochemistry of Reduction of Azo Compounds by Shewanella Strains Relevant to Electron Transport Chain." Applied Microbiology and Biotechnology 88 (3): 637–43. https://doi.org/10.1007/S00253-010-2820-Z.

Hong, Yiguo, Xingjuan Chen, Jun Guo, Zhicheng Xu, Meiying Xu, and Guoping Sun. **2007**. "Effects of Electron Donors and Acceptors on Anaerobic Reduction of Azo Dyes by Shewanella Decolorationis S12." Applied Microbiology and Biotechnology 74 (1): 230–38. https://doi.org/10.1007/S00253-006-0657-2.

Hosseini Koupaie, E., M. R. Alavi Moghaddam, and S. H. Hashemi. **2011**. "Post-Treatment of Anaerobically Degraded Azo Dye Acid Red 18 Using Aerobic Moving Bed Biofilm Process: Enhanced Removal of Aromatic Amines." Journal of Hazardous Materials 195 (November):147–54. https://doi.org/10.1016/j.jhazmat.2011.08.017.

Hou, Junxian, Zhongliang Liu, and Yanxia Li. **2015**. "Polyaniline Modified Stainless Steel Fiber Felt for High-Performance Microbial Fuel Cell Anodes." Journal of Clean Energy Technologies 3 (3): 165–69. https://doi.org/10.7763/JOCET.2015.V3.189.

Huang, Lihua, Xiufen Li, Yueping Ren, and Xinhua Wang. **2016**. "In-Situ Modified Carbon Cloth with Polyaniline/Graphene as Anode to Enhance Performance of Microbial Fuel Cell." International Journal of Hydrogen Energy 41 (26): 11369–79. https://doi.org/10.1016/J.IJHYDENE.2016.05.048.

Hubbe, Martin A, Junyeong Park, and Sunkyu Park. **2014**. "Cellulosic Substrates for Removal of Pollutants from Aqueous Systems: A Review. Part 4. Dissolved Petrochemical Compounds." *BioRes.* 9(4), 7782-7925.

Hübner, Uwe, Stephanie Spahr, Holger Lutze, Arne Wieland, Steffen Rüting, Wolfgang Gernjak, and Jannis Wenk. **2024**. "Advanced Oxidation Processes for Water and Wastewater Treatment – Guidance for Systematic Future Research." Heliyon 10 (9): e30402. https://doi.org/10.1016/J.HELIYON.2024.E30402.

Hunger, Klaus. **2004**. "Industrial Dyes: Chemistry, Properties, Applications." Industrial Dyes: Chemistry, Properties, Applications, March, 1–660. https://doi.org/10.1002/3527602011.

Husien, Sh, Reem M. El-taweel, Alyaa I. Salim, Irene Samy Fahim, Lobna A. Said, and Ahmed G. Radwan. **2022**. "Review of Activated Carbon Adsorbent Material for Textile Dyes Removal: Preparation, and Modelling." Current Research in Green and Sustainable Chemistry 5 (January):100325. https://doi.org/10.1016/J.CRGSC.2022.100325.

Islam, Md. Mynul, Allah Rakha Aidid, Jamshed Nawaj Mohshin, Himel Mondal, Sumon Ganguli, and Ashok

Kumar Chakraborty. **2025.** "A Critical Review on Textile Dye-Containing Wastewater: Ecotoxicity, Health Risks, and Remediation Strategies for Environmental Safety." Cleaner Chemical Engineering 11 (December):100165. https://doi.org/10.1016/J.CLCE.2025.100165.

Jalili, Payam, Amirhosein Ala, Parham Nazari, Bahram Jalili, and Davood Domiri Ganji. **2024**. "A Comprehensive Review of Microbial Fuel Cells Considering Materials, Methods, Structures, and Microorganisms." Heliyon 10 (3): e25439. https://doi.org/10.1016/J.HELIYON.2024.E25439.

Jamee, Radia, and Romana Siddique. **2019**. "Biodegradation of Synthetic Dyes of Textile Effluent by Microorganisms: An Environmentally and Economically Sustainable Approach." European Journal of Microbiology & Immunology 9 (4): 114. https://doi.org/10.1556/1886.2019.00018.

Jasińska, Anna, Aleksandra Walaszczyk, and Katarzyna Paraszkiewicz. **2024**. "Omics-Based Approaches in Research on Textile Dye Microbial Decolorization." Molecules 2024, Vol. 29, 29 (12). https://doi.org/10.3390/MOLECULES29122771.

Jayapal, Mohanapriya, Hema Jagadeesan, Manojkumar Shanmugam, Perinba Danisha J, and Shobana Murugesan. **2018**. "Sequential Anaerobic-Aerobic Treatment Using Plant Microbe Integrated System for Degradation of Azo Dyes and Their Aromatic Amines by-Products." Journal of Hazardous Materials 354 (July):231–43. https://doi.org/10.1016/J.JHAZMAT.2018.04.050.

Jegan Durai, N., G. V.T. Gopalakrishna, V. C. Padmanaban, and N. Selvaraju. **2020**. "Oxidative Removal of Stabilized Landfill Leachate by Fenton's Process: Process Modeling, Optimization & Analysis of Degraded Products." RSC Advances 10 (7): 3916–25. https://doi.org/10.1039/C9RA09415F.

Ji, Fangqi, Wei Zhou, Ze Zhang, and Bing Zhang. **2022**. "Effects of Relative Molecular Weight Distribution and Isoelectric Point on the Swelling Behavior of Gelatin Films." Frontiers in Chemistry 10 (May):857976. https://doi.org/10.3389/FCHEM.2022.857976.

Jiang, Laixin, and Zuolin Cui. **2006**. "One-Step Synthesis of Oriented Polyaniline Nanorods through Electrochemical Deposition." Polymer Bulletin 2006 56:6 56 (6): 529–37. https://doi.org/10.1007/S00289-005-0494-Y.

Jimenez, Luis, Margarita Kulko, Ryan Kim, Theranda Jashari, and Tina Choe. **2020**. "16S RRNA Analysis of Electrogenic Bacterial Communities in Microbial Fuel Cells Developed from Temperate Soils." Https://Doi.Org/10.1893/BIOS-D-18-00006 91 (1): 9–20. https://doi.org/10.1893/BIOS-D-18-00006.

Jong, Bor Chyan, Byung Hong Kim, In Seop Chang, Pauline Woan Ying Liew, Yeng Fung Choo, and Gi Su Kang. **2006**. "Enrichment, Performance, and Microbial Diversity of a Thermophilic Mediatorless Microbial Fuel Cell." Environmental Science and Technology 40 (20): 6449–54. https://doi.org/10.1021/ES0613512.

Kadhom, Mohammed, Noor Albayati, Hayder Alalwan, and Mustafa Al-Furaiji. **2020**. "Removal of Dyes by Agricultural Waste." Sustainable Chemistry and Pharmacy 16 (June):100259. https://doi.org/10.1016/J.SCP.2020.100259.

Kainth, Shagun, Piyush Sharma, and O. P. Pandey. **2024**. "Green Sorbents from Agricultural Wastes: A Review of Sustainable Adsorption Materials." Applied Surface Science Advances 19 (February):100562.

https://doi.org/10.1016/J.APSADV.2023.100562.

Kalaivani, R, V Janaki Devi, R Umarani, K Periyanayagam, and A K Kumaraguru. 2012. "Antimicrobial Activity of Some Important Medicinal Plant Oils against Human Pathogens." Journal of Biologically Active Products from Nature 2 (1): 30–37. https://doi.org/10.1080/22311866.2012.10719105.

Kamalesh, R., S. Karishma, A. Saravanan, and P. R. Yaashikaa. **2024**. "Emerging Breakthroughs in Membrane Filtration Techniques and Their Application in Agricultural Wastewater Treatment: Reusability Aspects." Sustainable Chemistry for the Environment 8 (December):100183. https://doi.org/10.1016/J.SCENV.2024.100183.

Kamati, Salmi Ndapandula, Jia Yan, and Jianwei Fan. **2024**. "A Review on Progresses in Reactive Dye-Containing Wastewater Treatment." Water Practice and Technology 19 (7): 2712–33. https://doi.org/10.2166/WPT.2024.142.

Kameche, Karima, Said Amrani, Samah Mouzaoui, and Hamid Aït-Amar. **2022**. "Biodegradation of Diazo Dye Evans Blue by Four Strains of Streptomyces Isolated from Soils of Algeria." Biocatalysis and Agricultural Biotechnology 46 (November):102529. https://doi.org/10.1016/J.BCAB.2022.102529.

Kapoor, Riti Thapar, Mohammed Danish, Ram Sharan Singh, Mohd Rafatullah, and Abdul Khalil Abdul. **2021**. "Exploiting Microbial Biomass in Treating Azo Dyes Contaminated Wastewater: Mechanism of Degradation and Factors Affecting Microbial Efficiency." Journal of Water Process Engineering 43 (October):102255. https://doi.org/10.1016/J.JWPE.2021.102255.

Karam, Ahmed, Emad S. Bakhoum, and Khaled Zaher. **2021**. "Coagulation/Flocculation Process for Textile Mill Effluent Treatment: Experimental and Numerical Perspectives." International Journal of Sustainable Engineering 14 (5): 983–95. https://doi.org/10.1080/19397038.2020.1842547.

Katuri, Krishna P., Keith Scott, Ian M. Head, Cristian Picioreanu, and Tom P. Curtis. 2**011**. "Microbial Fuel Cells Meet with External Resistance." Bioresource Technology 102 (3): 2758–66. https://doi.org/10.1016/J.BIORTECH.2010.10.147.

Keshava, Channa, Suna Nicolai, Suryanarayana V. Vulimiri, Florenz A. Cruz, Narges Ghoreishi, Sven Knueppel, Ariane Lenzner, et al. **2023**. "Application of Systematic Evidence Mapping to Identify Available Data on the Potential Human Health Hazards of Selected Market-Relevant Azo Dyes." Environment International 176 (June):107952. https://doi.org/10.1016/J.ENVINT.2023.107952.

Khalil, Noor Fadhil, Ali Mousa Ridha, and Mahmood K.H. Al-Mashhadani. **2023**. "Modification of Carbon Cloth/Polyaniline Nano-Titanium Dioxide Composite Electrodes for Enhancement Microbial Fuel Cells (MFCs)." AIP Conference Proceedings 2651 (1). https://doi.org/10.1063/5.0111660/2880551.

Khan, Mohammad Danish, Da Li, Shamas Tabraiz, Burhan Shamurad, Keith Scott, Mohammad Zain Khan, and Eileen Hao Yu. **2021**. "Integrated Air Cathode Microbial Fuel Cell-Aerobic Bioreactor Set-up for Enhanced Bioelectrodegradation of Azo Dye Acid Blue 29." Science of The Total Environment 756 (February):143752. https://doi.org/10.1016/J.SCITOTENV.2020.143752.

Khan, Mohammad Danish, Ankit Singh, Mohammad Zain Khan, Shamas Tabraiz, and Javed Sheikh. **2023**.

"Current Perspectives, Recent Advancements, and Efficiencies of Various Dye-Containing Wastewater Treatment Technologies." Journal of Water Process Engineering 53 (July):103579. https://doi.org/10.1016/J.JWPE.2023.103579.

Khan, Mohammad Danish, Shamas Tabraiz, Ravikumar Thimmappa, Da Li, Abdul Hakeem Anwer, Keith Scott, Mohammad Zain Khan, and Eileen Hao Yu. **2022**. "Polyaniline on Stainless Steel Fiber Felt as Anodes for Bioelectrodegradation of Acid Blue 29 in Microbial Fuel Cells." Frontiers in Chemical Engineering 4 (April):877255. https://doi.org/10.3389/FCENG.2022.877255.

Khan, Nishat, M. Danish Khan, Abdul Sattar Nizami, Mohammad Rehan, Azfar Shaida, Anees Ahmad, and Mohammad Z. Khan. 2018. "Energy Generation through Bioelectrochemical Degradation of Pentachlorophenol in Microbial Fuel Cell." RSC Advances 8 (37): 20726–36. https://doi.org/10.1039/C8RA01643G.

Khan, Sadia, Tayyaba Noor, Naseem Iqbal, and Lubna Yaqoob. **2024**. "Photocatalytic Dye Degradation from Textile Wastewater: A Review." ACS Omega 9 (20): 21751. https://doi.org/10.1021/ACSOMEGA.4C00887.

Khatri, Awais, Mazhar Hussain Peerzada, Muhammad Mohsin, and Max White. **2015**. "A Review on Developments in Dyeing Cotton Fabrics with Reactive Dyes for Reducing Effluent Pollution." Journal of Cleaner Production 87 (1): 50–57. https://doi.org/10.1016/J.JCLEPRO.2014.09.017.

Kim, Tak Hyun, Chulhwan Park, Jeongmok Yang, and Sangyong Kim. **2004.** "Comparison of Disperse and Reactive Dye Removals by Chemical Coagulation and Fenton Oxidation." Journal of Hazardous Materials 112 (1–2): 95–103. https://doi.org/10.1016/j.jhazmat.2004.04.008.

Kishor, Roop, Diane Purchase, Ganesh Dattatraya Saratale, Luiz Fernando Romanholo Ferreira, Muhammad Bilal, Hafiz M.N. Iqbal, and Ram Naresh Bharagava. **2021**. "Environment Friendly Degradation and Detoxification of Congo Red Dye and Textile Industry Wastewater by a Newly Isolated Bacillus Cohnni (RKS9)." Environmental Technology & Innovation 22 (May):101425. https://doi.org/10.1016/J.ETI.2021.101425.

Kitanou, Sarra, Mustapha Tahaikt, Mohamed Taky, and Azzedine Elmidaoui. 2025. "Response Surface Methodology to Investigate the Effects of Operational Parameters on Membrane Bioreactor." Water Science and Technology 91 (5): 453–68. https://doi.org/10.2166/WST.2025.031.

Kong, Fanying, Hong Yu Ren, Dong Liu, Zilong Wang, Jun Nan, Nan Qi Ren, and Qiang Fu. **2022**. "Improved Decolorization and Mineralization of Azo Dye in an Integrated System of Anaerobic Bioelectrochemical Modules and Aerobic Moving Bed Biofilm Reactor." Bioresource Technology 353 (June). https://doi.org/10.1016/j.biortech.2022.127147.

Kong, Fanying, Hong Yu Ren, Spyros G. Pavlostathis, Aijie Wang, Jun Nan, and Nan Qi Ren. **2018.** "Enhanced Azo Dye Decolorization and Microbial Community Analysis in a Stacked Bioelectrochemical System." Chemical Engineering Journal 354 (December):351–62. https://doi.org/10.1016/J.CEJ.2018.08.027.

Kouzuma, Atsushi, Takuya Kasai, Atsumi Hirose, and Kazuya Watanabe. **2015**. "Catabolic and Regulatory

Systems in Shewanella Oneidensis MR-1 Involved in Electricity Generation in Microbial Fuel Cells." Frontiers in Microbiology 6 (JUN): 609. https://doi.org/10.3389/FMICB.2015.00609.

Kurade, Mayur B., Tatoba R. Waghmode, Jiu Qiang Xiong, Sanjay P. Govindwar, and Byong Hun Jeon. **2019**. "Decolorization of Textile Industry Effluent Using Immobilized Consortium Cells in Upflow Fixed Bed Reactor." Journal of Cleaner Production 213 (March):884–91. https://doi.org/10.1016/J.JCLEPRO.2018.12.218.

Kusumlata, Balram Ambade, Ashish Kumar, and Sneha Gautam. 2024. "Sustainable Solutions: Reviewing the Future of Textile Dye Contaminant Removal with Emerging Biological Treatments." Limnological Review **2024**, Vol. 24, Pages 126-149 24 (2): 126–49. https://doi.org/10.3390/LIMNOLREV24020007.

La Cruz-Noriega, Magaly De, Santiago M. Benites, Segundo Rojas-Flores, Nelida M. Otiniano, Ana M. Sabogal Vargas, Rubén Alfaro, Luis Cabanillas-Chirinos, Walter Rojas-Villacorta, Renny Nazario-Naveda, and Daniel Delfín-Narciso. 2023. "Use of Wastewater and Electrogenic Bacteria to Generate Eco-Friendly Electricity through Microbial Fuel Cells." Sustainability **2023,** Vol. 15, Page 10640 15 (13): 10640. https://doi.org/10.3390/SU151310640.

Li, Chao, Zhen Zhang, Yi Li, and Jiashun Cao. **2015**. "Study on Dyeing Wastewater Treatment at High Temperature by MBBR and the Thermotolerant Mechanism Based on Its Microbial Analysis." Process Biochemistry 50 (11): 1934–41. https://doi.org/10.1016/J.PROCBIO.2015.08.007.

Li, Hai hong, Yang tao Wang, Yang Wang, Hai xia Wang, Kai kai Sun, and Zhen mei Lu. **2019**. "Bacterial Degradation of Anthraquinone Dyes." Journal of Zhejiang University: Science B 20 (6): 528–40. https://doi.org/10.1631/JZUS.B1900165.

Li, Jinmei, Lining Zhao, and Peng Liu. **2023**. "One-Step Electrodeposition of Polyaniline Nanorods on Carbon Cloth for High-Performance Flexible Supercapacitors." Langmuir 39 (40): 14297–307. https://doi.org/10.1021/ACS.LANGMUIR.3C01594.

Li, Tong, Luanxiao Wei, Yisu Fang, Yuhan Cui, Xiajiao Wang, and Yu Li. **2025**. "Risk Identification of Human Health, Ecotoxicity, and Degradation Products of Azo Dyes: Development of a Priority Control List." Environmental Pollution 386 (December):127180. https://doi.org/10.1016/J.ENVPOL.2025.127180.

Li, Wanlin, Xiangchun Quan, Liang Chen, and Yu Zheng. **2020**. "Application of Slow-Release Carbon Sources Embedded in Polymer for Stable and Extended Power Generation in Microbial Fuel Cells." Chemosphere 244 (April):125515. https://doi.org/10.1016/J.CHEMOSPHERE.2019.125515.

Li, Yanbo, Guohong Liu, and Huai Shi. **2023**. "Expansion of Carbon Source Utilization Range of Shewanella Oneidensis for Efficient Azo Dye Wastewater Treatment through Co-Culture with Lactobacillus Plantarum." Archives of Microbiology 205 (8): 1–9. https://doi.org/10.1007/S00203-023-03634-5.

Li, Yuan, Pengcheng Zhang, Yaqi Xu, Jiang Jin, and Hua Zhang. **2021**. "Polyaniline-Decorated Carbon as Composite Carrier for Improving PtNi Catalyst Durability." Journal of Electronic Materials 50 (6): 3488–97. https://doi.org/10.1007/S11664-021-08851-6.

Li, Yue, Xiaojing Li, Yang Sun, Xiaodong Zhao, and Yongtao Li. **2018**. "Cathodic Microbial Community

Adaptation to the Removal of Chlorinated Herbicide in Soil Microbial Fuel Cells." Environmental Science and Pollution Research 25 (17): 16900–912. https://doi.org/10.1007/S11356-018-1871-Z/FIGURES/8.

Liu, Guangfei, Jiti Zhou, Jing Wang, Xiujuan Wang, Ruofei Jin, and Hong Lv. **2011**. "Decolorization of Azo Dyes by Shewanella Oneidensis MR-1 in the Presence of Humic Acids." Applied Microbiology and Biotechnology 91 (2): 417–24. https://doi.org/10.1007/S00253-011-3273-8.

Liu, Jiale, Lu Fan, Wenjun Yin, Shusheng Zhang, Xiaomei Su, Hongjun Lin, Haiying Yu, Zhenghai Jiang, and Faqian Sun. **2023**. "Anaerobic Biodegradation of Azo Dye Reactive Black 5 by a Novel Strain Shewanella Sp. SR1: Pathway and Mechanisms." Journal of Environmental Management 347 (December):119073. https://doi.org/10.1016/J.JENVMAN.2023.119073.

Liu, Junwei, Yixuan Bao, Xuan Zhang, Kaiyun Zhang, Shuaimin Chen, Haiyan Wu, and Jian He. **2021**. "Proteiniclasticum Sediminis Sp. Nov., an Obligate Anaerobic Bacterium Isolated from Anaerobic Sludge." Antonie van Leeuwenhoek 114 (10): 1541–49. https://doi.org/10.1007/S10482-021-01620-9.

Liu, Shentan, Hongpu Xue, Xiaojuan Feng, and Sang Hyun Pyo. 2022. "Electrostimulation for Promoted Microbial Community and Enhanced Biodegradation of Refractory Azo Dyes." Journal of Environmental Chemical Engineering 10 (6): 108626. https://doi.org/10.1016/J.JECE.2022.108626.

Liu, Yanyan, Junyong Zhu, Ming Shuo Chi, Gilles Van Eygen, Kecheng Guan, and Hideto Matsuyama. **2025**. "Comprehensive Review of Nanofiltration Membranes for Efficient Resource Recovery from Textile Wastewater." Chemical Engineering Journal 506 (January):160132. https://doi.org/10.1016/J.CEJ.2025.160132.

Liu, Yundan, Long Ren, Zhen Zhang, Xiang Qi, Hongxing Li, and Jianxin Zhong. **2016**. "3D Binder-Free MoSe2 Nanosheets/Carbon Cloth Electrodes for Efficient and Stable Hydrogen Evolution Prepared by Simple Electrophoresis Deposition Strategy." Scientific Reports 2016 6:1 6 (1): 1–9. https://doi.org/10.1038/srep22516.

Logan, Bruce E., Bert Hamelers, René Rozendal, Uwe Schröder, Jürg Keller, Stefano Freguia, Peter Aelterman, Willy Verstraete, and Korneel Rabaey. **2006**. "Microbial Fuel Cells: Methodology and Technology†." Environmental Science and Technology 40 (17): 5181–92. https://doi.org/10.1021/ES0605016.

Long, Xizi, Xian Cao, Shentan Liu, Osamu Nishimura, and Xianning Li. **2019**. "The Azo Dye Degradation and Differences Between the Two Anodes on the Microbial Community in a Double-Anode Microbial Fuel Cell." Water, Air, and Soil Pollution 230 (11): 1–11. https://doi.org/10.1007/S11270-019-4325-4.

Lu, Yixin, Jiao Chen, Li Zhao, Zheng Zhou, Cheng Qiu, and Qianglin Li. **2020**. "Adsorption of Rhodamine B from Aqueous by Goat Manure Biochar: Kinetics,Isotherms, and Thermodynamic Studies." Polish Journal of Environmental Studies 29 (4): 2721–30. https://doi.org/10.15244/pjoes/112207.

Mani, Priyadharshini, V. T. Fidal, Kyle Bowman, Mark Breheny, T. S. Chandra, Taj Keshavarz, and Godfrey Kyazze. **2019**. "Degradation of Azo Dye (Acid Orange 7) in a Microbial Fuel Cell: Comparison Between Anodic Microbial-Mediated Reduction and Cathodic Laccase-Mediated Oxidation." Frontiers in Energy Research 7 (September):101. https://doi.org/10.3389/FENRG.2019.00101.

Mani, Sujata, and Ram Naresh Bharagava. **2016**. "Exposure to Crystal Violet, Its Toxic, Genotoxic and Carcinogenic Effects on Environment and Its Degradation and Detoxification for Environmental Safety." Reviews of Environmental Contamination and Toxicology 237:71–104. https://doi.org/10.1007/978-3-319-23573-8_4.

Marsili, Enrico, Daniel B. Baron, Indraneel D. Shikhare, Dan Coursolle, Jeffrey A. Gralnick, and Daniel R. Bond. **2008**. "Shewanella Secretes Flavins That Mediate Extracellular Electron Transfer." Proceedings of the National Academy of Sciences of the United States of America 105 (10): 3968–73. https://doi.org/10.1073/PNAS.0710525105.

Mehdinia, Ali, Minodokht Dejaloud, and Ali Jabbari. **2013**. "Nanostructured Polyaniline-Coated Anode for Improving Microbial Fuel Cell Power Output." Chemical Papers 2013 67:8 67 (8): 1096–1102. https://doi.org/10.2478/S11696-013-0381-1.

Merino, Estíbaliz, and María Ribagorda. **2012**. "Control over Molecular Motion Using the Cis–Trans Photoisomerization of the Azo Group." Beilstein Journal of Organic Chemistry 8:119 8 (1): 1071–90. https://doi.org/10.3762/bjoc.8.119.

Miklos, David B., Christian Remy, Martin Jekel, Karl G. Linden, Jörg E. Drewes, and Uwe Hübner. **2018**. "Evaluation of Advanced Oxidation Processes for Water and Wastewater Treatment – A Critical Review." Water Research 139 (August):118–31. https://doi.org/10.1016/j.watres.2018.03.042.

Millbern, Zoe, Alison Trettin, Rachel Wu, Morgan Demmler, and Nelson R. Vinueza. **2024**. "Synthetic Dyes: A Mass Spectrometry Approach and Applications." Mass Spectrometry Reviews 43 (2): 327–44. https://doi.org/10.1002/MAS.21818.

Mishra, Arti, Simran Takkar, Naveen Chandra Joshi, Smriti Shukla, Kartikeya Shukla, Anamika Singh, Anusha Manikonda, and Ajit Varma. **2022**. "An Integrative Approach to Study Bacterial Enzymatic Degradation of Toxic Dyes." Frontiers in Microbiology 12 (January):802544. https://doi.org/10.3389/fmicb.2021.802544.

Moh Rabti, Amel Taher, Akin Emrecan Gok, Burak Yuzer, and Huseyin Selcuk. **2025**. "Evaluation of a Sustainable Dye-Exhausted Resin Regeneration Method for Cost-Effective Decolorization and Detoxification of Textile Wastewater." Engineering Science and Technology, an International Journal 63 (March):101973. https://doi.org/10.1016/J.JESTCH.2025.101973.

Mohamad Hanapi, Nur Hanis, Sharifah Hanis Yasmin Sayid Abdullah, Zuriati Khairuddin, nor Hasima Mahmod, Hadieh Monajemi, Azimah Ismail, Fathurrahman Lananan, Zarizal Suhaili, Azizah Endut, and Hafizan Juahir. **2022**. "COD Removal and Colour Degradation of Textile Dye Effluents by Locally Isolated Microbes." International Journal of Environmental Analytical Chemistry 102 (19): 7835–50. https://doi.org/10.1080/03067319.2020.1839438.

Mohanty, Swati Sambita, and Arvind Kumar. **2021**. "Biodegradation of Indanthrene Blue RS Dye in Immobilized Continuous Upflow Packed Bed Bioreactor Using Corncob Biochar." Scientific Reports 2021 11:1 11 (1): 13390-. https://doi.org/10.1038/s41598-021-92889-3.

———. **2025.** "Microbial Decolorization of Anthraquinone Dyes: Batch and Continuous Treatment Systems - a Mini-Review." Frontiers in Environmental Engineering 4 (June):1553712. https://doi.org/10.3389/FENVE.2025.1553712.

Mohtasebi, Amirmasoud, Tanzina Chowdhury, Leo H.H. Hsu, Mark C. Biesinger, and Peter Kruse. **2016.** "Interfacial Charge Transfer between Phenyl-Capped Aniline Tetramer Films and Iron Oxide Surfaces." Journal of Physical Chemistry C 120 (51): 29248–63. https://doi.org/10.1021/ACS.JPCC.6B09950.

Morales-Florez, Alejandro, Colin W.J. Lockwood, Benjamin W. Nash, Marcus J. Edwards, Jessica H. van Wonderen, Amit Sachdeva, Julea N. Butt, and Thomas A. Clarke. **2025.** "Extracellular Catalysis of Environmental Substrates by Shewanella Oneidensis MR-1 Occurs via Active Sites on the C-terminal Domains of MtrC." Protein Science : A Publication of the Protein Society 34 (8): e70243. https://doi.org/10.1002/PRO.70243.

Morgan-Sagastume, Fernando. **2018**. "Biofilm Development, Activity and the Modification of Carrier Material Surface Properties in Moving-Bed Biofilm Reactors (MBBRs) for Wastewater Treatment." Critical Reviews in Environmental Science and Technology 48 (5): 439–70. https://doi.org/10.1080/10643389.2018.1465759.

Mousset, Emmanuel, Wei Hao Loh, Wei Shien Lim, Léa Jarry, Zuxin Wang, and Olivier Lefebvre. **2021**. "Cost Comparison of Advanced Oxidation Processes for Wastewater Treatment Using Accumulated Oxygen-Equivalent Criteria." Water Research 200 (July):117234. https://doi.org/10.1016/J.WATRES.2021.117234.

Moyo, Senelisile, Bukisile P. Makhanya, and Pinkie E. Zwane. **2022.** "Use of Bacterial Isolates in the Treatment of Textile Dye Wastewater: A Review." Heliyon 8 (6): e09632. https://doi.org/10.1016/J.HELIYON.2022.E09632.

Muniyasamy, Abaranjitha, Gayathri Sivaporul, Abarna Gopinath, Rajendran Lakshmanan, Ali Altaee, Anant Achary, and Padmanaban Velayudhaperumal Chellam. **2020**. "Process Development for the Degradation of Textile Azo Dyes (Mono-, Di-, Poly-) by Advanced Oxidation Process - Ozonation: Experimental & Partial Derivative Modelling Approach." Journal of Environmental Management 265 (July):110397. https://doi.org/10.1016/J.JENVMAN.2020.110397.

Murali, V., Soon-An Ong, Li-Ngee Ho, Yee-Shian Wong, and Nasrul Hamidin. **2013.** "Comprehensive Review and Compilation of Treatment for Azo Dyes Using Microbial Fuel Cells." Water Environment Research 85 (3): 270–77. https://doi.org/10.2175/106143012X13503213812481.

Murshid, Shabnam, Adithya Joseph Antonysamy, Gnana Prakash Dhakshinamoorthy, Arun Jayaseelan, and Arivalagan Pugazhendhi. 2023. "A Review on Biofilm-Based Reactors for Wastewater Treatment: Recent Advancements in Biofilm Carriers, Kinetics, Reactors, Economics, and Future Perspectives." Science of The Total Environment 892 (September):164796. https://doi.org/10.1016/J.SCITOTENV.2023.164796.

Mustafa, Ghulam, Ammara Younas, Muhammad Tariq Zahid, Deok Won Kim, Ihtisham Jamil, Nikita Yadav, Mayur B. Kurade, Shouvik Saha, Karishna Kumar Yadav, and Byong Hun Jeon. **2025**. "Bioremediation of Reactive Blue 19 Dye by Laccase-Producing Serratia Marcescens AY4 Strain." Journal of Environmental

Chemical Engineering 13 (2): 115605. https://doi.org/10.1016/J.JECE.2025.115605.

Mustafa, Ghulam, Muhammad Tariq Zahid, Shaukat Ali, Syed Zaghum Abbas, Mohd Rafatullah, Ghulam Mustafa, Muhammad Tariq Zahid, Shaukat Ali, Syed Zaghum Abbas, and Mohd Rafatullah. **2021**. "Biodegradation and Discoloration of Disperse Blue-284 Textile Dye by Klebsiella Pneumoniae GM-04 Bacterial Isolate." Journal of King Saud University – Science 33 (4). https://doi.org/10.1016/J.JKSUS.2021.101442.

Nagraj, Pankaj Kumar Chaurasia, Shashi Lata Bharati, Nagendra Sharma, Jaynath Kumar, and Azhagu Madhavan Sivalingam. **2025**. "Degradation of Dyes by Fungi: An Overview on Recent Updates." The Microbe 6 (March):100232. https://doi.org/10.1016/J.MICROB.2024.100232.

Nakagawa, Gen, Atsushi Kouzuma, Atsumi Hirose, Takuya Kasai, Gen Yoshida, and Kazuya Watanabe. 2015. "Metabolic Characteristics of a Glucose-Utilizing Shewanella Oneidensis Strain Grown under Electrode-Respiring Conditions." PLoS ONE 10 (9): e0138813. https://doi.org/10.1371/JOURNAL.PONE.0138813.

Naz, Iffat, Douglas Hodgson, Ann Smith, Julian Marchesi, Shama Sehar, Safia Ahmed, Jim Lynch, Claudio Avignone-Rossa, and Devendra P. Saroj. **2018.** "Investigation of the Active Biofilm Communities on Polypropylene Filter Media in a Fixed Biofilm Reactor for Wastewater Treatment." Journal of Chemical Technology & Biotechnology 93 (11): 3264–75. https://doi.org/10.1002/JCTB.5686.

Nazina, Tamara N., Salimat K. Bidzhieva, Denis S. Grouzdev, Diyana S. Sokolova, Tatyana P. Tourova, Sofiya N. Parshina, Alexander N. Avtukh, Andrey B. Poltaraus, and Azhdar K. Talybly. **2020**. "Soehngenia Longivitae Sp. Nov., a Fermenting Bacterium Isolated from a Petroleum Reservoir in Azerbaijan, and Emended Description of the Genus Soehngenia." Microorganisms 2020, Vol. 8, Page 1967 8 (12): 1967. https://doi.org/10.3390/MICROORGANISMS8121967.

Ndive, Julius Nnamdi, Simeon Okechukwu Eze, Somtochukwu Godfrey Nnabuife, Boyu Kuang, and Zeeshan A. Rana. **2025**. "Dual-Chamber Microbial Fuel Cell for Azo-Dye Degradation and Electricity Generation in Textile Wastewater Treatment." Waste Management Bulletin 3 (3): 100195. https://doi.org/10.1016/J.WMB.2025.100195.

Nerenberg, Robert. **2016.** "The Membrane-Biofilm Reactor (MBfR) as a Counter-Diffusional Biofilm Process." Current Opinion in Biotechnology 38 (April):131–36. https://doi.org/10.1016/J.COPBIO.2016.01.015.

Ngo, Anna Christina R., and Dirk Tischler. **2022**. "Microbial Degradation of Azo Dyes: Approaches and Prospects for a Hazard-Free Conversion by Microorganisms." International Journal of Environmental Research and Public Health 2022, Vol. 19, Page 4740 19 (8): 4740. https://doi.org/10.3390/IJERPH19084740.

Nguyen, Thu Huong, Nguyen Anh-Vu, Thi Thu Huong Nguyen, Taira Hidaka, Taku Fujiwara, Takahiro Watari, and Takashi Yamaguchi. **2025**. "Cosubstrates in Azo Dye Decolorization: From Conventional Anaerobic Systems to Microbial Fuel Cells." Bioresource Technology 436 (November):132962. https://doi.org/10.1016/J.BIORTECH.2025.132962.

Nybacka, Louise. n.d. "FTIR Spectroscopy of Glucose." Accessed February 10, **2025**.

http://www.teknat.uu.se/student.

O'Shea, Kevin E., and Dionysios D. Dionysiou. **2012**. "Advanced Oxidation Processes for Water Treatment." Journal of Physical Chemistry Letters 3 (15): 2112–13. https://doi.org/10.1021/JZ300929X.

Offei, Felix, Anders Thygesen, Moses Mensah, Kwame Tabbicca, Dinesh Fernando, Irina Petrushina, and Geoffrey Daniel. **2016**. "A Viable Electrode Material for Use in Microbial Fuel Cells for Tropical Regions." Energies 2016, Vol. 9, Page 35 9 (1): 35. https://doi.org/10.3390/EN9010035.

Öge, Ezgi, Belma Nural Yaman, and Yeliz Buruk Şahin. **2023**. "Optimization of Biodegradation Yield of Reactive Blue 49: An Integrated Approach Using Response Surface Methodology Based Marine Predators Algorithm." Journal of Microbiological Methods 206 (March):106691. https://doi.org/10.1016/J.MIMET.2023.106691.

Oliveira, Jean M.S., Jan S. Poulsen, Eugênio Foresti, and Jeppe L. Nielsen. **2024**. "New Insights into the Mechanism of Azo Dye Biodegradation by Lactococcus Lactis." Journal of Environmental Chemical Engineering 12 (5): 113670. https://doi.org/10.1016/J.JECE.2024.113670.

Oller, I., S. Malato, and J. A. Sánchez-Pérez. **2011**. "Combination of Advanced Oxidation Processes and Biological Treatments for Wastewater Decontamination-A Review." Science of the Total Environment 409 (20): 4141–66. https://doi.org/10.1016/j.scitotenv.2010.08.061.

Oplatowska, Michalina, Ryan F. Donnelly, Rita J. Majithiya, D. Glenn Kennedy, and Christopher T. Elliott. **2011**. "The Potential for Human Exposure, Direct and Indirect, to the Suspected Carcinogenic Triphenylmethane Dye Brilliant Green from Green Paper Towels." Food and Chemical Toxicology 49 (8): 1870–76. https://doi.org/10.1016/J.FCT.2011.05.005.

Ouyang, Jihong, Wenbo Yang, Zhaoyan Guo, Fujun Li, Wendong Liu, Pengfei Guo, Yumeng Zhou, Dali Gao, Lijing Zhang, and Shengyang Tao. **2024**. "Modular Cascade of Flow Reactors: Continuous Flow Synthesis of Water-Insoluble Diazo Dyes in Aqueous System." ChemSusChem 17 (19): e202400413. https://doi.org/10.1002/CSSC.202400413.

Ozturk, Emrah. **2022**. "Improving Water-Use Efficiency and Environmental Performances in an Integrated Woven-Knitted Fabric Printing-Dyeing Textile Mill." Journal of Cleaner Production 379 (December):134805. https://doi.org/10.1016/J.JCLEPRO.2022.134805.

Pandey, Anjali, Poonam Singh, and Leela Iyengar. **2007**. "Bacterial Decolorization and Degradation of Azo Dyes." International Biodeterioration & Biodegradation 59 (2): 73–84. https://doi.org/10.1016/J.IBIOD.2006.08.006.

Pereira, João, Yuniki Mediayati, H. Pieter J. van Veelen, Hardy Temmink, Tom Sleutels, Bert Hamelers, and Annemiek ter Heijne. **2022**. "The Effect of Intermittent Anode Potential Regimes on the Morphology and Extracellular Matrix Composition of Electro-Active Bacteria." Biofilm 4 (December):100064. https://doi.org/10.1016/J.BIOFLM.2021.100064.

Pérez-Díaz, Margarita Isabel, Paola Zárate-Segura, Luis Antonio Bermeo-Fernández, Khemlal Nirmalkar, Fernando Bastida-González, Jaime García-Mena, Janet Jan-Roblero, and Claudia Guerrero-Barajas. **2020**.

"'Bacterial Consortium from Hydrothermal Vent Sediments Presents Electrogenic Activity Achieved under Sulfate Reducing Conditions in a Microbial Fuel Cell.'" Journal of Environmental Health Science and Engineering 18 (2): 1189. https://doi.org/10.1007/S40201-020-00537-1.

Periyasamy, Aravin Prince. **2024**. "Recent Advances in the Remediation of Textile-Dye-Containing Wastewater: Prioritizing Human Health and Sustainable Wastewater Treatment." Sustainability 2024, Vol. 16, 16 (2). https://doi.org/10.3390/SU16020495.

———**. 2025**. "A Review of Bioremediation of Textile Dye Containing Wastewater." Cleaner Water 4 (December):100092. https://doi.org/10.1016/J.CLWAT.2025.100092.

Pham, The Hai, Nico Boon, Peter Aelterman, Peter Clauwaert, Liesje De Schamphelaire, Lynn Vanhaecke, Katrien De Maeyer, Monica Höfte, Willy Verstraete, and Korneel Rabaey. **2008.** "Metabolites Produced by Pseudomonas Sp. Enable a Gram-Positive Bacterium to Achieve Extracellular Electron Transfer." Applied Microbiology and Biotechnology 77 (5): 1119–29. https://doi.org/10.1007/S00253-007-1248-6.

Phu, Thi Kim Cuong, Phi Long Nguyen, and Thi Viet Bac Phung. **2025.** "Recent Progress in Highly Effective Electrocoagulation-Coupled Systems for Advanced Wastewater Treatment." IScience 28 (3): 111965. https://doi.org/10.1016/J.ISCI.2025.111965.

Pieczykolan, Barbara, Izabela Płonka, Edyta Kudlek, Rafał Kryst, Patrycja Stuchlik, Dominika Pokoj, Karolina Hanzlik, Nikodem Piekarczyk, Igor Orłowski, and Martyna Grodzicka. **2025**. "Application of Advanced Oxidation Processes for Effective Reactive Red 241 Degradation." Desalination and Water Treatment 323 (July):101308. https://doi.org/10.1016/J.DWT.2025.101308.

Pizzicato, Barbara, Severina Pacifico, Diana Cayuela, Gabriela Mijas, and Marta Riba-Moliner. 2023. "Advancements in Sustainable Natural Dyes for Textile Applications: A Review." Molecules 28 (16): 5954. https://doi.org/10.3390/MOLECULES28165954.

Porobić, Slavica J., Bojan Božić, Miroslav D. Dramićanin, Vesna Vitnik, Željko Vitnik, Milena Marinović-Cincović, and Dušan Mijin. **2020**. "Absorption and Fluorescence Spectral Properties of Azo Dyes Based on 3-Amido-6-Hydroxy-4-Methyl-2-Pyridone: Solvent and Substituent Effects." Dyes and Pigments 175 (April):108139. https://doi.org/10.1016/J.DYEPIG.2019.108139.

Potrykus, Szymon, Luis Fernando León-Fernández, Janusz Nieznański, Dariusz Karkosiński, and Francisco Jesus Fernandez-Morales. **2021**. "The Influence of External Load on the Performance of Microbial Fuel Cells." Energies 2021, Vol. 14, Page 612 14 (3): 612. https://doi.org/10.3390/EN14030612.

Pournaghi-Azar, M. H., and B. Habibi. **2007**. "Electropolymerization of Aniline in Acid Media on the Bare and Chemically Pre-Treated Aluminum Electrodes: A Comparative Characterization of the Polyaniline Deposited Electrodes." Electrochimica Acta 52 (12): 4222–30. https://doi.org/10.1016/J.ELECTACTA.2006.11.050.

Prasad, K. Rajendra, and N. Munichandraiah. **2002.** "Electrocatalytic Efficiency of Polyaniline by Cyclic Voltammetry and Electrochemical Impedance Spectroscopy Studies." Synthetic Metals 126 (1): 61–68. https://doi.org/10.1016/S0379-6779(01)00496-9.

Priyadarshini, Monali, Indrasis Das, Makarand M. Ghangrekar, and Lee Blaney. **2022**. "Advanced Oxidation Processes: Performance, Advantages, and Scale-up of Emerging Technologies." Journal of Environmental Management 316 (August):115295. https://doi.org/10.1016/J.JENVMAN.2022.115295.

Przystas, Wioletta, Ewa Zablocka-Godlewska, and Elzbieta Grabinska-Sota. **2012**. "Biological Removal of Azo and Triphenylmethane Dyes and Toxicity of Process By-Products." Water, Air, and Soil Pollution 223 (4): 1581. https://doi.org/10.1007/S11270-011-0966- 7.

Przystaś, Wioletta, Ewa Zabłocka-Godlewska, and Elżbieta Grabińska-Sota. **2019**. "Pleurotus Ostreatus as a Species with Potentially High Effectiveness in the Removal of Synthetic Dyes Belonging to Different Classes." Desalination and Water Treatment 161 (September):376–86. https://doi.org/10.5004/DWT.2019.24314.

Przystś, Wioletta, Ewa Zabłocka-Godlewska, and Elzbieta Grabińska-Sota. **2013.** "Effectiveness of Dyes Removal by Mixed Fungal Cultures and Toxicity of Their Metabolites." Water, Air, and Soil Pollution 224 (5): 1–9. https://doi.org/10.1007/S11270-013-1534-0.

Qu, Wanwan, Idrees B. Qader, and Andrew P. Abbott. **2021.** "Controlled Release of Pharmaceutical Agents Using Eutectic Modified Gelatin." Drug Delivery and Translational Research 2021 12:5 12 (5): 1187–94. https://doi.org/10.1007/S13346-021-00998-3.

Quan, Xiangchun, Hengduo Xu, Bo Sun, and Zhutian Xiao. **2018.** "Anode Modification with Palladium Nanoparticles Enhanced Evans Blue Removal and Power Generation in Microbial Fuel Cells." International Biodeterioration & Biodegradation 132 (August):94–101. https://doi.org/10.1016/J.IBIOD.2018.01.001.

Radhika Rajasree, S. R., M. Gobalakrishnan, L. Aranganathan, and M. G. Karthih. **2020.** "Fabrication and Characterization of Chitosan Based Collagen/ Gelatin Composite Scaffolds from Big Eye Snapper Priacanthus Hamrur Skin for Antimicrobial and Anti Oxidant Applications." Materials Science and Engineering: C 107 (February):110270. https://doi.org/10.1016/J.MSEC.2019.110270.

Rajesh, P. P., Md. T. Noori, and M. M. Ghangrekar. **2020.** "Improving Performance of Microbial Fuel Cell by Using Polyaniline-Coated Carbon–Felt Anode." Journal of Hazardous, Toxic, and Radioactive Waste 24 (3): 04020024. https://doi.org/10.1061/(ASCE)HZ.2153-5515.0000512.

Rajhans, Geetanjali, Adyasa Barik, Sudip K. Sen, and Sangeeta Raut. **2021.** "Degradation of Dyes by Fungi: An Insight into Mycoremediation." BioTechnologia 102 (4): 445. https://doi.org/10.5114/BTA.2021.111109.

Ramamurthy, Karthikeyan, Peter Snega Priya, Raghul Murugan, and Jesu Arockiaraj. **2024.** "Hues of Risk: Investigating Genotoxicity and Environmental Impacts of Azo Textile Dyes." Environmental Science and Pollution Research International 31 (23): 33190–211. https://doi.org/10.1007/S11356-024-33444-1.

Ramasamy, Vijayakumar, and Raja Suresh Selvapuram Sudalaimuhu. **2022**. "Aerobic and Anaerobic Decolorization of Textile Dyes Using Actinobacteria," 695–703. https://doi.org/10.1007/978-1-0716-1728-1_101.

Ramos, Ana Rose, Alvin Karlo G. Tapia, Chrysline Margus N. Piñol, Nacita B. Lantican, Ma Lourdes F. del

Mundo, Ronniel D. Manalo, and Marvin U. Herrera. **2019**. "Morphological, Electrical and Antimicrobial Properties of Polyaniline-Coated Paper Prepared via a Two-Pot Layer-by-Layer Technique." Materials Chemistry and Physics 238 (December):121972. https://doi.org/10.1016/J.MATCHEMPHYS.2019.121972.

Rane, Ashwini, and Sanket J. Joshi. **2021**. "Biodecolorization and Biodegradation of Dyes: A Review." The Open Biotechnology Journal 15 (1): 97–108. https://doi.org/10.2174/1874070702115010097.

Rashid, Md Al Mamunur, Dini Hayati, Kyungwon Kwak, and Jongin Hong. **2020**. "Theoretical Investigation of Azobenzene-Based Photochromic Dyes for Dye-Sensitized Solar Cells." Nanomaterials 10 (5): 914. https://doi.org/10.3390/NANO10050914.

Rathour, Ranju Kumari, Deepak Sharma, Saleem Ullah, El-Hassan M. Mahmoud, Nitish Sharma, Pradeep Kumar, Arvind Kumar Bhatt, Irshad Ahmad, and Ravi Kant Bhatia. **2024.** "Bacterial–Microalgal Consortia for Bioremediation of Textile Industry Wastewater and Resource Recovery for Circular Economy." Biotechnology for the Environment 2024 1:1 1 (1): 6-. https://doi.org/10.1186/S44314-024-00005-2.

Rathour, Rohit, Dishant Patel, Shabnam Shaikh, and Chirayu Desai. **2019**. "Eco-Electrogenic Treatment of Dyestuff Wastewater Using Constructed Wetland-Microbial Fuel Cell System with an Evaluation of Electrode-Enriched Microbial Community Structures." Bioresource Technology 285 (August):121349. https://doi.org/10.1016/J.BIORTECH.2019.121349.

Ravadelli, Mauana, Rayra E. Da Costa, Maria Angeles Lobo-Recio, Tiago Rogerio Vitor Akaboci, João Paulo Bassin, Flávio Rubens Lapolli, and Tiago José Belli. **2021**. "Anoxic/Oxic Membrane Bioreactor Assisted by Electrocoagulation for the Treatment of Azo-Dye Containing Wastewater." Journal of Environmental Chemical Engineering 9 (4): 105286. https://doi.org/10.1016/J.JECE.2021.105286.

Ravi, Ashwini, Ramkishore Krishnan, Mounesh Ravuri, Selvakumar Santhosh, Mohamad S. AlSalhi, Sandhanasamy Devanesan, Aruliah Selvarani, Aruliah Rajasekar, Rajaram Rajamohan, and Jayaraman Narenkumar. **2025.** "Sustainable Approach for the Degradation of Contrast Dye Evans Blue by Enterobacter Cloacae Strain SD4-1." Journal of the Taiwan Institute of Chemical Engineers 166 (January):105323. https://doi.org/10.1016/J.JTICE.2023.105323.

Reddy, Appanu Sushvanth, Sarita Kalla, and Z. V.P. Murthy. **2021**. "Textile Wastewater Treatment via Membrane Distillation." Environmental Engineering Research 27 (5). https://doi.org/10.4491/EER.2021.228.

Rodríguez-Narváez, Oscar M., Alain R. Picos, Nelson Bravo-Yumi, Martín Pacheco-Alvarez, Carlos A. Martínez-Huitle, and Juan M. Peralta-Hernández. **2021**. "Electrochemical Oxidation Technology to Treat Textile Wastewaters." Current Opinion in Electrochemistry 29 (October):100806. https://doi.org/10.1016/J.COELEC.2021.100806.

Roriz, Margarida S., Johann F. Osma, José A. Teixeira, and Susana Rodríguez Couto. **2009**. "Application of Response Surface Methodological Approach to Optimise Reactive Black 5 Decolouration by Crude Laccase from Trametes Pubescens." Journal of Hazardous Materials 169 (1–3): 691–96. https://doi.org/10.1016/J.JHAZMAT.2009.03.150.

Saha, Purbasha, and K. V.Bhaskara Rao. **2020**. "Immobilization as a Powerful Bioremediation Tool for Abatement of Dye Pollution: A Review." Https://Doi.Org/10.1139/Er-2020-0074 29 (2): 277–99. https://doi.org/10.1139/ER-2020-0074.

Saif Ur Rehman, Muhammad, Ilgook Kim, Naim Rashid, Malik Adeel Umer, Muhammad Sajid, and Jong In Han. **2016**. "Adsorption of Brilliant Green Dye on Biochar Prepared From Lignocellulosic Bioethanol Plant Waste." CLEAN – Soil, Air, Water 44 (1): 55–62. https://doi.org/10.1002/CLEN.201300954.

Sanchez-Herrera, Diana, Daniella Pacheco-Catalan, Ruby Valdez-Ojeda, Blondy Canto-Canche, Xochitl Dominguez-Benetton, Jorge Domínguez-Maldonado, and Liliana Alzate-Gaviria. **2014**. "Characterization of Anode and Anolyte Community Growth and the Impact of Impedance in a Microbial Fuel Cell." BMC Biotechnology 14 (1): 1–10. https://doi.org/10.1186/S12896-014-0102-Z.

Santhanarajan, Aalfin Emmanuel, Woo Jun Sul, Keun Je Yoo, Hoon Je Seong, Hong Gi Kim, and Sung Cheol Koh. **2021**. "Metagenomic Insight of a Full Scale Eco-Friendly Treatment System of Textile Dye Wastewater Using Bioaugmentation of the Composite Culture CES-1." Microorganisms **2021**, Vol. 9, 9 (7). https://doi.org/10.3390/MICROORGANISMS9071503.

Santoni, Francesco, Alessio De Angelis, Antonio Moschitta, Paolo Carbone, Matteo Galeotti, Lucio Cinà, Corrado Giammanco, and Aldo Di Carlo. **2024**. "A Guide to Equivalent Circuit Fitting for Impedance Analysis and Battery State Estimation." Journal of Energy Storage 82 (March):110389. https://doi.org/10.1016/J.EST.2023.110389.

Saratale, R. G., G. D. Saratale, J. S. Chang, and S. P. Govindwar. **2011**. "Bacterial Decolorization and Degradation of Azo Dyes: A Review." Journal of the Taiwan Institute of Chemical Engineers 42 (1): 138–57. https://doi.org/10.1016/J.JTICE.2010.06.006.

Sarkar, Shrabana, Aparna Banerjee, Urmi Halder, Raju Biswas, and Rajib Bandopadhyay. **2017**. "Degradation of Synthetic Azo Dyes of Textile Industry: A Sustainable Approach Using Microbial Enzymes." Water Conservation Science and Engineering 2 (4): 121–31. https://doi.org/10.1007/S41101-017-0031-5.

Saunders, Norman R., Katarzyna M. Dziegielewska, Kjeld Møllgård, and Mark D. Habgood. **2015**. "Markers for Blood-Brain Barrier Integrity: How Appropriate Is Evans Blue in the Twenty-First Century and What Are the Alternatives?" Frontiers in Neuroscience 9 (OCT): 166058. https://doi.org/10.3389/FNINS.2015.00385.

"SGS: New European Standard for Aromatic Amines Derived from Azo Colorants Released." n.d. Accessed January 25, **2026.** https://www.sgs.com/en-pl/news/2017/05/safeguards-08217-new-european-standard-for-aromatic-amines-derived-from-azo-colorants-released

Shahabuddin, Syed, Norazilawati Muhamad Sarih, Muhammad Afzal Kamboh, Hamid Rashidi Nodeh, and Sharifah Mohamad. **2016**. "Synthesis of Polyaniline-Coated Graphene Oxide@SrTiO3 Nanocube Nanocomposites for Enhanced Removal of Carcinogenic Dyes from Aqueous Solution." Polymers 2016, Vol. 8, Page 305 8 (9): 305. https://doi.org/10.3390/POLYM8090305.

Shahi, Amrita, Padmanaban Velayudhaperumal Chellam, Ankur Verma, and R. S. Singh. **2021**. "A Comparative

Study on the Performance of Microbial Fuel Cell for the Treatment of Reactive Orange 16 Dye Using Mixed and Pure Bacterial Species and Its Optimization Using Response Surface Methodology." Sustainable Energy Technologies and Assessments 48 (December):101667. https://doi.org/10.1016/J.SETA.2021.101667.

Shakibania, Sara, Taral Patel, Roman Turczyn, Manus J.P. Biggs, and Katarzyna Krukiewicz. **2025.** "Hybrid Conducting Polymer Films Promote Neural Outgrowth and Neural-Electrode Integration in Vitro." Bioelectrochemistry 165 (October):108985. https://doi.org/10.1016/J.BIOELECHEM.2025.108985.

Sharma, Jyotshana, Shubhangani Sharma, and Vineet Soni. **2021**. "Classification and Impact of Synthetic Textile Dyes on Aquatic Flora: A Review." Regional Studies in Marine Science 45 (June):101802. https://doi.org/10.1016/J.RSMA.2021.101802.

Sharma, Praveen, Lakhvinder Singh, and Neeraj Dilbaghi. **2009**. "Response Surface Methodological Approach for the Decolorization of Simulated Dye Effluent Using Aspergillus Fumigatus Fresenius." Journal of Hazardous Materials 161 (2–3): 1081–86. https://doi.org/10.1016/J.JHAZMAT.2008.04.085.

Shirani, Mahboube, Behrouz Akbari-adergani, Hamid Rashidi Nodeh, and Syed Shahabuddin. **2020**. "Ultrasonication-Facilitated Synthesis of Functionalized Graphene Oxide for Ultrasound-Assisted Magnetic Dispersive Solid-Phase Extraction of Amoxicillin, Ampicillin, and Penicillin G." Microchimica Acta 187 (11). https://doi.org/10.1007/S00604-020-04605-Z.

Singh, Gajendra B., Ankita Vinayak, Gaurav Mudgal, and Kavindra Kumar Kesari. **2024**. "Azo Dye Bioremediation: An Interdisciplinary Path to Sustainable Fashion." Environmental Technology & Innovation 36 (November):103832. https://doi.org/10.1016/J.ETI.2024.103832.

Singh, Pradeep Kumar, Pankaj Singh, Rajat Pratap Singh, and Ram Lakhan Singh. **2021**. "Biodecolorization of Azo Dye Acid Blue 113 by Soil Bacterium Klebsiella Variicola RMLP1." Journal of Ecophysiology and Occupational Health, June, 64–71. https://doi.org/10.18311/JEOH/0/27108.

Slama, Houda Ben, Ali Chenari Bouket, Zeinab Pourhassan, Faizah N. Alenezi, Allaoua Silini, Hafsa Cherif-Silini, Tomasz Oszako, Lenka Luptakova, Patrycja Golińska, and Lassaad Belbahri. **2021**. "Diversity of Synthetic Dyes from Textile Industries, Discharge Impacts and Treatment Methods." Applied Sciences 2021, Vol. 11, Page 6255 11 (14): 6255. https://doi.org/10.3390/APP11146255.

Solanki, Komal, Sindhu Subramanian, and Suddhasatwa Basu. **2013a**. "Microbial Fuel Cells for Azo Dye Treatment with Electricity Generation: A Review." Bioresource Technology 131 (March):564–71. https://doi.org/10.1016/J.BIORTECH.2012.12.063.

———. **2013b**. "Microbial Fuel Cells for Azo Dye Treatment with Electricity Generation: A Review." Bioresource Technology 131:564–71. https://doi.org/10.1016/J.BIORTECH.2012.12.063.

Soltani, Ali, Mehdi Faramarzi, and Seyed Aboutaleb Mousavi Parsa. **2021**. "A Review on Adsorbent Parameters for Removal of Dye Products from Industrial Wastewater." Water Quality Research Journal 56 (4): 181–93. https://doi.org/10.2166/WQRJ.2021.023.

Sonawane, Jayesh M., Sunil A. Patil, Prakash C. Ghosh, and Samuel B. Adeloju. **2018**. "Low-Cost Stainless-

Steel Wool Anodes Modified with Polyaniline and Polypyrrole for High-Performance Microbial Fuel Cells." Journal of Power Sources 379 (March):103–14. https://doi.org/10.1016/J.JPOWSOUR.2018.01.001.

Splitstoser, Jeffrey C., Tom D. Dillehay, Jan Wouters, and Ana Claro. **2016**. "Early Pre-Hispanic Use of Indigo Blue in Peru." Science Advances 2 (9): e1501623. https://doi.org/10.1126/SCIADV.1501623.

Sreedharan, Veena, Purbasha Saha, and Kokati Venkata Bhaskara Rao. **2021**. "Dye Degradation Potential of Acinetobacter Baumannii Strain VITVB against Commercial Azo Dyes." Bioremediation Journal 25 (4): 347–68. https://doi.org/10.1080/10889868.2020.1871317.

Stolz, A. **2001**. "Basic and Applied Aspects in the Microbial Degradation of Azo Dyes." Applied Microbiology and Biotechnology 56 (1–2): 69–80. https://doi.org/10.1007/S002530100686/METRICS.

Sultan, Maha, Hassan Ibrahim, Hossam Mohammed El-Masry, and Youssef R. Hassan. **2024**. "Antimicrobial Gelatin-Based Films with Cinnamaldehyde and ZnO Nanoparticles for Sustainable Food Packaging." Scientific Reports 2024 14:1 14 (1): 1–21. https://doi.org/10.1038/s41598-024-72009-7.

Sultana, Saima, Mohammad Danish Khan, Suhail Sabir, Khalid M. Gani, Mohammad Oves, and Mohammad Zain Khan. **2015**. "Bio-Electro Degradation of Azo-Dye in a Combined Anaerobic–Aerobic Process along with Energy Recovery." New Journal of Chemistry 39 (12): 9461–70. https://doi.org/10.1039/C5NJ01610J.

Sun, Jian, Zhe Bi, Bin Hou, Yun qing Cao, and Yong you Hu. 2011. "Further Treatment of Decolorization Liquid of Azo Dye Coupled with Increased Power Production Using Microbial Fuel Cell Equipped with an Aerobic Biocathode." Water Research 45 (1): 283–91. https://doi.org/10.1016/J.WATRES.2010.07.059.

Sun, Jian, Bihai Cai, Yaping Zhang, Yenping Peng, Kenlin Chang, Xunan Ning, Guoguang Liu, et al. **2016**. "Regulation of Biocathode Microbial Fuel Cell Performance with Respect to Azo Dye Degradation and Electricity Generation via the Selection of Anodic Inoculum." International Journal of Hydrogen Energy 41 (9): 5141–50. https://doi.org/10.1016/J.IJHYDENE.2016.01.114.

Sun, Jian, Youming Li, Yongyou Hu, Bin Hou, Yaping Zhang, and Sizhe Li. **2013**. "Understanding the Degradation of Congo Red and Bacterial Diversity in an Air-Cathode Microbial Fuel Cell Being Evaluated for Simultaneous Azo Dye Removal from Wastewater and Bioelectricity Generation." Applied Microbiology and Biotechnology 97 (8): 3711–19. https://doi.org/10.1007/S00253-012-4180-3.

Sun, Liping, Yinghui Mo, and Lu Zhang. **2022.** "A Mini Review on Bio-Electrochemical Systems for the Treatment of Azo Dye Wastewater: State-of-the-Art and Future Prospects." Chemosphere 294:133801. https://doi.org/10.1016/J.CHEMOSPHERE.2022.133801.

Suresh, R., Saravanan Rajendran, Wei Hsin Chen, Matias Soto-Moscoso, Thanigaivel Sundaram, Aishah Abdul Jalil, and Suresh Kumar Rajamani Sekar. **2024**. "A Review on Algae-Mediated Adsorption and Catalytic Processes for Organic Water Pollution Remediation." Frontiers in Materials 11 (August):1432704. https://doi.org/10.3389/FMATS.2024.1432704.

Takkar, Simran, Bhawna Tyagi, Naveen Kumar, Taruna Kumari, Khushboo Iqbal, Ajit Varma, Indu Shekhar

Thakur, and Arti Mishra. **2022**. "Biodegradation of Methyl Red Dye by a Novel Actinobacterium Zhihengliuella Sp. ISTPL4: Kinetic Studies, Isotherm and Biodegradation Pathway." Environmental Technology & Innovation 26 (May):102348. https://doi.org/10.1016/J.ETI.2022.102348.

Thiruppathi, Krithika, Kavitha Rangasamy, Mahendran Ramasamy, and Dinesh Muthu. 2021. "Evaluation of Textile Dye Degrading Potential of Ligninolytic Bacterial Consortia." Environmental Challenges 4 (August):100078. https://doi.org/10.1016/J.ENVC.2021.100078.

Thomas, Olusegun E., and Olajire A. Adegoke. **2022**. "Synthesis, Characterization and Solvatochromic Behaviour of New Water-Soluble 8-Hydroxy-3,6-Disulphonaphthyl Azohydroxynaphthalenes." Journal of Taibah University for Science 16 (1): 451–62. https://doi.org/10.1080/16583655.2022.2070903.

Thung, Wei Eng, Soon An Ong, Li Ngee Ho, Yee Shian Wong, Fahmi Ridwan, Yoong Ling Oon, Yoong Sin Oon, and Harvinder Kaur Lehl. **2015**. "A Highly Efficient Single Chambered Up-Flow Membrane-Less Microbial Fuel Cell for Treatment of Azo Dye Acid Orange 7-Containing Wastewater." Bioresource Technology 197 (December):284–88. https://doi.org/10.1016/J.BIORTECH.2015.08.078.

Tian, Fang, Yongbo Wang, Guang Guo, Keqiang Ding, Feng Yang, Chongyang Wang, Huiya Wang, and Mengdi Yan. **2023**. "Meta-Genome Analysis of a Newly Enriched Azo Dyes Detoxification Halo-Thermophilic Bacterial Consortium." Environmental Research 237 (November):116828. https://doi.org/10.1016/J.ENVRES.2023.116828.

Tian, Yongqiang, Kangli Wu, Shenghong Lin, Meiling Shi, Yang Liu, Xu Su, and Rehmat Islam. **2024**. "Biodegradation and Decolorization of Crystal Violet Dye by Cocultivation with Fungi and Bacteria." ACS Omega 9 (7): 7668. https://doi.org/10.1021/ACSOMEGA.3C06978.

Tkaczyk, Angelika, Kamila Mitrowska, and Andrzej Posyniak. **2020**. "Synthetic Organic Dyes as Contaminants of the Aquatic Environment and Their Implications for Ecosystems: A Review." Science of The Total Environment 717 (May):137222. https://doi.org/10.1016/J.SCITOTENV.2020.137222.

Tripathi, Manikant, Shivpujan Shukla, Ranjan Singh, Sangram Singh, Pankaj Singh, Pradeep Kumar Singh, Awadhesh Kumar Shukla, et al. **2024**. "Physicochemical Investigations of Textile Wastewater and Process Parameter Optimization for Biodecolorization of Congo Red Dye by Pseudomonas Aeruginosa MT-2 Strain." Journal of Pure and Applied Microbiology 18 (4): 2558–69. https://doi.org/10.22207/JPAM.18.4.29.

Tripathi, Manikant, Pankaj Singh, Ranjan Singh, Saroj Bala, Neelam Pathak, Sangram Singh, Rajveer Singh Chauhan, and Pradeep Kumar Singh. **2023**. "Microbial Biosorbent for Remediation of Dyes and Heavy Metals Pollution: A Green Strategy for Sustainable Environment." Frontiers in Microbiology 14 (April):1168954. https://doi.org/10.3389/FMICB.2023.1168954.

Tripathi, Manikant, Sakshi Singh, Sukriti Pathak, Jahnvi Kasaudhan, Aditi Mishra, Saroj Bala, Diksha Garg, et al. **2023**. "Recent Strategies for the Remediation of Textile Dyes from Wastewater: A Systematic Review." Toxics 11 (11): 940. https://doi.org/10.3390/TOXICS11110940.

Tüfekci, Neşe, Nüket Sivri, and İsmail Toroz. **2007**. "Pollutants of Textile Industry Wastewater and Assessment

of Its Discharge Limits by Water Quality Standards." Turkish Journal of Fisheries and Aquatic Sciences 7 (2): 97–103. https://www.trjfas.org/abstract.php?lang=en&id=319.

Ullah, Faheem, Ghulam Mustafa, Muhammad Tariq Zahid, Ihtisham Jamil, Syed Zaghum Abbas, Byong-Hun Jeon, Abdulrahman H Alessa, et al. **2024**. "Role of Acinetobacter Baumannii in Decolorization of Reactive Blue 224 Dye and Functional Analysis of Azoreductase Gene." Journal of King Saud University – Science 36 (7). https://doi.org/10.1016/J.JKSUS.2024.103279.

Usoltsev, Dmitrii, Vera Sitnikova, Andrey Kajava, and Mayya Uspenskaya. **2019**. "Systematic FTIR Spectroscopy Study of the Secondary Structure Changes in Human Serum Albumin under Various Denaturation Conditions." Biomolecules 9 (8). https://doi.org/10.3390/BIOM9080359.

Veluchamy, Ajithkumar, Jothika Jeyabalan, Anushka Singh, Selvaraju Narayanasamy, and Ankur Verma. **2024**. "A Review on Recent Insights of Azoreductases Mediated Dye Degradation: A Sustainable Approach for Bioremediation of Industrial Wastewater." Journal of Water Process Engineering 68 (December):106403. https://doi.org/10.1016/J.JWPE.2024.106403.

Villanueva, Xabier, Lili Zhen, José Nunez Ares, Thijs Vackier, Heiko Lange, Claudia Crestini, and Hans P. Steenackers. **2023**. "Effect of Chemical Modifications of Tannins on Their Antimicrobial and Antibiofilm Effect against Gram-Negative and Gram-Positive Bacteria." Frontiers in Microbiology 13 (January):987164. https://doi.org/10.3389/FMICB.2022.987164.

Vyavahare, Govind, Ranjit Gurav, Ravishankar Patil, Shubham Sutar, Pooja Jadhav, Devashree Patil, Yung Hun Yang, et al. **2021**. "Sorption of Brilliant Green Dye Using Soybean Straw-Derived Biochar: Characterization, Kinetics, Thermodynamics and Toxicity Studies." Environmental Geochemistry and Health 43 (8): 2913–26. https://doi.org/10.1007/S10653-020-00804-Y.

Wang, Guozhen, Yating Guo, Jiaying Cai, Hongyu Wen, Zhen Mao, Hao Zhang, Xin Wang, Lei Ma, and Mengqin Zhu. **2019**. "Electricity Production and the Analysis of the Anode Microbial Community in a Constructed Wetland-Microbial Fuel Cell." RSC Advances 9 (37): 21460. https://doi.org/10.1039/C8RA10130B.

Wang, Hui, Xizi Long, Yingying Sun, Dongqi Wang, Zhe Wang, Haiyu Meng, Chunbo Jiang, Wen Dong, and Nan Lu. **2022**. "Electrochemical Impedance Spectroscopy Applied to Microbial Fuel Cells: A Review." Frontiers in Microbiology 13 (July):973501. https://doi.org/10.3389/FMICB.2022.973501.

Wang, Hwai Lee, and Ted Weita Lai. **2014**. "Optimization of Evans Blue Quantitation in Limited Rat Tissue Samples." Scientific Reports 4 (1): 1–7. https://doi.org/10.1038/SREP06588.

Wang, Yuelei, Yuqi Liu, Xiaojun Zhang, Lu Cheng, Daizong Cui, Min Zhao, and Xianchun Zong. **2025**. "Rapid Biodecolorization of Azo Dyes by Shewanella Oneidensis MR-1 Under Aerobic Conditions." Catalysts 15 (8): 796. https://doi.org/10.3390/CATAL15080796.

Wei, Dong, Bingfeng Wang, Huu Hao Ngo, Wenshan Guo, Fei Han, Xiaodong Wang, Bin Du, and Qin Wei. **2015**. "Role of Extracellular Polymeric Substances in Biosorption of Dye Wastewater Using Aerobic Granular Sludge." Bioresource Technology 185 (June):14–20.

https://doi.org/10.1016/J.BIORTECH.2015.02.084.

Wojnárovits, László, and Erzsébet Takács. **2008**. "Irradiation Treatment of Azo Dye Containing Wastewater: An Overview." Radiation Physics and Chemistry 77 (3): 225–44. https://doi.org/10.1016/J.RADPHYSCHEM.2007.05.003.

Wu, Yongmin, Xiang Xiao, Cancan Xu, Danming Cao, and Daolin Du. **2012**. "Decolorization and Detoxification of a Sulfonated Triphenylmethane Dye Aniline Blue by Shewanella Oneidensis MR-1 under Anaerobic Conditions." Applied Microbiology and Biotechnology 2012 97:16 97 (16): 7439–46. https://doi.org/10.1007/S00253-012-4476-3.

Xiao, Xiang, Can Can Xu, Yong Min Wu, Pei Jie Cai, Wen Wei Li, Dao Lin Du, and Han Qing Yu. **2012**. "Biodecolorization of Naphthol Green B Dye by Shewanella Oneidensis MR-1 under Anaerobic Conditions." Bioresource Technology 110 (April):86–90. https://doi.org/10.1016/j.biortech.2012.01.099.

Yadav, Archana, Pankaj Kumar, Deepak Rawat, Shafali Garg, Paromita Mukherjee, Furqan Farooqi, Anurag Roy, Senthilarasu Sundaram, Radhey Shyam Sharma, and Vandana Mishra. **2022**. "Microbial Fuel Cells for Mineralization and Decolorization of Azo Dyes: Recent Advances in Design and Materials." Science of The Total Environment 826 (June):154038. https://doi.org/10.1016/J.SCITOTENV.2022.154038.

Yadav, Ravi Shankar, Weihua He, Dandan Liang, Chao Li, Yanling Yu, Kamran Ayaz, and Yujie Feng. **2024**. "High-Efficiency Hydrogen Recovery from Corn Straw Hydrolysate Using Functional Bacteria and Negative Pressure with Microbial Electrolysis Cells." Water (Switzerland) 16 (17): 2423. https://doi.org/10.3390/W16172423/S1.

Yadav, Shailendra, Kanha Singh Tiwari, Chitrasen Gupta, Mahendra Kumar Tiwari, Arbaj Khan, and Sankatha P. Sonkar. **2023**. "A Brief Review on Natural Dyes, Pigments: Recent Advances and Future Perspectives." Results in Chemistry 5 (January):100733. https://doi.org/10.1016/J.RECHEM.2022.100733.

Yamada, Shigeyuki, Junko Bessho, Hitoya Nakasato, and Osamu Tsutsumi. **2018**. "Color Tuning Donor–Acceptor-Type Azobenzene Dyes by Controlling the Molecular Geometry of the Donor Moiety." Dyes and Pigments 150 (March):89–96. https://doi.org/10.1016/J.DYEPIG.2017.11.002.

Yang, Pengfei, Yanqin Lu, Hua Zhang, Ronghua Li, Xiaozhe Hu, Asfandyar Shahab, Ashraf Y. Elnaggar, Abdulwahed Fahad Alrefaei, Mikhlid H. AlmutairiI, and Enas Ali. **2024**. "Effective Removal of Methylene Blue and Crystal Violet by Low-Cost Biomass Derived from Eucalyptus: Characterization, Experiments, and Mechanism Investigation." Environmental Technology & Innovation 33 (February):103459. https://doi.org/10.1016/J.ETI.2023.103459.

Yang, Suling, Fangzhou Du, and Hong Liu. . "Characterization of Mixed-Culture Biofilms Established in Microbial Fuel Cells." Biomass and Bioenergy 46 (November):531–37. https://doi.org/10.1016/J.BIOMBIOE.2012.07.007.

Yao, Linpeng, Xing Xue, Peipei Yu, Yicheng Ni, and Feng Chen. **2018**. "Evans Blue Dye: A Revisit of Its Applications in Biomedicine." Contrast Media & Molecular Imaging 2018 (April). https://doi.org/10.1155/2018/7628037.

Yates, Edwin, and Andrew Yates. **2015**. "Johann Peter Griess FRS (1829–88): Victorian Brewer and Synthetic Dye Chemist." Notes and Records of the Royal Society of London 70 (1): 65. https://doi.org/10.1098/RSNR.2015.0020.

Yuzer, Burak, and Huseyin Selcuk. **2021**. "Recovery of Biologically Treated Textile Wastewater by Ozonation and Subsequent Bipolar Membrane Electrodialysis Process." Membranes 2021, Vol. 11, 11 (11). https://doi.org/10.3390/MEMBRANES11110900.

Zabłocka-Godlewska, Ewa, Wioletta Przystaå, and Elzbieta Grabińska-Sota. **2014**. "Decolourisation of Different Dyes by Two Pseudomonas Strains under Various Growth Conditions." Water, Air, and Soil Pollution 225 (2): 1–13. https://doi.org/10.1007/S11270-013-1846-0.

ZABŁOCKA-GODLEWSKA, Ewa, Wioletta PRZYSTAŚ, and Maria GODLEWSKA. **2020**. "Isolation and Screening of Bacteria with Ability to Decolorize Selected Synthetic Dyes – Preliminary Results." Architecture, Civil Engineering, Environment 13 (2): 75–86. https://doi.org/10.21307/acee-2020-019.

Zablocka-Godlewska, Ewa, Wioletta Przystas, and Elzbieta Grabinska-Sota. **2012**. "Decolourization of Diazo Evans Blue by Two Strains of Pseudomonas Fluorescens Isolated from Different Wastewater Treatment Plants." Water, Air, and Soil Pollution 223 (8): 5259. https://doi.org/10.1007/S11270-012-1276-4.

Zafar, Sadia, Dilara A. Bukhari, and Abdul Rehman. **2022**. "Azo Dyes Degradation by Microorganisms – An Efficient and Sustainable Approach." Saudi Journal of Biological Sciences 29 (12): 103437. https://doi.org/10.1016/J.SJBS.2022.103437.

Zafar, Z., K. Ayaz, M. H. Nasir, S. Yousaf, I. Sharafat, and N. Ali. **2019**. "Electrochemical Performance of Biocathode Microbial Fuel Cells Using Petroleum-Contaminated Soil and Hot Water Spring." International Journal of Environmental Science and Technology 16 (3): 1487–1500. https://doi.org/10.1007/S13762-018-1757-0.

Zee, Frank P. Van Der, and Santiago Villaverde. **2005**. "Combined Anaerobic–Aerobic Treatment of Azo Dyes—A Short Review of Bioreactor Studies." Water Research 39 (8): 1425–40. https://doi.org/10.1016/J.WATRES.2005.03.007.

Zhang, Fei, Zheng Ge, Julien Grimaud, Jim Hurst, and Zhen He. **2013**. "Long-Term Performance of Liter-Scale Microbial Fuel Cells Treating Primary Effluent Installed in a Municipal Wastewater Treatment Facility." Environmental Science and Technology 47 (9): 4941–48. https://doi.org/10.1021/ES400631R.

Zhang, Guodong, Sansan Feng, Yan Jiao, Duu Jong Lee, Yanjun Xin, and Huifang Sun. **2017.** "Cathodic Reducing Bacteria of Dual-Chambered Microbial Fuel Cell." International Journal of Hydrogen Energy 42 (45): 27607–17. https://doi.org/10.1016/J.IJHYDENE.2017.06.095.

Zhang, Junqi, Wenjing Lv, Yangyang Wang, Jingxuan Tan, Qijing Liu, Huan Yu, Chao Li, et al. **2025**. "Engineering Shewanella Oneidensis to Efficiently Co-Utilize Glucose and Xylose for Converting Cellulose Hydrolysate from Corn Stover to Electricity." Chemical Engineering Journal 505 (February):159574. https://doi.org/10.1016/J.CEJ.2025.159574.

Zhang, Leyuan, Yucheng Zhang, Yang Liu, Sibo Wang, Calvin K. Lee, Yu Huang, and Xiangfeng Duan. **2024**.

"High Power Density Redox-Mediated Shewanella Microbial Flow Fuel Cells." Nature Communications 2024 15:1 15 (1): 1–11. https://doi.org/10.1038/s41467-024-52498-w.

Zhang, Yiqing, Kashif Shaad, Derek Vollmer, and Chi Ma. **2021**. "Treatment of Textile Wastewater Using Advanced Oxidation Processes—a Critical Review." Water (Switzerland) 13 (24): 3515. https://doi.org/10.3390/W13243515/S1.

Zhao, Juntao, Feng Li, Shutian Kong, Tao Chen, Hao Song, and Zhiwen Wang. **2023**. "Elongated Riboflavin-Producing Shewanella Oneidensis in a Hybrid Biofilm Boosts Extracellular Electron Transfer." Advanced Science 10 (9): 2206622. https://doi.org/10.1002/ADVS.202206622.

Zhong, Dengjie, Yaqi Liu, Xinrong Liao, Nianbing Zhong, and Yunlan Xu. **2018**. "Facile Preparation of Binder-Free NiO/MnO2-Carbon Felt Anode to Enhance Electricity Generation and Dye Wastewater Degradation Performances of Microbial Fuel Cell." International Journal of Hydrogen Energy 43 (51): 23014–26. https://doi.org/10.1016/J.IJHYDENE.2018.10.144.

Zhou, Feng, Wenyue Wang, Kaiyi Li, Weilong Yang, Jaewon Lee, Bing Xie, Bing Wu, Hongqiang Ren, Seungkwan Hong, and Min Zhan. **2024.** "Controlling of Irreversible Fouling and Mechanism in a Hybrid Ceramic Membrane Bioreactor (CMBR)-Reverse Osmosis (RO) Process for Textile Wastewater Reclamation." Desalination 586 (October):117914. https://doi.org/10.1016/J.DESAL.2024.117914.

Zin, Khairunnisa' Mohd, Mohd Izuan Effendi Halmi, Siti Salwa Abd Gani, Uswatun Hasanah Zaidan, A. Wahid Samsuri, and Mohd Yunus Abd Shukor. **2020**. "Microbial Decolorization of Triazo Dye, Direct Blue 71: An Optimization Approach Using Response Surface Methodology (RSM) and Artificial Neural Network (ANN)." BioMed Research International 2020:2734135. https://doi.org/10.1155/2020/2734135.